Chances in Wind Energy
A Probabilistic Approach to Wind Turbine Fatigue Design

Dick Veldkamp

Chances in Wind Energy

A Probabilistic Approach to
Wind Turbine Fatigue Design

Proefschrift

ter verkrijging van de graad van doctor
aan de Technische Universiteit Delft
op gezag van de Rector Magnificus prof. dr. ir. J.T. Fokkema
in het openbaar te verdedigen ten overstaan van een commissie,
door het College voor Promoties aangewezen,
op dinsdag 17 oktober 2006 om 15:00 uur

door

Herman Frederik VELDKAMP

werktuigkundig ingenieur
geboren te Kokonao, Nederlands Nieuw-Guinea

voor mijn ouders
voor Elizabeth
voor Dian, Lisette en Susan Rikke

iv

Contents

Foreword

The problem presents features of interest.

— Sherlock Holmes in 'The crooked man'

To boldly go where no one has gone before.

— From the opening lines of the television series 'Star Trek'

Sherlock Holmes' famous dictum gives the reason for starting this (and maybe any) piece of research: it just seemed an interesting problem. In this case the problem was to find out what our wind turbine design methods mean: if we follow all standards and do the best we can, what is the failure probability we obtain?

The ideal when doing PhD work is nicely captured in the second quotation (which must be the most well known split infinitive of all time): to boldly develop new methods and make ground breaking discoveries. However it soon becomes clear that much work has been done before; but if one thinks about it for a moment, one should not really be put off by this. After all, one of the pillars of science is that things done before are done again, i.e. checked and verified (a fact that is not always appreciated enough – why are there no funds for reproducing results for example?).

My ideal was to write a book in the style of 'Numerical Recipes' by Press *et al.* [167], which is not only a comprehensive and clear treatment of numerical methods (which, incidentally, was used extensively in the present work), but is also a publication that, rather than only solving the obvious problems, addresses less common and more tedious extensions too; on top of that it is 'notable for its accessibility and general not-too-serious tone' (Wikipedia)[1].

As regards the latter, I doubt whether this volume will be 'unputdownable'; but in relation to the former, I think I have covered the relevant aspects of the subject, and along the way tied up some loose ends: those things that have been lying around for years because nobody has the time to investigate them, or rules of thumb that everybody in the wind industry accepts without bothering to check them. Also I have tried to explain in detail what I did – it is my experience that there is a tendency to look down on the simpler details ('We experts know all this already, don't we?')

---

[1]Now that is a comment I would like to hear about this tome.

rather than describing all the steps taken, which sometimes makes it hard to find out what the researchers actually did.

When one is working so long on one project it is natural that many people contribute to it in one way or another. First of all I want to thank my supervisors Gijs van Kuik and Ton Vrouwenvelder, whose critical remarks greatly improved the manuscript (though I confess to always having looked forward to our meetings with a certain anxiety).

I thank the members of the committee for the time they took to go through the manuscript and for their valuable comments.

Then there are thanks to: Ivan Bech Lauridzen for doing some FEM calculations; Frank Goezinne for assisting with Measure-Correlate-Predict calculations; Kurt Hansen, Gunner Larsen and Karl Henrik Svendsen for supplying wind data; Wim Bierbooms, Bill Holley and Jacob Mann for discussions on modelling of turbulent wind fields; Raymond Downey for some additional work on uncertainties in wind climate prediction; Tjaard and Wybrand van Ellen for spotting two errors of arithmetic (which have been corrected in the PDF-version); Erik van der Pol for saving computer data at a critical moment; Kenneth Thomsen for sending me various articles and reports; Erik Carl Miranda and Conrad Trevelyan for text polishing; Nord Jan Vermeer for help with L^AT_EX, the scientific word processor that effortlessly couples magnificent lay out with user-unfriendliness of varying degrees; Michael Vormwald for indispensable information on fatigue issues; Ronald v/d Werken for making some nice drawings. And of course to all colleagues in Denmark and in the Netherlands.

Finally I want to thank NEG Micon (now Vestas) for giving me the opportunity to spend four years on this interesting project.

Houten, September 2006   Dick Veldkamp

Summary

Wind is becoming an ever more important source of renewable energy: installed wind turbine power now stands at 60,000 MW worldwide (roughly 60,000 turbines), providing 0.6% of world electricity demand. In spite of this success, wind energy has still not made a definitive breakthrough. The main reason for this is that it has to compete with conventionally generated electricity, which often is cheaper, or at least appears to be if environmental costs are not taken into account. For wind to make a really substantial contribution to world energy supply, it is therefore imperative that the cost of wind energy is brought down even further, which means that wind turbines must be designed to be exactly as strong as necessary, but no stronger.

Hence there is a need to investigate whether the conventional design procedure that has been developed over the last decade results in the right degree of conservatism, and if not, how it may be improved. The ideal is to make the design just conservative enough, i.e. to exactly attain the target failure probability. Because wind turbines tend to be located in remote areas, the target value is primarily determined by economic considerations, rather than by public safety issues.

The aims of this work are therefore:

1. To quantify total uncertainty in the design procedure, and the relative importance of stochastic parameters influencing fatigue loads and strength.

2. To conduct a comparative review of calculation models where necessary.

3. To derive partial safety factors giving minimum unit electricity cost.

Previous work on probabilistic design of wind turbines is discussed. On the basis of this the scope of the present research is limited to fatigue issues, since extreme loads have been investigated previously (at least to some degree). Because of the current market trend, the focus of this work is on pitch controlled, variable speed machines, although the methods developed are generally applicable.

Following this, some preliminary investigations into economic design are described. It is shown that current practice –where wind turbines reach maximum power at 12–16 m/s wind speed– is optimal, giving capacity factors (average power divided by rated power) between 15 and 35%. A model is derived for the sum of investment cost and cost of failures during the turbine's life, which can be used to establish optimal partial factors.

An inventory of stochastic parameters is made; these are divided into five different groups: parameters related to the wind climate, the sea climate, the aerodynamics, the structural model and the material fatigue properties. For each of the parameters the distribution is estimated, and the models currently used in wind turbine design (i.e. the procedures used to estimate characteristic parameters and how to use them in calculations) are reviewed. Two examples of the conclusions drawn about these models are:

1. The usual load calculation, which uses separate 10 minute periods, misses the low frequency changes in wind direction that produce large load cycles for the tower. These cycles do have influence on fatigue damage equivalent loads.

2. The concept of fatigue damage equivalent turbulence is useful, and it is slightly conservative.

A limit state function is derived using the concept of life fatigue damage equivalent load range. With the First Order Reliability Method (FORM) and Monte Carlo simulation (both of which yield similar results), yearly failure probabilities due to fatigue are estimated for a wind turbine that is designed exactly according to the standard, and installed following common site admission rules. Optimal partial factors are established, using the annual failure probabilities and the economic model.

The partial factor values found for blades are somewhat smaller than in the standard, while values for hub, nacelle and tower are higher. The explanation for the latter is that two things are currently not taken into account in design calculations according to the standard (at least not explicitly): firstly, variation and bias in fatigue life prediction; secondly, the fact that a combination of many critical locations (for example in the tower) yields a larger failure probability than just one location.

The sensitivity of the partial factor optimisation to changes in various assumptions made is investigated. These include: what the actual value of the material fatigue strength is (vs what is required by standards), how severe the actual site wind regime is (vs what is admissible), the definition of the equivalent fatigue load, the slope of the S-N curve, the desired wind turbine life, the terrain type (complex terrain and offshore vs flat smooth uniform terrain), and finally whether calculated loads are verified by measurements.

The main conclusions of the work are threefold:

1. Given available data, a larger partial (load or material) factor should be used in fatigue design for cast iron and weld seams. However, the effect of this on design might be limited since hidden safety exists in the construction: material quality and hence fatigue strength are better than assumed, wind turbines are placed in climates that are more benign than they were designed for, and finally, dimensions may be determined by stiffness or extreme load considerations rather than by fatigue.

2. The variation of the limit state function is determined mainly by uncertainty on fatigue strength and fatigue life prediction. Therefore, the way forward is

to accurately establish fatigue properties and calibrate fatigue life predictions for materials exactly as used in wind turbines. In this way variation may be reduced (and bias removed), and failure probability estimates may be refined. If better information is available, hidden safety may be removed and smaller partial factors used in calculations.

3. The number of critical locations and correlation of loads and fatigue strength at different locations must be taken into account in calculations to establish failure probabilities, and must have influence on the partial factors to be used. Variation and bias of fatigue life predictions must be an explicit input to fatigue design calculations.

Samenvatting

Wind is een steeds belangrijker bron van duurzame energie: het totaal geïnstalleerd vermogen staat nu op 60.000 MW wereldwijd (ruwweg 60.000 turbines), goed voor ongeveer 0.6% van de wereldelektriciteitsvraag. Echter ondanks dit succes is windenergie nog niet definitief doorgebroken. De hoofdreden hiervoor is dat geconcurreerd moet worden met conventioneel gegenereerde elektriciteit, die vaak goedkoper is, of dat in ieder geval lijkt als milieukosten niet in rekening worden gebracht. Om met wind een werkelijk belangrijke bijdrage aan de wereldenergieproductie te leveren, is het noodzakelijk dat de kosten van windenergie nog verder naar beneden worden gebracht, hetgeen betekent dat windmolens precies sterk genoeg moeten worden ontworpen, maar niet sterker dan dat.

Daarom is het nodig te onderzoeken of de gebruikelijke ontwerpmethode die gedurende het laatste decennium ontwikkeld is, resulteert in ontwerpen met de gewenste graad van conservatisme, en als dit niet zo is, hoe deze verbeterd kan worden. Het ideaal is om juist conservatief genoeg te ontwerpen, d.w.z. dat men precies de streefwaarde voor de veiligheid (en daarmee de toelaatbare faalkans) realiseert. Omdat windmolens zich in het algemeen in afgelegen gebieden bevinden, wordt de toelaatbare faalkans meer door economische overwegingen bepaald dan door het vraagstuk van publieke veiligheid.

De doelstellingen van dit onderzoek zijn daarom:

1. Het kwantificeren van de totale onzekerheid in de ontwerpprocedure, alsmede het relatieve belang van de stochastische parameters die invloed hebben op vermoeiingsbelasting en -sterkte.

2. Waar nodig het doen van vergelijkend onderzoek naar berekeningsmodellen die gebruikt worden.

3. Het afleiden van partiële veiligheidsfactoren die minimale eenheidskosten van elektriciteit geven.

Eerder werk betreffende probabilistisch ontwerp van windturbines wordt besproken. Op basis hiervan wordt het huidige onderzoek beperkt tot vermoeiing, omdat het onderwerp 'extreme belastingen' reeds (tenminste tot op zekere hoogte) onderzocht is. Vanwege de huidige markttrend gaat de aandacht vooral uit naar pitch-geregelde variabel-toerentalmachines; ontwikkelde methoden zijn echter algemeen toepasbaar.

Hierna wordt enig inleidend onderzoek gedaan op het gebied van economisch ontwerpen. Er wordt aangetoond dat de gangbare praktijk –waarin windmolens bij een windsnelheid van 12–16 m/s maximaal vermogen bereiken– optimaal is, en dat hiermee een capaciteitsfactor (gemiddeld vermogen gedeeld door nominaal vermogen) van 15–35% wordt gehaald. Er wordt een model opgesteld voor de som van investerings- en faalkosten gedurende de levensduur van de turbine, dat gebruikt kan worden om optimale partiële factoren vast te stellen.

Stochastische parameters worden geïnventariseerd en vervolgens verdeeld in vijf verschillende groepen: windklimaat, zeeklimaat, aërodynamica, structuurmodel en vermoeiing. Voor elke parameter wordt de verdeling geschat, en de gebruikelijke modellen voor windmolenontwerp (hoe parameters te schatten en te gebruiken in berekeningen) worden geëvalueerd. Twee voorbeelden van conclusies over modellen zijn:

1. De gebruikelijke belastingsberekening die gebruik maakt van losse perioden van 10 minuten, mist laagfrequente veranderingen van windrichting, die grote belastingswisselingen in de mast veroorzaken. Deze belastingswisselingen hebben invloed op de equivalente vermoeiingsbelasting.

2. Het concept van vermoeiingsschade-equivalente turbulentie is bruikbaar, en het is enigszins conservatief.

Een betrouwbaarheidsfunctie wordt afgeleid, gebruik makend van het concept vermoeiingsschade-equivalente belasting. Met de eerste orde betrouwbaarheidsanalyse (FORM) en Monte-Carlosimulatie (die vergelijkbare resultaten geven) worden de jaarlijkse faalkansen ten gevolge van vermoeiing geschat voor een turbine die precies volgens de norm is ontworpen, en geïnstalleerd volgens de gebruikelijke opstellingscriteria. Met de jaarlijkse faalkansen en het economische model worden de optimale partiële factoren bepaald.

De partiële factor gevonden voor bladen is iets kleiner dan volgens de norm, terwijl de factoren voor de naaf, de gondel en de mast groter zijn. De verklaring van dit laatste is dat twee dingen niet (expliciet) worden meegenomen in de ontwerpberekeningen volgens de norm: ten eerste variatie en systematische fout in voorspelling van de vermoeiingslevensduur, en ten tweede het feit dat een combinatie van meer kritieke plekken (bijvoorbeeld in de mast) een grotere faalkans geeft dan één plek.

De gevoeligheid van de optimalisatie van partiële factoren voor veranderingen in diverse aannamen wordt onderzocht, zoals de werkelijke vermoeiingssterkte (vergeleken met de vereiste volgens de norm), het werkelijke windregime (vergeleken met het toegestane), definitie van de equivalente vermoeiingsbelasting, helling van de Wöhlerkromme, de gewenste levensduur, terreintype (complex terrein en offshore), en verificatie van berekende belastingen met metingen.

De hoofdconclusies van het onderzoek zijn drievoudig:

1. Op basis van de beschikbare gegevens zou een grotere partiële factor (belastings- of materiaalfactor) gebruikt moeten worden in het ontwerp voor ver-

moeiing van gietijzeren delen en lasnaden. Het effect op het ontwerp zou echter beperkt kunnen zijn omdat er verborgen veiligheid in de constructie zit: materiaalkwaliteit en daarmee vermoeiingssterkte zijn beter dan aangenomen wordt in de berekeningen; windmolens worden geplaatst op plekken waar het windregime milder is dan verondersteld in het ontwerp, en tenslotte kunnen afmetingen bepaald zijn door overwegingen van extreme belasting of stijfheid in plaats van vermoeiing.

2. De variatie van de betrouwbaarheidsfunctie wordt voornamelijk bepaald door de onzekerheid in vermoeiingssterkte en levensduurvoorspelling. Vooruitgang kan daarom geboekt worden door het nauwkeurig bepalen van de vermoeiings-eigenschappen van materialen zoals gebruikt in windmolens, en het calibreren van levensduurvoorspellingen. Op deze manier kan de variatie worden verminderd (en de systematische fout gecorrigeerd), en de schattingen van de faalkansen verbeterd. Als betere informatie beschikbaar is, kan verborgen veiligheid worden vermeden, en kan gerekend worden met kleinere partiële factoren.

3. In berekeningen om de faalkansen vast te stellen moet rekening worden gehouden met het aantal kritieke plekken en correlatie tussen belastingen en vermoeiingssterkte op verschillende plekken. De te gebruiken partiële factor moet hier van afhangen. Variatie en systematische fout in levensduurvoorspelling moeten expliciet worden meegenomen in vermoeiingontwerpberekeningen.

Sammenfatning

Vindenergi spiller en stadig vigtigere rolle i el-produktionen; den installerede effekt er nu ca. 60,000 MW på verdensplan (fordelt på ca. 60,000 møller), svarende til godt 0.6% af verdens elektricitetsforbrug. Alligevel har vindenergi endnu ikke set det definitive gennembrud. Hovedårsagen til dette er konkurrencen mod konventionelt genereret elektricitet, som ofte er billigere, eller i det mindste virker sådan, hvis miljøomkostninger ikke indregnes. Hvis vind skal give et væsentligt bidrag til verdens energiforsyning, er det afgørende at prisen på vindelektricitet bliver bragt endnu mere ned, hvilket medfører at vindmøller skal designes praecist så stærke som nødvendigt, men ikke stærkere end det.

Derfor skal det undersøges om de konventionelle designmetoder som blev udviklet i det foregående årti resulterer i den rigtige grad af konservatisme, og hvis ikke, hvordan de kan forbedres. Det tilsigtes at opnå et design som er lige konservativt nok, dvs. som har nøjagtigt den tilsigtede svigtsandsynlighed. Fordi vindmøller ofte bliver placeret i afsides områder, er de tilsigtede værdier primært bestemt af økonomiske overvejelser fremfor spørgsmål om offentlig sikkerhed.

Arbejdets målsætninger er derfor:

1. At kvantificere den totale usikkerhed i designproceduren og den relative betydning af stokastiske parametre som påvirker udmattelselaster og styrke.

2. At lave en sammenligning af beregningsmodeller hvor det skønnes nødvendigt.

3. At aflede partialkoefficienter som giver minimum enhedspris til elektricitet.

Tidligere arbejde med probabilistisk design af vindmøller bliver diskuteret. Da ekstremlaster er undersøgt tidligere (til en vis grad), afgrænses det foreliggende arbejde til at omfatte udmattelse. På grund af markedets udvikling fokuseres på pitchregulerede variabel-hastighedsmaskiner. Imidlertid kan de udviklede metoder anvendes generelt.

Der udføres nogle forberedende undersøgelser vedrørende økonomisk design. Det vises at den nuværende praksis –hvor vindmøller opnår maksimaleffekt ved 12–16 m/s– er optimal, og resulterer i kapacitetsfaktor (middeleffekt divideret med maksimaleffekt) som er 15–35%. Der afledes en model til at estimere summen af investerings- og svigtomkostninger i løbet af møllens levetid, som senere bruges til at bestemme de optimale partielkoefficienter.

Der laves en inventarisering af stokastiske parametre, som fordeles på fem grupper: vindklimaet, havklimaet, aerodynamikken, strukturmodellen og udmattelsesegenskaberne. Parametrenes fordelinger estimeres, og modeller der bruges i vindmøllens design (dvs. procedurer til at skønne parametrene og bruge dem i beregninger) evalueres. To eksempler på konklusioner om modeller er:

1. Den traditionelle lastberegningsprocedure som bruger adskilte 10 minutters perioder mister lavfrekvente vindretningsændringer som giver store lastcykler i tårnet. Disse cykler har indflydelse på udmattelseskade-ækvivalente laster.

2. Konceptet af udmattelseskade-ækvivalent turbulens kan bruges, og det er lidt konservativt.

Der udledes en grænsetilstandsfunktion ved hjælp af udmattelseskade-ækvivalent lastvidde konceptet. Med en første ordens pålidelighedsmetode (FORM) og Monte Carlo simuleringer (som giver lignende resultater) estimeres årlige brudsandsynligheder af udmattelsesrevner til en mølle som er præcist normmæssigt designet, og placeret ifølge de normale opstillingsregler. Med de årlige brudsandsynligheder og den økonomiske model udledes optimale partialkoefficienter.

Partialkoefficienten til vingerne er lidt mindre end normen foreskriver, mens værdierne til navet, bundrammen og tårnet er større. Forklaringen på det sidstnævnte er at to ting ikke er taget i betragtning i normmæssige designberegningerne (i det mindste ikke eksplicit): for det første, variation og forskydning i udmattelselivsforudsigelser, og for det andet, at en kombination af flere kritiske steder (for eksempel i tårnet) giver større brudsandsynlighed end et sted.

Følsomheden af optimeringens resultater overfor ændringer i forudsætningerne undersøges. Dette inkluderer: hvad den virkelige udmattelsestyrke er (i forhold til den normmæssigt påbudte), hvor slemt det virkelige vindregime på siten er (i forhold til det tilladelige), definition af udmattelsesskadeækvivalent last, Wöhlerkurvens hældning, terræntype (kompleks terræn og offshore), og til sidst om beregningerne blev eftervist med målinger.

Arbejdet fører til tre hovedkonklusioner:

1. Med de data der står til rådighed nu, skal der bruges større partialkoefficient (last- eller materialefaktor) i udmattelsedesign til støbejerndele og svejsesømme. Alligevel kunne effekten af dette være begrænset, fordi der ligger skjult sikkerhed i konstruktionen. Materialernes kvalitet og dermed udmattelsestyrke er bedre end forudsat i beregningerne, møllerne kan være placeret i klimaer der er mildere end man har designet dem til, og til sidst kan konstruktionens dimensioner være bestemt af stivheds- eller ekstremlastovervejelser, og ikke af hensyn til udmattelse.

2. Variation af grænsetilstandsfunktionen bestemmes mest af usikkerhed i udmattelsesstyrke og levetidsforudsigelse. Derfor er vejen frem at bestemme udmattelsesegenskaber nøjagtigere, og at kalibrere levetidsforudsigelser til materialer som bruges i vindmøller. På denne måde kan variation reduceres (og forskyd-

ningen fjernes), og brudsandsynligheder estimeres mere præcist. Hvis man har bedre oplysninger, kan der fjernes skjult sikkerhed og regnes med lavere partialkoefficienter.

3. Der skal tages hensyn til hvor mange kritiske steder der er, og hvor meget lasterne og udmattelsesstyrken i forskellige steder er korreleret, når man beregner brudsandsynligheder. Dette skal også have indflydelse på partialkoefficienten. Variation og forskydning i udmattelselivforudsigelse skal eksplicit tages med i designberegninger.

Chapter 1

Introduction

1.1 Wind turbine use

The development of wind turbine use in the last decade is a success story, as is witnessed by the fact that wind turbines have become a common sight in the landscape. The following figures (mainly provided by the European Wind Energy Association [34]) show the rapid expansion of wind energy:

- The mean annual growth world wide (measured by installed wind turbine power) over the last decade was 30% (see figure 1.1, next page).

- Currently the world total installed power is 60,000 MW (end 2005). This is roughly 60,000 turbines, good for more than the entire electricity demand of the Netherlands (ca 110 TWh/year), or 0.6% of world demand (Madsen [129]).

- Wind generated electricity now is 20% of total consumption in Denmark and 5% in Germany and Spain.

- The estimated number of wind energy related jobs is 72,000 in Western Europe alone.

- The cost of wind turbines has come down to ca € 1100 per kW generator power installed; the cost of electricity produced to 0.04–0.05 €/kWh on the best land sites and to 0.06–0.08 €/kWh on inland sites[1]. In fact, if external costs (environmental damage due to global warming, acid rain, fine dust et cetera) are taken into account, wind energy is already cheaper than conventional energy: the European Commission estimates the external (environmental) costs of fossil fuel use at 0.03–0.04 €/kWh [63].

- The time it takes a turbine to generate the energy that was used for its production is only 6–12 months (Lenzen [128]). Therefore, in its 20 year life, the turbine generates 20–40 times the energy it took to produce it.

---

[1]These figures do not include cost of financing.
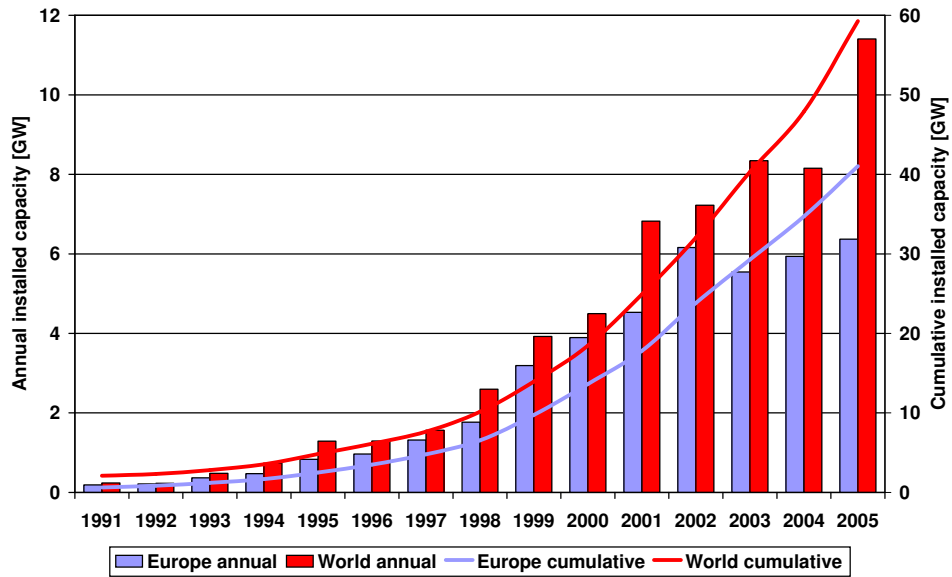
Figure 1.1: Installed windpower. Source BTM [129].

1.2   Issues

In spite of all the good news wind energy has still not made a definitive breakthrough. The main reason is of course that it has to compete against conventionally generated electricity, which often is cheaper, or at least appears to be if environmental costs are not taken into account. However valid the contention that these costs should be considered (to create the famous 'level playing field'), economic calculations are still mainly done with directly visible costs only. If we want a speedy transition to renewable energy, it is therefore imperative that the cost of wind energy is brought down even further, which means that wind turbines must be designed exactly as strong as necessary, but not more so.

This is even more pressing because wind turbines are growing in size so rapidly: the size of the average turbine has grown from 50 to 3000 kW in the last twenty-five years. For small turbines, conservative (= heavy) design was affordable, but this is no longer the case for current turbines. Their design is closer to the limit, and sometimes this has led to surprises. Some of these have proved to be costly due to the large volume of turbines installed: examples are the necessary refitting of gearboxes, and the occurrence of in-plane resonance in blades on stall turbines. Although both cited examples are somewhat special, they nevertheless indicate that design procedures are not quite good enough yet, in spite of the fact that they have considerably grown in complexity. The first turbines were simply designed for a few conservatively defined

> **1. Generate a 3-dimensional turbulent wind field for a chosen mean wind speed that represents a wind speed interval.**

> **2. Perform a step-by-step dynamic analysis on the turbine operating in the wind field to obtain force time histories in critical cross sections**

> **3. Convert the force time histories to stress time histories.**

> **4. Derive the number of cycles for each combination of mean stress and stress range by rainflow counting stress time histories into 'stress bins'.**

> **5. Scale up the number of cycles in each stress bin in line with the predicted number of hours of operation at the chosen wind speed.**

> **6. Repeat steps 1-5 for for different mean wind speeds and add all numbers of stress cycles.**

> **7. Factor the stresses and calculate partial fatigue damage for each (number of cycles, mean stress, stress range) combination.**

> **8. Add all partial damage to the total fatigue damage, and check whether the component under consideration can hold.**

Figure 1.2: Design process for fatigue loads.

extreme situations; nowadays all situations likely to be experienced by the turbine in its life must be checked for fatigue and ultimate load consequences, with full dynamic simulations and random wind and wave fields. Flow charts for wind turbine design are given in figure 1.2 for fatigue loads and in figure 1.3 (p4) for ultimate loads.

There are two areas where the design procedure is less than satisfactory: one is understanding and modelling rotor aerodynamics, and the other prediction of com-

1. Generate a 3-dimensional (possibly turbulent) wind field for a specified extreme wind condition and/or failure situation

2. Perform a step-by-step dynamic analysis on the turbine operating in the specified conditions to obtain force time histories in critical cross sections

3. Repeat steps 1 and 2 as many times as necessary to make statistical treatment of extreme values possible

4. Extract stress time histories and extreme stress value. Perform statistical treatment (averaging, extrapolation) as required.

5. Factor the stresses

6. Find the material strength and divide it by the material factor

7. Find the stress reserve factor by comparing the factored stresses with the reduced material strength.

Figure 1.3: Design process for ultimate loads. Cheng [36] showed that the most accurate way to find ultimate loads is not by defining extreme events (step 1), but by response extrapolation. However this is not yet the common method.

ponent life (or fatigue damage) under random loading.

As regards aerodynamics, blade loads are estimated with the Blade Element-Momentum method (BEM), an approximate method with a number of engineering corrections that capture the essence of a phenomenon but are lacking precision. However for design calculations six hours or so of turbine operation (representative of the turbine's life of 20 years) must be simulated, and BEM is currently the only method that can do this fast enough, and has the flexibility to cope with all operational situations that may arise (Snel [193]). The problem with fundamental methods, such as Navier-Stokes calculations, is that no models can be built that are small

and fast enough, and provide realistic loads. In fact reliable prediction of the wind turbine power curve from first principles is beyond us, even in ideal wind tunnel circumstances. Nevertheless Navier-Stokes calculations can be used to identify trends, and thus for improving parametric models incorporated in BEM. The load prediction problem is becoming even more difficult because wind turbines are installed in complex (mountainous) terrain and in windfarms in increasing numbers. Usually there are no good wind data for complex sites, and no good wake models are available for calculations in windfarms[2]. Also the errors caused by misprediction of aerodynamic loads may be amplified by resonance. Resonance is an inherent problem to wind turbines, because they are largely undamped structures, which are being excited by wind containing energy at all frequencies. All this means that we cannot design a wind turbine on the basis of theory alone, and must always use measurements for verification.

The problem of failure through fatigue has been with us since railway construction began in earnest ($\sim$1850). As far as accurate life prediction is concerned, there is still no better method than the linear damage summation first proposed by Palmgren and Miner, although fracture mechanics might be a candidate (see for example Eulitz [60], Haibach [77] and Schütz [185]). Of course there has been progress in the sense that control of material properties has substantially improved, considerable quantitative knowledge has been gained from testing, and a number of ad hoc rules have been developed (for example on how a notch influences crack growth). However it is still not possible to predict the expected life of a component more accurately than within a factor two or so, even if loads are perfectly known.

Related to aerodynamics and to fatigue is the description of the environmental parameters that must be used in load calculations (the wind climate and the definition of design load cases). Until now this was of no great concern, because wind turbines were mostly installed in flat smooth uniform terrain; however as more and more complex sites are being used for wind power (mountainous areas, possibly with forests, and also wind farms where turbines themselves influence climate), the matter gains importance.

Although there is work going on in the problem areas, for the present at least we must accept that current design procedures are the best ones available, and we should try to find out how conservative and how inaccurate they are. Once we know that, we may deal with the less-than-perfect state of affairs by using probabilistic methods, in which fixed parameters are replaced by stochastic ones. A probabilistic calculation yields the failure probability, which may then be compared to the target value.

For everyday use it may be convenient to use the partial safety factor[3] approach instead of full probabilistic design, for which the values of the partial safety factors are derived from the more elaborate probabilistic calculations. In the simplest form

---

[2]See section 4.9 for more on windfarm wake effects.

[3]From now on the shorter expression 'partial factor' will be used instead of 'partial safety factor'.

of this approach the characteristic load is multiplied by a load factor and the characteristic material strength is divided by a material factor. Both operations together intend to give the construction the desired low target failure probability. At present it is not clear which failure probability level is obtained for the following reasons:

1. To make the design process manageable, common sense decisions must be made on which load situations to investigate, which models to use, and how to set characteristic parameters. Many of these procedural decisions have not yet been investigated in detail.

2. Methods were conceived for solitary turbines in flat open terrain (where they were also verified to some extent), while current applications are likely to be in windfarms in complex terrain and offshore.

3. Although load verifications for individual turbines are standard, there has been no systematic load verification for many turbines in different situations (so we do not know how good predictions are for more complex situations).

4. Partial factors for loads and materials are mostly taken from building codes; one does not know to what degree they apply to wind turbines, and to what failure probability they lead.

While we do not have to be overly pessimistic (after all few turbines collapse, indicating that design is generally on the safe side), the state of affairs is unsatisfactory. What we would like to have, are recommendations for partial factors which fit the existing uncertainties, and ensure that some desired safety level is consistently reached throughout the turbine.

1.3   Previous work

General guidance on wind turbine design calculations can be found in handbooks, such as Burton [30] and Manwell [142]. Furthermore there are standards for land based turbines, for example the international IEC 61400-1 [93], and publications by certification bodies such as Det Norske Veritas [45] and Germanischer Lloyd [70]. More recently offshore wind turbine standards and guidelines have appeared, by DNV [46, 47], Germanischer Lloyd [71, 72] and by IEC [94]. All these publications tend to give general procedures for safe design, but are not very specific. Often various allowed procedures are listed, together with the caveats that are found in most handbooks. For example, only DNV [47] explicitly prescribes a target failure probability, but even here it is unclear to which extent the figure is adhered to if DNV rules are applied.

An overview of work on failure probabilities under fatigue and ultimate loading in connection with wind turbines is given in table 1.1.The methods for finding fatigue failure probabilities are closely related to those for ultimate load failures; therefore at least some of the work on ultimate loading is relevant.

Cheng's thesis [36] treats the merits of different extrapolation methods for finding the extreme (ultimate) load response of a wind turbine under combined wind and wave loading. Tarp-Johansen's report [204] is an exposition on how to find the failure probabilities for wind turbine ultimate loading, and which partial factors to use if wind and gravity loads are combined. He has taken most relevant uncertainties into account[4], and in addition he derives some specific numbers, which have found their way into IEC 61400-1 [93]. It could be interesting to see if and how the results would change if the latter work were combined with that by Cheng (Tarp-Johansen only uses the Gumbel distribution to find extreme wind speeds, while Cheng gives methods for evaluating different distributions). Ronold [177] does a safety factor calibration for blades in ultimate flap loading; the First order Reliability Method (FORM) is used with the measured site load distribution.

If we look at fatigue, there is the PRODETO-project (Braam [24]), which focuses on blade out-of-plane loads (flap moments). The measured distribution of these loads is approximated with a generalised Weibull function, of which the first three moments are functions of 10 minute mean wind speed and turbulence intensity. The advantage of this approach is that a reasonable guess may be made for load distributions occurring at any wind speed and turbulence intensity, even if no measurements are available for all combinations of these parameters. A probabilistic design is made with the First (Second) Order Reliability Method, in which the Weibull distribution moments are normally distributed stochastic variables. Load and material factors are derived.

Ronold [176, 178, 179] considers code calibration for wind turbine blade flap

---

[4]Tower stability and the uncertainty in buckling models is not considered.

Table 1.1: Summary of previous work (g=gravity, wa=waves, wi=wind)

author	fatigue	ultimate	calib.	loads	components
Cheng [36]		+		wi,wa	blade, tower
Tarp-Johansen [204]		+	+	wi, g	blade, tower
Ronold [177]		+		wi	blade
Braam [24]	+	+		wi,g	all
Ronold [176, 178, 179]	+		+	wi	blade
Lange [119]	+			wi	blade
Kashef [102], Kelly [106], Manuel [141], Veers [220]	+			wi,g	blade
Larsen [120]	+			wi,wa	blade, tower
Tarp-Johansen [203]	+		+	wi, g	hub, nacelle
Mousten [149]	+		+	wi	tower
Veers [219]	+			wi	blade
Dalsgaard Sorensen [198, 199]	+	+		wi,wa,g	tower

loading. He uses the same approach as in the PRODETO-project (in fact, he was involved in that project), but combines it with the use of the DNV probabilistic code PROBAN. Although he is not treating all uncertainty aspects, every step necessary for probabilistic design is described (if measured loads are accepted as given). Some of the theory used is found in the PRODETO-work as well (Braam [24]).

The work of Lange [119] is similar, but most attention is given to fits of generalised Weibull distributions to measured loads. In fact, at Sandia much effort has gone into the parametrisation of blade moments, mostly on blades for Vertical Axis Wind Turbines (VAWTs) (see Kashef [102], Kelly [106], Manuel [141], Veers [220]). These loads have been coupled to fatigue life and failure rate estimation programs, notably FAROW: Fatigue And Reliability Of Wind Turbine Components [236]. An issue which is raised is whether it is realistic to replace calculated (or measured) loads with finite amplitudes by a distribution that in principle gives load amplitudes to infinity. It seems that this question is not yet answered, instead the possibility of load truncation is offered to the user of FAROW.

Larsen [120] considers the relative contributions of stochastic parameters to total uncertainty. He determines the influence on uncertainty in load calculations caused by variation of aerodynamic coefficient, turbulence intensity and material fatigue properties. He finds that in all cases fatigue properties dominate total uncertainty.

Tarp-Johansen [203] treats the rotor hub, the main shaft and the machine frame. A limited number of uncertainties is investigated, and partial factors derived for parameter distributions with different coefficients of variation.

If we finally look at economics, Veers [219, 221] wrote an article in which he discusses the financial consequences of common and independent cause failures in a general way, again using the Sandia code FAROW.

More work on economics and optimal inspection intervals was done by Dalsgaard Sørensen [198, 199] and by Mousten [149], who looks at a specific detail: a bolt welded to the tower wall. Fatigue tests were used to calibrate a stochastic fracture mechanical model, which was then used to estimate failure probabilities.

1.4   Objectives

It is clear that useful work has been done already, and there are enough ideas to start from. However most work cited has a theoretical flavour, stopping short of giving practical numbers, and is therefore not easily used for everyday design (perhaps this is not surprising, since all authors are working in research institutes linked to the wind industry in one way or another, rather than at a manufacturer's). Another problem is that available publications are unconnected, and dealing with different (reduced) sets

of stochastic parameters. This makes it difficult to compare results, and to reach firm conclusions. What is needed, and what this work will attempt to provide, is:

1. A comprehensive study to determine how large total uncertainty (with respect to fatigue loading) is, and where the main uncertainties in the design process are. This should direct future research into the most profitable areas, where total uncertainty can be reduced most. *Motivation: only limited studies were done, usually starting from measured loads (which are then assumed to be exactly known). All studies use short cut assumptions about some uncertainties; it is not always clear on which evidence these assumptions rest.*

2. Where necessary, a comparative review of different models, which should give recommendations for models and for parameter choice. *Motivation: this has not been done yet. It is unsatisfactory that different models are allowed that may give significantly different answers.*

3. A derivation of partial factors that ensure that the desired safety level is obtained throughout the turbine. *Motivation: in previous work some safety factors have been derived, but results are generally presented as 'examples' and it is not clear what the range of validity of the derived factors is.*

4. A comparison of partial factors that are derived with values provided by various standards. *Motivation: while standard values are to some extent arbitrary and it is better to derive factors from first principles, standards contain considerable knowledge and experience that must not be ignored.*

1.5 Scope of this thesis

The intention is to describe all methods in such a way that they can easily be adapted for any turbine and for any load situation. However because of time constraints, efforts must be primarily directed at some important areas:

- In the opinion of the author the area of ultimate loads and extrapolation issues has been reasonably well covered before, in particular by Cheng [36] and by Tarp-Johansen [204]. Therefore this work will focus on fatigue loads.

- Only pitch controlled variable speed turbines will be considered, because this is the turbine type that is most common, and it looks like it will only become more dominant in the future.

- A selection of representative critical locations in the turbine and associated materials is made, in particular: the blade root (composite materials, such as glassfibre reinforced glassfibre, epoxy and wood); the rotor hub and the nacelle machine frame (both cast iron); the tower (welded steel).

1.6   Organisation

The probabilistic approach starts with setting the target failure probability, either from safety considerations or by financial optimisation: chapter 2 is dedicated to considerations on how to do this.

In chapter 3 the current wind turbine design procedure is described, to provide the reader with insight in models that are used. The conventional choices that are made are listed for later reference.

In chapters 4 to 7 the steps in the design procedure are studied in detail, and the probability distributions are derived for parameters that are taken to be constant in the conventional design procedure; where necessary the claims to accuracy of alternative models are examined. Specifically, chapters 4 and 5 deal with wind and sea climate, chapter 6 treats aerodynamics and the wind turbine structural model; finally chapter 7 is about material properties and estimation of fatigue damage.

In chapter 8 all information from previous chapters on parameter distributions is combined, to estimate which failure probability is obtained if the conventional design procedure is followed. Also the economically optimal partial factors are derived and compared to partial factors given in standards. In chapter 9 results are examined in more detail, and their sensitivity to changes in input parameters is investigated.

Finally conclusions and recommendations are found in chapter 10.

Various matters of detail are dealt with in the appendices.

1.7   Nomenclature

This work adheres as much as possible to symbols and terms that are in common use in the fields of wind energy, fatigue and probabilistic design. Unfortunately this means that some symbols may have multiple meanings; however from the context the correct one may usually be inferred. A complete list of symbols is provided in appendix A; moreover symbols are explained in the main text where they first occur. Perhaps a few conventions need mentioning:

- Partial safety factors are generally referred to as 'partial factors', which appears to be the preferred expression in the probabilistic design community.

- The influence of various parameters is quantified by the change in fatigue damage equivalent load range (see appendix C), which is the constant amplitude load range that, had it been applied some fixed number of times, would have produced the same fatigue damage as the actual variable amplitude load spectrum. Because the term 'fatigue damage equivalent load range' is so long, the shorter 'equivalent load' is normally used.

- The exponent of the S-N (Wöhler) curve m is commonly called 'slope'; strictly speaking this is not correct because the slope (derivative) of the curve is in fact $-1/m$ in a double logarithmic diagram.

Chapter 2

Economic design

We believe in low overhead costs.

— Micon chief engineer John T. Olesen, commenting on the shabby appearance of the premises of the fast growing company, 1993.

2.1 Introduction

Once it is decided that we want a wind turbine (rather than some other means to generate electricity), the task is to design the machine in an economic way. In all cases the goal is to arrive at a design that has the lowest cost per unit of electricity, averaged over the turbine's life. However there are two different situations:

1. The target failure probability is determined by safety considerations. This will be the case if sensitive objects are close to the turbine, or if there is risk of death or injury.

2. The target failure probability is free. For wind turbines, this is frequently the case, because they tend to be located in remote areas, where there is no safety issue. The failure probability yielding the lowest cost is to be found, by balancing initial investment against costs of service, failure and repair.

To establish the cost exactly is an undertaking in itself; preferably a full life cycle analysis should be performed in which all costs (including those to the environment) are taken into account: costs of materials, certification, production, transport, financing and insurance, inspection and maintenance, and finally decommissioning. Some of these costs are correlated, for instance if more material is used, less money might be spent on inspections and maintenance. However, most aspects of the problem may still be treated independently of the others. Thus, without rendering results invalid we may concentrate on material costs only (roughly proportional to component mass), principally determined by the partial factors used, which fix both the dimensions and the failure probability. Hence to achieve economic design, we must find the optimal

11

partial factors, either from the preset failure probability (if safety governs) or with some cost function (if financial considerations are defining).

The fatigue failure probability is not constant; it is zero at turbine installation and then rises with time. This means that rather than set one fixed number, one should define the desired behaviour of the failure probability over time, based on some optimisation that involves initial investment and cost of inspections and repairs. One may also do something more simple, like setting a maximum failure probability during the component's life, or some target mean. If one derives the failure probability from first principles, it is possible that the optimal target value or behaviour in time does not correspond to relevant standard and established figures that are in use (which may be values that are currently achieved in existing machines (and hence are implicitly accepted) or code values (which are explicitly accepted)).

When the target failure probability has been established, it can be used as input to a calculation which yields the corresponding partial factors. How to do this is the subject of chapters 4–9; this chapter is about establishing the target failure probability and the cost optimisation function. However first we will digress for a moment to derive reasonable design conditions (design wind speeds) for a wind turbine, because it is interesting to see why these speeds are chosen as they are, and because there are some misunderstandings about the issue.

2.2   Design conditions

The task of a wind turbine is to extract as much electricity as possible from the wind at reasonable cost. The cost qualification has important consequences for wind turbine design: it is clear that it is not economic to build a turbine that is so heavy that it can convert the maximum amount of wind energy to electricity above wind force 12 (hurricane force, more than 115 km/h $\approx$ 32 m/s). The extra investment would never be compensated by the extra energy generated, since wind speeds of this magnitude occur only rarely. So before going into the matter of minimum weight design, a question that must be answered is: what are economic design conditions?

Two important numbers governing design are the rated wind speed (the lowest wind speed at which maximum power is reached) and the stop or cut out wind speed. The rated wind speed may equal the stop wind speed, but it may also be smaller, if power is limited before the stop wind speed is reached. How must these parameters be chosen to obtain the lowest electricity cost? It turns out that reasonable values for these speeds can be found with some basic considerations about how energy output and turbine investment vary as function of these two speeds.

In what follows we assume the geometry of the turbine to be given. This means that the flow pattern around the blades and hence the properties of the rotor are fixed, such as the power coefficient (which is set to the realistic value $C_P = 0.45$ here). However we are still free to choose rated and stop wind speed, which will influence

the turbine's mass and energy output.

It is easy to calculate the average power generated P_{avg} and the total energy output E, by integrating the product of the time fraction some wind speed U occurs $f(U)$ and the power at that wind speed $P(U)$:

$$P_{avg} = \int_{U_{in}}^{U_{out}} P(U)\, f(U) dU \tag{2.1}$$

Here U_{in} and U_{out} are the wind turbine start and stop wind speeds. The wind speed probability density $f(U)$ is typically given by a Rayleigh distribution (Weibull distribution with shape factor $k = 2$). The life energy production E (in kWh) is:

$$E = L\, P_{avg} \tag{2.2}$$

where L is the turbine's life in hours (for example 175,200 hours = 20 years). The power that can be maximally extracted from the wind at some speed U is:

$$P(U) = C_P \frac{\rho}{2} AU^3 \leq \frac{16}{27} \frac{\rho}{2} AU^3 \tag{2.3}$$

Here P is the power, C_P the power coefficient, ρ the air density, A the rotor swept area and U the undisturbed (free stream) wind speed. The maximum value for $C_P = 16/27 \approx 0.59$, the famous Lanchester-Betz limit[1].

Let us assume that the total investment for some reference turbine is an amount c euros per kW rated (maximum) power[2], which would make the investment:

$$C_I = c\, P_{rat} \tag{2.4}$$

For current turbines the investment C_I is proportional to the rated power P_{rat}, which typically is the power generated at some speed in the interval 12–16 m/s wind speed and above. This is approximately true for the investment for most of the turbine, however some fraction f of the investment will be fixed (for example cost of obtaining permissions, rent for the site, grid connection, production metering). This means that if we want to optimise (starting from some fixed reference rated power $P_{rat,ref}$), the investment of a the turbine should be expressed more accurately as:

$$C_I = fc\, P_{rat,ref} + (1-f)c\, P_{rat} \tag{2.5}$$

Equation (2.5) reflects the assumption that the investment C_I depends linearly on rated (maximum) power P_{rat}. Actually, if the rated wind speed equals the stop wind

---

[1]It is only a matter of normalisation (to rotor swept area) that $C_P = 16/27$. Actually $3/2 \times 16/27 = 8/9 \approx 89\%$ of the kinetic energy of the air flowing through the rotor can be extracted. For a discussion of losses due to mixing in the far wake see Corten [40].

[2]For land based turbines c $\simeq$ 1100 €/kW, for offshore turbines c $\simeq$ 1500-2000 €/kW (2004).

speed the power goes with the cube of the wind speed, and forces with the square, so a constant diameter tower would require wall thickness and investment C_I that are proportional to the power 2/3 of the electric power P_{rat}. However the 2/3 power function can easily be linearised to have the form of equation (2.5) and it may even be argued that the 'experimental constant' c reflects this.

It is important for the validity of our argument whether equation (2.5) still holds if the rated wind speed is smaller than the stop wind speed. For stall turbines rotor thrust is almost constant above rated wind speed; for pitch-variable speed machines rotor thrust decreases, so the answer is 'yes' for both turbine types: maximum load is determined by rated wind speed. Combining equations (2.3) and (2.5), the total investment C_I can be written as:

$$C_I = c\, C_P \frac{\rho}{2} A \left(f U_{rat,ref}^3 + (1-f) U_{rat}^3 \right) \tag{2.6}$$

in which $U_{rat,ref}$ is the wind speed at which the fixed rated power $P_{rat,ref}$ is reached. The cost per kWh electricity p_{kWh} is:

$$p_{kWh} = \frac{C_I}{E} = \frac{c\, C_P \rho A \left(f U_{rat,ref}^3 + (1-f) U_{rat}^3 \right)}{2\, L\, P_{avg}(U_{in}, U_{rat}, U_{out})} \tag{2.7}$$

The electricity cost according to equation (2.7) is plotted in figure 2.1. Let us first consider the case where we simply try to get as much power as possible at any wind speed: the dotted lines. The rated wind speed U_{rat} equals the stop wind speed U_{out}: whenever the wind speed is below the stop wind speed the maximum power according to equation (2.3) is extracted. It is seen that the minimum electricity cost is reached with $U_{rat} = U_{out} = 12$ m/s if $U_{avg} = 7.5$ m/s, and with $U_{rat} = U_{out} = 16$ m/s if $U_{avg} = 10$ m/s. If the rated (and stop) wind speed are made larger, additional investment outweighs extra production, and the electricity cost goes up. Hence the optimal choice is to set rated and stop wind speeds at these values, 12 and 16 m/s respectively.

However (considering $U_{avg} = 7.5$ m/s) one can do even better by designing a machine with rated wind speed $U_{rat} = 12$ m/s, but stop wind speed around $U_{out} = 20$ m/s: if the power is limited to the rated power for $U > U_{rat} = 12$ m/s, the turbine investment will not increase for higher stop wind speeds, while one *does* have the benefit of the extra electricity.

Note that whatever the average wind speed, the electricity cost does not change significantly for stop wind speeds higher than 20 m/s: the time at these speeds, and hence the amount of electricity, is negligible. Therefore stop wind speeds higher than 20 m/s are unnecessary from a cost perspective (but they may be desirable because interruptions in windfarm power productions at high wind speeds are unwanted). With a simple approach we have established that a good choice for the design conditions
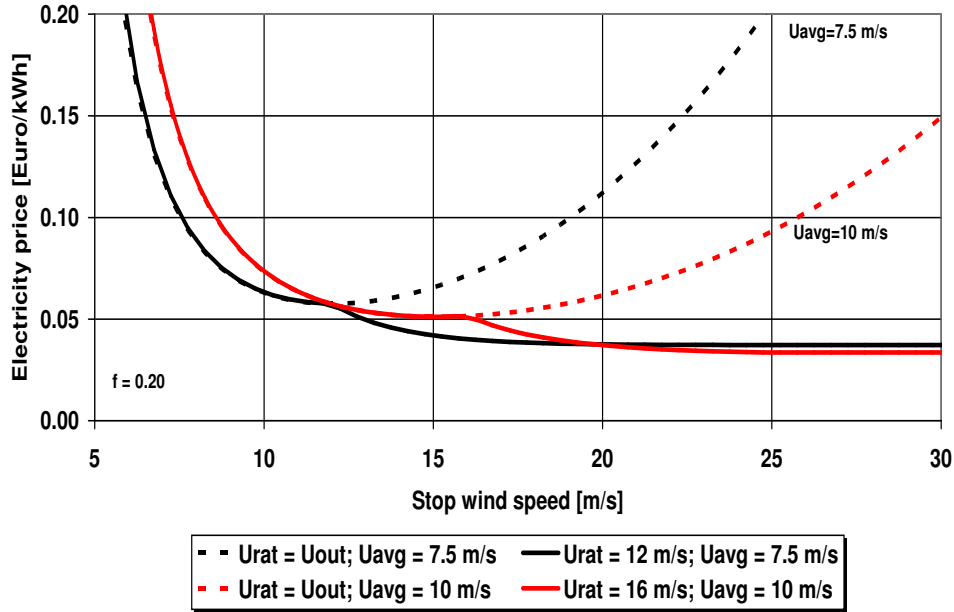
Figure 2.1: Cost of electricity as function of stop (cut out) wind speed according to equation (2.7). The wind regime has a Weibull distribution with $k = 2$; $c = 1100$ €/kW, $C_P = 0.45$, $f = 0.2$, $L = 20$ years. No discounting.

is (see figure 2.1):

$$12 \leq U_{rat} \leq 16 \ m/s$$
$$20 \leq U_{out} \leq 25 \ m/s$$

In the example we chose the fixed investment fraction to be $f = 0.2$; however the conclusion for the optimal speeds as given above is insensitive to the exact assumptions for this quantity.

With the speeds derived the capacity factor e can be calculated, which is the average power divided by the rated power:

$$e = \frac{P_{avg}(U_{in}, U_{rat}, U_{out})}{P_{rat}(U_{rat})} \tag{2.8}$$

A wind turbine's capacity factor is to be compared to capacity factors for conventional plants (see table 2.1, next page). Capacity factors for conventional plants are not 100%, but around 80% due to maintenance and fluctuating electricity demand. Calculated values for the capacity factor of wind plants are in the range $0.10 \leq e \leq 0.50$ (see figure 2.2, next page), depending on the average and the rated wind speed; actual figures that are obtained for the capacity factor are $0.15 \leq e \leq 0.40$. For
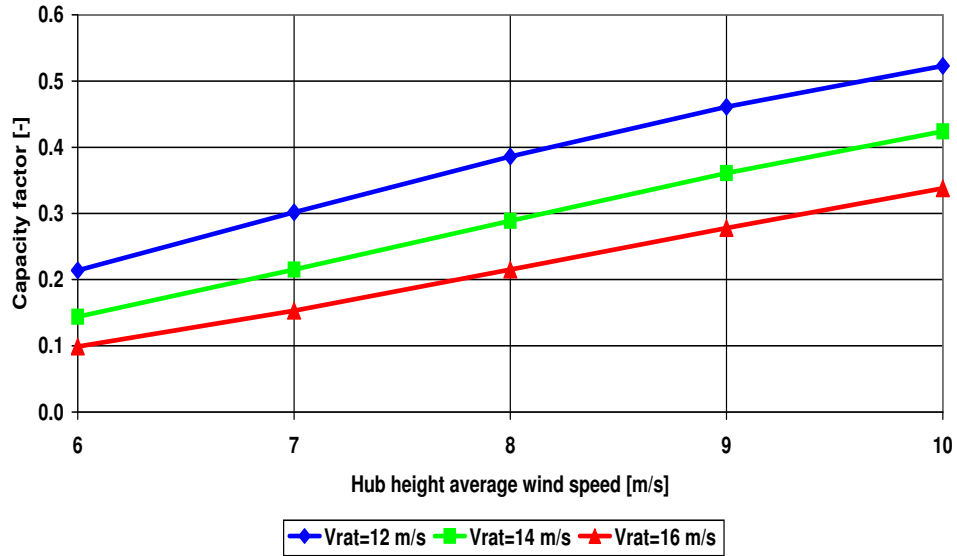
Figure 2.2: Capacity factor $e = P_{avg}/P_{rat}$ as function of wind speed. The wind follows a Weibull distribution with shape factor $k = 2$.

example the German electricity supplier E.ON states that in 2003 a capacity factor $e = 0.16$ was realised for 6250 MW installed power (Bouillon [23]; the low number indicates that wind speeds in Germany are generally low). These lower-than-unity capacity values are not the result of some inherent defect in wind turbines, but just originating from a design process homing in on the lowest electricity cost.

In the preceding example design conditions were just rated wind and stop wind speed; in reality a larger set of parameters is used that is considered to be representative for a large area, for example the coastal regions of North Western Europe. For practical reasons wind turbines are not designed for every individual site, but accord-

Table 2.1: Capacity factors for different power plants. Source: Milborrow [145].

Plant	Range	Average
Coal	68-90%	78%
Gas	68-90%	79%
Nuclear	75-85%	81%
Solar	8-25%	unknown
Wind	23-35%	30%

ing to a class definition. A turbine designed according to a class is then placed in any location where the climate is judged to be less severe (this may also be in a windfarm, where climate is influenced by neighbouring turbines). Thus –if we accept the standard design procedure as accurate for a moment– almost all turbines are designed conservatively and are too heavy. The advantages of this approach are fewer approval documents and fewer logistical problems (all turbines are the same), and reduced failure probability because of conservatism. The class definitions most used are those according to IEC 61400-1 (see table 2.2). For offshore wind turbines classes can still be used for the rotor and the nacelle, but not for the tower and foundation, which must be suitable for the local wave climate. In fact the entire turbine may be designed site specifically; this may be advantageous if the batch size is large enough.

2.3 Target reliability from a safety perspective

Failure is not an option.

— Mission Control flight director Gene Kranz, during the rescue of Apollo 13, 11–17 April 1970.

Whenever there is a disaster, the feeling is that 'this must never happen again', which may be translated as: 'a construction must *never* fail'. However this ideal is unreachable in a world of finite resources. Since the amount of money available for life and investment saving measures is finite, choices must be made, and it is not possible to have constructions that can never fail. In this section and the next we give some information about failure probability levels that are commonly accepted, and which may serve as background when we derive wind turbine optimal failure probabilities later. The quoted values are not necessarily optimal, only what is in common use.

Table 2.2: IEC 61400-1 wind turbine classes [93].

Class	I	II	III
Representative for	offshore	coastal	inland
Average wind speed	10 m/s	8.5 m/s	7.5 m/s
Wind speed distribution	Weibull: equation (3.1) with $k = 2$		
Turbulence intensity	prescribed: equation (3.3)		
Turbulence spectrum	Kaimal recommended: equation (3.4)		
Coherence	prescribed: equation (3.8)		
Wind shear exponent	0.2		
Air density	1.225 kg/m^3		
Yaw error	–		
Inflow angle (terrain slope)	8 deg		
Wake effect	prescribed: section 4.9		

Interesting literature exists on how to spend limited resources with optimal results, for example how to save the maximum number of quality life years (Nathwani [151], Rackwitz [171, 172]). Governments take many life saving measures, e.g. building hospitals, discouraging smoking and drinking, checking food quality, enforcing road safety laws, and –quite important– requiring the use of standards, such as building codes. The values of partial factors in codes reflect how much society is willing to spend to avoid death and injuries (since larger factors result in more expensive structures). If the cost for all life saving measures together is estimated, it is found that roughly 10^6 dollars is spent in developed countries per life saved ($\sim$30,000 dollars per life year saved). However Tengs [205] found that current spending practice is unbalanced with the amount of money spent per life year saved ranging from 0 to 10^{11} dollars (1993 dollars). The author notes that '*this kind of variation is unnerving because economic efficiency in promoting survival requires that the marginal benefit per dollar spent be equal across investment*'. Rational policies would of course require that the most cost effective measures are taken first, and that at any time all new measures taken cost approximately the same per life year saved.

Although the failure probability cannot be zero, obviously it must be small; the question is how small. Since we are usually interested in risk (defined as: failure probability times consequences), it is better to ask which risk level is acceptable instead. A pragmatic approach is to find it from current practice. For example, from the fact that not more money is spent on road safety, we may infer that currently in the Netherlands the accepted annual probability of dying in a traffic accident is:

$$p_d = \frac{number\ of\ road\ deaths\ per\ year}{population} = \frac{10^3}{1.6 \times 10^7} \approx 6 \times 10^{-5} \qquad (2.9)$$

The numbers found in practice can be generalised into a failure probability criterion (adapted from Vrijling [230]):

$$N_{di} = P_{d|fi}P_{fi}N_{pi} \leq 7 \times 10^{-6}\beta_i N_p \qquad (2.10)$$

where:

N_p	population [-]
N_{di}	number of deaths in activity i [-]
N_{pi}	number of people taking part in activity i [-]
$P_{d|fi}$	death probability. given an accident occurs in activity i [-]
P_{fi}	probability of an accident for activity i [-]
β_i	policy factor [-]

Equation (2.10) expresses that an activity i is allowed if it is expected to claim fewer than $N_{di} = 7 \times 10^{-6}\,\beta_i N_p$ deaths per year. The factor β_i is a policy factor reflecting the degree of involuntariness of an activity, and the (perceived) personal influence on

the risk. It ranges from $\beta = 10$ for activities as mountaineering (completely voluntary, large personal influence) to $\beta = 0.01$ for working in a factory (involuntary, small personal influence). According to the equation, for car driving in the Netherlands this means that ($\beta = 1$, car driving is not 100% voluntary for many people):

$$N_{di} \leq 7 \times 10^{-6} \times 1 \times 1.6 \times 10^7 = 112 \tag{2.11}$$

Equation (2.10) does not give the expected 1,000, which reflects the fact that it is an average over many different activities. Of course if we assumed total voluntariness we would have $\beta = 10$ and the answer would come out to ∼1,000. If we apply equation (2.10) to wind turbines, with $\beta = 0.01$ (involuntary, small personal influence) and $N_p = 1.6 \times 10^7$ (the whole population is 'involved' to the same degree in the activity 'being close to wind turbines occasionally'), we get:

$$N_{di} \leq 7 \times 10^{-6} \times 0.01 \times 1.6 \times 10^7 \approx 1 \tag{2.12}$$

This means that it is acceptable to society that 1 person per year dies in the Netherlands in a wind turbine related accident[3]. Since turbines typically are located in remote areas and fail during storms when there is even less chance that people are present, the requirement does not seem difficult to comply with, and it would not impose a limit on allowed failure probability; however this might change if turbines are going to be placed near roads and railways in larger numbers. Note that for people involved professionally with wind turbines the equation does not apply; the accepted personal risk is presumably on par with the value for all people working in an industrial environment, which is $p_{di} = 10^{-6}$ per year, or perhaps $p_{di} = 10^{-5}$ per year if we account for the fact that many people in the wind industry have especially chosen to work just there; in this case the risk is not related to turbine structural integrity, but rather to labour safety issues, such as electrical and falling hazards.

Building codes are calibrated to reflect the accepted risk level for structures of which failure will result in casualties. As matters stand, the same failure probabilities are used for wind turbine design, in spite of the fact that the risk of a person dying because of a wind turbine collapsing is much smaller, especially offshore.

2.4 Code values

Some wind turbine codes have appeared, such as the Danish standard DS472 [44], the DNV Guidelines [45], and the German standards [70, 71]. The most recent codes are IEC 61400-1 [93], and DNV-OS-J101 [46]. In DNV-OS-J101, the following values are given for offshore wind turbines: $p_F = 10^{-5}$ per year for normal safety class and $p_F = 10^{-4}$ per year for low safety class. In a predecessor of this standard [47], Det

---

[3]It should also be possible to derive the acceptable annual number of deaths with the Life Quality Index method.

Norske Veritas provides table 2.3 (next page), which is in line with the guidelines of the Nordic Building Commission [162].

ISO 19902 [95] gives some values for unmanned offshore structures (table 2.4, next page), which may be considered directly relevant for offshore wind turbines. Thus the standards agree on a value between 10^{-5} and 10^{-4} per year.

2.5   Currently achieved values

In the 'Handboek Risicozonering Windturbines' ('Handbook for wind turbine risk assessment') Rademakers [173] gives the following values (table 2.5). These values are not inconsistent with the value of $p_F = 10^{-3}$ per year derived by Tarp-Johansen [204] for extreme events, if it is assumed that most turbines are placed in a more benign environment than what they were designed for.

One should be skeptical about the accuracy of the numbers. There is no systematic collection of failure data (at least not publicly available) and accident reports that are available usually do not have enough information to reliably judge the nature and causes of failures. It is not even possible to say whether the numbers are biased towards the optimistic or pessimistic side. There are both reasons to expect figures to be too low and too high. Too low:

- There is a tendency not to report failures.

- The majority of turbines is still young (there has been no time for cracks to develop).

Table 2.3: Target annual failure probabilities for components. Source: DNV [47].

	Failure consequence		
	Less serious	Serious	Very serious
Failure type	Low safety class	Normal safety class	High safety class
Ductile failure with reserve capacity (redundant structure)	10^{-3}	10^{-4}	10^{-5}
Ductile failure with no reserve capacity (warning, non-redundant structure	10^{-4}	10^{-5}	10^{-6}
Brittle failure (no warning, non-redundant structure)	10^{-5}	10^{-6}	10^{-7}

Table 2.4: Target annual failure probabilities for offshore structures. Source: ISO [95].

Structure	Manned	Unmanned
Annual failure probability	3×10^{-5}	5×10^{-4}

- Smaller turbines tend to have some built-in conservatism (because conservative design is relatively cheap in smaller structures).

Too high:

- Data are for turbines designed 5–15 years ago. Part of the failures may be attributed to teething problems. Also design methods have improved.

If we want to use the figures to predict failure rates for current turbines of 2–3 MW power, the most reasonable guess is probably that they may be off by a factor 3 in each direction (hence the number of digits in the 'Handbook' figures (table 2.5) suggests an accuracy that is not really there).

2.6 Target reliability from a financial perspective

The standards that govern wind turbine design are (derived from) civil engineering standards. Thus the safety level of those standards has implicitly been adopted, a safety level which guarantees that an acceptably low risk of death and injury is achieved for structures such as bridges and utility buildings. However the consequences of wind turbine failure (number of dead and injured) are likely to be much smaller: as noted before, wind turbines are found in thinly populated areas, so the probability of somebody getting killed or injured if a blade is thrown off or a tower failing is low; also the impact of the failure outside the area directly affected by falling parts is essentially zero. Because no expenses are necessary to prevent deaths, the optimal failure probability for wind turbines may be higher than for other civil engineering structures. To find out what the optimal value is, we need to know how much the failure probability changes in relation to the production cost. In particular we want to minimise the expected difference between costs and benefits:

$$W(\gamma) = C_I(\gamma) + C_F(\gamma) + C_R(\gamma) - B(\gamma) \tag{2.13}$$

Here the parameter γ is the product of all partial factors[4], for example:

$$\gamma = \gamma_f \gamma_m \gamma_n \tag{2.14}$$

with:

---

[4]Note that it may not always be possible to multiply all safety factors like in this case.

Table 2.5: Annual failure probabilities (per turbine) currently achieved (Rademakers [173])

Scenario	Annual failure probability	
	Expected	95% confidence
Blade fails	6.3×10^{-4}	8.4×10^{-4}
Tower fails	2.0×10^{-4}	3.2×10^{-4}
Nacelle and rotor fall down	5.8×10^{-5}	1.3×10^{-4}

B	benefits over the turbine's life (energy sales) [€]
C_F	cost of failure (for example debris removal [€]
C_I	investment cost (for the entire installation) [€]
C_R	cost of component replacement in case of failure [€]
W	nett cost function [€]
γ	product of all partial safety factors [-]
γ_f	load factor [-]
γ_m	material factor [-]
γ_n	consequence-of-failure factor [-]

The investment cost $C_I(\gamma)$ can be written as some constant (say the investment for some standard value $\gamma = \gamma_0$) plus additional cost incurred if the component under consideration is made heavier (m is the mass of the component and c_m is the unit cost).

$$C_I(\gamma) = C_I(\gamma_0) + c_m \frac{\partial m}{\partial \gamma}(\gamma - \gamma_0) \tag{2.15}$$

The expected value of the cost of failure (removal of stumps and debris) is taken to be a fraction f_F of the standard investment $C_I(\gamma_0)$, multiplied by the sum of the failure probabilities for each year n, discounted with the interest rate r:

$$C_F = f_F C_I(\gamma_0) \sum_{n=1}^{N} \frac{p_F(\gamma, n)}{(1+r)^n} \tag{2.16}$$

The annual failure probability in year n is found from the cumulative failure probabilities:

$$p_F(\gamma, n) = p_{F,cum}(\gamma, n) - p_{F,cum}(\gamma, n-1) \tag{2.17}$$

Usually the cost of failure is small compared to cost incurred to replace components, given by:

$$C_R(\gamma) = \left(f_R C_I(\gamma_0) + c_m \frac{\partial m}{\partial \gamma}(\gamma - \gamma_0) \right) \sum_{n=1}^{N} \frac{p_F(\gamma, n)}{(1+r)^n} \tag{2.18}$$

The cost of replacing components is defined as a fixed fraction f_R of the initial investment $C_I(\gamma_0)$ plus extra cost of making the component under consideration heavier: if the component we are looking at is designed with a larger safety factor γ (rather than γ_0), replacement is more expensive. For a tower failure, we expect $f_R \sim 1$ (the whole turbine is lost), but if we look at blade failures f_R may be smaller. It is good to realise that equation (2.18) has some implicit assumptions (which are discussed in more detail below):

1. Investment cost is linearly dependent on the safety factor γ, which strictly is only valid for small changes in γ (however investigations for a tower actually showed validity over a great range).

2. The turbine's life is fixed at N years, and after this time the turbine is always removed.

3. Failed parts will always be replaced until the period of N years expires.

4. Multiple failures of the same component are neglected because the product probabilities are small.

The benefits (sales of electricity) over the turbine's life are (b are the average yearly benefits):

$$B = \sum_{n=1}^{N} \frac{b}{(1+r)^n} \tag{2.19}$$

For convenience, we assume instant replacement of failed components. Hence failures will not affect benefits, and $B(\gamma) = B = c$: we may leave B out of the optimisation problem. This is reasonable for land turbines; for offshore turbines it is probably too optimistic because due to bad weather there may go some time before component replacement is possible. Setting B to be constant also implicitly assumes that hub height is fixed, otherwise production would be a function of tower height and hence investment cost. The investment cost for the standard value $\gamma = \gamma_0$ is taken as:

$$C_I(\gamma_0) = c\, P_{rat} \tag{2.20}$$

with $c =$ €1100 per kW installed power. We normalise the W function by dividing by $C_I(\gamma_0)$ and setting $B = 0$ (since B is constant this makes no difference in the optimisation):

$$w(\gamma) = \frac{W(\gamma)}{C_I(\gamma_0)} = \frac{C_I(\gamma) + C_F(\gamma) + C_R(\gamma)}{C_I(\gamma_0)} \tag{2.21}$$

In the special case that $C_F = 0$ we end up with:

$$w(\gamma) = 1 - f_R + \left(f_R + \frac{c_m(\gamma - \gamma_0)}{C_I(\gamma_0)} \frac{\partial m}{\partial \gamma} \right) \left(1 + \sum_{n=1}^{n} \frac{p_F(\gamma, n)}{(1+r)^n} \right) \tag{2.22}$$

In equation (2.22) we see two factors counteracting each other ($1 - f_R =$ constant). If we increase safety γ, turbine mass increases (the first factor), increasing w and making the turbine more expensive; on the other hand more mass reduces the sum of the annual failure probabilities (the second factor), which decreases w.

The model is attractive because finding the safety factor producing the cost function minimum is easy; also the inherent uncertainties in the probabilistic approach

limit the value of more complex approaches[5]. However, equation (2.21) presupposes a fairly simple minded component replacement strategy. In the extreme case, if the tower were to fail in year 19 while the design life were $N = 20$ years, almost the whole turbine would instantly be replaced, in spite of the fact that the turbine would be removed in year 20 anyway. This matter deserves some more discussion.

An obvious extension of the model would be including inspections with a certain probability that cracks are detected and repaired. Dalsgaard Sørensen [198, 199] looked at such a model, and found that the money that can be spent on inspections is in the order of €500–2000 per inspection (for break even); these are marginal costs i.e. the costs for one extra inspection if all machinery (boats, people, equipment) is already available. His conclusion is that inspections are a promising option for cost reduction. The author of this work does not entirely agree with this: the amount of money available does not appear to give much room for inspections, and it appears that looking from the financial side one might just as well wait until failure as carry out regular inspections. There are two more arguments against the possibility of inspection and repair: firstly crack detection is difficult because parts cannot be well reached, and secondly repair is hard. Blades made of composites and cast iron components (hub and machine frame) cannot be repaired at all; even the welded tower construction is difficult to repair, and certainly the factory weld quality cannot be reproduced in the field. In practice the only 'repair' possible is to replace parts. All this is not to say that inspections cannot be desirable from a business point of view: obviously planning becomes easier if one can detect impending failures[6]. To which extent the inspection and repair strategy is feasible can only be settled by doing detailed calculations with actual numbers.

The important thing for us is that in the economic optimisation it does not make a big difference what is done: inspections and repairs roughly cost as much as they save in initial investment. This indicates that one does not have to worry overmuch about the inspection issue in a financial assessment, which leaves us with the question to what extent the proposed replacement-of-components strategy reflects reality.

What is the economically optimal strategy? As soon as the wind turbine has been erected, the money has been spent, and nothing can be done to reverse that[7]. Hence from this point on, the business is to generate energy at the lowest unit cost, given that the machine exists: the decision to be made is whether to spend money on maintenance and repair, or to scrap the turbine and buy a new one. At some point it will be cheaper to renew than to continue repairing, and at least in theory, replacing the existing structure must be considered all the time. In some cases, the renewal

---

[5]One may wonder whether this statement does not hold for many other economic models as well.

[6]Another strategy (not considered here) is rotation, possibly combined with condition monitoring: parts are replaced before failure occurs, and then repaired in the factory (where ideal conditions may be created, high quality inspections be done, special tools be used et cetera).

[7]Except of course sell the turbine, but that would only transfer the decision problem to the new owner, hence this option is irrelevant to the present discussion.

point may be far into the future; for example trains and aircraft are repaired (almost) endlessly.

For the case of wind turbines, we may quantify our options roughly as follows: the choice is between building a completely new turbine that lasts 20 years and costs 100 units, and replacing components costing anywhere between (say) 5 and 80 units (assume that the foundation need never be replaced). Both strategies would earn us a number of years of energy production, but in almost all cases the latter strategy (repair) would be cheaper. If for example we assume the extra period obtained by repair to be 5 years, then any replacement costing less than $5/20 \times 100 = 25$ units would be sensible. in fact there is no reason why we could not go on indefinitely with (e.g.) exchanging blades (if spare ones are available).[8]

Nevertheless there are several reasons why there is an end to the repair process. Several factors combine to make it attractive to replace old (small) turbines with new (larger) ones, even if the technical life has not run out (Kouwenhoven [113]):

- Newer machines are cheaper and better (for example initial investment has been €1000–1200 per kW installed power for a long time now, which means effectively that wind turbines become a few per cent cheaper every year).

- Suitable sites are in short supply, and the smallest machines tend to occupy the best sites. More energy could be generated if those turbines were replaced.

- Larger machines mean that projects generate larger profits in absolute terms. It may be that the unit cost of electricity generation with an old small turbine is low, but with a new machine much more energy can be generated.

- With time it becomes difficult to obtain spare parts for smaller machines.

- There is a tendency to concentrate wind power in fewer windfarms with larger units because this is deemed to be more visually appealing.

- There may be (politically driven) financial incentives to replace older, small machines, with newer, bigger ones.

- There is some 'headache' threshold to the failure probability (and hence life): although it might still be financially advantageous to continue with the old fleet, many failures cause too much hassle. Some minimum reliability of the entire windfarm is desirable. To put a number to this, an annual failure probability $p_F > 0.01$ is probably unacceptable for major components. The above extends to normal maintenance: at a certain point it is just too much trouble to maintain small wind turbines in relation to the energy output.

In fact, *even* if it is financially sound policy to continue operating old turbines and replace components for long periods, it is still expected that turbines that are installed now will be taken down in 10-15 years, and will certainly not operate beyond 20

---

[8]In reality one would take the interest (either public or private) into account, which would tend to decrease future benefits.

years. Conversely, in practice all failed parts are replaced until turbine renewal is very close, which is not optimal either. One may speculate whether human psychology plays a role here, and puts some limits on following the optimal investment strategy. On one hand one does not like endless replacements, on the other hand having some turbines in a wind farm that are not operating is deemed undesirable too, even if the whole farm is going to be replaced in the near future (of course there is also a public relations aspect to this).

In the author's opinion all this justifies using the simple cost function as given in equation (2.21). Life 20 years is used because this is the life required by IEC 61400-1; in section 9.6 the influence of using life values different from $N = 20$ years is investigated (for the blades there is almost no change, for the cast iron components optimal partial factors are 8% lower, and for the tower 14% lower).

To get back to the cost function proper, we will first be able to find out where the minimum is in chapter 8. However, which target value of the failure probability (or reliability index) is economically optimal if there is no human risk at all was already investigated by Dalsgaard Sørensen [198, 199] for solitary turbines. He finds that for a range of failure and reconstruction costs and interest rates the optimal reliability index range is $\beta = 3 - 3.6$, corresponding to annual failure probability $p_F = 2 \times 10^{-4}$ – 10^{-3} (averaged over the turbine's life; note that these numbers are close to the highest risk values found in the literature, see tables 2.3 and 2.4, p20). The figures hold both with and without systematic reconstruction. Three stochastic variables are used in his probabilistic model, with the following coefficients of variation: on wind fatigue load: $V = 0.15$, on stress estimation $V = 0.05$, on fatigue strength $V = 0.15$ (total variation is ca $V = 0.22$). Dalsgaard Sørensen states that this is approximately the safety level that is obtained if the Danish standard is used with $\gamma = \gamma_f \gamma_m = 1.42$.

Finally as a sidelight, Veers [219] considers the distribution over time of failures in a windfarm, depending on whether failure causes are independent or common, and what the financial effects are. No value for the optimal target reliability is derived.

2.7   Some philosophical issues

It may be objected that small values of failure probabilities found from a calculation have no absolute meaning: they are only relative (or *nominal*) because of uncertainty associated with the procedure, and because it is impossible to verify that the values calculated are correct (Melchers [144]). While this reasoning is formally correct, in practice some things may be said against it:

- If there are uncertainties associated with the calculation procedure these should be investigated by sensitivity studies; the result of the calculations would then be a range of answers (or a most likely answer), but it would not be just any number.

- It is difficult or impossible to verify small probabilities: however nobody would

deny that the probability to win the jackpot in a lottery (say that we find by standard probabilistic methods that the chance of winning is 10^{-7}) has absolute value, even though this cannot be verified either.

- The probability levels normally found (in wind turbine structures) are of the order of 10^{-5}, which is 4 standard deviations from the mean. This is still in the region where we would not expect problems with the validity of probability theory: it is likely to hold (and is verifiable to some extent).

Another objection against the validity of probabilistic methods is the 'tail problem', the problem that we do not know whether some distribution has the postulated shape, especially far from the mean. For example there may be some minimum and maximum material strength, resulting in a truncated strength distribution. However because we are dealing with many distributions, the shape of the combined distribution (that determines failure probability) will tend to be normal regardless of the exact properties of the underlying distribution. And again, with the failure probability magnitude we are dealing with we are not that far out in the tails.

Finally we must confront the fact the wind turbines do not often fail according to the fatigue failure modes that were imagined in the design. Often structural failures are the result of a control error or some unforeseen resonance phenomenon. However this does not invalidate the probabilistic approach; firstly everything is done to avoid this type of failure, secondly the approach is also a way of identifying weak spots and achieving consistent (and hence cost effective) design for the entire turbine.

Chapter 3

Conventional design

3.1 Introduction

In this chapter the conventional wind turbine design procedure is sketched, to provide the reader with insight in models that are used. In chapters 4 to 7 these models are examined more closely, and the probability distributions are derived for parameters that are taken to be constant in the conventional design procedure; where necessary alternative models are compared.

3.2 General procedure

The conventional design and site admission procedure is sketched in figure 3.1 (next page). After the design conditions have been selected from the standard, the design load calculations are done (more on this in section 3.4). Then a prototype is built and load measurements are done to check the wind turbine calculation model. If necessary the model is adjusted (section 3.5) until reasonable correspondence between calculated and measured loads is obtained (say $\pm 10\%$ for fatigue damage equivalent load ranges[1] of 10 minute periods). Finally a new load set is produced for the design of the 0-series with the adjusted model.

At present it does not seem possible to calculate more accurately than this[2] (although some investigations are being done where the measured wind history is used to generate constrained artificial random wind).

Further uncertainty in the design loads is introduced by the fact that a limited number of load cases is evaluated with different wind seeds for the artificial wind

---

[1] The expression 'fatigue damage equivalent load range' is very long. Therefore the shorter 'equivalent load' will be used henceforth. For the definition see appendix C

[2] There is the possibility to base the design loads 100% on measurements. However in most cases this is not a practical solution (results are only valid for one turbine at one site); besides there would still be variation in measured loads, even for (seemingly) identical conditions.

design conditions (e.g. class)

Load calculations

calculated loads

Prototype design

prototype

Measurements

measured loads

Comparison of loads
measured - calculated

Design adjustment
(0-series)

Difference small
enough?

yes

best estimate
design loads

calculated
loads

no

Adjustment of turbine
calculation model

adjusted model

New load
calculations

estimate of
site conditions

Estimate of site loads
(or full load calculation)

Comparison of design
and site loads

Admission / rejection

Figure 3.1: Conventional design and admission procedure

(for details, see section 4.2.2). If we wish, we may reduce this last uncertainty to an
arbitrarily low level by doing more or longer calculations.

Before wind turbines are installed, site conditions are evaluated, and the site loads
estimated (section 3.6). If site loads are judged to be small enough, the turbine may
be placed at the proposed site.

3.3   Ideal and simplified calculation

A wind turbine must withstand the environmental conditions, either those defined in a class representative for a large area (table 2.2, p17), or those at a particular site. As a thought experiment, assume that we had infinite resources at our disposal: time, computers, measuring equipment. Then we could reproduce the environment and the structure in a detailed way to get the right design:

- The atmospheric conditions could reflect reality to a high degree, for example for every square centimeter of rotor area a measurement of the three local wind speeds could be done with a 25 Hz sampling frequency.

- The flow around the blades (and the rest of the turbine) could be calculated with the Navier-Stokes equations (using very small cells of course).

- The structural model of the turbine could consist of tiny elements.

- By sophisticated manufacturing processes, quality control and measurements, the exact geometry would be established, which would make it possible to know the stress exactly in any location.

- Crack growth at various critical locations could be evaluated at every time step in the calculation.

- The whole calculation could be repeated as often as we wanted to get statistically significant results.

Obviously this approach is not feasible in reality. To be able to do calculations at all, many simplifying assumptions need to be made. These include:

- Making use of the fact that environmental conditions repeat themselves in time (for example a few dozen periods of 10 minutes of wind may suffice to represent 20 years of wind).

- Stationarity: for example that the wind speed has some distribution with mean and standard deviation that do not change with time.

- Using characteristic (weighed mean) values (for example the 90% fractile value for the turbulence intensity may represent the turbulence distribution, or 'yearly mean' vegetation at some site);

- Using models (for example a simplified structural model that ignores all resonance frequencies above 5 Hz).

- Parameterisations of important processes (for example crack growth).

Thus we end up with a calculation procedure for fatigue loads as given in the list of steps in figure 1.2 (p3). In the rest of this chapter the assumptions normally made are described (see table 3.1, next page), and in chapters 4–7 we will discuss in detail the validity of the calculation models and investigate how parameters that are assumed to be constant vary in real life.

There are three possible sources of discrepancy between the simplified approach and the ideal calculation:

- The model may not be a good enough approximation. For example a measured turbulence spectrum never has the ideal assumed shape.

Table 3.1: Simplifying design assumptions

area	subject	model
wind	wind speed history	small number of disjoint 10 min intervals
	wind speed distribution	Weibull ($k = 2$)
	wind direction distribution	unidirectional or fixed
	turbulence intensities	constant values
	turbulent wind field	gaussian (mostly)
	- turbulence spectrum	standard function
	- coherence	standard functions
	wind shear	logarithmic profile or power law
	tower shadow	potential flow or empirical model
	air density	constant value
	yaw error	constant value
	inflow angle (slope)	constant value
	wake effects in windfarm	as extra turbulence
	complex terrain	modification of standard parameters
sea	significant wave height	simple function of wind speed
	wave spectrum	standard function
	wave shape	sinusoidal shape
	wind/wave misalignment	constant value
	drag and inertia coefficients	constant value
	tide	correction on still water level
	current	constant value
aerodynamics	flow through rotor	independent annuli
	lift and drag	adjusted 2D wind tunnel values
	tip and root correction	engineering model
	oblique inflow	engineering model
	dynamic wake	engineering model
	dynamic stall	engineering model
wind turbine	control system behaviour	engineering model
	cut out wind speed	constant value
	structure	limited number of DOFs
	mass/stiffness	estimates
	geometry	ideal and simplified (for FEM)
	stresses	linear function of forces
material behaviour	S-N curve	const amplitude curve for (small) probes with corrections
	stress history	(rainflow) cycle count
	VA fatigue damage sum	linear summation by Miner's rule

- The representative (weighed) mean parameters used may not be conservative, or the degree of conservatism is uncertain.

- Only estimates of required parameters are available, and these may be biased. Even if a long term estimate is correct, the actual parameter values over the turbine's life may be different.

3.4 Conventional models

3.4.1 Wind

The first matter to look into is the wind climate in which the turbine must operate. To be able to do useful load calculations we are forced to describe the complex behaviour of the air flow at some proposed wind turbine site with a limited number of models and parameters. The first part of table 3.1 gives the usual wind climate models.

Wind speed history. For fatigue calculations, one starts by reducing the 20-years wind speed history of $\sim 10^6$ 10-minute intervals to a few dozen characteristic periods. To do this, the wind turbine operating wind speed range is divided into intervals, and each interval is assigned a representative average wind speed and turbulence[3]; table 3.2 gives an often used division. For each 10-minute interval short term wind fluctuations are well described by turbulence models (see below). Unfortunately the fatigue effect of long term-low frequency wind speed variations (over periods of days,

---

[3]In IEC 61400-1 'turbulence' is called 'turbulence standard deviation'. Here the shorter term 'turbulence' is preferred.

Table 3.2: Conventional load case definition consistent with IEC 61400-1.

wind speed interval (bin) [m/s]	representative wind speed [m/s]	turbulence intensity [-]			wind turbine state
		class A 'inland'	class B 'coastal'	class C 'offshore'	
0–3	3	0.419	0.366	0.314	idling
3–5	4	0.344	0.301	0.258	production
5–7	6	0.269	0.236	0.202	production
7–9	8	0.232	0.203	0.174	production
9–11	10	0.210	0.183	0.157	production
11–13	12	0.195	0.170	0.146	production
13–15	14	0.184	0.161	0.138	production
15–17	16	0.176	0.154	0.132	production
17–19	18	0.170	0.149	0.127	production
19–21	20	0.165	0.144	0.124	production
21–23	22	0.161	0.141	0.121	production
23–25	24	0.157	0.138	0.118	production
>25	30	0.150	0.131	0.112	idling or parked

say) is removed by this approach: large load cycles caused by the wind speed rising from zero to storm wind speeds and back again simply do not exist, because the 10-minute intervals are not linked.

Seed and time series length. Each 10-minute load case has its own set of 3 turbulent wind field components (u, v, w), generated with a different random seed. In this way loads are averaged (wind fields with turbulence producing larger loads are offset by others with more 'benign' turbulence), and it is therefore assumed that a limited number of calculations at each wind speed is sufficient to estimate average loads. Formerly 2×10 minutes at each wind speed was considered to be enough, but nowadays more calculations are done. This is not primarily to get the right average fatigue loads, but because it is required by the standard for load response extrapolation purposes.

Wind speed distribution. How many times each 10-minute interval with a certain average wind speed occurs in 20 years is described by a Weibull distribution:

$$F(U) = 1 - \exp(-(\frac{U}{C})^k) \tag{3.1}$$

$$C = \frac{U_{avg}}{\Gamma(1 + 1/k)} \tag{3.2}$$

According to IEC 61400-1 the distributions to be used have long term average wind speeds U_{avg} = 10 (class I), 8.5 (class II) or 7.5 m/s (class III) and shape factor $k = 2$.

Wind direction distribution. Except in critical cases, the fact that the wind comes from different directions is not used; instead all wind is assumed to come from the same direction (North for example). This is a matter of convenience. If terrain roughness in all directions is similar, it makes no difference for components above the yaw bearing, because the turbine yaw system makes the rotor follow the wind direction. The procedure will result in overprediction of tower loads (see section 4.3) however. If sectors around the turbine are significantly different with respect to roughness or obstacles, components above the yaw bearing do experience different loads depending on the wind direction distribution used, and it may be necessary to do detailed calculations.

Turbulence. In each wind speed bin the turbulence intensity $I(U)$ is taken according to the classes in IEC 61400-1 [93] (see table 3.2 and equation (3.3)). The equation reflects that at low wind speeds turbulence is higher due to thermal effects, while at higher wind speeds mechanical turbulence due to terrain roughness is dominant. The equation is an approximation for flat open terrain, and tuned in such a way that it produces 90% fractile turbulence values (approximately mean + 1.3 times the standard deviation for a lognormal distribution).

$$I_{char}(U) = \frac{\sigma_U}{U} = I_{ref}\left(0.75 + \frac{c_{90\%}}{U}\right) \tag{3.3}$$

Here:

$c_{90\%}$ constant = 5.6 m/s
I_{char} characteristic turbulence intensity (90% fractile) [-]
I_{ref} reference turbulence intensity (mean value at U = 15 m/s) [-]
     A (inland): $I_{ref} = 0.16$; B (coastal): $I_{ref} = 0.14$; C (offshore): $I_{ref} = 0.12$
U mean wind speed at hub height [m/s]
σ_U turbulence [m/s]

Within each 10-minute period the wind speed is assumed to be normally distributed, with average U and standard deviation $\sigma_U = I\,U$. The prescribed turbulence intensity value $I(U)$ is used in the creation of a 3-dimensional stochastic wind field that is moved through the rotor with a characteristic mean advection speed according to Taylor. How much power (variance) there is in the wind at a particular frequency is defined by the power spectral density function $S(f)$. Although there is some freedom in the choice of $S(f)$, all spectra must have the same $-5/3$ slope at high frequencies, and the difference is mostly in the length scales L_k which determine the shape of $S_k(f)$. A common choice is the spectrum for flat open terrain derived by Kaimal [98, 99]. In the IEC equation[4] it is given by:

$$\frac{fS_k(f)}{\sigma_k^2} = \frac{4fL_k/U}{(1 + 6fL_k/U)^{5/3}} \tag{3.4}$$

with:

$$L_u = 8.1\Lambda \qquad L_v = 2.7\Lambda \qquad L_w = 0.66\Lambda \tag{3.5}$$

$$\Lambda = 0.7H \quad (\Lambda \le \Lambda_{max}) \tag{3.6}$$

where:

f frequency [Hz]
H wind turbine hub height [m]
k index (u = longitudinal, v = transversal, w = vertical)
L_k length [m]
S_k one sided velocity component spectrum [m^2/s]
U average wind speed for the period considered [m/s]
Λ length scale [m]
Λ_{max} constant = 42 m

The turbulence values for the three directions u, v, w are set to the following ratios (for the coordinate system used, see appendix A):

$$\sigma_u : \sigma_v : \sigma_w = 1 : 0.8 : 0.5 \tag{3.7}$$

---

[4]The IEC formulas (3.4) are slightly different from Kaimal's original ones (Kaimal [98, 99]).

Finally the coherence function must be chosen, which defines dependency between wind speeds at locations some (lateral or vertical) distance r apart. IEC 61400-1 gives the same function for all wind speed components (f is frequency, L_c is a length scale, U is the mean wind speed)[5]:

$$Coh(r, f) = \exp\left(-12\sqrt{\left(\frac{fr}{U}\right)^2 + \left(\frac{0.12r}{L_c}\right)^2}\right) \tag{3.8}$$

If the Sandia/Veers model is used for wind field generation, spectrum and coherence as given here are reproduced exactly, if the Mann model is used, the functions are somewhat different (see appendix G for details).

Wind shear. If we were to remove all short term wind speed fluctuations, we would still not find uniform wind speed. Instead the average wind speed U varies with height, approximately according to:

$$\frac{U(z_2)}{U(z_1)} = \frac{\ln(z_2/z_0)}{\ln(z_1/z_0)} \tag{3.9}$$

where z_1 and z_2 are heights and z_0 is the terrain roughness. Often this profile is approximated by a power law[6]:

$$\frac{U(z_2)}{U(z_1)} = \left(\frac{z_2}{z_1}\right)^\alpha \tag{3.10}$$

For hub height $H = 80$ m and normal terrain roughness values ($z_0 = 0.1$ m), the exponent works out to $\alpha = 0.14$ to conform to the logarithmic profile. IEC 61400-1 prescribes $\alpha = 0.2$ for fatigue and $\alpha = 0.11$ for extreme loads.

Values for horizontal wind shear (which could occur in windfarms, or in mountainous terrain) are also given in the standard, but for ultimate load cases only, not for fatigue load calculations.

Tower shadow. For upwind rotors and circular towers the potential flow model is assumed to be valid (see for example Burton [30]). For normal blade tower clearance (1–2 times the tower diameter) the effect of the tower is small. For downwind rotors an empirical expression is used.

Yaw error (or wind misalignment). The wind turbine head does not follow the wind direction exactly for two reasons. Firstly wind direction changes are too fast to follow; this effect is (at least partially) taken into account in the turbulence field. Secondly the yaw error is difficult to measure: what is used is a wind vane on the

---

[5]This is only marginally different from the DS472 equation, that contains only the first term under the square root sign (DS472 [44]).

[6]Equations (3.9) and (3.10) can be 'made equivalent'. Let $z_1 = H$ (hub height); then require that the derivatives dU/dz are identical at $z = H$. Then $\alpha = 1/\ln(H/z_0)$. This is also the equation for turbulence intensity estimation: $I \approx \alpha$.

nacelle (in the rotor wake), a procedure that cannot be expected to give very accurate results. Therefore it must be assumed that there is a difference between the correct and the actual yaw position, and a fixed misalignment of 5–10° (both positive and negative) is used in calculations.

Inflow angle. Because the turbine is designed for some wide geographical area, it must be expected that average wind speed is not always horizontal: obviously this will be the case for hilly sites. A vertical inflow angle $S = 8°$ is therefore used. Together with the usual 5° main shaft tilt (to provide enough blade tower clearance), this results in 13° oblique inflow (a yaw error of 5° increases the total inflow angle to $\sqrt{13^2 + 5^2} = 14°$, see figure 4.11, p77).

Procedure to find wind speed seen by the blade. To summarise the above, the steps to find the wind speed seen by the blade are (for a solitary turbine):

1. Start with a constant, uniform wind speed.

2. Add vertical and horizontal wind shear and random turbulence in three directions to get the 'total' wind speed.

3. Incorporate the effects of tilt angle, wind direction, yaw error and terrain slope.

4. Take tower shadow into account.

5. Find the local wind speeds at the blade.

6. Convert these to relative wind speeds seen by the blades, taking into account blade movement and induction.

Air density. The air density is fixed to the value at temperature $T = 288$ K and pressure $p = 101,325$ Pa: $\rho = 1.225$ kg/m^3. For projects above sea level or offshore a different constant value is used, determined by site pressure and temperature.

Wake effects in windfarms. Wind turbine load calculations presume a solitary turbine in flat uniform terrain, while in reality more and more turbines are installed in windfarms, where wakes have an important effect on fatigue loads. One way to deal with this issue is to use the concept of *effective (or equivalent) turbulence*, which is imaginary turbulence that *would* have produced the same fatigue damage as the combined effect of actual turbulence and wake effects.

The practical advantage of using effective turbulence is that only a minor modification of the usual calculations is necessary; the disadvantage is that material properties (in the form of the slope of the S-N curve m) enter the load calculation, and that hence the loads become dependent on the material used and the crack growth model. This means that at least three parallel calculations would have to be done for blades (composites, $m = 9$–12), nacelle (cast iron, $m = 6$–8) and tower (welded steel, $m = 3$–4). Clearly this is inconvenient, so only one set of calculations is done for some high turbulence level, and later a check is performed whenever there is a proposal for a windfarm where wake effects are important (for more information on the relation between turbulence and fatigue damage see chapter 7 and appendix C).

In the turbulence wake model each turbine is assumed to have maximally 8 neigh-

bours[7], and only nearest neighbours are supposed to contribute with their wake to effective turbulence, as follows (Frandsen [64], IEC [93]):

$$\sigma_{eff} = \left[(1 - Np_w)\sigma_a^m + p_w \sum_{i=1}^{N} \sigma_{aw}^m \right]^{1/m} \tag{3.11}$$

$$\sigma_{aw} = \sqrt{\frac{0.9U^2}{(1.5 + 0.3s_i\sqrt{U})^2} + \sigma_a^2} \tag{3.12}$$

where:

m	slope of S-N curve [-]
N	number of neighbouring turbines [-]
p_w	fixed probability, $p_w = 0.06$
U	wind speed at hub height [m/s]
s_i	distance to neighbouring turbine i normalised by rotor diameter [-]
σ_a	ambient turbulence [m/s]
σ_{aw}	combined ambient and wake turbulence [m/s]
σ_{eff}	effective turbulence intensity [-]

Complex terrain. Most of the preceding theory is valid for 'flat smooth uniform terrain'. The concept is usually stretched somewhat, where 'flat' includes terrain with slopes up to 20° or so (or at least without flow separation), 'smooth' can mean 'with terrain roughness up to $z_0 = 0.3$ m ('high crops and bushes, numerous scattered obstacles') and 'terrain' can also mean 'offshore'. Still many sites where turbines are placed do not fit the description: a present we are looking at very complex mountainous areas, or sites with forests and clearings. If we want to employ the usual calculation methods, the only thing we can do is to adjust the parameters that are used in calculations (there is one exception: modern turbulence generators can also produce non-Gaussian wind fields - this can be used if there are indications that non-Gaussian

---

[7]The calculation is easily refined to any number of neighbours, where each neighbour occupies some sector.

Table 3.3: Adjustment of parameters for complex terrain. Source: Thomsen [206] except for shear parameter (spectral shape): Morfiadakis [147].

parameter	flat terrain	complex terrain
wind speed	Weibull distribution	Weibull corrected for speed up
inflow angle	$\sim 0°$	terrain slope (2–3D average)
turbulence intensity ratios	1.0 : 0.8 : 0.5	1.0 : 1.0 : 0.8
spectrum length scale ratios	1.0 : 0.3 : 0.1[1]	0.7 : 0.3 : 0.1
Mann's shear parameter Γ	3.9 (Kaimal)	0 (von Kármán)

[1]According to DS472 [44], in IEC 61400-1 [93] ratios are 1.0 : 0.33 : 0.08

approach is in order). Thomsen [206] suggests the following changes, which should be applied for 12 wind direction sectors of 30° (table 3.3). Following this procedure would make 12 separate calculations necessary for one turbine; however in the case of a wind farm in complex terrain one would normally select the worst case turbine for the design basis of all, and the computational burden would not be excessive. Morfiadakis [147] found that the von Kármán spectrum was a good fit for a complex site on the island of Andros (Greece); this spectrum has turbulence intensity ratios $1 : 1 : 1$, which is consistent with Thomsen's recommendation (measurements were done at 30 m height, which is a little low for today's turbines).

3.4.2 Sea

For offshore turbine the set of wind conditions described above needs to be extended with wave conditions.

Significant wave height. How much the sea surface elevation η varies might be characterised by the standard deviation σ_η, but traditionally the significant wave height H_s has been used for this, which is the mean height (from crest to trough) of the highest third of all waves. In this work the significant wave height definition used is:

$$H_s = H_{m0} = 4\sigma_\eta \tag{3.13}$$

which is slightly different. The significant wave height H_s and the zero crossing period T_z are usually known as a function of wind speed from measurements or from hindcast data. Suppose we consider 3 hour periods; for every period we record the averages of wind speed, significant wave height H_s and zero crossing period T_z. For every wind speed a matrix is now composed of which the elements are the frequencies of occurrence of each combination of significant wave height and zero crossing period[8]. Unfortunately this leaves us with many different load cases at each wind speed, so weighed average values for significant wave height and zero crossing period are computed (see for example Kühn [115]):

$$H_s(U) = \left(\sum p_i H_{s,i}^m\right)^{1/m} \tag{3.14}$$

$$T_z(U) = \left(\sum \frac{p_i}{T_{z,i}}\right)^{-1} \tag{3.15}$$

The method to get a fatigue damage equivalent significant wave height is analogous to what was done to include the effect of wind turbine wakes (equation (3.11), see also appendix C). Again one takes for granted that the material parameter m (slope of the S-N curve) enters the load calculations in order to simplify them. The procedure

---

[8]This matrix is also called scatter diagram.

results in simple curve fits for significant wave height as function of wind speed, and zero crossing period as function of significant wave height. The functions may be made dependent on wind direction.

Wave spectrum. The wave spectrum (that determines how much energy waves have as function of frequency) most used is the one sided Jonswap spectrum, given in equation (5.3) (p85); see for example DNV [47]. The spectrum has a peakedness parameter that makes it possible to tune it to measured data.

Wave kinematics. For fatigue calculations, 2-dimensional waves are assumed, like those in a (narrow) wave tank. Random Airy waves (first order sinusoidal waves) are generated according to the appropriate wave spectrum. The procedure is analogous to wind field generation (see appendix G). For circular cross sections the McCamy-Fuchs diffraction correction may be used on particle accelerations, which acts as a low pass filter. The first order calculation is fine for deep water waves, where the wave height-depth ratio $H/d \leq 0.2$, but the wave kinematics are not right for higher waves. It is especially difficult to find speeds and acceleration at the (varying) water surface, and the usual approximation is to calculate them at the average water surface, and stretch the speed and acceleration profiles to wherever the water surface is at a particular moment (for example Wheeler stretching).

Drag and inertia coefficient. Values for drag and inertia coefficients are derived from model tests or from standards and handbooks. For cylinders accepted values are $C_D = 0.6$–1.2 and $C_M = 1.3$–2.0, depending on the Reynolds and Keulegan-Carpenter numbers, and cylinder roughness (Gudmestad [76]). The influence of appurtenances (which gives a larger effective diameter) is incorporated by modifying these coefficients (IEC [94, appendix D.5]).

Wind/wave misalignment. Because it is not practical to do calculations for all combinations of wind and wave directions, wave/wind collinearity is used. Alternatively some constant misalignment in the order of $20°$ is used, which is probably a little more accurate. It is important to take the misalignment into account, because the aerodynamic damping of the structure is small in the direction perpendicular to the wind speed.

Tide. The (vertical) tide is included by modifying the mean sea level d. The corrected depth d' is dependent on the Wöhler exponent m of the material, and is found by integration of the depth over time:

$$d_{eq} = \left(\frac{1}{T} \int_T [d(t)]^{2m} dt \right)^{1/(2m)} \tag{3.16}$$

Current. Surface current speeds are usually small (< 1 m/s) in relation to wave speeds. Therefore one does not bother to calculate the correct modified kinematics: the current speed is just added to wave speeds.

3.4.3   Aerodynamics

The most common method to estimate wind turbine loads is the Blade Element-Momentum (BEM) method (see for example Burton [30] and Snel [193]). This is currently the only method that is fast and accurate enough to meet the demands made on load calculations. The basic assumption of this method is that ring shaped volumes of air flow through a perfectly aligned rotor without influencing each other:

- There is no radial flow.

- The wind field seen by the rotor is undisturbed by the presence of the rotor itself (apart from induction).

- Forces on blades can be found with simple calculations based on lift and drag coefficients.

To extend the range of validity of the model, various engineering corrections have evolved over the years such as:

- 3D correction on 2D lift coefficients (although it is possible to say something about what the correction should look like, no correction has been found that consistently improves calculations).

- Prandtl correction for flow around blade tips and blade roots

- dynamic stall model (there is a change of the lift coefficient between two levels with a time delay).

- Dynamic inflow (there is a wake model with time delay which governs induction)

- Skew inflow model.

All these models are approximations that capture the essence of a phenomenon. However it can hardly be a surprise that results are not always as good as desired. It is therefore essential that calculations are checked against measurements. The errors of the blade element-momentum method are normally corrected in the load verification process, by tuning of lift and drag coefficients (for an example in the public domain see Laino [116]).

3.4.4   Wind turbine

To be able to do calculations it is necessary to use a simplified model of the turbine, where the structure is reduced to a small number of idealised masses, dampers and stiffnesses.

Eigenfrequencies (mass, stiffness). Before the turbine is built, masses and stiffnesses are estimated. In reality, values may be different and eigenfrequencies will differ from those calculated with the model.

Structural model. The wind turbine is reduced to a number of connected beams. At present, the largest computational errors have to do with aerodynamics; by com-

parison the structural model may be considered to be almost perfect. Normal practice is to use mode shapes that have all frequencies smaller than 5–10 Hz, which means that tower first and second bending modes are taken into account, and the first three blade modes.

Stresses and geometry. From the deformation of the turbine and the acceleration of the parts, the forces in important cross sections can be computed. Then it is assumed that there is a linear relation between the 6-component stress vector $\underline{\sigma}$ and the 6-component force/moment vector $\underline{F}$:

$$A\underline{\sigma} = \underline{F} \tag{3.17}$$

The elements of the matrix A (areas and section moduli) are found with static finite element calculations (FEM) where unit forces and unit moments are put on the structure. It is customary to calculate the equivalent stress (von Mises stress) from the 6 stress components, and use this to judge whether failure will occur; to obtain sensible results in rainflow counting (see below) the equivalent stress is assigned the sign of the largest tensile stress. These calculation assume that the turbine is manufactured exactly according to specification, and geometry is perfect i.e. corresponds exactly to drawings. The inertia of the structure is taken into account in a lumped form in the calculation of the cross sectional forces; in reality there is of course continuous inertia, which has an influence on local stresses.

Control system. A simplified model of the wind turbine controller (which controls pitch angle and generator torque) is used, consisting of ideal components, such as sensors, inertias and time delays. The constants of the model are checked against some special measurements, for example a step in pitch action.

Cut out wind speed. The fact that the turbine is idling or parked above some cut out wind speed is taken into account in the load case definition. For example if the cut out wind speed is 25 m/s, it is assumed that the highest production interval is 23–25 m/s, and the turbine is parked or idling whenever $U > 25$ m/s.

3.4.5   Material behaviour

The last section of the table deals with material properties and crack growth.

S-N or Wöhler curve. The component fatigue curve may be found from tests on the component itself, or on representative probes. Sometimes there is no other possibility than to derive the Wöhler curve from constant amplitude tests on small probes, applying a number of corrections for surface roughness, mean stress, geometry, notch factor, heat treatment, et cetera.

Rainflow counting. The complex random stress history must be converted to a table with numbers of cycles and stress ranges, and possibly mean stresses (mean stress influence is important for cast iron and for blade materials). For this task, the rainflow method is employed. For details see for example Gudehus [74] or Haibach [77].

Fatigue damage. Total fatigue damage is found by adding the damage caused by each individual load cycle linearly (the Palmgren-Miner rule). In spite of its shortcomings (notably that sequence effects are disregarded), the method it is in near universal use.

3.5   Load verification and design adjustment

When the design is ready, a prototype is built and a load verification is done, in which measured loads are compared to calculated loads. In trying to reproduce measured loads, we allow ourselves some 'reasonable tuning' of various parameters. This does not mean that calculated loads are tweaked until they fit the measurements, but rather that some parameter values that *could not be exactly known* before the turbine was built are adjusted to their correct values. Tuning involves:

1. Eigenfrequencies. Eigenfrequency errors occur because masses, inertias and stiffnesses had to be estimated before the turbine was built. For example blade mass and stiffness, drive train stiffness and foundation stiffness may have to be adjusted (note that for the actual site foundation stiffness might again be different).

2. Damping. For example, from a braking test the tower damping may be estimated, and the assumed value improved.

3. Blade lift coefficients. Lift coefficients are adjusted until the right equivalent blade flap bending moments are found, while keeping the correct average power curve, average flap moment and average tower bending moment (this tuning is somewhat questionable from a physical point of view).

After tuning, the procedure to compare loads is as follows:

1. Select a number of representative 10-minute periods with different wind speeds and different turbulence levels, so-called 'load cases'. Periods where the turbine is in the wake of some other turbine, or where there was some turbine error, are excluded.

2. For each of these load cases, establish the yaw error, the air density and the turbulence intensity. One may also estimate wind shear, the turbulence spectrum and the turbulence coherence function. Generate artificial wind that corresponds to the measured wind to the desired degree.

3. Run the calculations and compare the damage equivalent loads for each load case to the measured ones.

Ideally calculated loads fit measured ones exactly. This is not always the case, and load correction factors may need to be used in future design calculations. These factors are a function of location in the wind turbine and a function of wind speed. For the turbine under consideration a redesign may now be done. Although in this

way calculated loads can be made to fit measured loads very well, predictive power of the calibration method is limited to designs that are very close to the one investigated, and every new design needs to be checked afresh.

3.6   Site admission

In reality site conditions will differ from the class definition. The usual case is that site conditions are estimated from a few years of measurements, possibly supplemented with data from wind atlases or stations nearby. Both for the vector of site conditions $\underline{x}_s$ and the vector of class conditions $\underline{x}_c$ equivalent load ranges can be derived, which may then be compared. The requirement for installation (site admission rule) is:

$$\Delta F_{eq}(\underline{x}_s) \leq SRF \, \Delta F_{eq}(\underline{x}_c) \tag{3.18}$$

where:

ΔF_{eq}	fatigue damage equivalent load [N, Nm]
SRF	stress reserve factor [-]
$\underline{x}_c$	vector of environmental parameters for the class
$\underline{x}_s$	vector of environmental parameters for the site

The stress reserve factor SRF comes into the equation because the design is almost never optimal in the sense that it is exactly at the limit; usually there is some small safety margin left, typically $1 \leq SRF \leq 1.1$. Therefore loads that are more severe than the class design loads may be admissible. The admission criterion (see figure 3.1, p30) is defined using the derivatives of the equivalent loads with respect to the components of the parameter vector $\underline{x}$. Linearising from the class definition point $\underline{x}_c$ yields:

$$\Delta F_{eq}(\underline{x}_s) \approx \Delta F_{eq}(\underline{x}_c) + \sum_{i=1}^{n} \frac{\partial \Delta F_{eq}(\underline{x}_c)}{\partial x_i} (x_{si} - x_{ci}) \tag{3.19}$$

Hence:

$$\sum_{i=1}^{n} \frac{\partial \Delta F_{eq}(\underline{x}_c)}{\partial x_i} (x_{si} - x_{ci}) \leq (SRF - 1) \, \Delta F_{eq}(\underline{x}_c) \tag{3.20}$$

If the stress reserve factor $SRF = 1$ then equation (3.20) simplifies to:

$$\sum_{i-1}^{n} \left(\frac{\partial \Delta F_{eq}(\underline{x}_c)}{\partial x_i} \right) (x_{si} - x_{ci}) \leq 0 \tag{3.21}$$

The method of equation (3.20) is useful in judging the suitability of sites and wind-farm configurations, especially if wake effects are incorporated as additional turbulence (IEC [93]). In practice equivalent loads are calculated in a few points (for example for a few values of the turbulence intensity and terrain slopes), and interpolation rather than extrapolation is used.

Chapter 4

Wind

4.1 Introduction

In chapter 3 and in table 3.1 (p32) the simplifying assumptions were listed that are made in conventional design practice. These assumptions are best guesses at the representative situation (for example the characteristic turbulence): the real situation at a site may be different. As a result of this, actual fatigue loads may be larger or smaller than estimated.

In chapters 4–7 we examine what the variation and bias are of the stochastic parameters describing the site and the wind turbine. The importance of a parameter is judged by examining its influence on relevant local loads[1], such as for example the blade root bending moment. The history of a local load is summarised in the equivalent load (see appendix C).

Models in common use are examined; some of them are good approximations of reality, but others perform less than satisfactory. However sometimes we will be forced to follow the time honoured practice of first listing everything that is wrong with a certain model, and then end up by using it anyway.

4.2 Wind speed history

4.2.1 Reduction to 10 minute load cases

For reasons of economy, the wind history during the turbine's life of twenty years or so is reduced to a few dozen 10 minute periods (or load cases) at certain average wind speeds: for example 3, 4, 6, ..., 24, 30 m/s (see table 3.2, p33). It would be unconservative of course to assume the wind speed to be constant within the load case: it varies with a distribution that is approximately gaussian in many cases (Mann

---

[1]Local loads (usually bending moments) are sometimes called 'sensors', because these loads are what would be measured by a strain gauge sensor at the location.

[135], Nielsen [154, 155], for more on non-gaussianity see section 4.5.4). This is of course what is called turbulence.

While with turbulence we have an accurate description of the wind for each individual load case, a disadvantage of the procedure is that large load cycles with periods longer than 10 minutes will be missed: for example a cycle of a few days: start at 4 m/s $\longrightarrow$ production at wind speeds between 4 and 25 m/s $\longrightarrow$ idling (stop) at 4 m/s, will never be found. An approach sometimes used to solve this problem is to have a number of additional load cases in which the wind speed history has an artificial low-high-low pattern (start-stop sequence).

Larsen and Thomsen [123] attempted to estimate the size of the effect on fatigue life by constructing an additional peak-trough signal from the global extremes of each 10 minute load case (in arbitrary order; either the minimum or the maximum may come first); the order of 10 minute load cases is based on the measured wind history. They report an increase of fatigue loads that is just on the edge of significance (see table 4.1). The matter was also investigated by Carlén [32] for four different sites (Jylland, Nasudden, Sprogø and Tystofte). He found that the transition probability for changing from one 10 minute average wind speed to another in the next 10 minute interval is well described by Weibull distributions. An analysis of the load cycles showed that for all sites there were 20,000–25,000 large wind speed cycles per year with a duration shorter than 3 hours and 100–200 cycles per year with a longer duration, the latter representing start-production-stop sequences. This circumvents (at least to some extent) the long standing argument about how long material memory is: if almost all cycles have a duration smaller than 3 hours, it seems reasonable to assume that the material 'remembers' these cycles; at least it is not necessary to assume memory of months or years. Carlén does not indicate how his results should be used to estimate additional fatigue damage, but presumably it would be along the lines of Larsen's method.

To estimate the influence of large wind speed cycles on all relevant load signals

Table 4.1: Ratio of equivalent fatigue load with and without large low frequency load cycles for Tystofte. Source: Larsen [123]. In this work, measured wind speeds were normalised to obtain average 8.5 m/s at hub height, which may explain the difference with Larsen's results.

Sensor[1]	material	slope m	load ratio	
			Larsen	this work
Blade root flap moment My11h[1]	weld seam	3	1.01	1.03
	cast iron	7	1.04	1.04
	composite	12	1.08	1.06
Nacelle tilt moment MyNf[1]	weld seam	3	1.00	1.01
	cast iron	7	1.00	1.02
	composite	12	1.02	1.06

[1]For nomenclature see appendix A.

and to be able to calibrate short cut methods, we will construct a time signal as a sequence of regular load cases, as follows:

1. Generate twelve different 10 minute load cases at each of the usual wind speeds: 3, 4, 6, ..., 24, 30 m/s (12 different wind directions).

2. Generate a wind speed and direction history. A measured wind history could be used, but an artificial history is preferable for research purposes, if it can be made to have realistic properties. Fortunately it turns out that a Markov chain based on the transition matrix of 1 h average wind speeds reproduces the measured low frequency wind spectrum for a number of sites well. Moreover spectra for these sites turn out to be similar.

3. Construct a sequence of load cases corresponding to the wind history.

4. Do a rainflow count on the entire history and compare with the conventional rainflow count.

The details of the procedure are, though interesting, too technical to go into here; the interested reader is referred to appendix E.

A summary of results is given in table 4.2. The explanation for the large increase in the nacelle roll (drive train) equivalent moment MxNf is the absence of start/stop cycles in the simplified load spectrum used here, which would be included in a normal design calculation[2]. The increase in tower base bending moments has to do with the

---

[2]In the beginning of the work it was decided to use a simplified load spectrum comprising load cases that give most fatigue damage: production and idling. It now turns out that starts and stops are important for the nacelle; however since all calculations of equivalent loads are relative (both design

Table 4.2: Influence of large low frequency load cycles on equivalent fatigue loads. Numbers are equivalent load ratios. Uniform wind direction distribution. Hourly wind directions are generated with a random walk process, where change in wind speed is governed by the normal distribution $N(\mu = 0°, \sigma = 15°)$.

Sensor[1]	m	IEC2 (land)		IEC1 (offshore)	
		mean	std.dev.	mean	std.dev.
Blade root lead-lag moment Mx11r	12	1.00	0.000	1.00	0.000
Blade root flap moment My11r	12	1.02	0.005	1.02	0.003
Hub lead-lag moment Mx11h	6	1.00	0.000	1.00	0.000
Hub flap moment My11h	6	1.03	0.004	1.03	0.002
Nacelle roll moment MxNf	6	1.06	0.001	1.08	0.002
Nacelle tilt moment MyNf	6	1.01	0.004	1.01	0.003
Nacelle yaw moment MzNf	6	1.01	0.005	1.01	0.004
Tower base moment Mxt0 (E-W)	4	1.05	0.01	1.02	0.004
Tower base moment Myt0 (N-S)	4	1.05	0.01	1.03	0.008
Mudline moment Mxf-20 (E-W)	4	–	–	1.01	0.004
Mudline moment Myf-20 (N-S)	4	–	–	1.02	0.008

[1]For nomenclature see appendix A.

fact that the change of wind direction is normally not taken into account. If it is, large load cycles are created because the mean load on the tower base is reversed if the wind turns 180°. This effect is less for offshore turbines, because a large part of total load is caused by waves, which produce a symmetric loading pattern. The procedure to generate artificial long time series is quite stable, as can be seen from the small standard deviations (table 4.2, all are smaller than 1%); a more important influence is the wind direction distribution. The algorithm used to generate random wind direction time histories leads to a uniform wind direction distribution.

In the probabilistic calculations it is assumed that if the right calculations (including start-stop sequences) are done, there will be no bias in results, except for the tower base bending moment. However even in the artificial histories there is some variation: $V \approx 1\%$ (except for the lead-lag moments). We will use the table figures in the calculations (influence of deviations from ideal wind speed and wind direction distributions are dealt with in section 4.3).

4.2.2   Influence of seed factors

Typically the calculation of the load spectrum was done with 2 calculations of duration 600 s at each wind speed[3]. This gives 26 load cases (see table 3.2, p33). For each calculation, random seeds are used for the generation of the wind field; this means that the turbine life equivalent loads vary: different seeds will yield different loads. To establish the coefficient of variation of the equivalent loads, 12 load cases of 600 s each, were calculated at 3, 4, 8, ..., 24, 30 m/s. Each individual wind field was normalised to yield the desired turbulence intensity level. From this collection of load cases, 100 sets of 26 independent samples were drawn, constituting 100 different realisations of the same load spectrum. Some results are given in table 4.3, together with some figures for a stall turbine published by Thomsen [207]. Obviously the coefficient of variation may be reduced by doing more calculations, for example with four times the original number all coefficients of variation decrease by a factor two. While it may turn out that the uncertainty is not large compared to others, it must be said that doing more calculations is a cheap way of reducing uncertainty; some extra reduction of variation may be achieved by doing extra calculations at wind speeds where most fatigue damage occurs.

There are various technical matters regarding the generation of turbulent wind fields, such as how many points to use, and which frequency interval, and how to handle loss of variance. However since these hardly introduce additional uncertainty, they need not concern us here. Details are discussed in appendix G. For more on the shape of the turbulence spectrum and coherence see section 4.5.2.

---

loads and actual loads would increase) no change is expected in results.

[3]With the third edition of IEC 61400-1 [93] the number of load cases was increased to at least 6 for each wind speed.

4.3 Wind speed and wind direction distributions

4.3.1 Idealised distributions

Basically one should use the measured site wind speed and direction distributions for a full load calculation. However for convenience, the combined site wind speed and wind direction distribution are approximated by simple fits:

- For land based turbines, the wind speed distribution is approximated by a Weibull fit (equation (3.1)), and all wind is assumed to come from the same direction. This introduces some conservatism in tower and foundation design (the rule of thumb is ca 10% overestimation of tower base moments). For land based turbines this is not a great problem, since the extra investment in tower and foundation is not overwhelming.

- For offshore turbines, the cost of the foundation is large, and it becomes attractive to perform a calculation that uses the combined wind speed/wind direction. Still one might want to approximate distributions from different directions by Weibull fits.

There are two reasons that the Weibull distribution fits measured distributions well. Firstly, if one assumes that the North-South and East-West wind speed are independent and normally distributed (with zero mean and equal variance), the length of the sum wind vector has a Rayleigh distribution, a special case of the Weibull distribution with shape factor $k = 2$ (Tuller [217]); often this is almost true in reality. Secondly, the Weibull distribution is really a distribution family, which can be made to fit a

Table 4.3: Coefficient of variation of fatigue damage equivalent load ranges. Weibull distributions $U = 8.5$ and 10 m/s, $k = 2$, 26 load cases of 600 s = 15,600 s. Note that Thomsen's figures are for a different total calculation time.

		This report		Thomsen [207]
Turbine type		PRVS		stall
Total time [s]		15,600		6,000
Average wind speed [m/s]		8.5	10	10
Equivalent load range	m			
Blade root lead-lag moment Mx11r	12	0.002	0.002	
Blade root flap moment My11r	12	0.014	0.007	0.027
Hub lead-lag moment Mx11h	8	0.003	0.002	
Hub flap moment My11h	8	0.018	0.011	
Nacelle driving moment MxNf	8	0.017	0.017	
Nacelle tilt moment MyNf	8	0.012	0.015	0.030
Nacelle yaw moment MzNf	8	0.010	0.010	0.029
Tower base side-side moment Mxt0	4	0.028	0.030	
Tower base fore-aft moment Myt0	4	0.031	0.029	0.058
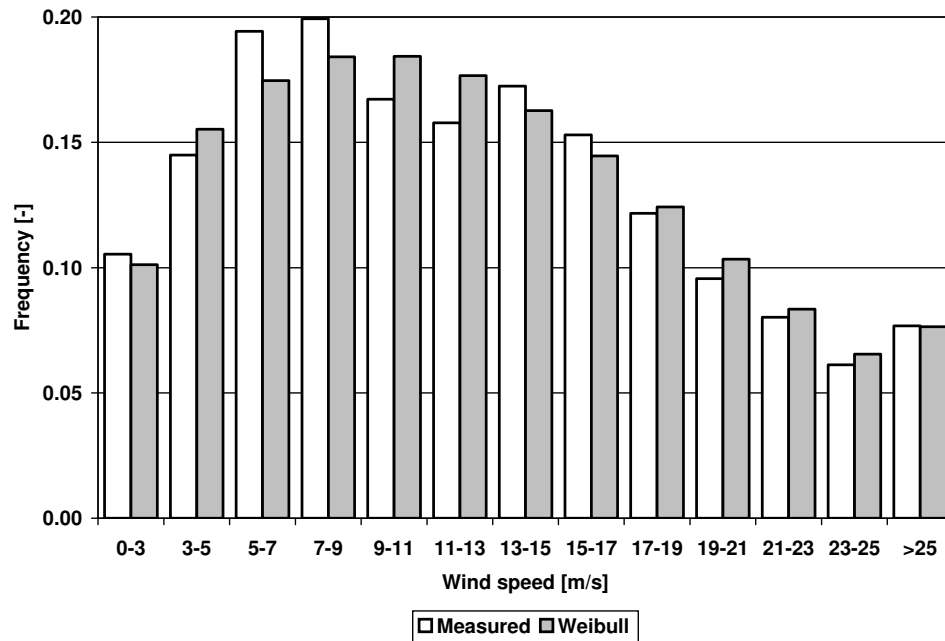
Figure 4.1: Wind speed distribution for Den Helder 1972–2002 (transformed to 70 m height) and Weibull fit. Source: KNMI.

range of different sets of measurements. After all 10-minute simulations are done, load cycle counting is done for each load case, and the numbers of cycles per load case are multiplied with a number corresponding to the number of hours at the load

Table 4.4: Normalised equivalent loads for different approximations of the wind speed and wind direction distribution. Results for the measured Den Helder distributions are set to unity.

speed		as measured	Weibull fit	as measured	Weibull fit
direction		as measured	uniform fit	unidirectional	unidirectional
eqv. load	m				
Mx11r	12	1.00	1.00	1.00	1.00
My11r	12	1.00	0.98	1.02	1.00
Mx11h	6	1.00	1.00	1.00	1.00
My11h	6	1.00	0.99	1.00	0.99
MxNf	6	1.00	1.00	0.99	1.00
MyNf	6	1.00	0.99	1.00	0.99
MzNf	6	1.00	0.99	1.00	0.99
Mxt0	4	1.00	0.94	0.55	0.52
Myt0	4	1.00	1.04	1.31	1.29
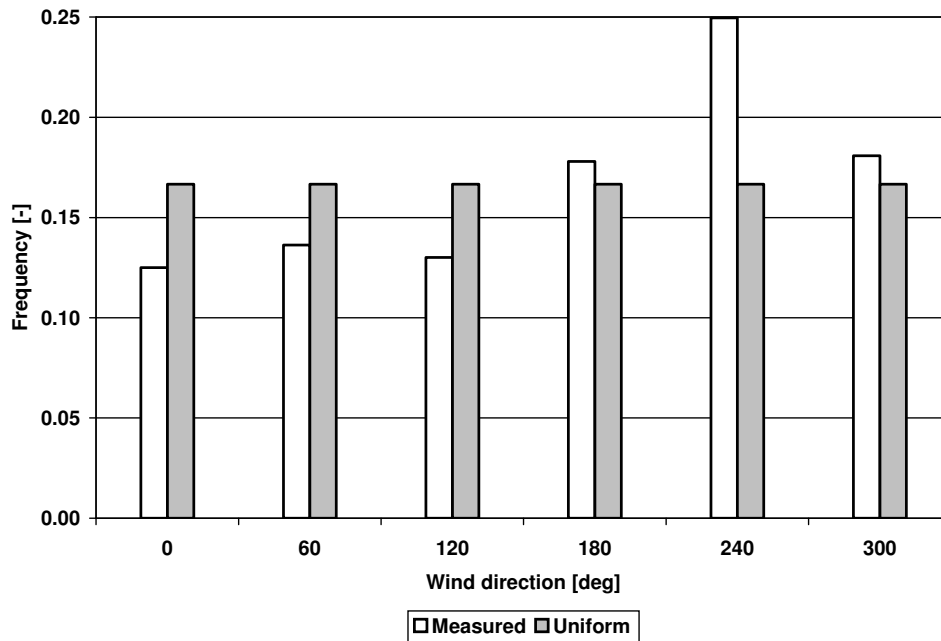
Figure 4.2: Wind direction distribution Den Helder 1972–2002 and uniform fit. Source: KNMI.

case wind speed. To see how much error is introduced by using idealised distributions we investigate a coastal site that is probably representative for North Western Europe: Den Helder (Netherlands). In figure 4.1 the wind speed distribution is shown, and in figure 4.2 the wind direction distribution. In table 4.4 some results are given for four different calculations. It is seen all loads above the yawing system are independent of the wind direction distribution used, because the head of the wind turbine follows the wind direction. Also using a Weibull fit instead of the actual distribution does not make much difference. For the tower loads we have a different situation: although the actual wind direction distribution may be approximated by a uniform distribution with reasonable accuracy, it is conservative to use unidirectional wind. For example, in case a unidirectional calculation is used for a land based turbine, the conservatism on the tower base bending moment is 1.29 relative to the measured distributions and 1.29/1.04 = 1.24 relative to the combination Weibull/uniform. In other words, the loads to be expected in reality are 0.78 and 0.81 times the calculated loads.

Even when the measured wind direction distribution is used, there is still some uncertainty: the actual wind direction distribution may deviate from the assumed (or measured) long term wind direction distribution. The question is how much this will influence tower and foundation loads.

The influence of variation in wind direction distribution was estimated as follows. First an omnidirectional calculation was done for the test turbine, with wind coming from 6 different directions (0, 60, ..., 300°). Then rainflow counts were done for bending moment in 6 wind directions; for each rainflow count a measured 1 year wind speed and direction distribution was used. Wind speeds were corrected to get the same overall average wind speed at hub height. Some results are given in table 4.5. It is seen that the coefficient of variation is small: the variation on bending moment over a 20 year period is only $V = 1\%$. This means that the actual equivalent load range over the turbine's life will be distributed with $V = 1\%$.

4.3.2 Estimation of wind speed

The scale parameter C (or the average wind speed U_{avg}) and the shape parameter k at a site are normally unknown and must be estimated. This may be done in several ways:

1. From site measurements. Sometimes wind turbines are placed close to a meteo station; in those rare cases a long term estimate is directly available. Otherwise, if it is known in advance where wind turbines are going to be placed, one may put up a measuring tower to get wind speed measurements. This is usually done for only a short period (6–12 months); however these wind data are normally not used directly, but in the Measure-Correlate-Predict procedure (see below). In the last decade alternatives for meteo masts have become avail-

Table 4.5: Coefficient of variation V of fatigue damage equivalent load ranges due to variations in wind direction distribution.

Elevation [m]	Wind direction [°]	V (1 year)	V (20 years)
Tower top	0 = NS	0.036	0.008
	60	0.024	0.005
	120	0.025	0.006
SWL+38	0 = NS	0.051	0.011
	60	0.033	0.007
	120	0.038	0.008
SWL+13	0 = NS	0.052	0.012
	60	0.034	0.008
	120	0.039	0.009
SWL	0 = NS	0.053	0.012
	60	0.033	0.007
	120	0.040	0.009
SWL–20 Mudline	0 = NS	0.047	0.011
	60	0.032	0.007
	120	0.038	0.008

able, such as SODAR (SOund Detection And Ranging) and LIDAR (LIght Detection And Ranging), which have the potential of making measurements at any height up to a few hundred meters without erecting a tower (see Antoniou [4]), and especially for offshore applications satellite measurements (see for example Hasager [83]).

2. With the Measure-Correlate-Predict (MCP) procedure (see Anderson [1] and Bass [10]), wind speeds at the site are measured during 6–12 months. Then the 10-minute or 1-hour values are correlated with one or more meteo stations nearby, and the correlation is used to predict long term site wind speed from the long term meteo station wind speed. The strength of MCP is that no assumptions about wind or terrain need to be made, except that there *is* a correlation between the two sites.

3. With the Wind Atlas Analysis and Application Program procedure (WAsP, Troen [214]). The two main ideas of WAsP are:

   (a) The wind speed at greater heights is independent of the terrain roughness.

   (b) There is a simple relation (for example a logarithmic law dependent on terrain roughness) between wind speed at higher altitudes and close to ground level.

   This makes it possible to find the wind speed at a site by first transforming the measured wind speed up (at the meteo station) and then down again (at the site). The reason that WAsP works rather well is that there is a good chance that any error introduced in the up transform is compensated by a corresponding error in the down transform.

4. With a large scale Navier-Stokes calculation combined with WAsP. This is an extension of WAsP. Instead of relying on wind speeds measured at 10 m height, high altitude wind speed data are used in combination with model flow calculations. The wind speeds at turbine hub height are found by correcting model wind speeds with WAsP procedures.

5. With a full Navier-Stokes calculation. Measured wind speeds at several sites are used for a Navier-Stokes calculation for a limited domain around the wind turbine site. A problem is that many good wind speed measurements are needed at the boundary of the domain. Even then it is hard to see how this procedure can be more accurate than (for example) MCP.

6. With a wind tunnel experiment on a terrain model. This procedure is the experimental analogon of procedure no 5.

Since MCP and WAsP are the industry standard, we will focus on these two procedures; at present there is no evidence that other procedures are significantly better. In addition something will be said about satellite measurements.

WAsP. A primary source of WAsP data is the European Wind Atlas [214], which provides tests of the procedure for most countries in the European Union. Table 4.6 gives a summary of results. No systematic error was found, but the coefficient of variation of the cross prediction distribution varies from $V = 0.03$ for the North Sea (good) through $V = 0.06$ for flat terrain (acceptable) to values as high as $V = 0.14$–0.25 for complex mountainous terrain (useless). In some cases there are obvious explanations for discrepancies, and predictions may be improved by taking only stations from the right group. The problem is that it is not always clear that this grouping can be done a priori. Some results from other sources are given in table 4.7. These confirm the findings from the European Wind Atlas.

MCP. On Measure-Correlate-Predict methods, good references are Anderson [1, 2] and Bass [10], in which 9 different MCP-methods are evaluated. The main conclusions of Bass [10, p69] are: *'In terms of overall average bias error, the simple sector ratio method is the best.'* [4] and *'For the best class A method, 95% of all*

---

[4]Some authors prefer variations of the basic method, see for example King [107] and Woods [237]

Table 4.6: Inaccuracy of cross predictions with WAsP. Source: European Wind Atlas [214]. Values are coefficients of variation of the ratio predicted/measured.

EWA ref	region[1]	all	N_S	best group	N_S
9.2	Ireland	0.086	9	0.015	3
9.3	United Kingdom and Ireland	0.090	8	0.081	4
9.4	United Kingdom and Scotland	0.100	6	0.054	2
9.5	United Kingdom	0.078	9	0.058	2
9.6	Denmark	0.068	9	0.026	3
9.7	Germany	0.041	7	0.031	5
9.8	Germany	0.119	6	0.041	3
9.9	North Sea	0.033	6		
9.10	Netherlands	0.054	6	0.042	5
9.11	Belgium, Luxembourg, Netherlands	0.060	7	0.033	6
9.12	France and Belgium	0.098	9	0.046	4
9.13	France, Germany, Luxembourg	0.045	8		
9.14	France (South West)	0.129	7	0.029	5
9.15	France (Massif Central)	0.077	4		
9.16	France (Massif Central/Rhone/Med)	0.246	9		
9.22	Spain (Canary Islands)	0.158	6		
9.25	Portugal	0.169	5	0.044	2
9.28	Italy	0.144	6	0.078	3
9.30	Greece	0.147	7		
	Average	0.102		0.044	
	Best	0.033		0.015	
	Worst	0.246		0.081	

[1]Regions considered to validate WAsP are 'geographically natural' and may include (parts of) different countries.

bias errors, over a range of climatologies and terrain, will lie within ±10% of the true value.'. If we assume that the errors are normally distributed, this means that the coefficient of variation of the ratio predicted/measured is $V = 0.05$. These results are confirmed by other sources (see table 4.8).

For this report, some additional calculations were done for the Netherlands, for which the Royal Netherlands Meteorological Institute (KNMI) makes hourly wind speeds available for all meteo stations. All wind speeds are potential wind speeds i.e. normalised to 10 m measuring height over open terrain (terrain roughness $z_0 = 0.03$ m). A typical example is given in figure 4.3 (next page). In this case the long term Schiphol wind speed is predicted 47 times, in each case with one year of hourly data from IJmuiden; wind speeds from all directions are combined. If we perform the same procedure for all 1722 station pairs (30,020 yearly wind speed pairs for

Table 4.7: Inaccuracy of wind speed estimates with WAsP from various sources.

Reference, location	Stations N_S	Predictions N_P	Mean ratio pred/msrd	COV V
Barthelmie [8]				
Nysted (DK)	1	2	0.93	-
Omo Stalgrunde (DK)	1	2	1.06	-
Berge [12]				
Norway	5	15	1.02	0.08
Frank [66]				
Pyhatunturi (SF)	1	1	0.87	-
Sodankyld (SF)	1	1	1.22	-
Hollis [92]				
United Kingdom	26	26	1.00	0.15
Landberg [117]				
Portugal	5	15	1.01	0.13

Table 4.8: Inaccuracy of wind speed estimates with MCP.

Reference, location	Station pairs	Predictions N_P	Mean Ratio pred/msrd	COV V
Anderson [1]	(53 sites)	unknown	1.00	0.035
Bass [10]	82	unknown	1.00	0.05
Barthelmie [8]				
Nysted (DK)	1	2	0.91	-
Omo Stalgrunde (DK)	1	2	1.04	-
This report				
Netherlands	1,722	30,020	1.00	0.06
Landberg				
Portugal	5	unknown	0.90	0.06
Hollis [92]				
United Kingdom	21	21	0.98	0.08

IJmuiden-Schiphol (d=23 km, Mean=0.996, COV=7.6%)
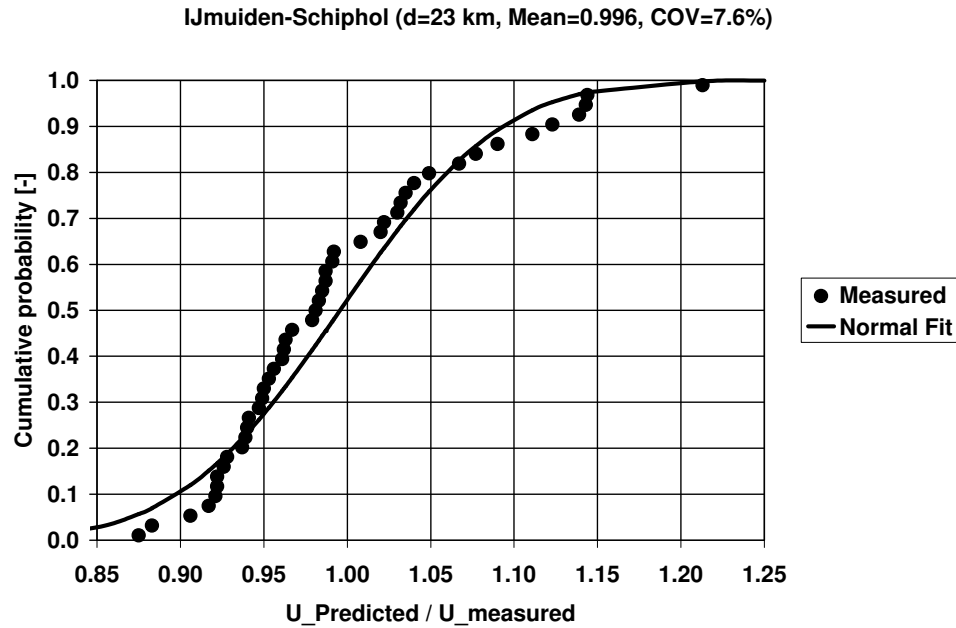
Figure 4.3: MCP predictions of Schiphol long term wind speed with IJmuiden data.

predictions), we find that the average prediction ratio converges to unity (as it should: the whole procedure is symmetric), and that the coefficient of variation on predicted wind speed/actual wind speed ratios is $V = 0.06$. The distribution of ratios fits a normal distribution very well, which means that 90% of all predictions are in the interval 0.90–1.10. This is consistent with Bass [10] who found $V = 0.05$ (note that overall wind speed ratios were used for the Dutch predictions instead of the better sector ratios used by Bass).

With the available data it was investigated whether predictions became better with smaller distance. The result is seen in figure 4.4 where the coefficients of variation of all cross predictions for all 1722 station pairs are plotted. Surprisingly, predictions do not improve at all with smaller distances; in fact there is zero correlation with distance. This probably has to do with the fact that all local wind speeds are correlated with the same geostrophic wind, and that wind speed variations are due to local terrain features. If this is true, this would make it possible to improve predictions by simply using more reference stations (this was not checked).

Satellite measurements. Wind speeds over water can be measured from a satellite with the Synthetic Aperture Radar (SAR), which relies on measuring how much radiation is back scattered from the sea surface, something that depends on surface roughness. The roughness in turn is correlated to wind speed at (for example) 10 m
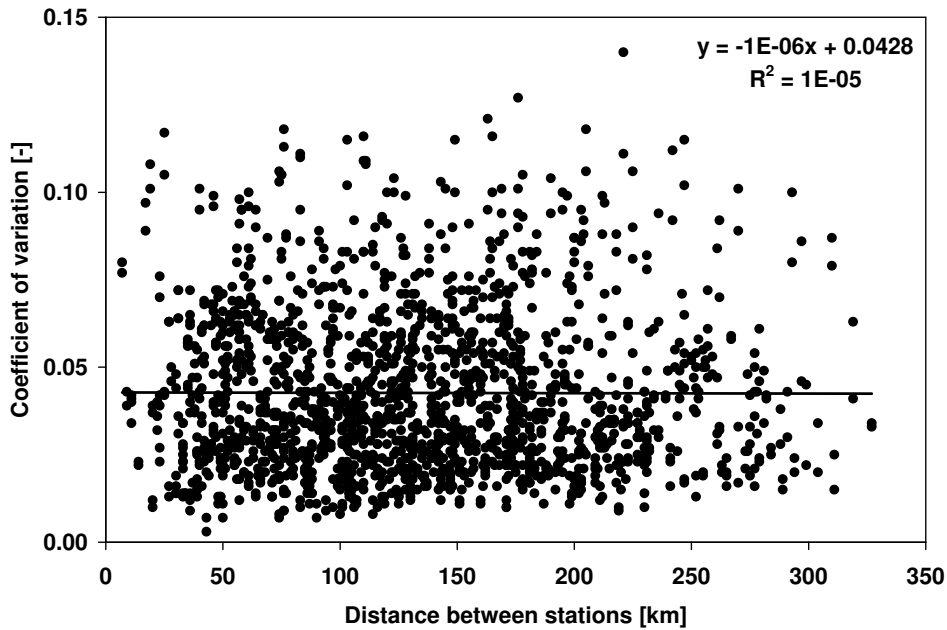
Figure 4.4: Coefficient of variation of ratio predicted / measured wind speed

height. By calibrating against tower measurements, near perfect long term averages can be obtained from satellite measurements in spite of the fact that the accuracy of individual measurements is not very good (± 1 m/s). Unfortunately this holds for wind speeds at 10 m over the water surface, and these values must still be converted to hub height wind speeds (see section 4.3.3). For further information on satellite measurements see Barthelmie [7, 9], Hasager [82, 83] and Pryor [170].

In summary: in the author's view MCP-methods are superior over WAsP for predicting wind speeds at (ca) 10 m height. They yield a consistent coefficient of variation $V \simeq 0.05$ on the ratio predicted/actual wind speed over a range of terrain types. With WAsP the coefficient of variation may be as high as $V = 0.25$, depending on terrain type. For offshore sites satellite measurements may be a good alternative.

4.3.3 Transformation to hub height

The most common methods described in the previous section (MCP, WAsP, SAR) provide us with an estimate of the wind speed at 10 m height. From this wind speed the wind speed at rotor hub height (say 70–120 m) must be found[5]. For the wind

---

[5]WAsP can provide estimates at any height (see for example Lange [118]), but the mechanism to compensate errors in the height transform does not work if the heights at the two sites differ too much,

speed as function of height there is the well known equation (see e.g. Lange [118]):

$$\frac{U(z_2)}{U(z_1)} = \frac{\ln (z_2/z_0) - \Psi (z_2/L)}{\ln (z_1/z_0) - \Psi (z_1/L)} \tag{4.1}$$

where:

L	Monin-Obukhov length [m]
U	wind speed [m/s]
z	height [m]
z_0	terrain roughness [m]
Ψ	stability function [-]

What we see is the logarithmic profile dependent on terrain roughness z_0 plus an atmospheric stability correction Ψ dependent on the ratio of height z and Monin-Obukhov length L. Turbulence may be produced by shear (speed differences) or by buoyancy (density differences); the length L is the height at which shear and buoyancy produce the same amount of turbulent kinetic energy. While equation (4.1) is based solidly in physics, the problem is that the Monin-Obukhov length L must be estimated, which can only be done indirectly from temperatures.

As long as wind speeds are high enough (above 6 m/s or so) thermal effects play no role above land, and neutrality may be assumed ($\Psi = 0$), at least for the lowest 50 m or so (Wieringa [235, p37]). Then the wind speed follows a logarithmic profile determined by terrain roughness z_0 and equation (4.1) reduces to equation (3.9), repeated here:

$$\frac{U(z_2)}{U(z_1)} = \frac{\ln (z_2/z_0)}{\ln (z_1/z_0)} \tag{4.2}$$

Although the wind speed height profile at any particular time may differ considerably from this equation, as an average it is not a bad estimator (as will be shown). The roughness of the terrain z_0 may be estimated with the Petersen classification or from measurements of turbulence intensity I at some reference height z_r, using:

$$I(z_r) = \frac{1}{\ln(z_r/z_0)} \tag{4.3}$$

which gives for the 'objective terrain roughness':

$$z_0 = z_r \exp(-1/I(z_r)) \tag{4.4}$$

For complex terrain it is not possible to use a simple wind speed profile law; the best solution is probably the use of Navier-Stokes calculations. However for the moment we ignore this and try to use the turbulence intensity method anyway.

---

so a larger error must be expected. For the probabilistic calculations presented in this work, it is assumed that prediction at 10 m height is followed by a height transform.
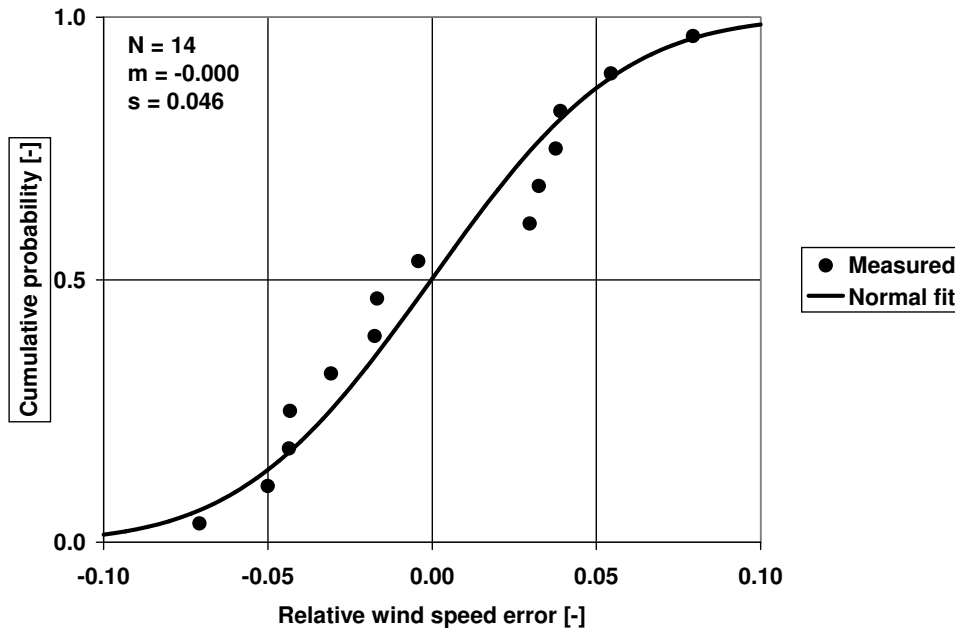
Figure 4.5: Prediction of wind speed at hub height. There are 8 sites of which 2 inland, 2 coastal, 3 offshore and 1 complex; prediction heights are between 60 and 116 m. For the prediction of the speed ratio the average of all wind speeds between 10 and 20 m/s (at 10 m height) were used. Source: Downey [48]. For all data see table D.7.

Some predictions are shown in figure 4.5. Downey [48] extracted data from the database <u>winddata.com</u> for all eight sites that have wind speed measurements above 60 m height. The terrain roughness was established with equation (4.4), and a logarithmic profile assumed. It appears that the mean of all 14 predictions is zero, giving an indication that on average the logarithmic profile is correct; the standard deviation on the ratio measured/predicted is $\sigma = 0.046$. Maybe predictions could be improved, for example by making separate predictions for each sector and for individual wind speed bins; however the figure found is probably a conservative upper bound.

So far we have ignored the fact that offshore applications are different from land sites. Obvious differences are the absence of a fixed terrain roughness and the non-neutrality of the atmosphere.

Terrain roughness is not a big problem: to estimate 'terrain roughness' there is the Charnock equation (see section 4.4), which makes the sea surface roughness dependent on wind speed, but maintains the logarithmic profile. Unfortunately several authors (Barthelmie [7], Frank [65] and Lange [118]) conclude that possible errors in roughness estimate are less important than atmospheric stability and stratification.

In investigations for four different Danish offshore sites, Motta [148] found the following figures for stability (table 4.9), which make it clear that neutrality cannot be taken for granted.

Lange [118] tried to predict 10 minute average wind speeds at 50 m height using data gathered at 10 m height. Using variations of equation (4.1) he found biased (under)predictions of 91–99% (see table 4.10), which however may be improved if his empirical correction is applied.

Motta [148] found corresponding results for Vindeby, Rødsand and Omø. A logarithmic profile (based on Charnock) tends to underpredict, but if a stability correction is applied the prediction ratio is close to unity.

McQueen [143] predicted wind speed at 30 m above sea level directly using 13 different methods, for example WAsP and numerical weather prediction methods. It appears that WAsP (with stability correction) is doing best with errors of 3–10%, while most other methods are performing worse.

4.3.4   Yearly variation

Even if the long term wind speed U and shape factor k known, one must still consider variations in yearly mean. Fortunately, the mean for a period of L years has standard deviation that is reduced by a factor $\sqrt{L}$ compared to the yearly value. A summary of data found is given in tables 4.11 and 4.12. Stations are in coastal and flat terrain (see appendix D). The coefficient of variation for 20 years wind speed was found to be $V_U = 0.015$, while $V_k = 0.015$ for the 20 years average Weibull shape factor[6].

---

[6]For data for the Netherlands it was found that the shape factor k is weakly correlated with wind speed ($r \sim 0.3$, see table D.1); however since this is a small value and influence of k on loads is minimal, U and k are assumed to be independent anyway.

Table 4.9: Average stability conditions for four Danish offshore sites. Source: Motta [148].

Class	Monin-Obukhov length L [m]	Frequency [%]
very stable	$0 < L < 200$	23
stable	$200 < L < 1000$	16
neutral	$|L| > 1000$	32
unstable	$-1000 < L < -200$	20
very unstable	$-200 < L < 0$	9

Table 4.10: Offshore wind speed predictions for Rødsand (Nysted) at 50 m height from measurements at 10 m height using Monin-Obukhov theory. Source: Lange [118, p77]

	all data	stable data	unstable data
mean prediction U_{pred}/U_{msr} [-]	0.94–0.98	0.91–0.96	0.97–0.99
rms [-]	0.03–0.05	0.03–0.06	0.02–0.03

4.4 Turbulence intensity

4.4.1 Introduction

The turbulence σ_U is defined as:

$$\sigma_U^2 = \frac{1}{T} \int_T \left(U(t) - \overline{U} \right)^2 dt \tag{4.5}$$

and the turbulence intensity is:

$$I = \frac{\sigma_U}{\overline{U}} \tag{4.6}$$

where $U(t)$ is the wind speed measured during an interval T, for example 10 minutes[7]. Because turbulence at wind speeds above ca 5 m/s is primarily caused by terrain roughness, variations in yearly average turbulence intensity are not to be expected (there are seasonal variations of course in case there is significant vegetation). However the turbulence is dependent on average wind speed, and moreover even a plot of 10 minute turbulence values for the same wind speed will show random variation. Hansen [79] investigated 6 different sites (offshore, mountainous, flat open

---

[7]Some authors prefer to detrend the wind speed before calculating the turbulence (i.e. subtract for example the least squares linear fit from the measured signal). In most cases the difference with the turbulence according to equation (4.5) is small.

Table 4.11: Coefficient of variation for yearly average wind speed and Weibull shape factor.

region	reference	average wind speed U		shape factor k	
		1 year	20 years	1 year	20 years
Netherlands	table D.1	0.062	0.014	0.065	0.015
Denmark	table D.2	0.047	0.011	-	-
Northern Germany	table D.3	0.065	0.015	0.073	0.016

Table 4.12: Coefficient of variation for average wind speed. Source: Pryor [169]. Note: Pryor gives coefficients of variation for the energy index, which is proportional to wind speed to the third power; these have to be divided by ~ 3 to find the corresponding number for wind speed (see table D.4).

Country	NCEP/NCAR 1960–1989		ECMWF 1990–2001	
	1 year	20 years	1 year	20 years
Denmark	0.034	0.008	0.031	0.007
Norway	0.030	0.007	0.043	0.010
Sweden	0.037	0.008	0.032	0.007
Finland	0.029	0.007	0.035	0.008
Baltic States	0.041	0.009	0.040	0.009
Iceland	0.030	0.007	0.041	0.009

terrain; measuring heights from 20 to 200 m), and found that the turbulence distribution at one particular wind speed can be well approximated as being lognormal, with distribution parameters M and S dependent on wind speed, height and terrain roughness:

$$F(\sigma) = N\left(\frac{\ln \sigma - M}{S}\right) \tag{4.7}$$

The mean and standard deviation of the turbulence distribution are found with:

$$\mu_\sigma = \exp(M + \frac{S^2}{2}) \tag{4.8}$$

$$\sigma_\sigma = \mu_\sigma \sqrt{\exp(S^2) - 1} \tag{4.9}$$

For offshore sites Vindeby and Gedser the suitability of the lognormal distribution was confirmed by Larsen [121], and DNV found the same result for the Danish coastal site Lammefjord [47, p34]. For heights that are relevant for wind turbines (50–200 m) we find: $M = 1.5$–2.3 and $S = 0.2$–0.3 ($\approx V$) for the representative wind speed 15 m/s (consult Hansen [79] for detailed results). The question now is how accurately we can predict the average turbulence intensity.

4.4.2   Estimation of average turbulence

To repeat, for flat uniform terrain the relation between turbulence intensity I at hub height H and terrain roughness z_0 is approximately:

$$I(H) = \frac{1}{\ln(H/z_0)} \tag{4.10}$$

The terrain roughness may be found with equation (4.4). For offshore, Frandsen (in IEC 61400-3 [94]) proposes the following. If we combine the well known friction velocity equation:

$$U(H) = \frac{u_*}{\kappa} \ln \frac{H}{z_0} \tag{4.11}$$

with the Charnock equation (Charnock [35]):

$$z_0 = A\frac{u_*^2}{g} \tag{4.12}$$

we get an implicit relation for the friction velocity u_*:

$$u_* \ln \frac{gH}{Au_*^2} = \kappa U(H) \tag{4.13}$$

where $A = 0.011$ for coastal waters, $\kappa \approx 0.4$, $g = 9.81$ m/s, and the wind speed $U(H)$ and hub height H are known. The mean turbulence σ is estimated with:

$$\sigma \approx 2.5 u_* \tag{4.14}$$

As approximation of the fatigue damage equivalent turbulence, the 90% fractile is estimated by adding 1.3 times the standard deviation to the mean. If the standard IEC value [93] for the standard deviation of the turbulence σ_σ is taken:

$$\sigma_{90\%} = 2.5 u_* + 1.3 \times \sigma_\sigma \tag{4.15}$$

Independent of wind speed, the value for σ_σ according to IEC 61400-1 is (in [m/s]):

$$\sigma_\sigma = 1.4 \, I_{ref} \tag{4.16}$$

Hence:

$$\sigma_{90\%} = 2.5 u_* + 1.3 \times (1.4 \, I_{ref}) \tag{4.17}$$

The constant I_{ref} is the mean turbulence intensity at hub height at 15 m/s. The procedure gives a reasonable estimate in a qualitative sense: in particular it correctly gives increasing turbulence intensity at higher wind speeds over water. The only problem is that the constant A is not very well known. Therefore, to estimate the mean turbulence intensity at hub height $I(H)$ (onshore or offshore) we combine equations (4.4) and (4.10), which leads to a relation between turbulence intensity at hub height $I(H)$ and at (low) reference height $I(z_r)$:

$$I(H) = \frac{I(z_r)}{1 + I(z_r)\ln(H/z_r)} \tag{4.18}$$

The results of this procedure are shown in figure 4.6 (next page), from which we see that the average bias is +0.017 (we overestimate) and the standard deviation is $\sigma_I = 0.008$.

4.4.3 Influence on loads

If the turbulence distribution (conditional on wind speed) is known, it is possible to make a load calculation for every combination of 10 minute wind speed and turbulence. However it is more economical to use one representative value for the turbulence, that ideally produces the same equivalent load range (or fatigue damage) as a calculation with a large number of different turbulence values.

The first definition of representative turbulence we consider is the 90% fractile value specified by IEC 61400-1. Because of the lognormal assumption and standard deviation according to equation (4.16), the mean turbulence is:

$$\mu_\sigma = I_{ref} \left(0.75 U + c_\mu \right) \tag{4.19}$$
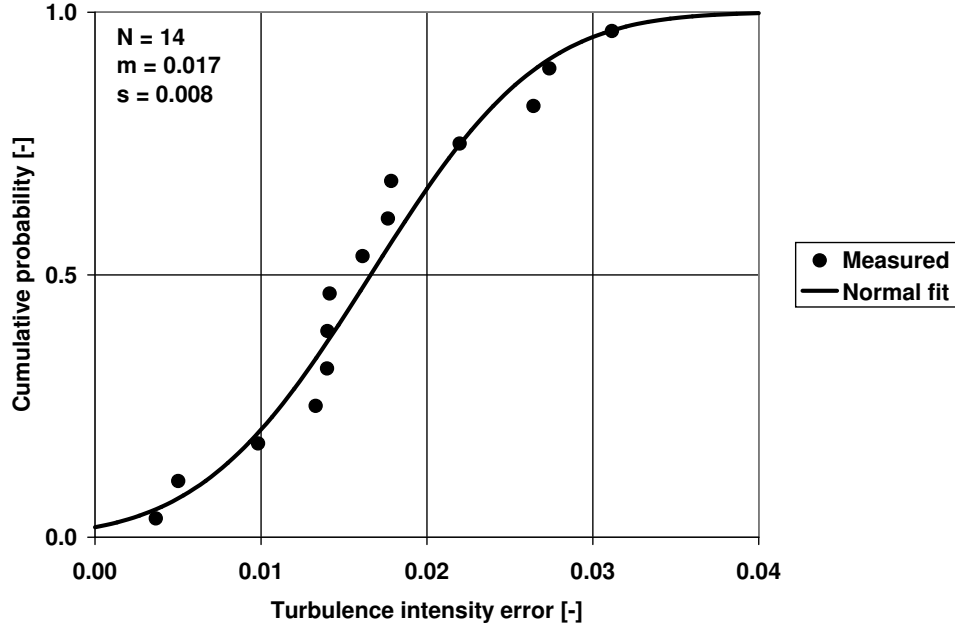
Figure 4.6: Prediction of turbulence intensity at hub height. There are 8 sites of which 2 inland, 2 coastal, 3 offshore and 1 complex; prediction heights are between 60 and 116 m. For the prediction of the turbulence intensity all wind speeds between 10 and 20 m/s (at 10 m height) were used. Source: Downey [48]. For all data see table D.7.

with $I_{ref} = 0.12$, 0.14, 0.16 and $c_\mu = 3.8$ m/s. The 90% fractile representative turbulence is:

$$\sigma_{90\%} = I_{ref}\left(0.75U + c_{90\%}\right) \tag{4.20}$$

with $c_{90\%} = 5.6$ m/s. The turbulence standard deviation is (5.6 – 3.8)/1.4 = 1.3 standard deviations above the mean μ_σ. The prescribed turbulence intensity $I_{90\%}$ is:

$$I_{90\%} = \frac{\sigma_{90\%}}{U} = \frac{I_{ref}\left(0.75U + c_{90\%}\right)}{U} \tag{4.21}$$

The second definition of representative turbulence often used is the so-called equivalent turbulence $\widehat{\sigma}_{eq}$ (we give it a hat because it is in fact an estimate of the exact equivalent turbulence that would produce exactly the same loads as a full calculation would do):

$$\widehat{\sigma}_{eq} = \left[\int\limits_0^\infty \sigma^m f(\sigma)d\sigma\right]^{1/m} \tag{4.22}$$

where m is the exponent of the relevant component's S-N curve, and $f(\sigma)$ is the marginal distribution of the turbulence. With the lognormal distribution according to equation (4.7) one finds::

$$\widehat{\sigma}_{eq} = \left[\exp(mM + \frac{1}{2}m^2 S^2) \right]^{1/m} = \exp(M + \frac{m}{2}S^2) \tag{4.23}$$

The corresponding approximate equivalent load is:

$$\widehat{\Delta F}_{eq} = \Delta F_{eq}(\widehat{\sigma}_{eq}) \tag{4.24}$$

The find out how conservative the two definitions of representative turbulence are, we calculate the exact equivalent load. From load calculations it appears that in good approximation the equivalent load range at a given wind speed varies linearly with turbulence σ:

$$\Delta F_{eq}(\sigma) = a\sigma + b \tag{4.25}$$

This is so because the aerodynamic loads are (in first approximation) proportional to the square of the relative wind speed U_{rel} seen by a blade:

$$F \propto U_{rel}^2 \tag{4.26}$$

The relative speed can be written as a mean speed multiplied by one plus a fraction s that is characteristic for the turbulence σ. Because most of the relative speed is due to the speed of the blade itself (which is constant) and not to the wind speed, the fraction s is small and:

$$F \propto U_{rel}^2 = \overline{U}_{rel}^2(1+s)^2 \approx \overline{U}_{rel}^2(1+2s) \tag{4.27}$$

If equation (4.25) holds, the exact equivalent load $\Delta F_{eq,x}$ at a given average wind speed is:

$$\Delta F_{eq,x} = \left[\int_0^\infty f(\sigma)\Delta F_{eq}^m(\sigma)d\sigma \right]^{1/m} = \left[\int_0^\infty f(\sigma)(a\sigma + b)^m d\sigma \right]^{1/m} \tag{4.28}$$

with $f(\sigma)$ being the marginal turbulence distribution. This integral can be solved analytically (appendix C.4). The corresponding exact equivalent turbulence based on the load integral σ_{eq} that would have given $\Delta F_{eq,x}$ is:

$$\sigma_{eq} = \frac{\Delta F_{eq,x} - b}{a} \tag{4.29}$$

For wind turbine loads it turns out that the ratio between the correct calculation based on loads and the approximate calculation based on turbulence is close to unity:

$$\frac{\Delta F_{eq,x}}{\widehat{\Delta F}_{eq}} = \frac{\left[\int\limits_0^\infty f(\sigma)(a\sigma + b)^m d\sigma\right]^{1/m}}{a\left[\int\limits_0^\infty \sigma^m f(\sigma) d\sigma\right]^{1/m} + b} \approx 1 \tag{4.30}$$

The ratio is exactly 1 if either $a = 0$ (loads independent of turbulence) or $b = 0$ (loads proportional to turbulence), but also if the turbulence distribution is narrow. These conditions are satisfied for all wind speeds larger than 5 m/s.

In figures 4.7 and 4.8 it is seen that it is conservative to use equivalent turbulence intensity (turbulence divided by mean wind speed); the largest deviations occur at low wind speeds. Fortunately one does not need to worry about this, because almost all turbulence dependent fatigue damage occurs for wind speeds between 10 and 20 m/s (see table 4.13). In cases where there is significant fatigue damage for $U < 10$ m/s, such as the blade root lead lag moment, the load is largely independent of turbulence, so it does not matter much which turbulence value is used.

The IEC 90% turbulence intensity value is slightly conservative (approximately 0.01–0.02, say if the exact value is $I = 0.15$ the 90% fractile is $I = 0.165$). Again the largest deviations from the correct approach occur at low wind speeds where no fatigue damage is incurred (see table 4.13). A detailed calculation in appendix C.4 shows that equation (4.23) is a good estimator of the equivalent turbulence (conservatism less than 0.01).

Table 4.13: Fatigue damage distributions over wind speed intervals [%].

IEC Class I	slope m	wind speed U [m/s]		
		<10	10–25	>25
Blade lead-lag moment Mx11r	12	21	79	0
Hub lead-lag moment Mx11h	8	25	75	0
Blade flap moment My11r	12	0	100	0
Hub flap moment My11h	8	2	98	0
Nacelle roll moment MxNr	8	12	88	0
Nacelle tilt moment MyNf	8	1	99	0
Nacelle yaw moment MzNf	8	0	100	0
Tower base side-side moment Mxt0	4	1	27	72
Tower base fore-aft moment Myt0	4	2	98	0
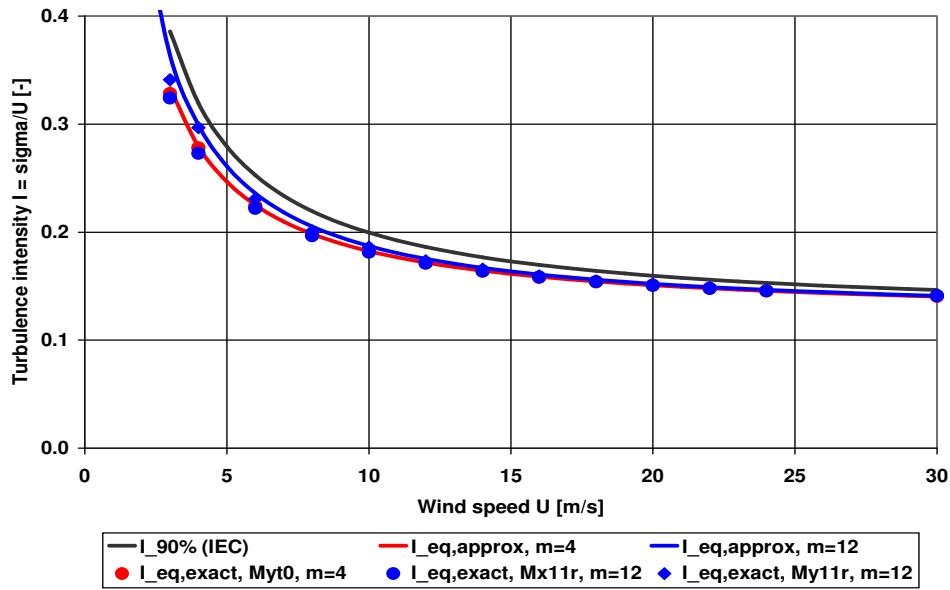
Figure 4.7: Comparison of IEC turbulence intensity $I_{90\%}$ and approximately equivalent turbulence intensity $\widehat{I}_{eq}$ with exact equivalent turbulence intensity $I_{eq,exact}$ found with load calculations. Wind regime IEC class A with $I_{ref} = 0.16$.
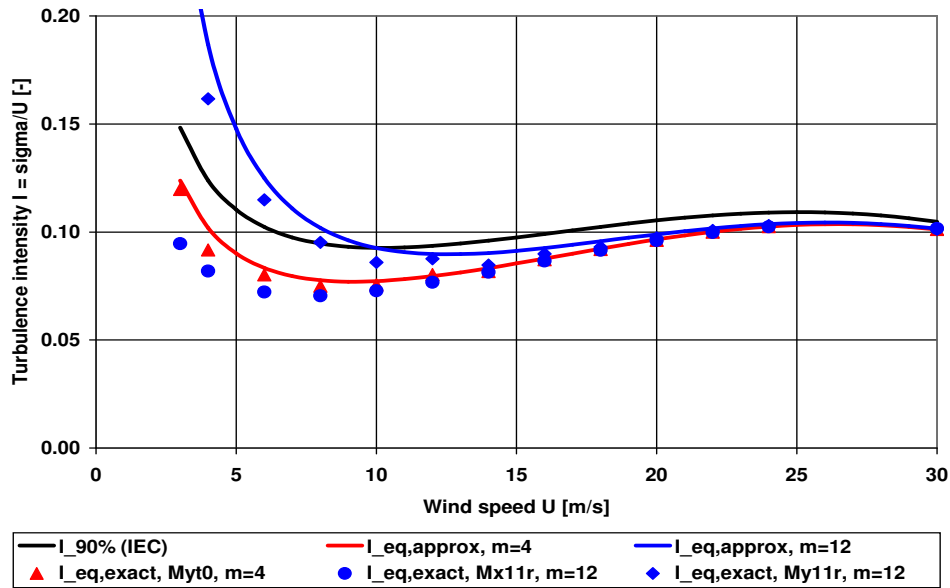
Figure 4.8: Comparison of IEC turbulence intensity $I_{90\%}$ and approximately equivalent turbulence intensity $\widehat{I}_{eq}$ with exact equivalent turbulence intensity $I_{eq,exact}$ found with load calculations. Wind regime: Vindeby.

4.5 Wind field

4.5.1 Introduction

The IEC 61400-1 standard allows the use of different methods to generate turbulent wind fields. The methods most commonly used are the Sandia method, developed by Veers [218] (see appendix G.2) and the Mann method, developed by Mann [133, 134, 138] (see appendix G.5). Both methods go back on the work of Shinozuka and Jan [190], who seem to have been the first to propose to write a random signal as a sum of sinusoids with random amplitudes or random phase angles.

There is no doubt that the Veers method is the easiest. However objections raised against this method are:

1. Wind speed components u and w are uncorrelated in the generated wind field (while in reality they are).

2. There is no mass conservation.

3. The Navier-Stokes equations are not satisfied.

4. Coherence functions are not in the model, but must be introduced manually.
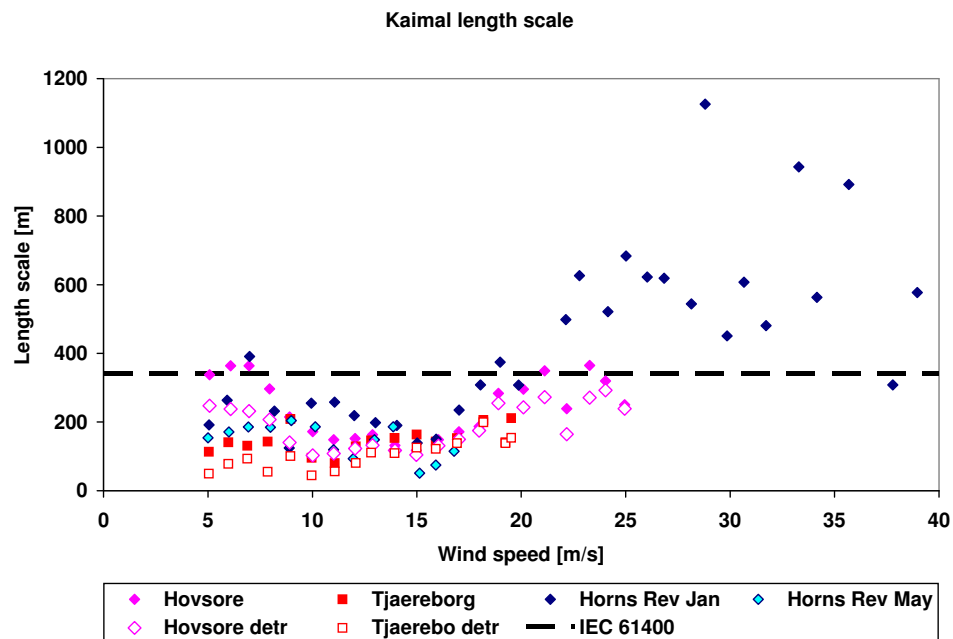
Figure 4.9: Length scales for Kaimal spectrum found from wind speed measurements at three different locations

It was shown by Veldkamp [223] that problem 1. is unimportant: the Veers wind fields can be modified to have the right (u, w) coherence (see appendix G.3). However loads resulting from wind fields having the correct (u, w) coherence are indistinguishable from those resulting from zero coherence wind fields. This is perhaps not surprising since the wind speed in u direction is by far the most important driver for loads (80–90%).

It is not known how important problems 2, 3 and 4 are. Various load verifications were done with Veers wind and Mann wind (within Vestas), but no consistent pattern emerged.

Nevertheless, all four problems do not exist in the Mann method. Mass conservation and the (linearised) Navier Stokes equations are inherent parts of the method, and all coherence functions are automatically generated, as well as the right turbulence intensity ratios. The only input parameter for the program is a wind shear number. The method can also be extended to include other boundary conditions, for example with the requirement that vertical speed is zero at ground level.

A nice feature of the Veers method is its stepwise build up, which makes it easy to incorporate measured (or otherwise prescribed) wind directly into the generated turbulence field (see appendix G.4 and Bierbooms and Veldkamp [14]). In the Mann method the same things can be done, but involving more complex mathematics (Nielsen [155]).

4.5.2 Spectrum

For open flat terrain the Kaimal spectrum in the IEC 61400-1 formulation is normally used. The Kaimal spectrum is based on extensive measurements done by Kaimal [98,99] in Kansas at 5.66, 11.3 and 22.6 m height over open terrain. The IEC equation for the spectrum is (for the 3 directions $k = u, v, w$):

$$\frac{S(f)}{\sigma_k^2} = \frac{4L_k/U}{(1 + 6fL_k/U)^{5/3}} \tag{4.31}$$

Here f is the frequency, L_k is a length scale, U is the average wind speed in wind direction and σ_k is the turbulence. There is only one free parameter in the Kaimal spectrum: the length scale L_k. For the most important spectrum (u, in the direction of the wind speed U) IEC 61400-1 prescribes that length scale $L_k = L_u = 340$ m be used for heights above 60 m. Actually curve fits for measured spectra yield values that are somewhat lower, at least for wind speeds up to 25 m/s (see figure 4.9).

It is difficult to find the length scale from a fit to a measured spectrum because the value found is very dependent on the variance at low frequencies (where the spectral density $S(f) \to 4L_k/U$), which in turn depends on the type of windowing used, and whether or not the signal is detrended. The problem is solved here (to some extent) by using the average of many unsmoothed spectra. In the Mann model there are two adjustable parameters: a length scale L_M and a shear parameter Γ.

Of these, the length scale shifts the spectral energy to higher or lower frequencies, while the shear parameter determines the spectral shape. If it is zero, the von Kármán isotropic spectrum appears, and if it is set to 3.9, the Kaimal spectrum is recovered, with –rather convincingly– the correct turbulence ratios for the three wind speed components[8]. Mann [133] derived best fit values for a few sites and spectra (see table 4.14). It is noted that the shear parameters found by Mann are less than the value that is the best fit for the Kaimal spectrum ($\Gamma = 3.9$). This is probably due to the fact that Kaimal's measurements were done at small heights, where shear is more pronounced than at current wind turbine hub heights (50–100 m).

A number of other authors have derived spectrum formulations: for example von Kármán [101], ESDU [56–59], Morfiadakis [147], Smedman [192], Tieleman [213]. However all of these spectra have similar shapes, and may be approximated by the Kaimal type spectrum with suitable length scale.

4.5.3   Coherence function

A disadvantage of the Veers method is the coherence function must be input independently of the spectrum. This is not the case in the Mann method, where the coherence functions appear automatically, and are always consistent. Mann found good correspondence with measurements at the Great Belt [138]. Larsen and Hansen [122] investigated a further 8 sites; on the basis of their data they derive an empirical model for exponential decay, and they conclude that the Mann coherence is closest to their measurements,

From the probabilistic perspective it is best to use Mann's shear parameter as stochastic variable, because it controls the spectral shape and the coherence functions in a consistent way, taking into account the fact that they are correlated.

On the other hand the independence of spectral shape and coherence function in the Veers method gives us the opportunity to investigate the influence of both parameters (length scale and decay parameter) separately (should we want to).

---

[8]As a matter of fact, the dependence of turbulence ratios on the shear parameter Γ makes it possible to estimate shear directly from the measured standard deviations ($\sigma_u, \sigma_v, \sigma_w$) without knowing the spectra.

Table 4.14: Mann length scale and shear parameter for three different locations. The Kaimal length scale is for the Kaimal spectrum that fits Mann's best. Source: Mann [134]; length scales derived by the author.

Site/spectrum	character	shear parameters	Length scale [m]	
			Mann	Kaimal
Great Belt	offshore	3.2	61	510
Lamex	coastal	2.6	42	270
Kaimal IEC	open terrain	3.9	34	340

4.5.4 Non-gaussian turbulence

Usually turbulence is taken to have a gaussian distribution within 1 to 60 minute intervals. In reality turbulence is non-gaussian, and the question is to which extent this invalidates load calculations.

Investigations by Nielsen [155] show that the gaussian assumption is correct to approximately 2.5 standard deviations from the wind speed mean (99% of all probability mass). Nielsen [154] provides data for 8 different sites (10–80 m measuring heights) and finds skewness values lower than 0.2 for all but one site, and kurtosis values 3 ± 0.3. So while the non-gaussian character may be a problem for the determination of extreme wind events, as far as fatigue is concerned the assumption is probably justified.

Thomsen [208] compared loads on a 'gaussian' and a 'non-gaussian' site, and found a small influence on fatigue loads. This is in contrast to Nielsen [154], who claims that blade flap moments may go up by as much as 20%. Unfortunately he only looked at operation at 12 m/s with a rather high turbulence intensity of $I = 0.2$.

While this matter certainly warrants further investigations, we set the matter aside for now, at least for flat coastal and offshore sites. With a view to further investigations, information on how to generate non-gaussian wind fields may be found in Yamazaki [238] and Nielsen [154, 155].

4.5.5 Modelling of uncertainty

As remarked before, the Mann model provides a consistent model of the wind field: dependent on the shear parameter Γ and the length scale L_M all coherence functions are automatically generated, as well as the turbulence ratios in the three directions (u, v, w). The model is capable of generating a range of wind spectra from the isotropic von Kármán spectrum ($\Gamma = 0$) to the Kaimal spectrum ($\Gamma = 3.9$); besides the length scale may be varied to get even more flexibility. Thus it would be best to use both Γ and L_M as stochastic variables. However because there is not much information on length scale we take a shortcut here. Both Γ and L_M have more or less the same influence on loads: they shift energy to higher or lower frequencies. Therefore it is possible to use only the shear parameter Γ. For flat open terrain we take for the distribution $\Gamma = N(\mu = 3.0, \sigma = 0.3)$. The length scale derived by Mann ($L_M = 34$ m) is kept, which corresponds to the IEC length scales given by equation (3.5) (p35).

4.6 Wind shear

IEC 61400-1 assumes neutrality, and prescribes wind shear with a power law giving the wind speed at height h as function of wind speed at hub height H:

$$U(h) = \left(\frac{h}{H}\right)^{\alpha} U(H) \tag{4.32}$$

with $\alpha = 0.2$. This is just a curve fit, however for historical reasons it is still widely used. The physically correct equation is equation (4.1). If we assume neutrality it reduces to the now familiar:

$$U(h) = \frac{\ln(h/z_0)}{\ln(H/z_0)} U(H) \tag{4.33}$$

If we want to make the two expressions equivalent in the sense that the wind shear $\partial U / \partial (h = H)$ has the same value in both equations, we have to set:

$$\alpha = \frac{1}{\ln(H/z_0)} \tag{4.34}$$

This gives us the possibility of estimating the power law exponent from the terrain roughness z_0, which may be estimated with Petersen's classification method, or may be found from the turbulence intensity measured at reference height z_r (compare section 4.4.2). We reapply equation (4.18) to get:

$$\alpha(H) = I(H) = \frac{I(z_r)}{1 + I(z_r)\ln(H/z_r)} \tag{4.35}$$

Downey [48] predicted wind shear at large (hub) heights using the procedure sketched above; his results are given in table 4.15. Unfortunately it appears that wind shear prediction on the basis of turbulence intensity has no added value. For lack of data, the best recipe is in fact the simplest:

- For flat land sites set $\alpha = 0.2$.

- For offshore sites set $\alpha = 0.1$.

- For complex sites, set $\alpha = 0.0$.

Table 4.15: Wind shear exponent predictions. Source: Downey [48]. See table D.7 for all data. The exponent found from wind speeds at h_1 and h_2 is assumed to be the true one, which is estimated using the roughness (found from turbulence intensity) and the reference height.

Site	type	h_1	h_2	h_r	z_0	wind shear exponent [-]		
		[m]	[m]	[m]	[m]	$\alpha(h_1, h_2)$	$\alpha(h_r, z_0)$	error
Egmond	offshore	70	116	21	9.1e-5	0.09	0.07	–0.01
Horns Rev	offshore	45	62	15	5.8e-4	0.13	0.09	–0.04
Læsø	offshore	45	62	15	2.3e-4	0.13	0.08	–0.05
Skipheia	coastal	72	101	11	3.0e-3	0.12	0.10	–0.02
Tjæreborg	coastal	60	90	30	6.9e-3	0.21	0.11	–0.11
Toboel	pastoral	45	62	15	4.8e-2	0.20	0.14	–0.06
Cabauw	pastoral	80	140	20	9.3e-3	0.16	0.10	–0.05
Oak Creek	complex	65	79	10	2.8e-3	-0.02	0.10	0.12
Mean						0.13	0.10	–0.03
Standard deviation						0.07	0.02	0.07
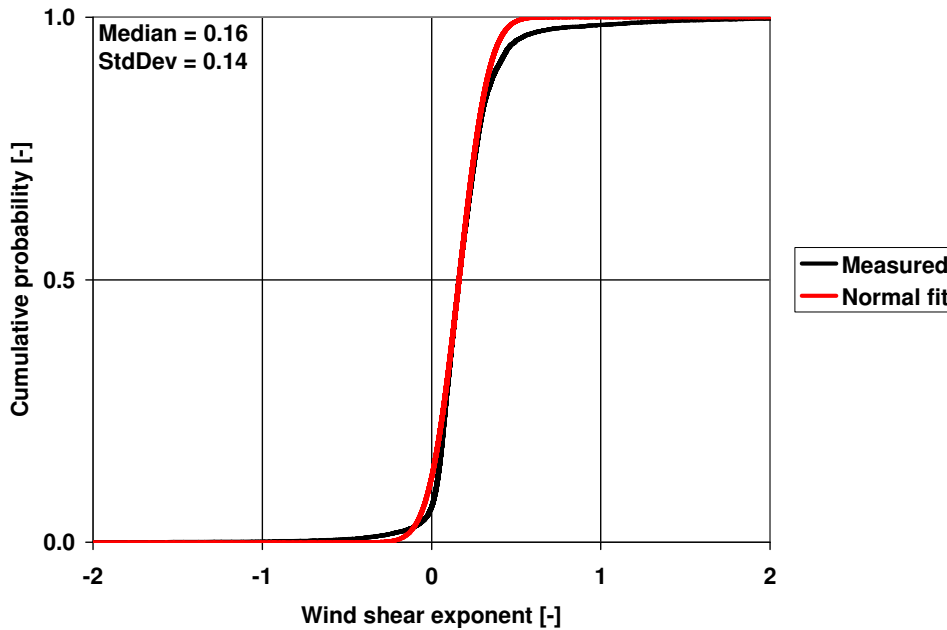
Figure 4.10: Wind shear exponent measured at Høvsøre (average over 10 minutes; H = 60 and 80 m; wind speed 10–25 m/s; N=13,751)

In all cases we set standard deviation $\sigma_\alpha = 0.02$.

In some other research For Tjæreborg (open terrain on the coast with turbulence intensity $I = 0.02$–0.10) the median value for the exponent was found to be $\alpha = 0.18$ which is close to $\alpha = 0.2$ (Veldkamp [223]). Measurements from Høvsøre (also on the Danish west coast) show that very large wind shears may occur. Nevertheless the median shear (most important for fatigue loads) is $\alpha = 0.16$ (figure 4.10).

4.7   Air density

In the coastal areas of North Western Europe, yearly average density variations are small, and air density and wind speed are uncorrelated. Therefore it is just a matter of finding the correct density value. For some sites (for example in the USA) there are considerable density variations over the year; however these can be accounted for by (for example) running two sets of calculations at different densities and combining results.

4.8   Inflow angle

The rotor loads are dependent on the angle between wind speed and the normal on the rotor plane. The total angle is (see figure 4.11):

$$\alpha(t) = \sqrt{(S(t) + T)^2 + (W(t) - Y(t))^2} \tag{4.36}$$

From load calculations it appears that the equivalent loads are well described by linear functions of the mean angles. Thus the wind direction may be set to $W = 0$, and we may skip the dependence on time t. Equation (4.36) simplifies to:

$$\alpha = \sqrt{(S + T)^2 + Y^2} \tag{4.37}$$

The equivalent load range becomes:

$$\frac{\Delta F_{eq}(\alpha)}{\Delta F_{eq}(\alpha_d)} \approx 1 + \frac{\partial F_{eq}}{\partial \alpha} \frac{(\alpha - \alpha_d)}{\Delta F_{eq}(\alpha_d)} \tag{4.38}$$

where:

ΔF_{eq}	equivalent load range [Nm]
S	vertical inflow angle $\approx$ terrain slope [°]
T	rotor tilt [°]
W	wind direction (North = 0°) [°]
Y	yaw angle (North = 0°) [°]
α	total inflow angle [°]
d	design (e.g. class value)

As expected, some simulations showed that the equivalent rotor blade loads are almost only dependent on α, and that it does not matter whether the main contribution comes from yaw errors or from terrain slope. To get enough tower clearance, the tilt angle is usually set at 5°. Turbines are put up on hill slopes that are 20–30°; however the inflow angles are usually much smaller: 0–10°. Current yaw systems operate by measuring misalignment on the nacelle. It seems unlikely that the yaw error can be kept below 5°, and an average error of 5–10° is probably realistic. Because IEC 61400 prescribes the terrain slope to be at least 8°, a normal design angle is:

$$\alpha = \sqrt{(5 + 8)^2 + 10^2} = 16.4 \text{ deg} \tag{4.39}$$

In this study we set rotor tilt $T = 5°$; we assume that the slope $S = 0$ (constant) for offshore and for flat terrain, and that it can be determined with an accuracy of $\pm 3°$ in complex terrain, which gives us a normal distribution with standard deviation 1°:

$$S = N(\mu = S_{est}, \ \sigma = 1°) \tag{4.40}$$

For the yaw error values of 5–10° have been reported, so we set:

$$Y = N(\mu = 8°, \ \sigma = 1°) \tag{4.41}$$

The values given above do not account for the occurrence of large coherent gusts and changes of direction.
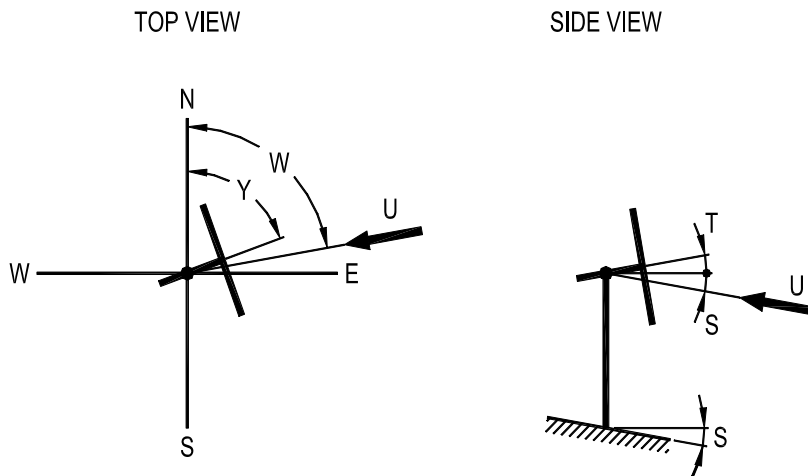
Figure 4.11: Definition of wind direction, yaw angle, terrain slope and tilt.

4.9 Wake effects

When turbines are placed in a windfarm, it is inevitable that they will be in each other's wake part of the time, which results in increased loads. Much work, both fundamental and practical, has been done on the development of the wake, on estimation of the speed deficit and on the added turbulence; an overview is given by Vermeer [226]. Perhaps the easiest way of incorporating wake effects on loads is by using artificial higher turbulence. This is the approach found in IEC 61400 [93] as proposed by Frandsen [64]. It is a simple model that is calibrated against measurements from a number of windfarms (see equations (3.11) and (3.12) (p38)).

The main objection to the equivalent turbulence approach is that it is too simple to capture the relevant physics; changes in mean wind speed in the wake are not accounted for, and hence predictions of extreme speeds will be off; also the different shape of the wake turbulence spectrum compared to free stream conditions is neglected. Furthermore the method was calibrated for flat smooth uniform terrain, and it is unclear how well it will perform in more complex conditions.

Recently a new approach based on air pollution dispersion theory was published by Thomsen [210–212]. First the wake of a wind turbine as function of the induction and the distance behind the rotor is found with a Navier-Stokes calculation (the rotor is modeled as an actuator disk). Now the rotor is placed in a large turbulence field; it is continuously 'shedding wakes' which evolve according to the sequence of precalculated shapes, as they get further from the rotor. Rotor and wakes are considered to be part of a large turbulence field, in which the wake is moving downwind with the average wind speed. At every time step, the (fixed) wake has the lateral

wind speed that is the integral of the turbulence field's speeds over the wake circular area. Integrating this average wake speed over one time step yields the new position of the wake in the field. The result of this procedure is a meandering wake. The method looks promising, for example the fact that no clear distinction is seen between full wake and half wake operation is neatly explained; also there is good qualitative agreement with measurements performed on turbines at the Tjæreborg test site. Verification is ongoing (see Mann [136], where it is shown that the wake indeed persists, and meanders in fair agreement with predictions based on wind speed measurements at the rotor).

According to Thomsen [210] the increased turbulence method seems to be good enough for calculation of fatigue loads (notwithstanding its physical shortcomings); Jørgensen [97] comes to the same conclusion in an evaluation of measurements from Middelgrunden windfarm.

If we assume an average wind farm (square configuration with distance 5D and uniformly distributed wind direction), then the additional turbulence is ca 0.02 according to the Frandsen method. Therefore, for now it is assumed that the additional turbulence intensity is lognormally distributed with mean $\mu = 0.02$ and standard deviation $\sigma = 0.01$. The windfarm turbulence is added to the natural turbulence before the turbulence dependent load ranges are estimated.

4.10   Complex terrain

As stated before, the assumptions underlying the estimates given above break down in complex, mountainous terrain, where terrain slopes are larger than $20°$ and terrain roughness is larger than $z_0 = 0.3$ m (in fact the whole concept of 'obstacle' loses its meaning). In load calculations the usual strategy is to tinker with some input parameters:

- The speed up for the wind at hub height and the wind shear are estimated with rules based on experience or theoretical models (for example flow over 2D hills).

- The inflow angle is determined on the basis of the terrain slope averaged over a distance of 2–3 rotor diameters upwind.

- Adjusted (u, v, w) turbulence values are used because typically turbulence is known to be more isotropic, i.e. it is more appropriate to use the von Kármán spectrum instead of Kaimal's (see Antoniou [5], Thomsen [206]).

The correct way to proceed would be to do wind speed measurements at hub height; however tall meteo towers are expensive, especially if it one wants to measure at more than one wind turbine location. A promising possibility is to use SODAR, which avoids the necessity of a tower. Maeda [131] used this method to compare the exact wind shear up to 100 m height with the estimates based on measurements at 20

and 30 m only. His result show an average estimated exponent for all wind directions $\alpha = 0.17$ that is almost correct (the measured value was $\alpha = 0.18$), but dependent on wind direction there are errors that have standard deviation $\sigma_\alpha = 0.08$. Here the worst will be assumed, and values $\sigma_\alpha = 0.04$–0.08 will be investigated.

Alternatively, wind speed estimates may be made using 2D or 3D Navier-Stokes calculations of the flow, which is a good approach for prediction of wind speed-height profiles, especially upstream of hills. Bitsuamlak [15] gives an overview; see for example Eidsvik [54] for some specific calculations (the model HIRLAM in combination with low altitude measurements is used to model the atmosphere at high altitudes). Table 4.16 gives an indication of errors in such calculations; wind tunnel measurements on sinusoidal 2D hills were compared to Navier-Stokes calculations and to predictions from the National Building Code of Canada (NBCC).

Nielsen [156] published an overview of 20 case studies where windfarm outputs were predicted on the basis of local wind measurements. Energy production in complex terrain may be off by as much as 50% (Portugal), which translates to ca 15% wind speed error. However it is difficult to judge results because apparently no strict protocol was used to ensure that only data that were known a priori were used for predictions.

Since the NBCC results from table 4.16 probably give a fair impression of the state of the art, a wind speed coefficient of variation $V_U = 0.20$ will be investigated (the worst case).

In mountainous terrain exceptional extreme conditions may also occur. Examples were found in reports of measurements that were done in connection with siting of wind turbines at complex sites:

- High turbulence intensity: Lausen [125].

- Non-gaussian turbulence: Mann [137].

- Large horizontal wind shear (wind direction shear): Hansen [81].

- Large vertical wind shear: Brandt Christensen [25], Courtney [42], Hansen

Table 4.16: Normalised speed up ratio predictions 40 m over hill crests for sinusoidal 2D hills. Values are compared to wind tunnel measurements (measured wind tunnel value = 1). Source: Bitsuamlak [15, figure 9].

| | shallow hill, $H/B = 1/8$ | | steep hill, $H/B = 1/4$ | |
	CFD	NBCC	CFD	NBCC
single hill	0.86	1.05	1.07	1.17
hill 1	0.95	1.10	1.16	1.26
hill 2	1.03	1.24	1.20	1.60
hill 3	1.00	1.26	0.97	1.39
Average	0.96	1.16	1.10	1.36
Coefficient of variation	0.07	0.11	0.10	0.19

[80], Lausen [125], Nielsen [153].

Judging by the number of references, of the extreme conditions wind shear seems to be occurring most often. However although (repeated) extreme conditions may cause difficulties for wind turbines, it is not clear that average fatigue conditions are significantly worse than on site where the wind is more well behaved.

In this work focus is on getting an impression of how additional uncertainty of the wind climate in complex terrain affects failure probability, rather than finding exact values. Based on the available information, distributions are adjusted as follows:

- Standard deviation on wind speed at hub height, wind shear exponent and turbulence intensity are increased.

- More isotropic turbulence is assumed, which corresponds to reducing Mann's shear parameter.

The modified distributions are summarised in table 4.17.

Table 4.17: Adjusted mean and standard deviation for complex terrain

parameter	FSU terrain		Complex terrain	
	mean	std.dev	mean	std.dev.
wind speed [m/s]	U_{avg}	$0.07\,U_{avg}$	U_{avg}	$0.20\,U_{avg}$
turbulence intensity [-]	0.16	0.01	0.16	0.02
wind shear exponent [-]	0.2	0.02	0.1	0.08
Mann's shear parameter [-]	3	0.3	1	0.6

Chapter 5

Sea

5.1 Introduction

If a turbine is placed in an offshore environment, the set of wind conditions described in the previous chapter needs to be extended with sea conditions, for estimating combined wind and wave loads. For fatigue, waves are most important: currents and tides have only minor influence on loads. Suppose that we wanted to do a full calculation, then we could describe the environmental conditions with sets of five parameters for each 3-hour period:

- Wind speed.
- Wind direction.
- Significant wave height.
- Zero crossing period (or peak period).
- Wave direction.

We would then lump 3-hour periods with identical conditions together, which would result in a reduced number of different combinations, each having some frequency of occurrence. While these five are the most important parameters, there are a few more things that have to be considered:

- The shape of the wave spectrum, mainly the peak enhancement factor γ and the peak period T_p (or the zero crossing period T_z).
- The drag coefficient C_D.
- The inertia coefficient C_M.
- The wave kinematic model.

We will consider these items in the following sections.

5.2   Lumping of load cases

It is not very practical (and not necessary) to do a separate calculation for each 5-parameter set. Instead parameter sets are lumped into a small number of relevant combinations, according to some simple (and uncontroversial) rules. The first thing to do is to sort significant wave height-zero crossing period combinations into wind speed bins; then the equivalent significant wave height and zero crossing period are computed according to equations (3.14) and (3.15) (p39). The method to get a fatigue damage equivalent significant wave height is analogous to what was done to include the effect of wind turbine wakes (equation (3.11), see also appendix C). Kühn [115] showed that this method works with negligible loss of accuracy in equivalent loads[1]. Moreover it appears that if the real wind direction distribution is used, for each wind direction all wave directions may be combined into one. Either co-directionality may be assumed, or some fixed error, typically between 10° and 20° misalignment. Thus it turns out that the lumping issue does not present a problem.

5.2.1   Estimation of significant wave height

When an offshore wind farm is planned for some site, it is possible that no metocean data are available just there. Then it will be necessary to use data from some other site close by. Cerda Salzmann [33] looked into this matter for the North Sea, and found rather small differences in estimated fatigue damage and equivalent load (see table 5.1). Moreover, for the whole of the North Sea there is an extensive database (NESS/NEXT, see Peters [166]), so we may consider the long term sea parameters to be known.

---

[1]This was confirmed in work done by Garrad Hassan for the IEC working group that prepared the wind turbine offshore standard IEC 61400-3.

Table 5.1: Calculated relative fatigue damage and equivalent load at the mudline using wave data from different sources. Source: Cerda Salzmann [33].

source	data type	water depth [m]	distance to shore [km]	relative fatigue damage (Ness/Next=1)	relative equivalent load (m=4) (Ness/Next=1)
Argoss N53^o	satellite	23	66	0.98	0.99
Argoss N52^o	satellite	20	19	0.77	0.94
IJmuiden MS	waverider + anemometer	21	37	1.07	1.02
MP Noordwijk	step gauge + anemometer	18	9	0.68	0.91
Ness/Next [166]	hindcast	19	16	1.00	1.00
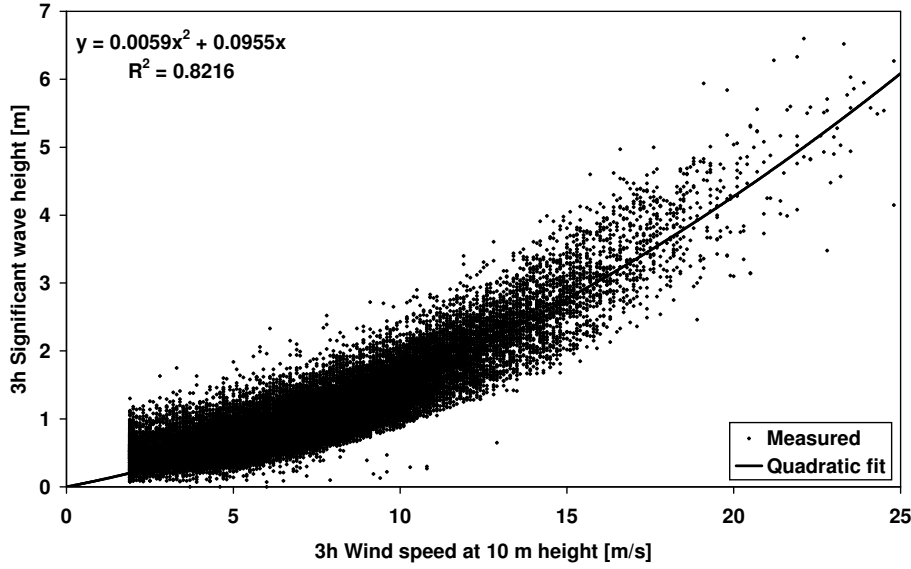
Figure 5.1: Three hour average significant wave height as function of wind speed (NESS/NEXT database, grid point NL-1)

5.2.2 Yearly variation of significant wave height

From 32 years of NESS/NEXT data (1972-1995) for a grid point close to the first Dutch windfarm, it appears that the yearly average significant wave height has mean $\mu = 1.27$ m and standard deviation $\sigma = 0.12$ m.[2] For the same period, the wind speed distribution at 10 m over the water surface is described by a Weibull distribution with average wind speed $U_{avg} = 8.1$ m/s and shape factor $k = 2$. The best fit for the relation between 3 hour mean values of wind and significant wave height is ($H_{s,3h}$ in [m] and U_{10} in [m/s]):

$$H_{s,3h} = 0.0059\, U_{10}^2 + 0.0955\, U_{10} \quad (r^2 = 0.82) \tag{5.1}$$

This relation is shown in figure 5.1. For the yearly averages the relation is ($H_{s,1\ year}$ in [m] and $U_{10,1\ year}$ in [m/s]):

$$H_{s,1\ year} = 0.22\, U_{10,1\ year} - 0.5 \quad (r^2 = 0.94) \tag{5.2}$$

---

[2]In fact, the distribution is well described as being lognormal (median $M = 1.27$, $V \approx S = 0.12$):

$$F(H_s) = N\left(\frac{\ln H_s - \ln M}{S}\right)$$
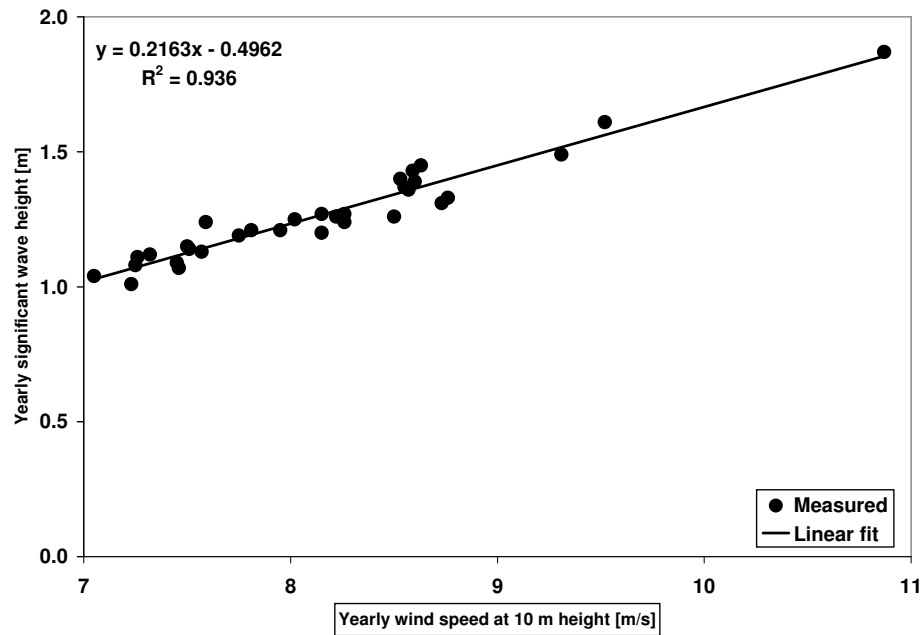
Figure 5.2: Yearly average significant wave height as function of yearly average wind speed
(from NESS/NEXT database, grid point NL-1)

which is shown in figure 5.2. It is easily verified that the two equations are consistent with each other if the yearly wind speed distribution is Weibull shaped.

Because wind and significant wave height are closely correlated, we may establish the sensitivity of wind turbine loads to the combined effects of wind speed and waves by first doing calculations where the significant wave height is given as function of wind speed by equation (5.1), and then varying the frequencies of occurrence of the different load cases to simulate change in wind speed.

5.3 Wave spectrum

Given the wave data that are available, it is often possible to use the wave spectrum obtained from measurements and hindcast data instead of a synthetic spectrum. However the severity of the wave loads is mainly determined by the total energy in the spectrum (i.e. by the significant wave height) and the frequency where most energy is in relation to the resonance frequency of the structure. Therefore there is no big problem in using synthetic spectra, even though they may deviate somewhat from the actual spectrum. The wave spectrum most used is the one sided Jonswap spectrum,
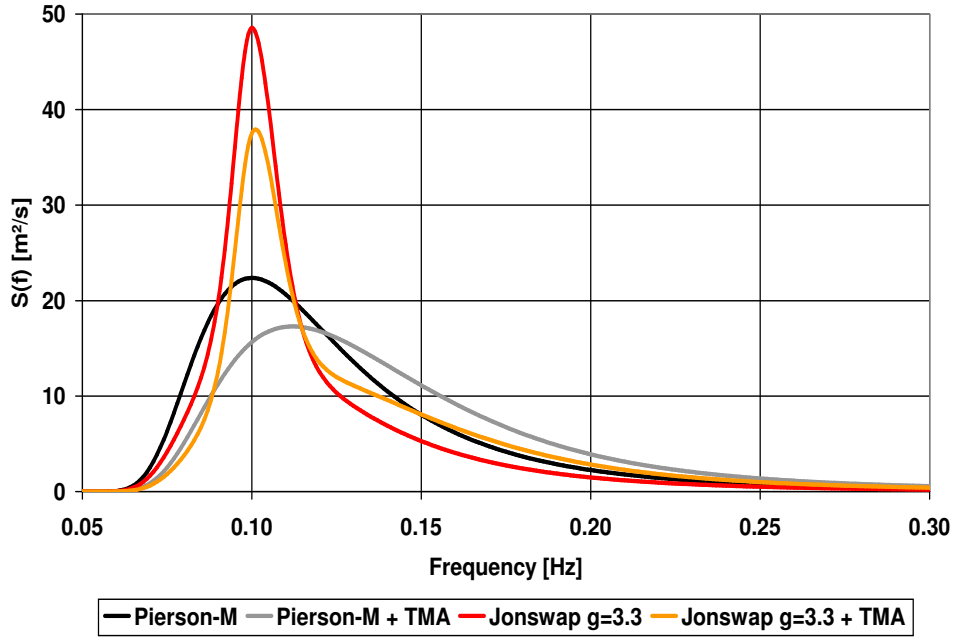
Figure 5.3: Pierson-Moskowitz and Jonswap spectra, original and with TMA correction. Significant wave height H_s = 5 m, peak frequency 0.1 Hz.

given by:

$$S_J(f) = \gamma^\alpha (1 - 0.287 \ln \gamma) \, S_{PM}(f)$$

$$= \gamma^\alpha (1 - 0.287 \ln \gamma) \, \frac{5}{16} \frac{H_s^2 f^5}{T_p^4} \exp\left(-\frac{5}{4}\left(\frac{f_p}{f}\right)^4\right) \quad (5.3)$$

With:

$$\alpha = \exp\left(-\frac{1}{2}\left(\frac{f - f_p}{\sigma f_p}\right)^2\right) \qquad \begin{array}{l} \sigma = 0.07 \; for \; f \leq f_p \\ \sigma = 0.09 \; for \; f > f_p \end{array} \quad (5.4)$$

Where:

f	frequency [Hz]
f_p	spectrum peak frequency [Hz]
H_s	significant wave height [m]
S_J	Jonswap spectral density [m²/Hz]
S_{PM}	Pierson-Moskowitz spectral density [m²/Hz]
T_p	peak period [s]
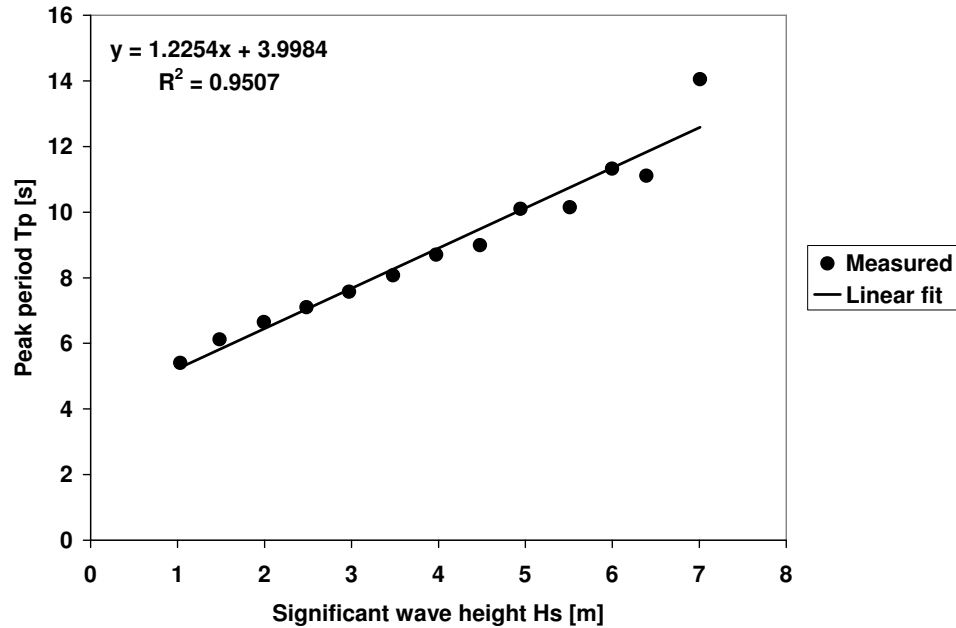
Figure 5.4: Peak period as function of significant wave height. Data for Munitiestortplaats IJmuiden, 1990, 1993–95. Data kindly supplied by Rijkswaterstaat (RIKZ).

α	exponent [-]
γ	peak parameter [-]
σ	help parameter [-]

The advantage of this spectrum is that it can be 'tuned' to any sea state with the peak enhancement factor γ, while the Pierson-Moskowitz spectrum is meant for fully developed waves. Additionally the TMA correction may be applied (Van der Tempel [224]). Thus almost any wave climate can be approximated with a synthetic spectrum; see figure 5.3 (previous page) for some examples of spectra. The zero crossing period T_z or the peak period T_p is usually known as function of significant wave height H_s and can be described with a simple function (see figure 5.4). From this the peak frequency may be established ($f_p = 1/T_p$). If the significant wave height and the peak frequency are known, it remains to fix the peak enhancement factor γ. An estimation formula is given by DNV [47]:

$$\gamma = \exp\left(5.75 - 1.15\frac{T_p}{\sqrt{H_s}}\right) \qquad 3.6 \leq \frac{T_p}{\sqrt{H_s}} \leq 5 \tag{5.5}$$

In figure 5.5 it is seen that the formula somewhat overestimates the peak enhancement factor found from curve fitting measured spectra.
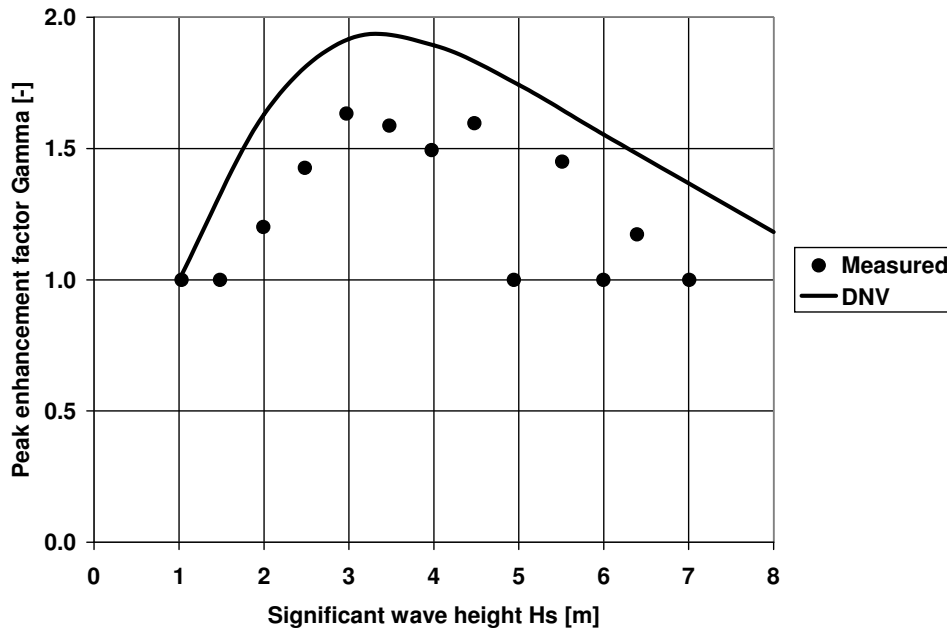
Figure 5.5: Peak enhancement factor γ as function of significant wave height. Data for Munitiestortplaats IJmuiden, 1990, 1993–95. Data kindly supplied by Rijkswaterstaat (RIKZ).

Still the conclusion of this section is that we do not need to introduce extra uncertainty for the waves, since they are correlated to wind, and various stochastic parameters are as well known as we care to determine them.

5.4   Wave kinematics

For the calculation of fatigue load on structures in the water, 2-dimensional linear (Airy) waves are assumed, like those in a very deep, narrow wave tank. The right combination of waves of different height is created by summing sinusoids of different frequencies of which the amplitudes are dictated by the wave spectrum. Assuming linearity admits simple hyperbolic solutions of the speed and acceleration profile; the profiles from the bottom up to the still water level are stretched (or compressed) to the actual water level including elevation (see for example Wheeler [234]). If we purely look at the kinematics of the water, there are four possible problems associated with the approach:

- If not enough different waves are superposed, statistical properties of (groups of) waves may be off (section 5.4.1).

- If the water is not deep enough (compared to wave height) real waves cannot be approximated by linear ones, and speeds and accelerations are different from those in first order waves (section 5.4.2).

- Waves are not 2-dimensional, the real wave field is 3-dimensional and has waves running in different directions.

- If the structure is large compared to the length of a wave it may no longer be regarded as a vertical line; the structure will change the wave kinematics (section 5.5).

5.4.1   Wave field generation

Random Airy waves (first order sinusoidal waves) are generated according to the appropriate wave spectrum, and then superposed. The procedure is analogous to wind field generation (see appendix G); the advantages of the method are simplicity and speed. It can easily be extended to generation of waves at multiple points in space (by phase shifting in the frequency domain) or to 3-dimensional waves (see Mittendorf [146]).

Tucker [216] cautions against using the fixed amplitude-random phase method because this would lead to the wrong 'groupiness' of waves (statistical properties of wave groups). However according to Elgar [55] there is no problem if enough sinusoidal components are used; alternatively the random gaussian amplitude method may be employed. In the author's experience there is no problem with today's computers to use a sufficient number of frequencies for generating waves[3].

5.4.2   Wave kinematics

The first order calculation with profile stretching is adequate for deep water waves, where the wave height-depth ratio $H/d \leq 0.2$, but the wave kinematics are not right for higher waves (see Gudmestad [75] for an overview of the merits of various stretching methods). It is possible to do efficient second order correction for random waves, which makes the wave kinematics right up to $H/d \simeq 0.3$ (see Sand and Mansard [140, 180], Duncan [49] and Van der Tempel [224]), but this procedure cannot be practically extended to higher order corrections. The surface elevation may reasonably be predicted with this sort of correction, but in more extreme cases it is not accurate enough to find correct speeds and acceleration at the varying water surface,

Alternatives that avoid the kinematics problem are random wave fields created in a numerical wave tank described by Clauss [38] and Steinhagen [201], and the use of Boussinesq waves, reported by Madsen [130] and Correa Bomholt Pedersen [39]. Both methods are feasible with currently available computing power, so the question

---

[3]In the author's opinion there is no evidence for special group properties of waves. If enough frequencies are used in wave field generation, statistical properties will be right.

which error is introduced by using linear wave kinematics will probably become less important in the near future.

However state-of-the-art is still first order waves. While speed and acceleration errors are non-negligible in extreme waves, by nature fatigue waves are smaller (in relation to depth), which makes it likely that simple models are enough for our needs.

The matter was investigated by van der Tempel and Veldkamp [224] for 70 m hub height and 15 m water depth; they found small differences in equivalent loads (see table 5.2). Trumars [215] looked at 80 m hub height and 20 m water depth, and found that with nonlinear waves fatigue damage is 7% higher with a 1-slope curve ($m = 3$) and 51% higher with a 2-slope curve according to Eurocode 3 ($m_1 = 3$, $m_2 = 5$). If this is converted to stress the numbers are 2% (conversion with $m = 3$) and 11% (conversion with $m = 4$). At present the best estimate seems to apply a bias of 1.05 (i.e. actual loads are 5% larger than calculated) and standard deviation $\sigma = 0.02$.

5.5 Drag and inertia coefficient

If wave speed and acceleration are known, the force on a stationary cylinder cross section $f(z)$ is obtained with Morison's equation:

$$f(z) = C_D \frac{\rho}{2} U|U|D(z) + C_M \rho \dot{U} \frac{\pi}{4} D(z)^2 \qquad (5.6)$$

where:

C_D	drag coefficient [-]
C_M	inertia coefficient [-]
$f(z)$	force at height z [N/m]
U	wave particle speed (perpendicular to cylinder) [m/s]

Table 5.2: Equivalent fatigue load ranges (bending moments, Wöhler exponent $m = 4$) for a 92 m, 2750 kW wind turbine on a 70 m tower + monopile ($f_0 = 0.30$ Hz) in 15 m water depth. Average wind speed 9.6 m/s, omnidirectional loads with measured wind speed and direction distribution and wind/wave collinearity. Source: Van der Tempel and Veldkamp [224].

Equivalent load range [%]	1st order	2nd order	Nonlinear
SWL+10 m			
North-South	100	105	101
East-West	100	105	111
SWL			
North-South	100	105	102
East-West	100	105	112
SWL-15 m			
North-South	100	104	102
East-West	100	105	112

z height [m]
$\dot{U}$ wave particle acceleration (perpendicular to cylinder) [m/s^2]
ρ water density [kg/m^3]

The equation works reasonably well, also for inclined cylinders (canonical values used are $C_D = 0.7$, $C_M = 2$ and $\rho = 1030$ kg/m^3). Nevertheless there is some difficulty in finding forces with precision.

Firstly this is because of difficulties with kinematics which were discussed in section 5.4.2.

Secondly there is the fact that dimensions of the structure are not (always) small compared to wave length. For the important special case of a cylinder in linear waves there is an analytical solution according to MacCamy-Fuchs diffraction theory, which gives a correction on the inertia coefficient and phase angle of the acceleration. The MacCamy-Fuchs corrected theoretical inertia coefficient C'_M is given by:

$$C'_M = \frac{16}{\pi k^2 D^2 \sqrt{[J'_1(kD/2)]^2 + [Y'_1(kD/2)]^2}} \tag{5.7}$$

and the phase lag of the particle acceleration is:

$$\alpha = \arctan \frac{J'_1(kD/2)}{Y'_1(kD/2)} \tag{5.8}$$

where:

C'_M MacCamy-Fuchs corrected inertia coefficient [-]
D cylinder diameter [m]
J'_1 derivative of Bessel function J_1 [-]
k wave number [1/m]
Y'_1 derivative of Bessel function Y_1 [-]
α particle acceleration phase lag [rad]

Effectively the correction works as a low pass filter: high frequency accelerations are 'damped'. Table 5.3 gives some numbers; the correction results in loads that are ca 10% smaller.

Thirdly there is the difficulty of establishing correct values for the drag and the inertia coefficient. Even in the laboratory there is large variation in individual measured values, see for example Høgedal [91], Shafiee-Far [188]: values depend on the Reynolds and the Keulegan-Carpenter number and on cylinder roughness. Typical variation on individual measurements is $0.5 \leq C_D \leq 1.0$ and $1.0 \leq C_M \leq 2.0$. However for fatigue applications there is much averaging and therefore one can live with the constant value approach.

An example of an experiment particularly relevant for us is the Christchurch compliant cylinder experiment, described by Burrows [29] and Najafian [150]. In this

experiment force measurements were done on a 12 m long 480 mm diameter smooth cylinder in random seas. The authors present values for C_D and C_M as function of the Keulegan-Carpenter number Kc and Reynolds Re for random waves[4]:

$$Kc = \frac{2\pi\sqrt{2}}{D}\frac{u_{rms}^2}{\sigma_{\dot{u}}} \tag{5.9}$$

$$Re = \frac{\sqrt{2}u_{rms}D}{\nu} \qquad (\nu = 1.43 \times 10^{-6}\ m^2/s) \tag{5.10}$$

where:

D	monopile diameter [m]
Kc	Keulegan-Carpenter number [-]
Re	Reynolds number [-]
u_{rms}	root mean square value of wave particle speed [m/s]
$\sigma_{\dot{u}}$	standard deviation of wave particle acceleration [m/s^2]
ν	water kinematic viscosity = 1.43×10^{-6} [m^2/s]

In the tests $Kc = 0$–20 which means that loads are inertia dominated, just like in the case of wind turbine monopiles. The main finding is that the method of using average values in Morison's equation works well, although there is large variation in individual force measurements. If least squares coefficient values for a run are reused to predict forces, correlations are better then 97% (Burrows [29, figure 3]). Moreover no significant improvement is possible with more complicated formulations (for example with time dependent coefficients). The dominance of inertia is confirmed by

---

[4]For one sinusoidal wave with period T, Keulegan-Carpenter and Reynolds reduce to:

$$Kc = \frac{u_{max}T}{D} \qquad Re = \frac{u_{max}D}{\nu}$$

Table 5.3: Equivalent fatigue load ranges (bending moments, Wöhler exponent $m = 4$) for a 92 m, 2750 kW wind turbine on a 70 m tower + 4.6 m diameter monopile ($f_0 = 0.30$ Hz) in 20 m water depth. Average wind speed 10 m/s (IEC class I), uniform wind direction distribution with wind/wave collinearity.

Equivalent load range [%]	normal		MacCamy-Fuchs	
location	1st order	2nd order	1st order	2nd order
SWL + 68 m	100	100	97	97
SWL + 38 m	100	97	84	85
SWL + 13 m	100	97	84	85
SWL	100	97	84	85
SWL – 10 m	100	98	89	91
SWL – 20 m	100	100	93	95

some calculations (see table 5.4). It is remarkable that the loads all along the tower up to the yaw system are influenced by the wave inertia loads. Paradoxically loads decrease slightly at larger C_D-values, this could be because drag forces are out of phase with inertia forces, and provide some damping. For a turbine with $D = 4.6$ m typical values are (at 16 m/s) $Kc = 0.75$ and $Re = 3.2 \times 10^6$. For this low Kc-value the inertia coefficient is close to $C_M = 2$. The value found for the drag coefficient is $C_D = 0.8$ for $Kc = 17$ (however the loads are totally inertia dominated (see table 5.4), so the exact value drag coefficient is not of concern). Unfortunately, since both the experiment and actual monopiles are in real waves our Re is off by a decade, possibly making the C_M-value invalid.

Probably the best is to stick with the standards, such as API [76] ($C_D = 0.6$–1.2, $C_M = 1.3$–2.0), ISO [95] and IEC [94]; in the latter standard there are also prescriptions on how to increase coefficients to take care of attachments such as ladders and J-tubes, and marine growth.

For the probabilistic calculations we assume that the correct values are known, and that the standard deviation is 0.1, which gives us a range 0.6 for both coefficients: $C_D = N(\mu = 0.9, \sigma = 0.1)$ and $C_M = N(\mu = 2.0, \sigma = 0.1)$. The mean values of the distributions are the values according to Burrows [29] for the Keulegan-Carpenter numbers representative for fatigue conditions.

Table 5.4: Equivalent fatigue load ranges for different values of the drag coefficient (bending moments, Wöhler exponent $m = 4$) for a 92 m, 2750 kW wind turbine on a 70 m tower + 4.6 m diameter monopile ($f_0 = 0.30$ Hz) in 20 m water depth. Average wind speed 10 m/s (IEC class I), uniform wind direction distribution with wind/wave collinearity.

location	$C_D = 0.0$	$C_D = 0.5$	$C_D = 0.95$	$C_D = 1.5$
$C_M = 2.15$				
SWL + 68 m	100	100	100	100
SWL + 38 m	101	100	100	99
SWL + 13 m	101	100	100	99
SWL	101	100	100	99
SWL – 10 m	101	100	100	99
SWL – 20 m	101	100	100	99
	$C_M = 1.0$	$C_M = 1.5$	$C_M = 2.0$	$C_M = 2.5$
$C_D = 0.95$				
SWL + 68 m	96	98	100	104
SWL + 38 m	69	81	100	124
SWL + 13 m	68	80	100	125
SWL	68	80	100	124
SWL – 10 m	67	80	100	122
SWL – 20 m	64	79	100	123

5.6 Tide

The influence of the tide is predictable and incorporated according to formula (3.16). Let us check whether this approach is correct.

We would like to replace the changing sea level $d(t)$ by a constant equivalent level d_{eq}, which gives us the same fatigue damage equivalent bending moment at the mudline. Let us make a couple of simplifying assumptions:

- The monopile has a constant diameter.

- Waves do not change with a change in water level.

- The wave force profile from the mudline (0) to the waterline (d) is only stretched.

For some water level d, the fatigue load range (equivalent bending moment) $\Delta M_{eq,0}$ is found by integrating the cross sectional load $f(z)$:

$$\Delta M_{eq,0} = \int_0^d f(z)\, z\, dz \tag{5.11}$$

If the still water level changes from d to d', then we have the corresponding integral:

$$\Delta M'_{eq,0} = \int_0^{d'} f(z\frac{d}{d'})\, z\, dz \tag{5.12}$$

If we set $z' = z\, d/d'$ then $z = z'\, d'/d$ and we find:

$$\Delta M'_{eq,0} = \int_0^d f(z') \left(z'\frac{d'}{d}\right)\, d\left(z\frac{d'}{d}\right) = \Delta M_{eq,0} \left(\frac{d'}{d}\right)^2 \tag{5.13}$$

This immediately proves equation (3.16) (repeated here):

$$d_{eq} = \left(\frac{1}{T}\int_T [d(t)]^{2m} dt\right)^{1/(2m)} \tag{5.14}$$

5.7 Current

The influence of current on fatigue is negligible, because current speeds are typically below 1 m/s, while particle speeds in waves may be as high as 5-10 m/s. Current practice is to simply add the current speed to the particle speed, which is accurate enough.

Chapter 6

Aerodynamics and wind turbine

6.1 Introduction

In this chapter the errors introduced by using blade element-momentum theory are discussed, as well as some uncertainties that are created because we have to model the turbine as a simple idealised structure in our calculations. First the aerodynamics are treated, and then the wind turbine structure.

6.2 Blade element momentum method

Most aerodynamic load calculations are done with the blade element-momentum method (BEM), a method that assumes that independent annuli of air go through the rotor, and that forces on a blade element may be found from relative local wind speed and blade lift and drag coefficients (usually obtained from two dimensional wind tunnel experiments). For reviews of BEM, see Leishman [127], Rasmussen [174] and Snel [193] (also other methods). All authors express the view that BEM overlooks important aspects of the flow through a wind turbine rotor, and is especially wrong when the rotor is in oblique flow. Be that as it may, BEM is the only method quick enough to do the hundreds of calculations that are now customary, and in fact it manages to reproduce complex real phenomena remarkably well, such as for example edgewise instability of rotor blades. The main problems of BEM are to a large extent cured by engineering corrections; furthermore calculations are normally checked against measurements. Key assumptions underlying BEM are discussed below.

Flow through rotor. It is assumed that only flow perpendicular to the blade axis contributes to blade forces: in the calculations there is no radial flow along the blade (while in reality there is). To some extent the effects of radial flow (also in oblique inflow) may be simulated by modifying the 2D lift and drag coefficient (see below).

Lift and drag. Wind tunnel values from 2D experiments are used, for profiles with ideal geometry. It is known that there are 3D effects in reality due to radial flow,

95

and deviations from the ideal geometry due to errors in the manufacturing process: especially the geometry of the leading edge is important as it influences the flow along the rest of the chord (for an interesting example, see Corten [41]). Some corrections on the 2D data have been proposed (Bak [6], Corten [40], Snel [193]), but (to the author's knowledge) there are no convincing improvements that always work. Hence 'tuning' of profile data is done to fit the measured power curve and the measured flap load ranges. Tuning becomes difficult if devices such as vortex generators or stall strips are used. Recently a new method was presented to modify the coefficients with a method that uses a fictitious angle of attack, based on Navier-Stokes calculations (Wen Zhong Shen [189]).

Dynamic wake. The rotor takes energy out of the wind, and thus the axial wind speeds behind the rotor are smaller than in front. Also rotation is introduced into the flow by the reaction forces of the rotor on the air. It appears that, in good approximation, the speeds seen by the blades are the vectorial average of wind speed before and after the rotor plane: hence they can be found by subtracting half the difference (the induced wind speed) from the sum of wind speed before the rotor and blade element speed. This seems to pose a problem: how can the speeds after the rotor be established if the amount of energy taken out by the rotor (which influences the wind speed after the rotor) has not been found yet? For equilibrium conditions the problem can be solved by iteration; for transient states the inertia of the wake saves the day. Since it takes time for the wake to change, the wake situation of the previous time step may be used for the blade force calculations at the present. Unfortunately the speed of wake change cannot be found from BEM, and thus some numbers (time constants) are used that fit measurements and calculations with more advanced methods. Sensitivity analyses with wakes with different time constants have shown that the influence on loads is small, as soon as some delay (more than 0 seconds) is introduced. See Snel [194] for further information.

Dynamic stall. For common blade profiles, the blade lift coefficient has an easy-to-measure stable value up to an angle of attack of ca 25 deg, and for angles of attack between ca 40 and 180 deg (the exact angle values depend on the profile shape). In between, two instable situations are possible, with high lift (attached flow) or with low lift (separated flow). It was found that the situation is reasonably well described by a time constant governed model that changes the lift coefficient smoothly from separated to unseparated and vice versa: Øye's model [165]. Other similar models are the Beddoes-Leishman model [127] and the Risø *fgh*-model (Snel [193]). All these models are engineering models with tuning parameters. Fortunately (as far as this problem is concerned), at present the trend is towards pitch-variable speed turbines, where the matter is less important, because operation is mostly at small angle of attack. The unfortunate side of this is that there is no incentive any more to solve this flow problem.

Tip and root correction. The Prandtl model is used to take into account flow around the blade tip and root from the high to the low pressure side (see Burton [30]).

Oblique inflow. In oblique inflow BEM is not valid. In spite of this, BEM is still capable of predicting loads with (according to some) surprising accuracy. Again an engineering model is used, that produces increased wind speed on the upwind rotor part, and decreased wind speed on the rotor downwind part (one model goes back to Glauert (1935), see Snel [194] for details and further references). As a matter of fact, the fact that modelling of oblique inflow is incorrect is not very important for fatigue calculations, because wind turbines are not supposed to operate in situations with large inflow angles: the loads become too big (it is important for extreme loading though).

Tower shadow. For upwind rotors and cylindrical (possibly conical) towers the potential flow model is assumed to be valid (see for example Burton [30]). Investigations have shown that this model is conservative (Björck [16], Graham [73]); however for normal blade tower clearance (1–2 times the tower diameter) the effect is small. For downwind rotors an empirical expression is used.

6.3 Resulting distribution for BEM uncertainty

Wind turbines are designed using experience with previous models. For example the same blade profiles are used as before, or corrections on profile data are employed that are known to have worked on previous blades. In any case load calculations are always verified by measurements, which means that the shortcomings of the blade element-momentum theory are not such a serious problem at they appear to be at first sight.

In the author's view the main problematic area is the effect of radial flow and its influence on the lift coefficient; since lift is the main driver for blade loads, blade root flap moments and tower base bending moments are affected. Thus the amount of flapping of a blade and the aerodynamic damping of the whole rotor (influencing tower loads) are usually miscalculated to some degree. Measurements are therefore essential; however if they are available, measured loads can be fairly well reproduced if the inflow angle is not too large (sometimes except for the bending moment in the tower base). Typical data from a load verification are given in figures 6.1 and 6.2 (next page). For individual 10 minute load cases there are considerable differences (circles, $R^2 \approx 0.7$); however if results are averaged in 1 m/s wind speed bins the scatter almost disappears (dots, $R^2 > 0.9$). The reason for the scatter is that loads are to a large extent determined by the high frequency content of the turbulence at the rotor, which cannot be predicted from the high frequency content at the measuring mast ca 250 m upwind. If only load cases are selected where the wind direction is close to 270 deg (so the rotor sees the measured wind) scatter is hardly reduced; not even if the measured wind in multiple points is used to generate a constrained wind field for the load calculation (see Bierbooms [14]).

Because the error is not determined by the accuracy of the load calculations (re-
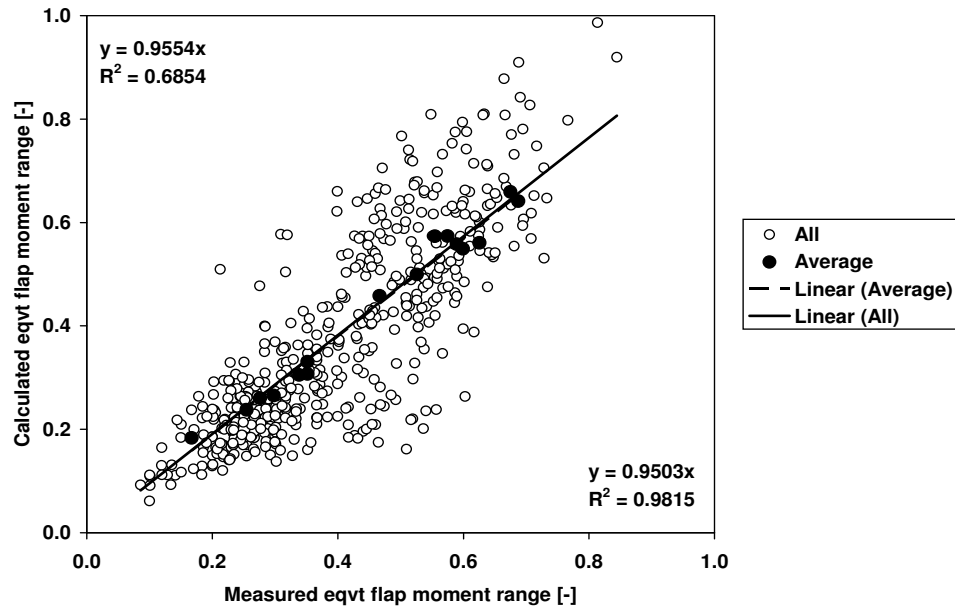
Figure 6.1: Comparison of measured and calculated equivalent blade root flap moment range for 500 10-minute periods (Vestas V90-3 MW). Normalised values, exponent $m = 12$)

sults converge to the right value if enough cases are considered), the important factor becomes the bias, which is maximally $\sim$10%, and hence the coefficient of variation may be set to $V = 0.03$ (otherwise more tuning would be done). To establish what the beneficial effect of load verification and tuning is, we consider the case where no measured loads are available. Recently a blind experiment was done in which many institutes tried to predict loads that were measured on a 10 m diameter wind turbine in the NASA Ames 24$\times$36 m^2 wind tunnel (Simms [191], Schreck [184]). Before the experiment, participants only received geometrical data of the turbine, and 2D profile data measured in a wind tunnel. Measured results were not revealed until load predictions had been completed.

While the best predictor was the EllipSys3D CFD-code (Sørensen [200]), of most interest to us is the performance of BEM-codes that participated. Unfortunately, it is difficult to judge the results, firstly because some results are so far off that they almost must be due to gross errors, and secondly because all results are average loads (not load ranges) in constant flow without turbulence. Main shaft torque predictions range from 50 to 150% of the true value and blade bending moment predictions from 70 to 130%. We assume here that the coefficient of variation on equivalent fatigue loads due to inaccurate aerodynamic modelling is $V = 0.10$–0.15.
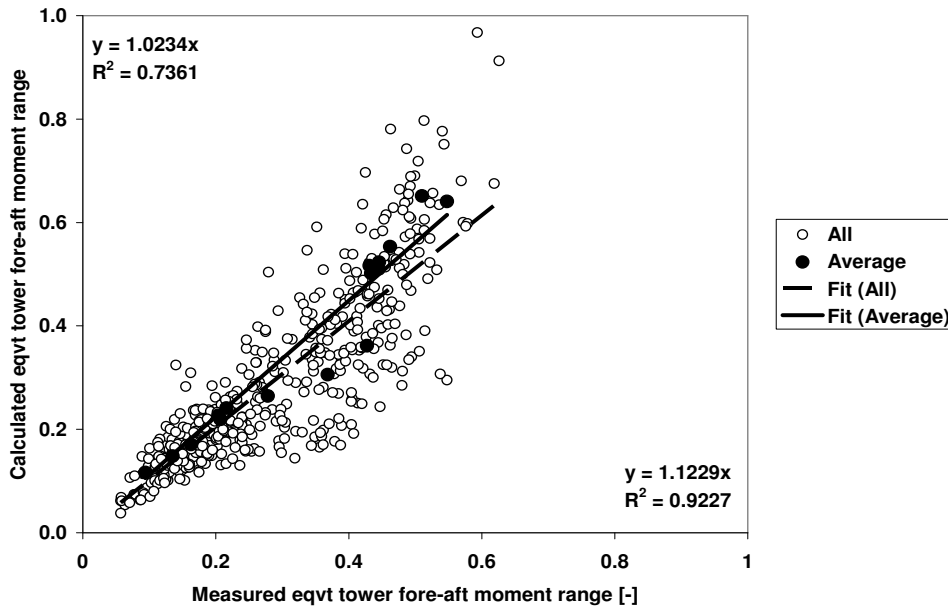
Figure 6.2: Comparison of measured and calculated equivalent tower base fore-aft moment range for 500 10-minute periods (Vestas V90-3 MW, normalised values, exponent $m = 4$)

6.4 Control system

In pitch controlled variable speed wind turbines, the control system keeps the power and rotor speed within bounds. Electrical converters can handle generator speed intervals of 700–1300 rpm, therefore the usual control strategy is (numbers are just examples):

- At wind speeds below 8 m/s or so, maintain generator constant speed at 800 rpm; power varies with wind speed.

- At wind speeds between 8 and 14 m/s, keep constant tip speed ratio (but within the interval 800–1100 rpm); speed and power vary with wind speed.

- At wind speeds over 14 m/s, keep constant speed (1100 rpm) and constant power.

This is just the basic recipe; in fact it does not work that well if it is not improved with some special measures to take care of the transitions from one state to another, and to avoid drive train oscillations. Manufacturers are beginning to realise the possibilities of control systems: the ultimate goal is to keep remove all blade and tower load variations due to turbulence and oblique inflow, while still obtaining maximum energy output (see for example Bossanyi [20–22] for overviews - but there is an entire field devoted to the subject). Things that can be done to get nearer to that goal are to use

blade pitch control (and to a lesser degree generator torque control) to:

- Damp tower vibrations in fore-aft and side-side direction.

- Nullify the effect of wind shear and wind directions variations (this is usually called *cyclic pitching* because all blades make a sinusoidal pitch motion with 120 deg phase shift).

- Keep blade loads completely constant over a revolution by using *individual pitch control*, where blade pitch angle depends on root flap moment, or on 3/4 span angle of attack.

All this means that loads will become less dependent on site parameters and that considerable load reductions may be reached; on the other hand one gets increasingly dependent on correct controller tuning, which is a tricky thing because of many different (undamped) eigenmodes that may get excited, with unwanted consequences for loads.

In this work the choice is made to use a simple controller that is doing the basic power and speed control, because that is proven state-of-the-art. This controller is robust, and that is why it is felt that it can be justified to assume that parameter changes in the controller will not affect fatigue loads significantly.

6.5   Cut out wind speed

In calculations it is assumed that the wind turbine stops at exactly the specified cut out wind speed. In reality this may not be the case, because the wind speed must be determined from an anemometer on top of the nacelle, operating in the rotor wake. This creates some uncertainty in the actual wind stop wind speed, which has influence on the equivalent fatigue loads. It is difficult to say what the inaccuracy is, but a maximum error of ± 1 m/s cannot be too far off, which would make the standard deviation $\sigma = 0.3$ m/s. However effect on equivalent fatigue loads is negligible.

6.6   Structural model

There are two methods in use in wind turbine modelling, the finite element method (FEM) or 'multibody dynamics' approach (in which the turbine is represented as an arbitrary number of masses, beams, springs et cetera), and the mode shape approach (in which modelling is restricted a priori to a number of mode shapes judged to be relevant, typically mode shapes with frequencies less than 10 Hz). The advantage of the FEM approach is that any turbine and any support construction can be modeled with the same method; the mode shape approach is less flexible. The advantage of the mode shape approach is its great speed: FEM beam modelling generates many high frequency modes, that make it necessary to either use small time steps or suppress higher modes with the use of implicit integration schemes. So far it has not been

shown that the FEM method is more accurate; in fact, an investigation by Thomsen [209] in which he compared Stig Øye's Flex5 (mode shape) and Risø's HAWC (FEM/MD), showed identical results. In the author's view this is not surprising, since the modelling problem does not have to do so much with mass-damper-spring systems (which are quite accurate), but with aerodynamics. Incidentally, all calculations for this work were done with the code Flex5, developed by Stig Øye. Flex5 belongs to the mode shape family, and has all customary engineering models described in chapter 6.

6.6.1 Blade representation

Blades may be represented in a more or in a less sophisticated way:

1. Flap and lead-lag mode shapes assumed to be perpendicular to each other. Typically 2 flap and 1 lead-lag mode with $f < 5$ Hz are used. In this approach the blade is assumed to have a beam inside it that is rotated over an angle taken to be the blade twist at mid span. It can be shown with accurate finite element calculations that the first three 'real' blade modes are very close to these simplified modes.

2. Combined flap/lead-lag modes. Typically 2 predominantly flap modes and 1 predominantly lead-lag mode are used.

The different approaches are compared in table 6.1 for an arbitrary load case, production at 20 m/s. Except for the calculations with 2 modes, results are all close to each other. If we assume that the 5 mode calculation is accurate, the maximum error introduced by using only 3 modes is less then 1%, and may be neglected.

Table 6.1: Influence of the number of blade modes (production at 20 m/s). Table values are the difference in equivalent load compared to the standard approach with 3 modes assumed to be perpendicular to each other) (Veldkamp [222])

modes (+ = used)		3 perp.	2	3	4	5
1. 0.69 Hz (1Flap)		+	+	+	+	+
2. 1.31 Hz (1Edge)		+	+	+	+	+
3. 1.76 Hz (2F)		+		+	+	+
4. 3.15 Hz (3F)					+	+
5. 4.46 Hz (2E)						+
load component	m	difference in [%]				
Mx11r	10	0	+2.7	+1.1	+1.6	+2.0
My11r	10	0	-2.7	+0.9	+1.4	+1.0
MxNf	8	0	-3.8	-1.8	-2.1	-1.0
MyNf	8	0	0.0	0.0	+0.9	+0.5
MzNf	8	0	+1.1	-0.5	-0.7	-0.8
Mxt0	4	0	-0.9	+0.4	-0.4	-0.1
Myt0	4	0	+0.4	-0.3	+1.0	-0.1

6.6.2   Tower representation

Until a few years ago, towers were modeled as springs attached to the nacelle, for example with two linear springs in horizontal directions and one torsional spring (for yawing motion). This is all right for short towers (say up to 50 m). Nowadays towers are so high that it is necessary to include second order effects (bending of the tower produces an additional bending moment) and higher modes. Modern programs can have 2×2 tower modes plus 2×2 monopile modes (or even more), resulting in 2×4 bending modes for a tower-monopile combination. It was shown (in some internal company investigations) that results are identical to results obtained with a full finite element calculation. Again this source of uncertainty may be neglected.

6.6.3   Eigenfrequency errors

The exact representation of the structure may be of little consequence, but eigenfrequency errors may be important because of the energy distribution in wind and in waves. The variation in eigenfrequency can not be accounted for if there is some gross design error, like for example tower frequency being close to the wave peak frequency. The only thing one can do is to look at the variation that occurs in loads if frequencies vary in a normal design.

For both the tower and the blades the matter was investigated by varying the stiffness ±10%, which results in 5% change in resonance frequency. For a 'normally designed' turbine the influence on loads is small (see tables 6.2 and 6.3), and hence the uncertainty is simply incorporated with a multiplication factor having a normal distribution $N(\mu = 1, \sigma = 0.01)$.

Table 6.2: Influence of blade eigenfrequency variation on 20 years equivalent fatigue loads. Land turbine, IEC class II standard load calculation.

Load	m	Frequency ratio		
		0.95	1.00	1.05
Blade root lead-lag moment Mx11r	12	1.03	1.00	0.98
Blade root flap moment My11r	12	1.00	1.00	1.02
Hub lead-lag moment Mx11h	6	1.02	1.00	0.99
Hub flap moment My11h	6	0.99	1.00	1.02
Nacelle roll moment MxNf	6	1.00	1.00	1.00
Nacelle tilt moment MyNf	6	0.98	1.00	1.02
Nacelle yaw moment MzNf	6	0.99	1.00	1.01
Tower base fore-aft moment Myt0	4	1.03	1.00	1.00

6.7   FEM modelling

The Finite Element Method has been in use for decades now to find stresses in complicated structures, but recently it has become common practice to generate finite element models of components directly from 3D drawing tools, like ProEngineer. This makes it possible to establish stresses in critical locations as function of external loads with high accuracy. Also freedom in FE modelling is limited and agreement in results from different firms improved. However there is still some room for individual choices: element and fillet size for example. A full list of possible error sources comprises:

- Limitations in element size and order (for example 2D plate/shell elements are used instead of 3D bricks).

- Mesh generation (element shape and mesh size).

- Boundary conditions.

- Selection of critical locations (hot spots).

- Linear transfer function.

- Geometrical deviations.

Mesh generation. To get an idea of the influence of mesh size, test calculations were done by Bech Lauridzen [11]. For 10 critical locations in a hub unit stresses were determined, using different mesh sizes. From blade load histories, stress time histories at critical locations were calculated, which were rainflow counted in the usual way. Finally fatigue damage and stress reserve factors were established. Results are given in table 6.4 (next page), where the value of the stress reserve factor for the coarsest mesh is arbitrarily set to $SRF = 1$. In this case it is seen that stress reserve factors tend to increase with smaller mesh size (but not always).

We cannot establish mean conservatism, because it is unknown which calculation would have been used; however we can establish the coefficient of variation for all

Table 6.3: Influence of tower eigenfrequency variation on 20 years equivalent fatigue loads. Land turbine, IEC class II standard load calculation.

Load	m	Frequency ratio		
		0.95	1.00	1.05
Blade root lead-lag moment Mx11r	12	1.00	1.00	1.00
Blade root flap moment My11r	12	1.01	1.00	1.01
Hub lead-lag moment Mx11h	6	1.00	1.00	1.00
Hub flap moment My11h	6	1.01	1.00	1.02
Nacelle roll moment MxNf	6	1.01	1.00	1.00
Nacelle tilt moment MyNf	6	1.00	1.00	1.00
Nacelle yaw moment MzNf	6	1.01	1.00	1.00
Tower base fore-aft moment Myt0	4	1.05	1.00	0.99

stress reserve factors, which is $V = 0.04$. Given the much reduced cost of FEM calculations at present, it would seem advisable to do sensitivity studies in every project, to remove this source of uncertainty.

Boundary conditions. A difficulty in determining correct unit stresses is the influence of boundary conditions. Over the years it has become apparent that hubs or machine frames cannot just be 'fixed to the infinitely stiff world', but that detailed models of supporting elements are necessary, like the main shaft for the hub, or the yaw bearing plus tower top for the nacelle machine frame.

In the case we consider, the hub is not connected to a main shaft with bolts, but to a ring bearing located in the front of the nacelle. In the FEM calculation the bearing may either be considered to be infinitely stiff, or have some finite stiffness EI. Here E is Young's modulus and I is some areal moment representative for the bearing, that was estimated from the dimensions of the bearing ring and rollers. Apart from the best estimate EI, more flexible bearing rings were also considered with stiffnesses $EI/2$ and $EI/4$.

Results are given in table 6.5, where values of the stress reserve factor are given for critical locations in the wind turbine hub. Stress reserve factors for the infinitely stiff case are arbitrarily set to $SRF = 1$. The pattern that emerges is that critical locations in the front of the hub (locations 1–4) are not affected at all, while correct modelling of the stiffness is critical for locations close to where the boundary conditions are (locations 5–10, and especially 6–7).

Selection of critical locations. The selection of critical locations is not a problem. Either it is very clear where they are, or else many locations are chosen (which is no problem with the available computer capacity, in fact all elements may be checked if one so desires).

Table 6.4: Influence of mesh size on stress reserve factor found in FEM calculations for a wind turbine hub. Source: Bech Lauridzen [11].

Mesh size [mm]		40	28	22		COV
location 1	edge of	1.00	1.03	1.01		0.02
location 2	a hole	1.00	1.00	1.01		0.01
location 3		1.00	0.97	0.98		0.02
location 4		1.00	1.04	1.01		0.02
Mesh size [mm]		4	3	2.6	2	
location 5	fillet	1.00	1.14	1.11	1.11	0.06
location 6		1.00	1.01	1.06	0.98	0.03
location 7		1.00	1.15	1.07	1.03	0.06
Mesh size [mm]		8	5	4	3	
location 8	fillet	1.00	1.14	1.16	1.16	0.07
location 9		1.00	1.12	1.05	1.06	0.05
location 10		1.00	1.02	1.06	1.02	0.02
Average						0.04
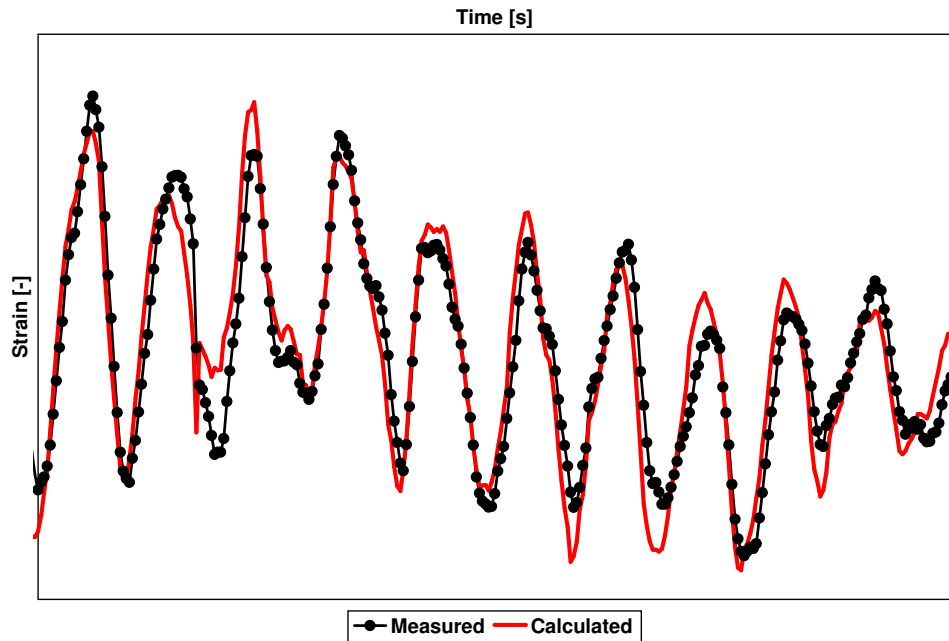
Figure 6.3: Comparison of measured and FEM-calculated strain signal. Source: Last [124], reproduced by permission.

Linear transfer function. A question is how good the linear transfer function is that is assumed in equation (3.17) (p42), and whether local stresses are simple linear functions of the varying external loads. Because of the linearity of steel behaviour,

Table 6.5: Influence of boundary conditions on stress reserve factor found in FEM calculations for a wind turbine hub. The number EI is an estimate of the bearing ring stiffness. Source: Bech Lauridzen [11].

location	no	stiff	EI	$EI/2$	$EI/4$
front of	1	1.00	1.01	1.02	1.02
the hub	2	1.00	1.01	1.01	1.01
	3	1.00	1.01	1.01	1.01
	4	1.00	1.01	1.01	1.01
close to	5	1.00	1.25	1.11	1.01
bearing	6	1.00	1.44	1.29	1.19
ring	7	1.00	1.61	1.68	1.68
	8	1.00	1.13	1.11	1.09
	9	1.00	0.96	0.95	0.94
	10	1.00	0.98	0.98	0.97

one would of course expect good agreement, and this is what was found by Last [124], in an experiment where the strain at a weld toe was considered (see figure 6.3, previous page). The strain was calculated by extrapolation from stresses measured with strain gauges, and the corresponding calculation was done with data from a FEM-model, subjected to the same external loads. Correspondence is not perfect but the correlation coefficient in the example is high: $r^2 = 0.88$.

It is difficult to say what the influence of the last two things (errors in boundary conditions and transfer functions) is on stress. For want of better information it is assumed that there is no bias, and that the coefficient of variation is the same as found in meshing: $V = 0.04$. This gives a combined coefficient of variation $V = 0.06$ (this holds for the blade, the hub and the nacelle machine frame; the tower is such a simple structure that no additional uncertainty needs to be used: $V = 0.03$).

Geometrical deviations. Real components will generally not have dimensions specified on drawings, but rather show scatter. Usually requirements are set to ensure that (for example) 95% of all plates has a thickness larger than the nominal value.

As far as geometrical deviations are concerned, for steel plates investigations were done by Byfield [31]. He found the following (see table 6.6): dependent on whether the stress depends on area or on section modulus, the coefficient of variation varies somewhat, but the distribution $N(\mu = 1,\ V = 0.03)$ seems a good choice for the circumferential welds in the wind turbine tower.

The same value is also used for other components considered, because no specific data are available.

Table 6.6: Mean and coefficient of variation of geometrical properties. Source: Byfield [31].

Parameter	Eurocode 3		Measured	
	mean μ	COV V	mean μ	COV V
Area [m^2]	1	0.03	0.99	0.022
Section modulus (y) [m^3]			1.00	0.019
Section modulus (z) [m^3]			0.98	0.029
Inertia (y) [m^4]	1	0.03	1.00	0.025
Inertia (z) [m^4]	1	0.03	0.98	0.037

Chapter 7

Fatigue

Aussagen wie "die Miner-regel ist falsch" halten einer sachlichen Prüfung nicht stand.

— E. Haibach [77]

Die rechnerische Lebensdauerabschätzung schwingbelasteter Bauteile unter Anwendung von Schadensakkumulationshypothesen gelingt bisher trotz umfangreicher Anstrengungen auf diesem Gebiet im algemeinen nicht mit der erforderlichen Zuverlässigkeit.

— P. Heuler [89]

7.1   Introduction

The fifth and last part of the stochastic parameter investigation concerns the fatigue properties of the material. Even if the climate were exactly known, stresses could be found with 100% accuracy and the manufacturing process had zero tolerance, there would still be variation in component life.

Fatigue is the phenomenon that small varying loads may eventually cause failure, in spite of the fact that they are well below the static yield limit. This happens because locally there are always stresses higher than the yield limit due to (surface) imperfections and associated stress concentration, which cause local plastic deformation. If the load is varying there may be new plastic deformations with every load cycle, leading to a micro crack, which via the stage of a 'technical crack' (a few tenths of a mm), finally develops into a large crack which will cause collapse. In composites the failure mechanisms are different, damage may for example be caused by fibre micro-buckling. The challenge is to predict component life with sufficient accuracy for any type of variable loading (life is the time until a crack of defined length or depth is formed, or until collapse). Before going into various approaches, we shortly

discuss some background and definitions[1]. For comprehensive treatment of the issues involved, two good references are Haibach [77] and Schijve [183].

7.1.1   S-N or Wöhler curve

The S-N or Wöhler curve (figure 7.1) gives the number of load cycles that can be withstood as function of the cyclic, constant amplitude (CA) load. It is established by applying a certain cyclic load to a specimen and recording the number of cycles until failure, or sometimes until a crack of some predefined size is created. The cyclic load is defined by the stress ratio R, given by the cycle minimum stress divided by the maximum:

$$R = \frac{\sigma_{min}}{\sigma_{max}} \tag{7.1}$$

Thus a sinusoidal load which is symmetric around zero has $R = -1$, while a sinusoidal load with zero minimum value has $R = 0$. Usually the curve (for some fixed R) is well described with a power law:

$$N = N_D \left(\frac{\Delta\sigma_A}{\Delta\sigma} \right)^m \tag{7.2}$$

The fatigue strength (fatigue limit, endurance limit) $\Delta\sigma_A$ is the load level below which no failure occurs under constant amplitude loading. The intersection of the tilted and horizontal part of the curve is at N_D cycles, and m (the Wöhler exponent) is conventionally called the slope of the curve. The number N is the fatigue life if the load range is $\Delta\sigma$. The bold curve in figure 7.1 is called the 'Original Miner curve'. It is derived from the experimental data: the black dots (for some discussion of how accurately the curve may be established, see appendix C.5).

If the load situation is more complicated than a signal varying with constant amplitude, the original curve with fatigue limit is no longer valid. Small load cycles cannot start a crack (that is why the fatigue limit is found), but can nevertheless contribute to growth of an existing crack (because the crack is a notch that creates large local stresses). The question is how to modify the original curve to account for the effect of small cycles. The simplest proposal is to just extend the left part of the curve with the same slope (Elementary Miner or Corten-Dolan). This seems conservative; however according to Liu and Zenner [239] the relevant curve for life prediction under variable loading must also be steeper (see discussion below in section 7.1.3). Another possibility is the correction proposed by Haibach [77], where the slope of the right part of the curve is taken to be:

$$m_{right} = 2\,m_{left} - 1 \tag{7.3}$$

---

[1]The following discussion is primarily about metals and not necessarily valid for composites. We do not consider multiaxial fatigue (for example the Critical Plane Approach), because firstly, almost all stress situations are two dimensional (critical locations are at the surface) and dominated by one tensile stress, and secondly, there is no evidence that more complicated methods yield superior results.
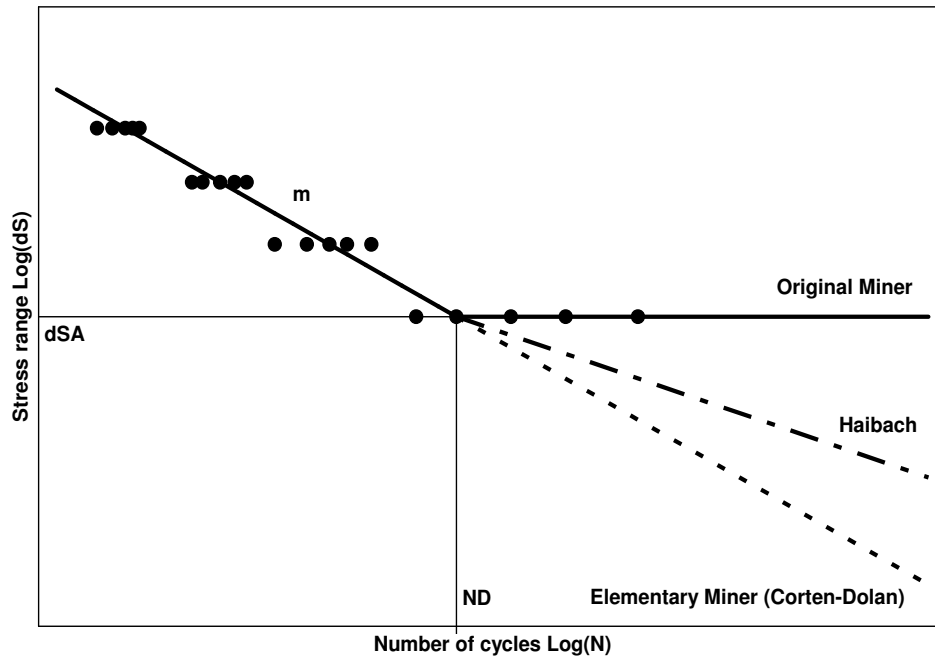
Figure 7.1: S-N or Wöhler curve with different extensions to deal with variable amplitude loading (schematic).

This is for example seen in the Eurocode 3 S-N curves for welded details (m_{left} = 3, m_{right} = 5). Although Haibach provides a theoretical justification for this correction, it is also appealing on the grounds that the right curve must be somewhere in between the original and elementary Miner lines.

7.1.2 Scatter

If fatigue tests are done, measurements may not be on the curve, but scatter around it (figure 7.1). There are two causes for this: firstly there is variation in the time a crack at the surface starts due to variations in the state of the surface, and secondly there is variation in the growth speed of the crack, due to variation in material bulk properties (Schijve [182, 183]). If the surface of a component is smooth and there is no stress concentration, the first source of variation is most important: most of the time until failure is spent in the crack initiation stage (Gudehus [74]); the S-N curve tends to be flat (large exponent m). This is because if loads are large, a crack will start soon (regardless of the surface condition), while if loads are small, it may take very long before a crack starts. If the load is smaller than $\Delta\sigma_A$ life is infinite, because no crack will be initiated (see figure 7.1, 'Original Miner'). If there is a crack present, like

there may be in the case of a weld seam, there is (almost) no crack initiation stage, and the curve will be steeper (small exponent m).

The amount of variation in life at a certain load (number of load cycles until failure) is expressed by the scatter number T_N, the ratio of the life attained by the best 10% of all test specimens $N_{10\%}$ divided by the life attained by 90% of all test specimens $N_{90\%}$:

$$T_N = \frac{N_{10\%}}{N_{90\%}} \tag{7.4}$$

If the life distribution $F(N)$ is assumed to be lognormal (and in many cases there is no evidence to the contrary, Eulitz [60]), then:

$$F(N) = N\left(\frac{\ln N - \ln M_N}{S_N}\right) \tag{7.5}$$

and the scale parameter S_N is (N_{inv} is the inverse of the standard normal distribution):

$$S_N = \frac{\ln T_N}{2\, N_{inv}(0.90)} \approx \frac{\ln T_N}{2.563} \tag{7.6}$$

The coefficient of variation on life V_N is:

$$V_N = \sqrt{\exp\left(S_N^2\right) - 1} \tag{7.7}$$

If $S_N \ll 1$, then:

$$V_N \approx S_N \tag{7.8}$$

For completeness we give the median of the distribution:

$$N_{50\%} = M_N \tag{7.9}$$

the mean:

$$\mu_N = M_N \sqrt{\exp S_N^2} \tag{7.10}$$

and finally the standard deviation:

$$\sigma = \mu_N V_N = M_N \sqrt{\exp\left(S_N^2\right)\left(\exp(S_N^2) - 1\right)} \tag{7.11}$$

If the slope of the S-N curve is m, conversion from life scatter to stress scatter is straightforward. The scale parameter S_σ and the scatter number T_σ are found with:

$$S_\sigma = \frac{S_N}{m} \tag{7.12}$$

$$T_\sigma = T_N^{1/m} \tag{7.13}$$

The coefficient of variation V_σ can be calculated exactly with an expression similar to equation (7.7). It may be approximated by:

$$V_\sigma \approx \frac{V_N}{m} \tag{7.14}$$

This concludes the overview of the distribution formulas to be used in the calculations.

7.1.3   Variable amplitude loading

If we are dealing with constant amplitude loading, and relevant tests are available, life prediction is trivial: at some load level the best prediction is simply the median number of cycles established in the tests. Now consider the case of a random load signal, consisting of a mix of large and small load cycles. The method most used to make predictions is the linear damage summation or Palmgren-Miner rule (see appendix C). However in the case of VA-loading it is usually found that the Palmgren-Miner rule is unconservative, and overestimates fatigue life. The reason for this is that the original S-N curve no longer applies under random loading. There are bound to be some large load cycles in the spectrum, that quickly initiate a crack; once there is a crack, smaller cycles below the fatigue limit will contribute to fatigue damage. Hence the first thing that must be done to improve the curve, is to extend it below the fatigue limit, for instance according to Corten-Dolan, or according to Haibach (see figure 7.1, p109). However Eulitz [60, 61] found no life prediction improvement if either of these extensions were used. A possible explanation for this is that because the crack initiation stage is short, the component must be treated as sharply notched from the start, and the S-N curve becomes steeper. Together with the lowering of the fatigue limit, this forms the essence of the Liu-Zenner correction (see figure 7.2 (next page) and Zenner [239]), where the curve is rotated around the point of the largest load cycle. Both the slope m and the fatigue limit $\Delta\sigma_A$ are modified:

$$m' = \frac{m + 3.6}{2} \tag{7.15}$$

$$\Delta\sigma'_A = \frac{\Delta\sigma_A}{2} \tag{7.16}$$

Note that equation (7.15) is consistent with results for welded connections which are known to have a crack (notch) and have slope $m = 3$–4 to start with (see Ritter [175] and Sedlacek [187] (background document for Eurocode 3)). Because there already is a crack, the slope of the S-N curve should not change if VA-loading is considered instead of CA-loading. It is easily seen that for $m = 3.6$ one finds $m' = 3.6 = m$.
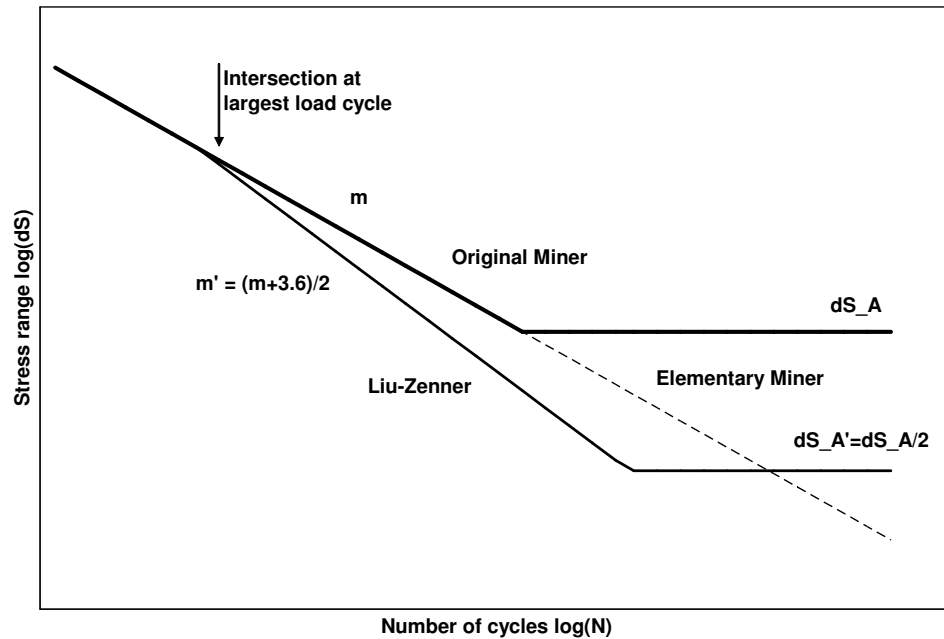
Figure 7.2: S-N curve with correction according to Liu and Zenner [110].

7.1.4   Life curve

For many applications, characteristic load spectra have been developed, for example Twist (Transport Wing Standard) for airplanes, Wawesta (Walzwerkstandard) for rolling machines, and Wisper/WisperX for wind turbine blades. All these spectra have a fixed loading sequence and are scalable, which means that they may for example be characterised by the largest load cycle in the spectrum. Thus it becomes possible to construct a pseudo S-N curve or life curve, where the number of cycles until failure is given as function of the largest load cycle of the spectrum; in this case the life curve will of course be to the right of the normal S-N curve for constant amplitude loading (see figure 7.3).

If the life curve is predicted using Palmgren-Miner linear damage summation it is often found that life is overpredicted, i.e. the number of cycles until failure found in test is less than calculated. One way of making the predictions fit observations is using the relative Miner rule: one simply states that under a certain load spectrum the (fictitious) damage at failure is $D = 0.5$ rather than $D = 1$.

Another way is to prescribe that the life prediction must not be done with the original experimental S-N curve, but with a curve reduced by multiplication with the
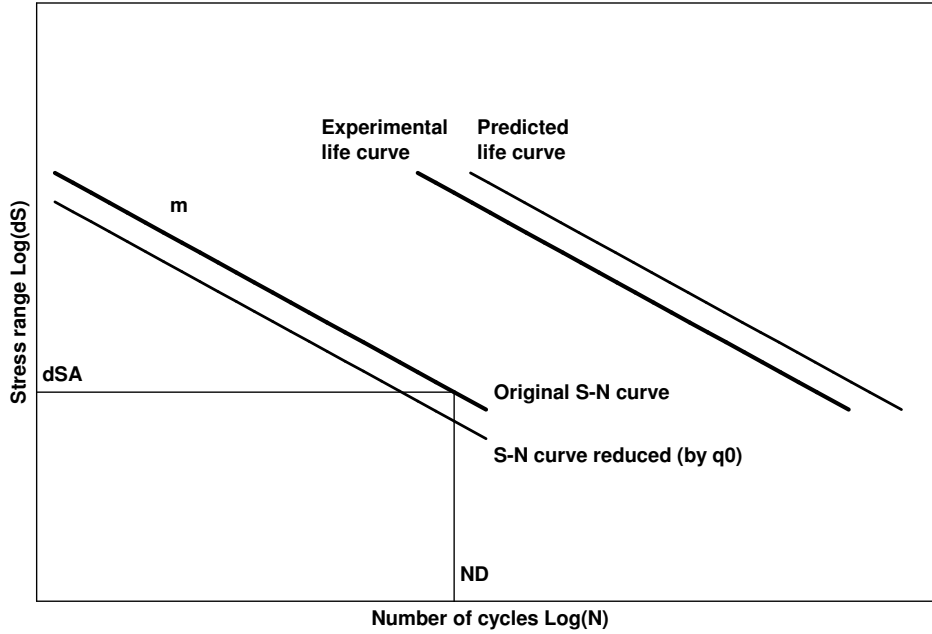
Figure 7.3: Life curve and application of q_0 method (relative Miner rule).

stress factor q_0. The damage D calculated from a test to failure is:

$$D = \sum_i \frac{n_i}{N_D} \left(\frac{\Delta\sigma_i}{\Delta\sigma_A} \right)^m \neq 1 \tag{7.17}$$

We modify the S-N curve on which the prediction was based by a stress factor q_0 to obtain a new damage sum $D' = 1$:

$$D' = \sum_i \frac{n_i}{N_D} \left(\frac{\Delta\sigma_i}{q_0\Delta\sigma_A} \right)^m = 1 \tag{7.18}$$

From these two equations it follows immediately that:

$$\frac{D}{D'} = D = q_0^m \tag{7.19}$$

The q_0 method may be combined with the Liu-Zenner correction.

7.2 Fatigue life prediction

7.2.1 Acceptable scatter

If we consider fatigue life prediction, we may define the fatigue damage that a component is calculated to be able to sustain as $D = 1$. Experimental results (the damage calculated from all actual load cycles sustained) will scatter around this value. The scatter in experimental damage may be treated in the same way as before with:

$$T_D = \frac{D_{10\%}}{D_{90\%}} \tag{7.20}$$

with D being the experimental fatigue damage. Schütz [185] gives some guidelines on which accuracy is acceptable if the life of some individual component is predicted (see table 7.1). It is interesting to see whether these demands can be met. Eulitz [61] derived some best possible values for the scatter number T_N (scatter on life) from the test database he compiled. The S-N curve is typically derived as follows: constant amplitude (CA) tests are done at $n_{\Delta\sigma}$ stress levels with n_S specimens each (for example at $n_{\Delta\sigma} = 4$ stress levels, with $n_S = 5$ specimens at each level); thus $n_{\Delta\sigma}$ estimated points of the 50% survival S-N curve are found. The scatter numbers for variation of individual lives and median life (at one stress level) are related as:

$$T_{N,50\%} = T_N^{\frac{1}{\sqrt{n_S}}} \tag{7.21}$$

Using all his data, Eulitz found average scatter $T_{N,50\%}$ = 1.51 for the median life, i.e. for 50% points of the CA S-N curve at some given load level. For *individual* lives found in tests with variable amplitude loading, the average scatter was T_D = 3.2. Eulitz considers the two scatter numbers to be independent, because the causes

Table 7.1: Indicative values for lifetime predictions (based on Schütz [185]).

Fatigue damage	$D_{90\%}$	$D_{10\%}$	T_D	V_D
Good	0.67	1.50	2.25	0.324
Acceptable	0.50	2.00	4.00	0.583
Stress factor	$q_{0,90\%}$	$q_{0,10\%}$	T_σ	V_σ
$m = 4$				
Good	0.90	1.11	1.22	0.080
Acceptable	0.84	1.19	1.41	0.139
$m = 8$				
Good	0.95	1.05	1.11	0.040
Acceptable	0.92	1.09	1.19	0.068
$m = 12$				
Good	0.97	1.03	1.07	0.026
Acceptable	0.94	1.06	1.12	0.045

of scatter are different in the case of CA-loading (mainly time to crack initiation) and VA-loading (mainly the load sequence). Therefore, even if we have a perfect prediction algorithm, the total scatter cannot be smaller than:

$$T = \exp\left(\sqrt{\ln^2 1.51 + \ln^2 3.2}\right) \approx 3.4 \tag{7.22}$$

for the predictions of the life of an individual component under VA loading based on the CA S-N curve. The scatter number $T = 3.4$ corresponds to a coefficient of variation $V = 0.51$ on life. Admittedly Eulitz's considerations are somewhat pessimistic because uncertainty on the entire CA-curve is likely to be smaller than the uncertainty on one point of the curve (the curve is based on the experiments at all stress levels, hence the uncertainty is smaller), but even if the curve is known exactly, $T = 3.2$ is an absolute minimum. This means that $V_\sigma = 0.11$ (for welds with $m \sim 4$) and $V_\sigma = 0.08$ (for cast iron with $m \sim 6$) if we convert from life to stress.

We now discuss various ways to predict fatigue life, to see how well they do compared to the minimum possible scatter. It must be noted that scatter numbers given by various authors usually refer to *median* values i.e. on the basis of more individual tests the 50% survival damage (or life) is estimated, which is compared to the prediction. The scatter results given are all experimentally found, no assumption are made about the origin of scatter.

7.2.2 Synthetic S-N curve

The S-N curve is established on the basis of fatigue tests that are done on small, smooth specimens under CA loading[2]. The main reason to do this is that this type of experiment is comparatively cheap and fast. The S-N curve for ideal material is then modified in order to make it representative for the actual component. Effects that have to be taken into account are:

- Size effect. If two specimen have the same geometry but differ in size, the probability that some crack will develop is greater in the larger specimen, because there are more weak locations to start from. This is the statistical size effect (see appendix F.4). Another effect is that the stress situation will be different in larger specimens.

- Surface roughness. If the surface is not smooth, the situation is like a crack is already present, and life will be shorter than for a smooth surface.

- Stress concentration factor. Local stress concentration decreases the fatigue strength, but not as much as would be found if the maximum stress were compared to the S-N curve found. Therefore a 'notch factor 'or 'effective stress concentration factor' is estimated to reduce the curve.

---

[2]Weld seams are an exception. The equivalent of the small smooth test probe for welds is (in most cases) a test piece with a short seam, typically 100–200 mm long.

- Quality. In larger components it is more difficult to obtain the same material quality. Furthermore, in cast iron there may be gas cavities, slag inclusions and graphite (flakes or chunks).

- Mean stress. Generally, positive mean stress will reduce fatigue strength, while a negative mean stress tends to increase it.

After all corrections have been done, a *synthetic* S-N curve is obtained (see for example Gudehus [74] and Haibach [77] for procedures, also to estimate the curve from static properties only), which ideally should fit results obtained with the large component under constant amplitude loading. To estimate the fatigue damage under VA loading, the rainflow procedure is used to reduce the varying load signal to an ordered table with triplets of load range, mean load and number of cycles. For each triplet fatigue damage is separately assessed, and assumed to be independent of the rest of the load history (linear summation according to the Palmgren-Miner rule). The medians and scatter numbers for fatigue damage D and stress factor q_0 are given in table 7.2. The main problems with the use of synthetic S-N curves are the corrections that have to be made to go from small smooth probes to large components, which are based on curve fitting without (sufficient) physical basis, and the incorrectness of the linear summation rule, in which sequence effects are ignored.

7.2.3   Measured S-N curve

In this approach, tests to arrive at the CA S-N curve are done with the actual component, or with specimens that are representative for it in size and/or stress concentration factor. Thus the exact CA S-N curve is immediately available without the need for corrections. This obviously solves the correction problem, but not the inadequacy of the Palmgren-Miner rule. The approach was extensively investigated by Eulitz (see Eulitz [61], the research was also reported in Eulitz [60] and Kotte [109]). For steel, cast iron and aluminium, about 300 CA S-N curves were directly obtained from experiments, and these were used to predict component life found from 2,000 corresponding VA tests; in all the work was based on 18,000 individual tests. A great deal of attention was paid to details in the procedure: all tests results used were critically

Table 7.2: Results for fatigue life predictions using synthetic S-N curves. Each test represents a median life prediction on the basis of a CA S-N curve. The damage D is the calculated damage sustained on failure. Source: Eulitz [61].

material	load type	number of tests	damage D median	scatter T_D	stress factor q_0 median	scatter T_σ
steel	all	317	0.52	12.6		
steel	tension/compress.	179			0.84	1.65
steel	bending	244			0.90	1.63
cast iron	all	89	4.07	10.3	1.31	1.60

re-evaluated and missing information was added where possible; different methods for estimating the best S-N curve from scattered measurements were compared, as well as extensions of the S-N curves beyond the fatigue limit and how to count load cycles. During the work all information was stored in a database (DABEF = *Datensammlung Betriebsfestigkeit*) which might for example be used for testing fracture mechanical approaches (see below). The main results relevant to our study are:

- Of all counting methods, rainflow counting with mean stress correction is to be preferred.

- The Liu-Zenner correction must be used, according to which the S-N curve is rotated, accounting for the difference between CA and VA loading (Zenner [239]).

- The medians and scatter numbers for fatigue damage D and stress factor q_0 are given in table 7.3.

7.2.4 Life curve and relative Miner rule

In this approach, tests are done with variable amplitude loading according to some standardised pseudo random load sequence, for example a gaussian one, or some spectrum representative for actual loading. If test spectra only differ by a scale factor, it is possible to define each spectrum by some characteristic stress (for example the highest stress), and for each characteristic stress plot the number of cycles that was sustained until failure: the fatigue life curve (figure 7.3, p113). If one assumes that the damage accumulation rule according to a one slope S-N curve holds, one can calculate where the life curve ideally should have been. If this is compared to the experimental life curve one finds a reduction factor that should have been applied to the original S-N curve to arrive at the correct life prediction. This ratio of the stresses (which we call q_0 following Heuler [88], see equation (7.19)) is assumed to be constant for a particular shape of the spectrum, and thus some damage $D < 1$ is allowed (or a reduced S-N curve used). This approach, called the relative Miner rule, was described by Gassner [68, 69] and further researched by Buch [27, 28] and

Table 7.3: Results for fatigue life prediction using measured S-N curves with Liu-Zenner correction. Each test represents a median life prediction on the basis of a CA S-N curve. The damage D is the calculated damage sustained on failure. Source: Eulitz [61].

material	load type	number of tests	damage D		stress factor q_0	
			median	scatter T_D	median	scatter T_σ
steel	tension/compr.	179	0.44	6.2	0.87	1.39
steel	bending	244	0.69	8.1	0.91	1.59
cast iron	bending	89	1.19	10.4	1.03	1.46
aluminium	tension/compr.	219	0.63	6.1	0.92	1.40
aluminium	bending	86	1.09	6.5	1.02	1.50

Heuler [88, 89]. Heuler's approach is simplest, because the equivalent fatigue load is calculated according to the elementary (one slope) S-N curve and then a factor is applied to either life or stress to arrive at unity mean predicted life. The results that were obtained are given in table 7.4. One test (which yields one value for q_0) consists of enough individual fatigue tests to establish the 50% survival CA S-N curve and the 50% survival life curve. Thus the scatter numbers given refer to median values, not scatter in individual specimen tests. In individual tests done to establish the life curve, all load spectra are the same on a cycle by cycle basis (except for a size factor).

7.2.5   Fracture mechanics

In this approach fracture mechanics is used to estimate crack growth. The simplest forms of fracture mechanics deal with the situation where there is a sizable (technical) crack, and material behaviour is fully elastic. Given some macro crack, life until failure can be estimated (Schijve [183]). However in many cases most of the component's life is spent in the formation of this technical crack, and once this has developed into a technical crack (a few tenths of a mm) there is not much time left until failure. Conventional fracture mechanics is not suitable to treat this situation. However Vormwald [227, 229] developed a new fracture mechanical approach especially for microcrack using an energy integral (the P_J-integral), which takes plasticity and crack closure into account. His approach was further developed by Anthes [3] and Dankert [43], for an overview see Haibach [77]. Anthes [3] provides some convincing examples that the approach works well for smooth specimens under variable loading: the median life prediction is close to unity, and the scatter number $T_D = D_{10\%}/D_{90\%} = 3.5$. Perhaps this approach could be extended to real components, but calibration would be necessary. Also it would have to be checked whether the method is useful for very large numbers of cycles encountered in wind turbines $(10^8 - 10^9)$.

The JCSS probabilistic code [96] describes a simple fracture mechanical method that must be calibrated against fatigue tests; inaccuracies are accounted for by con-

Table 7.4: Results for fatigue life prediction using the relative Miner rule (q_0-approach). Each test represents one value for q_0 derived from a CA S-N curve and a life curve. Numbers for damage are derived (by the author) from numbers for the stress factor q_0 with exponent $m = 5$. Source: Heuler [88].

material	load type	number of tests	damage D median	damage D scatter T_D	stress factor q_0 median	stress factor q_0 scatter T_σ
steel/	gaussian spectrum	60	(0.42)	(4.2)	0.84	1.33
cast	Straight line spect.	17	(0.19)	(6.9)	0.72	1.47
iron	LBF spectrum	123	(0.70)	(3.9)	0.93	1.31

sidering the constants governing crack growth as stochastic parameters. The method does not take sequence effects into account however.

7.2.6 Overview

In table 7.5 a summary is given of the accuracy that can be reached for lifetime predictions with various methods for steel and cast iron. A few remarks are in order here.

Firstly it should be stated that the decimals in the table are only given to achieve consistency between table numbers. It is clear that as far as accuracy goes, the number of decimals for life scatter T_N should be zero, and for stress scatter T_σ one.

Secondly it is seen that the scatter found by Eulitz [61] is high compared to numbers that were found by Heuler [88, 89], while they are essentially using the same procedure. The difference is that Heuler derives scatter numbers for each individual random load spectrum, while Eulitz considers many types of random loading simultaneously. According to Haibach [77] the large scatter found by Eulitz could (in part) be due to the fact that VA-test fatigue data from many different sources were used, which may not be comparable, i.e. laboratories were not using identical procedures in their experiments. In any case it seems clear that the numbers found by Heuler provide a lower limit for the scatter that can be obtained with this procedure (relative Miner rule for standardised pseudo random spectra). Since one only knows the statistical properties of loading sequences in wind turbines, the situation there may be worse.

Thirdly, it must be stressed that the numbers found by Heuler and Eulitz are related to median curves. Essentially both authors compared 50% survival CA S-N curves with 50% survival VA life curves. If we consider the life of individual components, we must also take into account variation in individual strength. Eulitz provides a scatter number (from experiments) $T_N = 3.2$, which translates into $T_\sigma = 1.21$ ($m = 6$) to $T_\sigma = 1.34$ ($m = 4$). These numbers appear to be reasonable, if one compares them to the scatter in CA tests on welds: $T_\sigma = 1.35$ (Olivier [163]), and

Table 7.5: Accuracy of various life prediction methods (numbers as given by the authors are given in bold). The scatter numbers in columns 2 and 3 represent scatter on medians (life and fatigue strength). To get the total scatter, these numbers must be combined with scatter on values in individual predictions.

Life prediction method	T_N medians	T_σ medians	T_σ individ.	T_σ total	V_σ total
Synthetic S-N curve [61]	**10.3-12.6**	**1.60-1.65**	1.3	1.71-1.76	0.21-0.22
Measured S-N curve [61]	**6.2-10.4**	**1.39-1.59**	1.3	1.52-1.70	0.17-0.21
Random loading test [88]	5-8	**1.31-1.47**	1.3	1.47-1.59	0.15-0.18
Fracture mechanics [3]	**3.5**	1.23-1.37	1.3	1.40-1.50	0.13-0.16

on cast iron: $T_\sigma = 1.20$ (Kaufmann [103, 105], Nerdahl [152]). For a fixed pseudo random load spectrum there is no reason why scatter should be larger than in CA tests (Schweiger [186]). However we probably should use a larger number for the case of wind turbines, because we are not sure of the exact load sequence. In the table the individual scatter was set to $T = 1.3$ as a reasonable mean value (for cast iron $T = 1.2$, for welds $T = 1.2$–1.4). Example: the total scatter if random loading tests are used is:

$$T_{\sigma,low} = \exp \sqrt{\left(\ln^2 1.31 + \ln^2 1.3\right)} = 1.46 \tag{7.23}$$

$$T_{\sigma,high} = \exp \sqrt{\left(\ln^2 1.47 + \ln^2 1.3\right)} = 1.59 \tag{7.24}$$

It is interesting to compare the numbers in table 7.5 with those given by the Joint Committee on Structural Safety in their proposal for a probabilistic code for weld seams [96]. Here the number of cycles until failure in CA tests is assumed to be lognormally distributed, as is the damage sum reached upon failure under VA loading. The former has coefficient of variation $V_{N,CA} = 0.58$, while the latter has $V_{N,VA} = 0.3$; both distributions are unbiased. The corresponding scatter numbers are (related to life):

$$T_{N,CA} \approx \exp\left(2.56 \times 0.58\right) = 4.4 \tag{7.25}$$

$$T_{N,VA} \approx \exp\left(2.56 \times 0.3\right) = 2.2 \tag{7.26}$$

If we convert to strength (with exponent $m = 3$), we find:

$$T_{\sigma,CA} = 4.4^{1/3} = 1.64 \tag{7.27}$$

$$T_{\sigma,VA} = 2.2^{1/3} = 1.29 \tag{7.28}$$

The total scatter number T_σ becomes:

$$T_\sigma = \exp \sqrt{\ln^2 1.64 + \ln^2 1.29} = 1.75 \tag{7.29}$$

And the coefficient of variation V_σ:

$$V_\sigma \approx \frac{\ln 1.75}{2.56} = 0.22 \tag{7.30}$$

This is the same order of magnitude as the numbers in table 7.5. If we take the specific numbers for weld seams (table 8.5, p145), we have $V_{\sigma,CA} = 0.11$ and $V_{\sigma,VA} = 0.17$, which together yield:

$$V_\sigma = \sqrt{0.11^2 + 0.17^2} = 0.20 \tag{7.31}$$

Hence there seems to be agreement on the total scatter on material fatigue properties, at least for welds. What the JCSS does (apparently) not consider however is that life predictions may be biased.

Fourthly, the low number for the fracture mechanical approach assumes that the method is calibrated for real size specimens. At present it is not sure whether the method could be applied with the same success.

All in all the conclusion is that the methods that take the load sequence into account (standard random load spectrum and fracture mechanics) have an advantage over the conventional method that does not, even if it is based on measured S-N curves. However it is not certain that this advantage can be realised for wind turbines, since the load sequence is only known in a statistical sense.

The most physical approach would be to model the structure's strength as some function decreasing with time, and subject the structure to a representative random load time history that includes all extremes that naturally occur. One could for instance look at 10 minute loading intervals: each time interval would either result in some crack growth (possibly zero), or result in failure (if one of the load cycles in a particular interval are larger than the remaining strength). In this approach there is no fatigue failure, there is only ultimate load failure: when this happens depends on how much the structure has deteriorated. The fracture mechanical methods developed by Vormwald and others could be used in this way (Anthes [3], Dankert [43], Vormwald [227]). Doing things like this is attractive because the artificial division between fatigue loads and ultimate loads is removed: in reality of course there is no such division: there is a continuous spectrum from small to large load cycles. In some cases it is even possible that what is classified by standards as a 50 years extreme event, occurs every few months or so.

However this is not (yet) the usual way of doing things: as matters stand, fatigue and ultimate loads are treated separately. This can be done because most of the component's life is spent in the crack initiation phase, and the strength is not much diminished until there is a sizable crack, and failure is imminent ('sudden death'). The approach is correct if there are few extreme events, because in that case fatigue damage caused by these events may be neglected. The situation becomes more complicated if large load cycles occur often: still one could deal with the problem by redefining the set of fatigue load cases to include the right number of extreme events.

7.3 Treatment of uncertainty

Now that we have some data on scatter of fatigue life predictions and on stress factor, the question is how to use these data in the probabilistic calculation. There are two uncertainties:

- Scatter on the median damage that is due to load sequence effects. The scatter numbers found by Eulitz may be the most representative; it is true that scatter

may be less in Heuler's life curve prediction method, especially because we are dealing with only one material (cast iron GGG40 for example), but on the other hand we do not have the required fatigue data, and neither do we know the actual load sequence in wind turbines.

- Scatter due to differences between individual components. A priori there is no reason why the scatter in tests to establish a life curve (with a fixed pseudo random load spectrum) would differ significantly from scatter on tests to establish a CA curve. In fact, if influence of the slope is removed by converting all variation to stress, it may well be argued that standard deviation on fatigue strength must be close to standard deviation on static strength. Therefore scatter numbers found in CA tests will be used as estimate for scatter in VA tests. Some fatigue experiments on $\varnothing 25$ mm notched aluminium cylinders reported by Schweiger [186] support the contention that scatter under CA and VA loading is similar.

Thus two separate lognormal distributions will be used to model uncertainty in fatigue behaviour, one characterised by Heuler's scatter numbers, and the other by scatter numbers on CA fatigue tests. The justification to proceed in this way is twofold: firstly, these are the data are available to us, and secondly, using the data in this way is (at least) approximately right.

7.4 Material data

7.4.1 Cast iron

Nodular cast iron is used for the nacelle machine frame and for the hub. Because of complex geometry it is convenient to cast these parts, and nodular cast irons have good fatigue properties. There are few public references in which fatigue data are given. Kaufmann [103] is a report of research at the Fraunhofer Institute, in which investigations are described on large cast iron specimens (40 x 70 mm cross section) taken from one large block, with a large quality range (from defect free specimens to specimens having chunky graphite, and with various stress concentration factors), The report gives all relevant details, such as the exact probe geometries and results of individual tests. The same research is also described in an article (Kaufmann [105]). Data are summarised in table 7.6.

For the uncertainty due to fatigue life prediction for VA-loading we have Eulitz's data [60, 61], which are for cast iron: median damage $D_{50\%} = 1.19$, $T_D = 10.4$; median stress factor: $q_{0,50\%} = 1.03$, $T_\sigma = 1.46$, $V_\sigma = 0.15$.

In this case there are some more data on life prediction: Kaufmann [104] and Sonsino [196] looked at a range of cast irons (GTS-35, GTW-S38, GGG40, GGG70. GGG100) treated in various ways to improve fatigue strength: sandblasting, grinding, rolling, and induction hardening. They investigated life under constant loading

and random loading (gaussian spectrum), both for stress ratios $R = -1$ and $R = 0$, and also tried to predict fatigue life under VA-loading on the basis of the S-N curves derived from the CA tests, This is essentially what Eulitz did; however no investigation was made into the accuracy of various calculation procedures; it appears that Kaufmann and Sonsino just used one simple recipe for all damage estimates. Because there are 58 test series, it is interesting to make some plots of the damages found, to put the numbers found by Eulitz in perspective. In figure 7.4 (next page) all data are plotted; the scatter number is $T_D = 45$. On one hand this is not surprising, since no attempt at all was made to group the data, or to use the optimal prediction tool: we simply pooled all available data without any critical evaluation. On the other hand it is disappointing that results are *so* bad: after all every damage prediction is based on the measured CA curve for identical specimens, and the method used (S-N curve with Haibach correction (see figure 7.1, p109) is in common use. In figure 7.5 (next page) all data points for the 'exotic' treatments are left out (leaving only grinding, grit blasting and sandblasting). Especially for stress ratio R = -1 the scatter is reduced dramatically to $T_D = 8$ ($T_\sigma = 1.41$ if $m = 6$), not unlike what was found by Heuler [88, 89], see figure 7.6 and table 7.7 (p125). Even though this data treatment is crude, we nevertheless can see that on one hand Eulitz's numbers are probably not overly pessimistic, and that on the other hand Heuler's numbers *can* be reached if one limits oneself to a sufficiently homogeneous group of specimens.

Table 7.6: Fatigue data for cast iron GGG40 in CA tests. Specimens are taken from one large block. Source: Kaufmann [103].

Material	Cast iron GGG40			
Reference	Kaufmann [103]			
Treatment	Unmachined sandblasted, machined			
Quality	Defect free, small defects, large defects			
Cross section	40 x 70 mm			
Loading	Constant amplitude; axial, bending			
Fatigue data (for small defects, 50% survival)				
Slope m	6.5			
Knee point N_D	2×10^6			
Stress concentration α	1.10		1.75	
Stress ratio R	−1	0	−1	0
Fatigue strength range $\Delta\sigma$ [MPa]	270	210	210	164
Mean stress sensitivity M	0.29		0.28	
Coefficient of variation V_σ	0.07			
Scatter number T_σ	1.20			
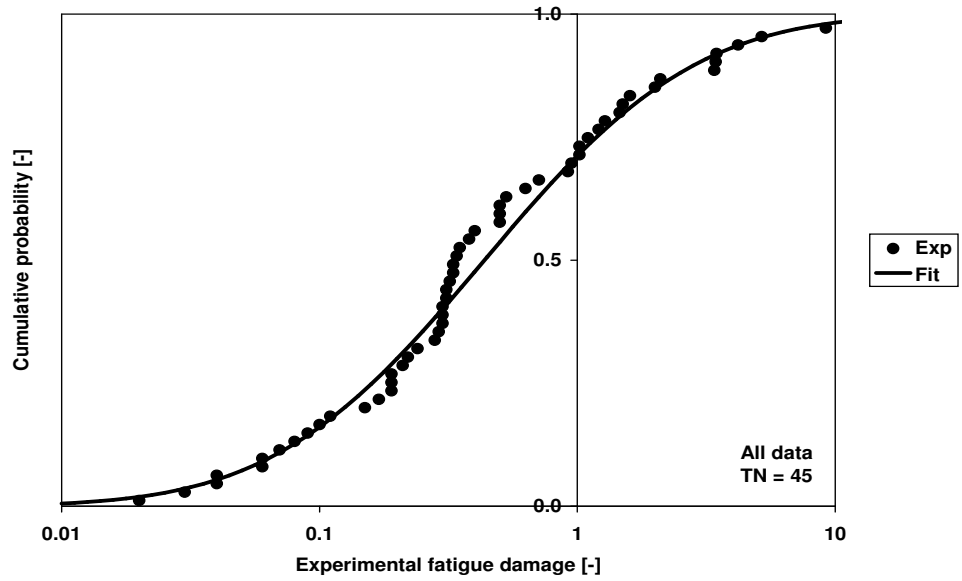
Figure 7.4: Experimental fatigue damage for various cast irons (ground, grit blasted, sand blasted, rolled, induction hardened). Source: Sonsino [196].
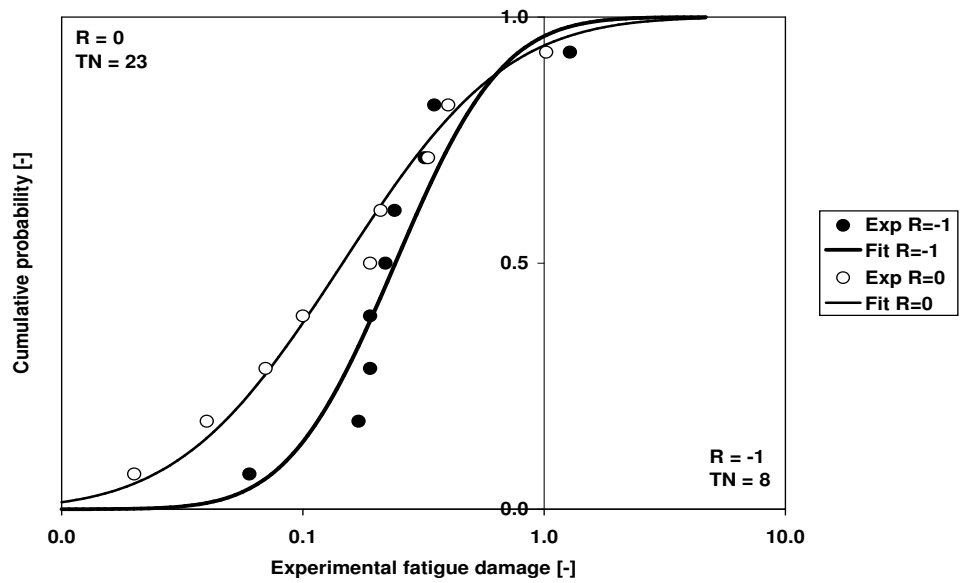
Figure 7.5: Experimental fatigue damage for various cast irons (ground, grit blasted, sand blasted). Source: Kaufmann [104].
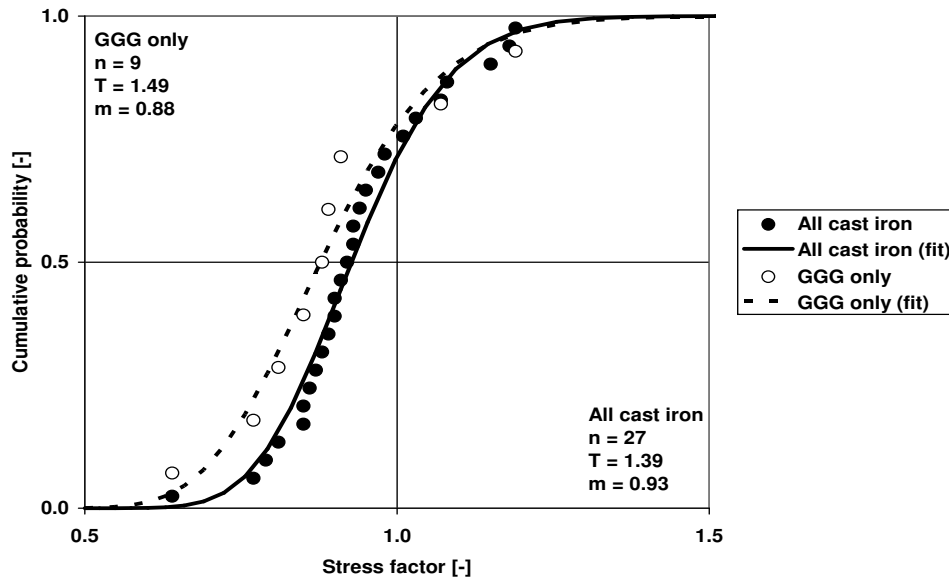
Figure 7.6: Stress factor q_0 for various cast irons. Source: Heuler [88].

Table 7.7: Estimates of the lognormal distribution of the stress factor q_0 for cast iron (see section 7.1.2. Source: Heuler [88]). Estimates are done with the bootstrap method (Efron [52, 53]). Minimum and maximum indicate 68% confidence interval.

material	parameter	minimum	median	maximum
all cast iron ($n = 27$)	*estimated*			
(GGG, GS, GTS,	scale parameter M (median)	0.90	0.93	0.95
GTW, Sikufond)	shape parameter S	0.11	0.13	0.15
	derived			
	scatter number T_σ	1.32	1.39	1.47
	coefficient of variation V_σ	0.11	0.13	0.15
nodular only ($n = 9$)	*estimated*			
(GGG42, GGG50)	scale parameter M (median)	0.83	0.88	0.93
	shape parameter S	0.12	0.16	0.19
	derived			
	scatter number T_σ	1.35	1.49	1.65
	coefficient of variation V_σ	0.12	0.16	0.20

7.4.2 Welds

Welding is used in the turbine tower and in the rear nacelle frame. A great amount of testing has been done on fatigue of welds, described for example in the back-

ground document to Eurocode 3 (Sedlacek [187]) and in the catalogues issued by DVS (Olivier and Ritter [164]). Results have found their way into the standards Eurocode 3 and the IIW Guidelines [90].

Especially interesting is the work by Köttgen and Olivier [111, 112, 163], that was partly done in connection with a weld seam failure on the Growian wind turbine. A number of different weld geometries were investigated, and it turns out that all S-N curves can be made to collapse into one if the local stress is calculated while assuming notch radiuses $r = 1$ mm. Some data are given in table 7.8; according to the IIW Guidelines [90] it is allowed to use this approach.

A question that may arise if circumferential weld seams in wind turbine towers are considered, is whether these welds have greater fatigue strength than found in 2D-specimens with limited width: one would expect that cracks in these specimens always start at the edges because generally the stress situation is more unfavourable than in the centre, something which is not possible in circumferential weld seams because there is no edge. However according to Vormwald [228] tests have shown that this is not the case: cracks do not start more often at edges; nor did one observe a preference for cracks to start near starts and stops in the weld seam. Hence the problem of transferability is reduced to finding the fatigue strength of a long homogeneous seam based on data found with short seams. This may be done with the Weibull weakest link model (see appendix F.4).

It is not entirely settled what the slope of the S-N curves for weld details must be. Eurocode 3 prescribes the same curve for all weld details, with the knee point at 5×10^6 cycles, $m = 3$ for the left part of the curve and $m = 5$ for the right part of the curve. The background document to the Eurocode (Sedlacek [187]), that lists

Table 7.8: Fatigue data for weld seams in CA tests ($r = 1$ mm approach). Source: Köttgen [111, 112], Olivier [163].

Material	Weld seams for low carbon steel			
Reference	Köttgen [111, 112], Olivier [163]			
Treatment	Stress relief			
Quality				
Cross section	8 - 80 mm thickness			
Loading	Constant amplitude; axial, bending			
Fatigue data (local stress values, 50% survival)				
Slope m	3.75			
Knee point N_D	$\simeq 5 \times 10^6$			
Number of cycles N	2×10^6		infinite life	
Stress ratio R	-1	0	-1	0
Fatigue strength range $\Delta\sigma$ [MPa]	486	348	422	312
Mean stress sensitivity M	0.40		0.35	
Coefficient of variation V_σ	0.13	0.11	0.09	0.11
Scatter number T_σ	1.41	1.31	1.25	1.34

the experimental data, gives a wide range of slopes. It is the author's impression that Eurocode 3 has adopted $m = 3$ as a convenient blanket value that is not too far wrong. Ritter [175] wrote a report dedicated to the matter, and found that slopes tend to vary dependent on which weld detail is considered (table 7.9). For plate butt welds, the dominant weld in wind turbine towers, the slope is $m = 3.77$ for test pieces and $m = 3.46$ for H-beams.

As far as damage sum prediction is concerned, according to Sonsino [197] the median damage for welds under various types of loadings (uniaxial and multiaxial, CA and VA) is $D = 0.45$ or lower (down to $D = 0.10$), with $T_D = 4$ (for exponent $m = 4$: $T_\sigma = 1.41$; S-N curve reduction $q_0 = 0.45^{1/4} = 0.82$ ($V_\sigma = 0.135$). These numbers fit in with those found by Heuler [88], who provides some data for weld seams (see figure 7.7). From Heuler's data points for welds we find the results given in table 7.10 with the bootstrap method.

Table 7.9: Slope of S-N curve m for various weld details. Source: Ritter [175].

weld type			as welded	stress relieved
plate butt weld (I, V, X, Y)	test piece		3.77	3.98
	H-beam		3.46	–
cruciform joint				
- double fillet, partial penetration	test piece		3.58	–
- double bevel, partial penetration	test piece		3.46	–
- double bevel, full penetration	test piece		3.52	–
lap joint with fillets	test piece		3.57	–
longitudinal weld seam				
- double fillet, partial penetration	test piece		3.54	–
	H-beam		3.36	–
- full penetration	test piece		2.93	2.93
	H-beam		3.03	–
circumferential weld in shear	test piece		4.83	5.32

Table 7.10: Estimates of the lognormal distribution of the stress factor q_0 for weld seams (see section 7.1.2; data source: Heuler [88]). Estimates are done with the bootstrap method (Efron [52, 53]). Minimum and maximum indicate 68% confidence interval.

material	parameter	minimum	median	maximum
weld seams ($n = 7$)	*estimated*			
	scale parameter M (median)	0.75	0.80	0.86
	shape parameter S	0.12	0.17	0.22
	derived			
	coefficient of variation V_σ	0.12	0.17	0.22
	scatter number T_σ	1.37	1.55	1.74
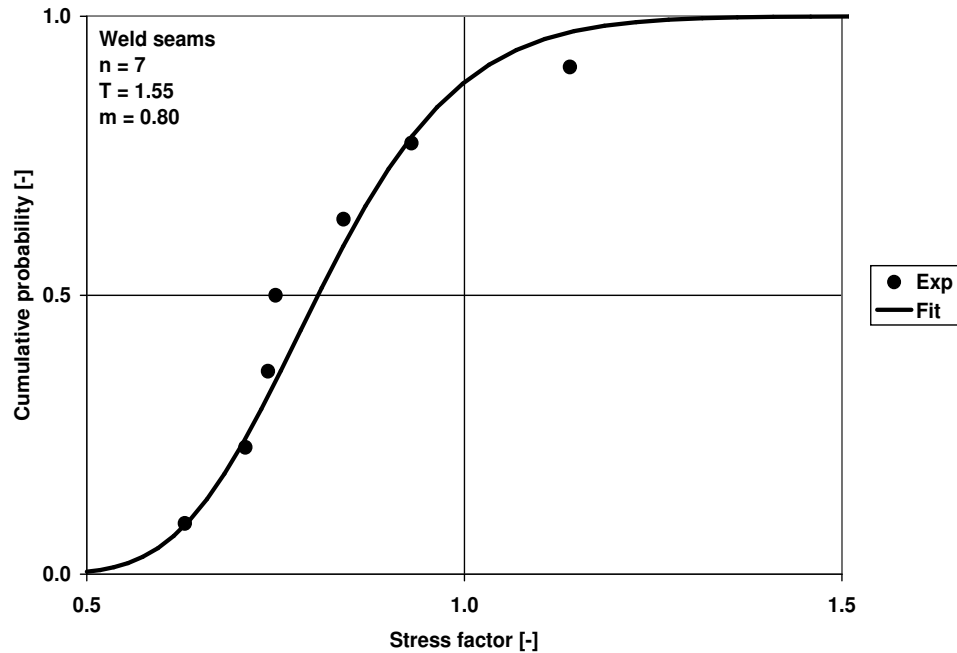
Figure 7.7: Stress factor q_0 for weld seams. Source: Heuler [88].

7.4.3 Bolts

In the blade-hub connections, the hub-main shaft connection, the tower top (yaw bearing), and the tower flanges bolts are used, usually of quality 8.8 or 10.9. Although bolt connections will not be further investigated here (bolt connection are redundant, so failure probabilities are small), some data are given in table 7.11. It is difficult to give definite numbers for the fatigue strength (these should be obtained by testing); however most coefficients of variation (on stress) are in the order of $V_\sigma = 0.10$.

Two useful publications that treat the subject of bolted connections are the standard VDI 2230 [225], and a report by Schaumann and Seidel [181] on bolted flanges in wind turbines. Both publications discuss how to estimate the stress in the bolts dependent on connection geometry and load, and also give some guidelines on which fatigue strength to use.

7.5 Fatigue of blades

7.5.1 Introduction

For composite materials used in wind turbine blades the situation is different from that for steel and cast iron. Composites represent a heterogeneous group of materials with widely varying properties: as the name 'composites' implies, a composite can consist of any combination of materials, although common composites have one material primarily providing strength (like fibres) and another material acting mainly as filler (the latter is also adding some strength by keeping the former in place). Brøndsted [26] gives a handy introduction to all the issues involved, with many references; here we are only concerned with uncertainty on fatigue strength; unfortunately there is more than enough of that in composite materials. The CA fatigue strength depends on:

- The fibre material (glass, carbon, aramid, wood).

- The volume ratio fibre material to polymer resin (the matrix material which is filling up the space between the fibres).

- The orientation of the fibres.

- The type of resin (thermoset (polyester, epoxy, vinyl ester) or thermoplastic).

Table 7.11: Fatigue properties for bolts. Note: fatigue strengths are amplitudes, not ranges.

Material	Bolt material 8.8, 10.9, 12.9							
Treatment	Hardened (HR=before rolling, RH=after rolling)							
Quality								
Cross section	M16 - M72							
Loading	axial loading under pre-stress)							
Fatigue data	treatm.	m	N_D [-]	mat	$F_M/F_{0.2}$ [-]	fat. str. [MPa]	T_σ [-]	COV [-]
Dunkel [50] M16	RH	3	-	10.9	0.7	45	1.31	0.104
Kloos [108] M16	RH	3	2×10^6	8.8	0.6	65	1.41	0.13
M16				12.8	0.6	68	1.43	0.14
M24				8.8	0.6	63	1.22	0.08
M24				12.9	0.6	63	1.65	0.20
Hanenkamp [78] M34x4	HR	6	7×10^5	10.9	0.7	78	1.31	0.11
M42x4.5				10.9	0.7	72	1.31	0.10
M48x5				10.9	0.7	76	1.34	0.12
2" UNC				10.9	0.7	48	1.36	0.12
M64x6				10.9	0.7	47	1.22	0.08
M72x6				10.9	0.7	44	1.18	0.06

- Whether the blades are hand or machine laid, and whether resin infusion is used to fill the mould (nowadays machine laying and vacuum infusion is standard procedure; this removes some variation).

- The presence of wrinkles, misalignments and porosities.

- At what temperature and how long the material is cured.

- How sensitive the material is to moisture.

- Size. It is not known precisely how coupon tests relate to full scale tests.

Other than ferrous materials, composite materials may fail not only in tension, but also in compression (micro buckling of fibres); furthermore fatigue strength is strongly dependent on mean stress.

7.5.2   S-N curve

Because of different failure modes, it is not possible to use one S-N curve with a general correction for mean stress. Instead tests must be done for many different stress ratios. An example of a constant life diagram is given in figure 7.8. It is clear that the shape of the lines cannot be described by simple models, and that prediction based on a linear or bilinear diagram must necessarily be off, as also observed by Nijssen [157] who shows an even more irregular diagram based on many tests (see also section 7.5.3). Because of all the variation, it is hardly surprising that there are no generic fatigue data that can be used. Manufacturers do tests on their own material, and these data are proprietary. However in our calculations we do not need specific values for the fatigue strength or fatigue strain: we may assume that a blade was designed according to the standard (i.e. has unity stress reserve factor), and only need to determine generic uncertainty in the values. From the literature it can be seen that the scatter on life is $T_N \simeq 10$ (Bond [19], Van Leeuwen [126], Nijssen [161]; however usually no statistical evaluation is included, and the scatter has to be read from graphs. Fortunately from the OPTIMAT project statistical results from a large database are available for glassfibre reinforced epoxy (GRE) (Nijssen [157]).

Van Leeuwen [126] showed that variation in fatigue life is not larger for blades

Table 7.12: Some fatigue data for glassfibre reinforced epoxy (GRE) test specimens. Source: Nijssen [157]; values for T_N, V_σ and T_σ are derived from the original data, assuming a lognormal life distribution.

Test probe	R	m	V_N	T_N	V_σ	T_σ
MD R0400	-1	9.63	1	8.4	0.09	1.25
	0.1	9.96	0.3–1	2.1-8.4	0.03–0.08	1.08–1.24
	10	25.35	>1	>12.8	>0.03	>1.09
UD R0300	-1	9.0	1	8.4	0.09	1.27
	0.1	9.1	0.3–1	2.1–8.4	0.03–0.09	1.09–1.26
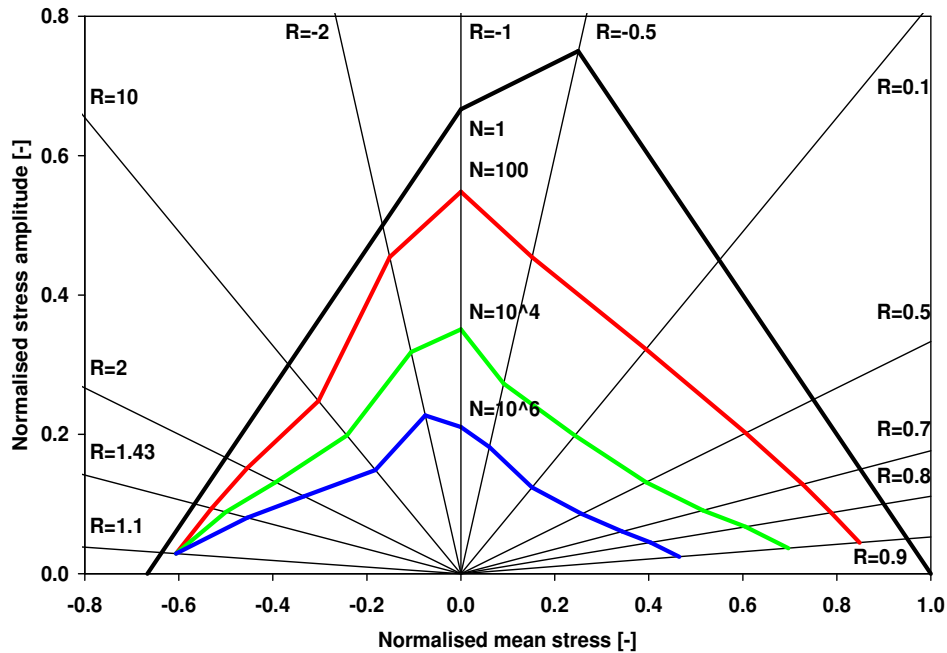
Figure 7.8: Example of a constant life diagram (schematic). The coloured lines represent the fatigue strength at the given number of cycles as function of mean stress.

compared to coupons.

Following Nijssen (see table 7.12), we will assume $T_N = 8.4$ for scatter on individual fatigue lives. As slope of the curve we will consider values $m = 9$–12; $m = 9$–10 is representative for glassfibre materials and carbon fibre, while higher exponents are more fitting for wooden blades. All curves used for calculations are median minus two standard deviations.

7.5.3   Fatigue life prediction

It is difficult to apply fracture mechanical concepts developed for isotropic, homogeneous material. Nevertheless work is going on in this direction; other methods being investigated are the use of a strength degradation model (Nijssen [159, 160]), possibly in combination with monitoring the material stiffness as indicator of residual strength. However the state-of-the-art is still to use the constant life diagram and Palmgren-Miner summation.

Articles tend to give ad hoc fatigue damage estimation rules fitting the data set that the author had available. The general approach is to use CA test data for different stress ratios to predict the life found in tests with the WISPER-spectrum or the

reduced WISPERX spectrum (see for example Bond [19], Echtermeyer [51], Mandell [132], Nijssen [161]). Usually good results are obtained after a modification of some sort has been applied to the standard procedure. It is not possible to judge the general validity of such procedures results to wind turbines, in particular because the WISPER/WISPERX load spectrum -while being a useful spectrum for comparing results by different investigators and to do at least some testing of prediction algorithms- is not very representative of real blade loading.

Sutherland [202] investigated for how many R-ratios tests must be done, by comparing life predictions with simplified constant life diagrams and with a 'complete' constant life diagram having 13 R-ratios (see figure 7.8, previous page). He shows that at least 5 lines are required for typical edgewise loading (R = -2, -1, -0.5, 0.1 and 0.5), while 6 lines are enough for flapwise loading (R = -2, -1, -0.5, 0.1, 0.5 and 0.7). A diagram with only three R-values (which seems to be the customary diagram) yields life prediction that are 0.85–0.99 for edgewise loading and 0.22–2.43 for flapwise loading, and hence is not sufficiently accurate. We may conclude that it is not unrealistic to assume T_D = 2.43/0.22 ≈ 10 for damage prediction, which would translate into $T_\sigma = 10^{1/9} = 1.29$, or $V_\sigma = 0.10$ (note that the nice thing about Sutherland's approach is that variations in material properties do not enter at all in the life estimates). This scatter results is confirmed to some extent by results of Echtermeyer [51], who presents obtained lives of 0.2–1.6, i.e. a scatter factor $T \approx 8$.

A recent overview and evaluation of prediction methods is given by Nijssen [158]; his main conclusion is in line with Sutherland's [202], that constant life diagrams based on tests with many R-values yield the best prediction.

Another attempt to describe the entire constant life diagram is the multislope approach presented by Boerstra [17], in which S-N curves for various R-values are combined into one by using a variable slope m.

Given the available information, we set T_D = 10 for life prediction scatter due to insufficiently accurate modelling. Unfortunately we have insufficient data to say anything about bias; however we are helped somewhat by the fact that fatigue curves for composite are very flat. For example if the bias on life prediction is 0.5, then the corresponding bias on strength is $0.5^{1/10} = 0.93$, which is only a minor correction.

Chapter 8

Optimal partial factors

8.1   Introduction

Now that all relevant probability distributions have been established (chapters 4–7, for a summary see section 8.7), we can estimate the component probability of failure due to fatigue loads for any combination of partial factors, design parameters and site parameters. The procedure to do this is as follows:

1. Choose the parameters for the wind turbine design (for example the wind class definition according to IEC 61400-1).

2. Choose a site according to the site admission rules (equation (3.20), p44), and estimate the site parameter distributions (for example the distribution of the site yearly mean wind speed).

3. Choose a set of partial factors (for example according to IEC 61400-1).

4. Calculate the probability that the relevant wind turbine components fail.

Obviously the procedure sketched above may be used in reverse: partial factors may be varied until some target failure probability is reached. In particular we are interested in economic optimisation, where we want to find the partial factors that give us the lowest electricity generation cost (see section 2.6). The product of partial factors influences both the mass of a component and its failure probability; thus it is a matter of balancing extra mass (a larger initial investment for construction material) against reduced failure probability (and associated smaller cost of failures). It is easy to establish the influence of the partial factor product on a component's mass, but how extra safety influences failure probability is more difficult to assess. To do this, we have to examine the limit state function, a matter to which we now turn.

It should be noted that no safety factor calibration is carried out, as is done for example by Ronold [178]. Such a calibration would involve deriving partial factors for (a subset of) all stochastic parameters, and selecting a set of factors that holds the failure probability close to the target value for a wide variety of load situations and

critical locations. Instead we consider fatigue failure of four different components (listed in table 8.1); failure of a component occurs because loads acting on it cause a crack in a critical location to form and grow. For each component the optimal partial factor and associated failure probability will be derived, for which the cost function (incorporating initial investment and cost of replacement of parts) has a minimum.

8.2 Limit state function

Under which conditions a component fails is determined by examining the limit state function Z, which is the difference of the resistance $R(\underline{x})$ and the load $S(\underline{x})$:

$$Z(\underline{x}) = R(\underline{x}) - S(\underline{x}) \tag{8.1}$$

Both the resistance $R(\underline{x})$ and the load $S(\underline{x})$ depend on a vector of stochastic parameters $\underline{x}$ (wind speed, turbulence intensity, fatigue strength, et cetera); the construction fails if the load $S(\underline{x})$ is larger than the resistance $R(\underline{x})$, or $Z(\underline{x}) < 0$. The probability of this happening $p_F = P(Z(\underline{x}) < 0)$, defined by the following integral:

$$p_F = \int\limits_{Z(\underline{x})<0} f(\underline{x}) \, dx = \int\limits_{\mathbb{R}_n} f(\underline{x}) \, H\left(-Z\left(\underline{x}\right)\right) \, dx \tag{8.2}$$

Here $f(\underline{x})$ is the probability density, and $H\left(-Z\left(\underline{x}\right)\right)$ is the Heaviside function, which is $H = 1$ if $Z(x) < 0$ (failure) and $H = 0$ if $Z(x) > 0$ (no failure). To show how the failure probability is found in practice, as example we take the vector $\underline{x}$ to be:

$$^{t}\underline{x} = (q_0, x_{dim}, x_{\Delta\sigma_A}, I_a, I_{wf}, U_{avg}, Y, \alpha, \Gamma) \tag{8.3}$$

with:

Table 8.1: List of components, loads acting on it, and consequences of failure.

component	load causing failure	consequences
blade	edgewise moment Mx11r flapwise moment My11r	one blade fails and is destroyed
hub	edgewise moment Mx11h flapwise moment My11h	the hub fails and is destroyed; the rotor (hub and blades) falls down
machine frame	driving moment MxNr tilt moment MyNf yaw moment MzNf	the machine frame (nacelle) fails and is destroyed; the rotor (hub and blades) falls down.
tower	tower base W-E moment Mxt0 tower base N-S moment Myt0	the tower fails, and the entire wind turbine collapses

I_a ambient turbulence intensity [-]

I_{wf} windfarm added turbulence intensity [-]

q_0 stress factor (load sequence reduction factor on fatigue strength) [-]

U_{avg} long term average wind speed [m/s]

x_{dim} dimension factor (for deviations in section modulus) [-]

$x_{\Delta\sigma_A}$ material fatigue strength divided by characteristic value [-]

Y yaw misalignment [rad]

α wind shear exponent [-]

Γ Mann's shear parameter [-]

Although formally both R and S may be functions of every component of $\underline{x}$, more natural dependencies are:

$$R(\underline{x}) = R(\underline{x}_R) = R(q_0, x_{dim}, x_{\Delta\sigma_A}) \tag{8.4}$$

$$S(\underline{x}) = S(\underline{x}_S) = S(I_a, I_{wf}, U_{avg}, Y, \alpha, \Gamma) \tag{8.5}$$

The task is to find the integral given in equation (8.2) by evaluating the resistance R and the load S. This is what a certification body is doing: given a design, check whether the resistance R is large enough compared to the load S to achieve the target failure probability.

In what follows we will assume that both R and S have dimension of moment [Nm]. However this is not essential and the whole calculation could also be done with R and S having dimension of stress of force ([Pa] or [N]), or be cast in dimensionless form.

8.3 Site equivalent fatigue load

When considering fatigue failures, it is convenient to establish both the resistance and the load as equivalent fatigue load. The advantage of this concept is that any load history, no matter how complex, can be reduced to one number, which greatly increases computational efficiency. This comes at the cost of some additional inaccuracy, but probably not much (see section 9.4 and appendix C).

The site equivalent fatigue load is the load that, when applied N_{eq} times, would produce the same amount of fatigue damage as the actual random load history; it is found by calculating the load history representative for the turbine's life under the set of site conditions $\underline{x}$, and rainflow counting all cycles in that history. The rainflow procedure converts the random load history into a table of triplets (number of cycles n_i, load range ΔF_i, mean load $F_{mean,i}$), that can be used to estimate fatigue damage. For each load cycle, characterised by extreme values $F_{max,i}$ and $F_{min,i}$, we find the range ΔF_i and the mean $F_{mean,i}$:

$$\Delta F_i = F_{max,i} - F_{min,i} \tag{8.6}$$

$$F_{mean,i} = \frac{1}{2}\left(F_{max,i} + F_{min,i}\right) \tag{8.7}$$

The value of $S(\underline{x})$ is for example given by (other definitions of the equivalent load are possible, see appendix C):

$$S(\underline{x}) = \Delta F_{eq}(\underline{x}) = \left(\frac{\sum n_i(\underline{x})\Delta F_i^m(\underline{x})}{N_{eq}}\right)^{1/m} \tag{8.8}$$

Here n_i is the frequency of occurrence for a particular load cycle i; the equivalent number of cycles N_{eq} may be set to any value[1]. A common choice is to set $N_{eq} = 5 \times 10^6$ to enable direct comparison with fatigue tests or standards (for example Eurocode 3 puts the fatigue limit at 5×10^6 cycles). Alternatively N_{eq} is set to the number of cycles that a 1 Hz signal would have during the wind turbine's life; the advantage of this last choice is that equivalent loads found in calculations for periods of different length are directly comparable. It is straightforward to calculate the site equivalent load for any vector $\underline{x}$, the only problem is that it is expensive in terms of computation time.

8.4   Fatigue resistance

The fatigue resistance R of a cross section with associated nominal section modulus W is:

$$R(\underline{x}) = x_{dim}W\Delta\sigma_A \tag{8.9}$$

where x_{dim} is a factor accounting for deviations from ideal geometry (for example due to manufacturing inaccuracy), and $\Delta\sigma_A$ is the fatigue strength (here a stress). The fatigue strength $\Delta\sigma_A$ is:

$$\Delta\sigma_A = q_0 x_{\Delta\sigma_A}\Delta\sigma_{A,char} \tag{8.10}$$

Here $x_{\Delta\sigma_A}$ represents the ratio of actual fatigue strength and characteristic fatigue strength (under constant amplitude loading):

$$x_{\Delta\sigma_A} = \frac{\Delta\sigma_A}{\Delta\sigma_{A,char}} \tag{8.11}$$

The characteristic fatigue strength $\Delta\sigma_{char}$ is for example the 2.3% value (two standard deviations below the mean). The number q_0 is a factor on fatigue strength accounting for the effect that the fatigue damage (the Palmgren-Miner sum) that can be

---

[1]The equivalent number of cycles N_{eq} is not equivalent in the sense that (for example) it is determined as a weighed sum of numbers N. The subscript 'eq' only indicates that N_{eq} is associated with equivalent load ΔF_{eq}. A better name would be 'N_{ref}' but for clarity we stick with the convention.

sustained by some critical location ('hot spot') depends on the properties of the load spectrum: the frequency distribution of small and large cycles and sequence effects[2]. Combining equations (8.9) and (8.10) yields the actual resistance $R(\underline{x})$:

$$R(\underline{x}) = q_0 x_{dim} x_{\Delta\sigma_A} W \Delta\sigma_{A,char} \tag{8.12}$$

In a certification process the value of the section modulus W would be taken from a drawing of the specific turbine under consideration, and one could then proceed to compare the resistance R with the load S, to establish whether the wind turbine had sufficient strength. However our aim is to do general calculations for any wind turbine, and therefore we want to eliminate the section modulus W and express $R(\underline{x})$ directly in terms of the characteristic load effect $S_{avg}(\underline{x}_{char})$. To do this, we use the conventional design equation, which links the characteristic resistance R_{char} to the characteristic load effect $S_{avg}(\underline{x}_{char})$:

$$\frac{R_{char}}{\gamma_m} = SRF \gamma_f S_{avg}(\underline{x}_{char}) \tag{8.13}$$

First a set of characteristic load conditions $\underline{x}_{char}$ is defined (for example a wind regime class according to IEC 61400-1); for fatigue calculations on wind turbines these conditions are set in such a way that they reflect conservative estimates of representative conditions. If we do a full fatigue load calculation with this set of conditions, the result is the average characteristic load effect $S_{avg}(\underline{x}_{char})$[3]. For additional safety, the load is inflated with the load factor $\gamma_f \geq 1$, and the characteristic fatigue strength is reduced by the material factor $\gamma_m \geq 1$. The stress reserve factor SRF is not an input to, but a residual of the design process, where dimensions are initially chosen conservatively and increased if strength is insufficient, but not usually decreased if there a small extra safety margin. Ideally we would have $SRF = 1$, but a more usual situation is $SRF \simeq 1.05$. Because:

$$R_{char} = W \Delta\sigma_{char} \tag{8.14}$$

Equation (8.12) may be rewritten as:

$$R(\underline{x}) = q_0 x_{dim} x_{\Delta\sigma_A} R_{char} \tag{8.15}$$

---

[2]Because we are dealing with the properties of the load here, it may be argued that (the inverse of) the factor q_0 should be put on loads, rather than on fatigue strength. However this is not essential, and by defining a reduction on fatigue strength we follow common practice in fatigue literature.

[3]There is a minor complication here: what we would like to have is the *average* characteristic load effect $S_{avg}(\underline{x}_{char})$; but because we are using random wind fields with different seeds in the calculations, we end up with a characteristic load effect that is different from the average value by a factor x_{seed}. However it is current practice to evaluate many load cases, all having different wind fields, resulting in x_{seed} being very close to unity:

$$S(\underline{x}_{char}) = x_{seed} S_{avg}(\underline{x}_{char}) \simeq S_{avg}(\underline{x}_{char})$$

The fact that x_{seed} is a stochastic parameter is taken into account in the calculations, but we will not burden the discussion with it.

Using equation (8.13), we eliminate R_{char} to get:

$$R(\underline{x}) = q_0 x_{dim} x_{\Delta\sigma_A} \; SRF \; \gamma_f \gamma_m \; S_{avg}(\underline{x}_{char}) \tag{8.16}$$

The section modulus W has now been removed and the fatigue resistance $R(x)$ is defined in terms of a set of characteristic site conditions $\underline{x}_{char}$, and the components of $\underline{x}_R$:

q_0	parameter for variation in fatigue strength due to load sequence effects
x_{dim}	parameter for variation in material dimensions
$x_{\Delta\sigma_A}$	parameter for variation in constant amplitude fatigue strength

The wind turbine designer would use equations (8.13) and (8.14) to find the section modulus W, which would then be communicated to the certification body for a check against the characteristic loads. What we have done is eliminate the wind turbine specific section modulus in order to make the evaluation of the limit state function Z valid for any machine.

8.5   Failure probability

To work out the failure probability we need to calculate the integral in equation (8.2), something that for example may be done with the Monte Carlo method, or with the First Order Reliability Method (FORM).

The Monte Carlo method works by doing N (simulated) experiments to obtain an estimate of the failure probability. In every experiment each component x_i of the stochastic variable vector $\underline{x}$ is randomly sampled according to its distribution, and the limit state function $Z(\underline{x})$ is evaluated. Every time $Z(\underline{x}) < 0$, a failure is recorded (N_F is increased by one), and when N experiments have been performed, the failure probability p_F is found with:

$$p_F = \frac{N_F}{N} \tag{8.17}$$

The strength of the method is its great generality: any limit state function and any distribution can be handled; its disadvantage is slow convergence: for example if the failure probability is in the order of $p_F = 10^{-6}$, then something like 10^8 numerical experiments are required to get a reliable answer. If the evaluation of Z is costly it becomes important to speed up convergence, and several schemes have been developed to do this; for details see for example Press [167, 168].

The First Order Reliability Method (FORM) relies on replacing all probability distributions involved by suitable normal distributions, which make it possible to approximate the n-dimensional surface consisting of all vectors $\underline{x}$ for which $Z(\underline{x}) = 0$ by a hyperplane. This hyperplane is found with a fast iterative method, and the

failure probability may then be calculated directly. The advantage of the method is its speed, which is gained at the price of some (small) loss of accuracy. The theory of FORM can be found in any book on probabilistic design; a description of the version used here is given in appendix F.1. What is used is standard FORM, except for the evaluation of the limit state function Z, which is done with an approximate method (see below).

Both methods involve evaluation of the Z-function: in the Monte Carlo method we need function values directly, in FORM we mostly need derivatives, but these can only be established numerically in our case, so again function values are required. If we put equation (8.16) back into the limit state function Z (equation (8.1)), we get:

$$Z(\underline{x}) = q_0 x_{dim} x_{\Delta\sigma_A} \; SRF \; \gamma_f \gamma_m S_{avg}(\underline{x}_{char}) - S(\underline{x}) \tag{8.18}$$

The work of evaluating $Z(\underline{x})$ consists of:

1. Finding the characteristic average load effect $S_{avg}(\underline{x}_{char})$. This is not difficult. It involves the calculation of (say) 5 load spectra of 26 load cases = 130 load cases (or some more depending on how sure we want to be of having found the true average value $S_{avg}(\underline{x}_{char})$). If characteristic conditions are fixed for a calculation (for example an IEC class), this only needs to be done once. The resistance is found by multiplication with the stochastic parameters.

2. Finding the site load effect $S(\underline{x})$. This is the real problem, since we need the site load effect for any vector $\underline{x}$ that may turn up in the calculation. Worse yet, the first order reliability method operates with an iterative scheme that needs values of Z *and* all its derivatives $\partial Z/\partial x_i$ (which often can only be found numerically). Because $\underline{x}$ has 15–20 independent components, it is not feasible to redo the whole calculation each time a new value of Z is needed.

What we need is a fast way to estimate $Z(\underline{x})$ for any vector $\underline{x}$. One way of doing this is to use Taylor expansion, which may be done from any point $\underline{x}_0$. In our case $\underline{x}_0 = \underline{x}_{char}$ would be an obvious choice:

$$Z(\underline{x}) \approx q_0 x_{dim} x_{\Delta\sigma_A} \; SRF \; \gamma_f \gamma_m S_{avg}(\underline{x}_{char})$$
$$- S(\underline{x}_{char}) - \sum_j (x_j - x_{char,j}) \left(\frac{\partial S}{\partial x_j} \right)_{\underline{x}=\underline{x}_{char}} \tag{8.19}$$

Establishing each derivative necessitates (as a minimum) one new full calculation (the fixed point $S(x_{char})$ is known already), but calculations need only be done once, so there is a clear speed advantage in this approach. However the Taylor approximation is only accurate as long as we do not get too far from the fixed point, which may not always be the case.

As a matter of fact, if we need accurate derivatives over larger intervals, we may just as well be smart and use the same amount of work in a more precise approach. What we do is calculate the value of $Z(\underline{x})$ for a few points over the intervals of interest

of $\underline{x}_j$ and then fit low order polynomials through the points found. If a change in one variable x_j always changes the load $S(\underline{x})$ by the same relative amount independent of the value of other components of $\underline{x}$, then $S(\underline{x})$ can be written as a product of independent functions $S_j(\underline{x})$:

$$S(\underline{x}) = \prod_j S_j(\underline{x}) \tag{8.20}$$

and results will be exact for any $\underline{x}$ (in appendix F.2 it is shown that the product approximation of equation (8.23) yields acceptable results for the important site parameters wind speed and turbulence intensity, and is superior to the first order Taylor expansion). If we divide equation (8.18) by $S_{avg}(\underline{x}_{char})$ we get an alternative (but equivalent) limit state function Z':

$$Z'(\underline{x}) = q_0 x_{dim} x_{\Delta\sigma_A} \, SRF \, \gamma_f \gamma_m - \frac{S(\underline{x})}{S_{avg}(\underline{x}_{char})} \tag{8.21}$$

Because of assumption (8.20) we have:

$$\frac{S(\underline{x})}{S_{avg}(\underline{x}_{char})} = \prod_j \frac{S(\underline{x} = \underline{x}_{char}, x_j \neq x_{char,j})}{S_{avg}(\underline{x}_{char})} \tag{8.22}$$

This may be verified by writing out the product expression. Hence:

$$Z'(\underline{x}) = q_0 x_{dim} x_{\Delta\sigma_A} \, SRF \, \gamma_f \gamma_m - \prod_j \frac{S(\underline{x} = \underline{x}_{char}, x_j \neq x_{char,j})}{S_{avg}(\underline{x}_{char})} \tag{8.23}$$

In summary, if we assume that a change in some component x_j changes the site load by the same relative amount regardless of the rest of the vector $\underline{x}$, then the function $S(\underline{x})$ can be accurately calculated beforehand for sufficiently large ranges of x_j. In the Monte Carlo or FORM calculation, the behaviour of $S_j(\underline{x})$ is approximated by first or second order polynomials, something which turns out to give accurate fits, and also takes care of the problem how to obtain the correct average value for $S(\underline{x})$, since curve fitting removes some noise in the calculations. In standard FORM or Monte Carlo calculations, the limit state function Z would be evaluated exactly wherever necessary, for example with the two-level factorial method (Larsen [120]) or if need be with a complete hypersurface (the response surface). Strictly speaking the product approximation proposed here makes the method used non-standard FORM.

8.6 Example

To show how the calculation operates in practice, we work out an example calculation with only 3 stochastic variables. Let us consider a solitary turbine designed for IEC

class II (average wind speed at hub height U_{char} = 8.5 m/s). The estimate of the climate at the sites where the turbine is to be installed is that the average wind speed is U = 8.0 m/s, and we assume in this example that the turbulence corresponds exactly to the one in the standard. We are interested in a fatigue failure of the tower base, a welded structure. There is only one critical location: the door. There are three variables, the (normalised) CA fatigue strength $x_{\Delta\sigma_A}$, the load sequence stress factor q_0 and the site wind speed U. The vector of basic variables $\underline{x}$ is:

$$\underline{x} = \begin{pmatrix} x_1 \\ x_2 \\ x_3 \end{pmatrix} = \begin{pmatrix} x_{\Delta\sigma_A} \\ q_0 \\ U \end{pmatrix} \tag{8.24}$$

The variables $\Delta\sigma_A$ and q_0 act on resistance R, while the variable U acts on the load S. We define the limit state function as:

$$Z = R_0 R_1 R_2 - S_0 S_1 \tag{8.25}$$

Here R_0 and S_0 are constants, and R_1, R_2, S_1 are functions of the vector $\underline{x}$.

Constant parameters. According to IEC 61400-1 partial factors for fatigue design are load factor γ_f = 1.0 and material factor γ_m = 1.27. We assume that the tower has a stress reserve factor SRF = 1.05 (it is just a little too heavy, this is often the case in the final design); then the factor R_0 is:

$$R_0 = SRF\ \gamma_F \gamma_M = 1.05\ \times\ 1.0\ \times\ 1.27 = 1.33 \tag{8.26}$$

The site mean fatigue load is taken to be S_0 = 0.9, because the wind direction distribution is taken to be unidirectional in the evaluation of this load, while in fact wind can come from any direction. Next we consider the basic stochastic variables.

1. Variation in normalised fatigue strength. $R_1(\underline{x}) = R_1(x_1) = R_1(x_{\Delta\sigma_A}) = x_{\Delta\sigma_A}$. For welds the coefficient of variation of the CA fatigue strength is $V_{x_{\Delta\sigma_A}} = 0.134$ (Köttgen [112], table 7.8, p126), and the standard (for example Eurocode 3) provides the median values minus two times the standard deviation. This means that the mean of the normalised CA fatigue strength is approximately

$$\mu_{x_{\Delta\sigma_A}} = \frac{1}{1 - 2 \times 0.134} = 1.37 \tag{8.27}$$

The distribution is assumed to be lognormal.

2. Variation in stress factor. $R_2(\underline{x}) = R_2(x_2) = R_2(q_0) = q_0$. According to the data in table 7.10 (p127), the best estimates for median and coefficient of variation are $(q_{0,50\%} = 0.80, V = 0.17)$; the estimates that are one standard deviation from these values are $(q_{0,50\%} = 0.75, V = 0.12)$ and $(q_{0,50\%} = 0.86, V = 0.22)$ respectively.

3. Uncertainty in wind speed seen by the turbine. The equivalent load depends on the average wind speed as follows:

$$S_1(\underline{x}) = S_1(x_3) = S_1(U) = 1 + 0.123\,(U - 8.5) \tag{8.28}$$

Some values for the equivalent fatigue load (S-N curve slope $m = 4$ for welds) are given in table 8.2, together with the values from a linear least squares fit. It is clear that both sets of values are almost identical. The values in the bottom row are described by equation (8.28). There are three sources of uncertainty in the wind speed influence on the equivalent load:

1. The long term average site wind speed. The wind speed at 10 m height is for example found with the Measure-Correlate-Predict procedure (MCP) (see section 4.3.2). The distribution of the prediction is unbiased on average, but the coefficient of variation varies: $V_{MCP} = 0$–0.12 with an average of $V_{MCP} = 0.04$ (section 4.3). We do two calculations, with $V_{MCP} = 0.04$ and $V_{MCP} = 0.08$.

2. The yearly variation in wind speed, which was found to be $V_1 = 0.06$ (section 4.3.4). For wind turbine life L years the coefficient of variation of the wind speed over the life is $V_L = V_1/\sqrt{L}$.

3. The uncertainty caused by transforming the wind speed from 10 m height up to hub height. If we assume a maximum error of 0.5 m/s $\approx 3\sigma$ at hub height, then $\sigma \approx 0.5/3 = 0.17$ and $V = (0.5/3)/8.0 = 0.02$.

We may estimate the combined coefficient of variation for wind speed with vector summation. For example for 20 years life:

$$V_U = \sqrt{0.04^2 + \frac{0.06^2}{20} + 0.02^2} = 0.047 \qquad (8.29)$$

Table 8.2: Equivalent fatigue load ranges as function of average wind speed. Bending moment at the tower base, 20 years life, slope of S-N curve for welds $m = 4$.

U [m/s]	6	7	8	9	10
ΔF_{eq} [kNm] (calculated)	1941	2273	2624	2972	3303
ΔF_{eq} [kNm] (linearised)	1938	2280	2623	2965	3307
$\Delta F_{eq}(U)/\Delta F_{eq}(8.5)$	0.69	0.82	0.94	1.06	1.18

Table 8.3: Distribution data for limit state function (equation 8.31)

Stochastic parameter	Name	Median	V	Dist.
Average load reduction	S_0	0.9	-	D
Wind speed:				
-MCP		1	0.04, 0.08	
-Yearly wind speed (20 years)		1	$0.06/\sqrt{20}$	
-Height transform		1	0.02	
Wind combined (20 years)	S_1	1	0.047, 0.084	N
Average strength	R_0	1.33	-	D
CA fatigue strength factor $x_{\Delta\sigma}$	R_1	1.37	0.134	LN
Stress factor q_0	R_2	0.75, 0.80, 0.86	0.12, 0.17, 0.22	LN

If the coefficient of variation V_{MCP} is twice as large then:

$$V_U = \sqrt{0.08^2 + \frac{0.06^2}{20} + 0.02^2} = 0.084 \tag{8.30}$$

Data summary. All data are summarised in table 8.3. To recapitulate:

$$Z = R_0 R_1 R_2 - S_0 S_1 \tag{8.31}$$

With:

$$\begin{aligned}
R_0 &= 1.33 \\
R_1 &= R_1(x_1) = R_1(x_{\Delta\sigma_A}) = x_{\Delta\sigma_A} \\
R_2 &= R_2(x_2) = R_2(q_0) = q_0 \\
S_0 &= 0.9 \\
S_1 &= S_1(x_3) = S_1(U) = 1 + 0.123\,(U - 8.5)
\end{aligned} \tag{8.32}$$

Results. The results of the calculation are given in figure 8.1 (next page), for different estimates of the distribution of the stress factor q_0: mean, and mean plus or minus one standard deviation. The characteristic picture is seen that the cumulative failure probability is almost zero in the first years, and starts to become significant after a few years. This is of course due to the fact that the creation of fatigue damage takes time. Cumulative failure probabilities seem fairly high, something that can be directly attributed to the large scatter on fatigue life under variable amplitude loading (or, in stress terms: large scatter on the stress factor q_0). However if we look at the average yearly failure probability found $p_F = 6 \times 10^{-4}$, this figure is not so different from what is achieved in practice: $p_F = 2 \times 10^{-4}$ (see table 2.5, p21), or the figure $p_F = 10^{-3}$ derived by Tarp-Johansen [203].

Although results are different, it is seen that the exact choice of the q_0-distribution does not have a large influence on what happens in the second half of the turbine's life; this is because the estimates of median and coefficient of variation were assumed

Table 8.4: Results of example calculation: influence factor α^2, failure probability p_F and reliability index β. V is the coefficient of variation of the stochastic parameters.

Stochastic parameter	V	α^2	V	α^2
Fatigue strength $\Delta\sigma_A$	0.13	0.36	0.13	0.33
Stress factor q_0 (median 0.80)	0.17	0.58	0.17	0.54
Wind speed U	0.047	0.05	0.084	0.13
Cumulative failure probability p_F (20 years)	1.2×10^{-2}		1.6×10^{-2}	
Reliability index β (20 years)	2.25		2.14	
Average yearly failure probability $p_{F,avg}$	6.0×10^{-4}		8.0×10^{-4}	
Reliability index β (1 year)	3.24		3.16	
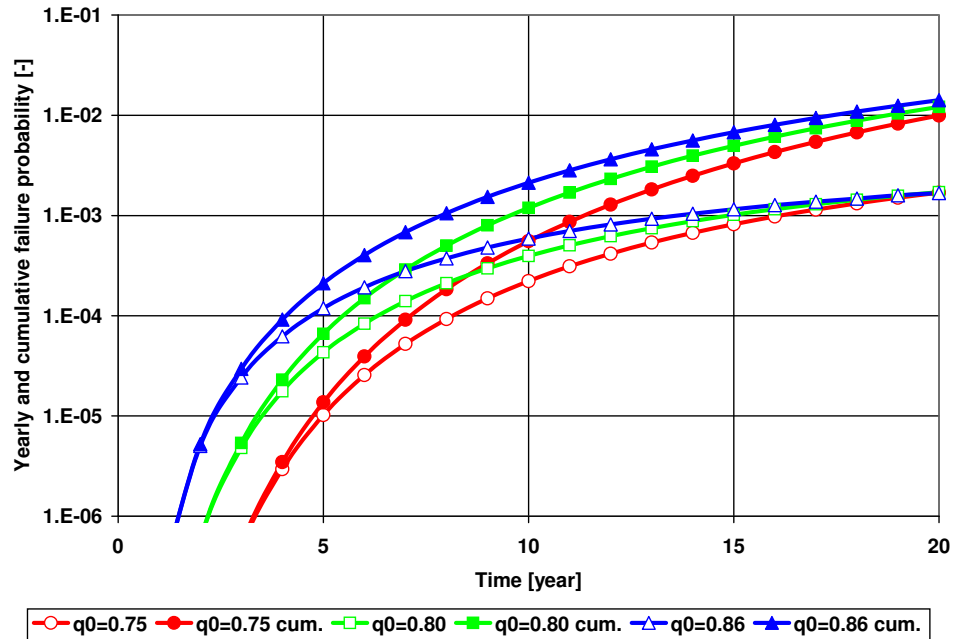
Figure 8.1: Tower fatigue failure probability a function of time (example). Note that values of the median and standard deviation of q_0 are combined according to columns in table 7.10.

to be correlated; for example a small value of the median goes with a small coefficient of variation.

The FORM calculation also provides the influence factors (table 8.4), that indicate how the variation of the limit state function is distributed over the set of stochastic variables. In this case almost all variation is due to uncertainty in the stress factor q_0 and in the CA fatigue strength of welds. If the uncertainty on wind speed estimation is increased, failure probability becomes somewhat larger, but not much because stress factor and fatigue strength uncertainties are dominating.

8.7 Standard calculation

We estimate the failure probabilities if we were to do a design calculation according to the standard, and install the turbine on a site exactly corresponding to the assumed conditions, according to the site admission rule, equation (3.20) (p44). In table 8.5 the design values chosen for all relevant parameters are given. Also the distributions that are the result of the investigations in the previous chapters are listed.

Table 8.5: Overview of distributions used in the standard calculation.

parameter	dist.	ref. x_r	fractile $P(x_r)$	std dev σ	COV V	design x_d
low cycle fatigue conservatism	N	1	0.5	*(see table 4.2)*		1
- tower fore-aft moment Myt0	N	1.05	0.5		0.01	1
average wind speed U_{avg} [m/s]	N	8.5	0.5		0.07[1]	8.5
Weibull shape factor k	N	2	0.5		0.015	2
wind dir. dist. conservatism	D	1				1
- tower fore-aft moment Myt0	N	0.77	0.5		0.01	1
wind field seed	N	1	0.5	*(see table 4.3)*		1
turbulence intensity I	N	0.16	0.5	0.01		0.18
wind field shear Γ	N	3.2	0.5	0.3		3.9
wind shear exponent α	N	0.2	0.5	0.02		0.2
air density ρ [kg/m^3]	D	1.225				1.225
yaw error Y [°]	N	0	0.5	1		6
inflow angle (slope) S [°]	N	4	0.5	1		8
wake effect model (as turb.)	LN	0.02	0.5	0.01		0
significant wave height H_s [m]	LN	1.27	0.5	0.03		1.27
wave spectrum peak parameter γ	N	2				2
wave nonlinearity	N	1.10	0.5	0.03		1
wind/wave misalignment	D	1				1
drag coefficient C_D	N	0.7	0.5	0.1		0.7
inertia coefficient C_M	N	2.0	0.5	0.1		2.0
tide factor d_{eq}	D	1				1
current	D	1				1
all aerodynamics						
- edge mom. Mx11r, Mx11h	N	1	0.5		0.01	1
- tower fore-aft mom. Myt0	N	1	0.5		0.03	1
- other moments	N	1	0.5		0.03	1
control system	D	1				1
cut out wind speed U_{out} [m/s]	N	25	0.5	0.5		25
structural model	D	1				1
eigenfrequencies	D	1				1
geometry	N	1	0.5		0.03	1
FEM unit stresses	N	1	0.5		0.06	1
- tower	N	1	0.5		0.03	1
fatigue strength $x_{\Delta\sigma_A}$						
- blade (m=12)	LN	1	0.023		0.07	1
- cast iron (m=6.3)	LN	1	0.023		0.07	1
- weld (m=3.5)	LN	1	0.023		0.11	1
stress factor q_0						
- blade (m=12)	LN	1	0.5		0.10	1
- cast iron (m=6.3)	LN	0.93	0.5		0.13	1
- weld (m=3.5)	LN	0.80	0.5		0.17	1

[1]Combination of prediction at 10 m, transformation to hub height and yearly variation.

Each distribution for the actual turbine at some site is characterised by a reference value x_r, the corresponding fractile $P(x_r)$, and either the standard deviation σ or the coefficient of variation V. Furthermore for all components we set the stress reserve factor $SRF = 1$ and load factor $\gamma_f = 1$; following common practice, we set the material factor $\gamma_m = 1.50$ for the blades, $\gamma_m = 1.27$ for the tower and $\gamma_m = 1.38$ for the hub and the nacelle (cast iron). The results of the calculation according to the standard are given in table 8.6. There are a few interesting things to be observed here:

1. Results of the First Order Reliability Method and the Monte Carlo method are close to each other in all cases. This shows that it is justified to use the faster FORM in our calculations; of course in some final stage one might always do an 'exact' calculation with the Monte Carlo method.

2. For all components most uncertainty is associated with the fatigue strength and the stress factor (i.e. the fatigue damage sum). For most components these two parameters are totally dominating, with sum of the variation above 0.60.

Table 8.6: Overview of failure probabilities p_F, reliability indices β and influence factors α. Standard calculation according to IEC 61400-1 class II for $L = 20$ years life. The definition of fatigue damage equivalent load includes mean stress influence, except for the tower welds.

load component	Mx11r	My11r	Mx11h	My11h	MxNr	MyNf	MzNf	Myf0
$p_{F,MC,L}$	9.3e-5	2.3e-4	1.0e-2	1.5e-2	1.3e-2	3.0e-2	2.0e-2	7.3e-2
$p_{F,FORM,L}$	9.1e-5	2.1e-4	1.0e-2	1.4e-2	1.3e-2	2.9e-2	1.9e-2	7.2e-2
$\beta_{FORM,L}$	3.74	3.53	2.31	2.17	2.21	1.90	2.08	1.46
$\beta_{FORM,1}$	4.44	4.26	3.28	3.18	3.20	2.98	3.11	2.69
α^2 [%]								
Fatigue strength	24	21	18	17	17	14	15	23
Stress factor	48	42	62	59	58	47	52	53
Wind seed		1			1			2
Geometry	5	4	3	3	3	3	3	2
FEM	22	18	15	14	14	11	12	2
Avg. wind speed		3	1	2	3	9	6	10
Weibull shape								
Wind dir. dist.								
Turb. intensity		4		1		8	6	3
Spectrum shape						1		3
Wind shear						1		
Windfarm wake		3		1		4	3	1
Aerodyn. model		4		3	3	2	3	2
Yaw error								
Terrain slope								
Low cycle fatigue								1
Stop wind speed								

3. Second most important is FEM, for all components but the tower $\alpha^2 \geq 0.10$.

4. Of moderate importance are average wind speed (for the nacelle and the tower) and turbulence intensity (for the nacelle).

5. Not important at all are the following uncertainties: Weibull shape factor, wind direction distribution, the spectral shape (characterised by Mann's shear parameter) wind shear, yaw misalignment, inflow angle (terrain slope), low cycle fatigue, and finally the stop wind speed.

From these results we may immediately draw the conclusion that efforts to reduce uncertainty should focus mainly on fatigue issues and perhaps on FEM-calculations (see also section 8.9).

8.8   Optimisation and comparison to standard values

Now that all the machinery to find failure probabilities is in place it is time to return to the question what the optimal failure probability and target reliability are from a financial point of view. To recapitulate: we want to minimise the function $w(\gamma)$, given by equation (2.21) (repeated here):

$$w(\gamma) = \frac{W(\gamma)}{C_I(\gamma_0)} = \frac{C_I(\gamma) + C_F(\gamma) + C_R(\gamma)}{C_I(\gamma_0)} \tag{8.33}$$

The value of the product of partial safety factors γ for which $w(\gamma)$ reaches its minimum is the economically optimal one.

For the calculation we use the standard land turbine NM92/2750-70 (see appendix B). We look at the tower, the blade, the hub and the nacelle in turn. In each case, we assume that dimensions are fully determined by fatigue loads (something which is not true, but reasonable because we want consistent fatigue design).

Tower. For the tower the derivative of mass with respect to the total safety factor (product of partial factors) γ is established by finding the minimum weight tower for various values of γ. It turns out that the relation safety factor-tower mass is almost linear, with $1/m_0 \; \partial m/\partial \gamma = 0.7$ (where m_0 is the tower mass for the base case with $\gamma_0 = 1.27$). The fraction repair (or replacement) cost divided by investment cost is $f_R = 0.9$ because it may reasonably be assumed that almost the entire turbine must be replaced if the tower fails (see table B.3). Following Dalsgaard Sørensen [198, 199] the additional failure cost (debris removal and loss of revenue) C_F is set to 3% of the investment cost $C_I(\gamma_0 = 1.27)$.

For the tower we investigate the sensitivity of the optimal reliability index to three factors: the interest rate r, the failure cost fraction f_F and the number of critical locations N.

The optimal tower reliability index β (and therewith the optimal γ) depends on the interest rate r: if r is larger it is advantageous to invest less now (investing present
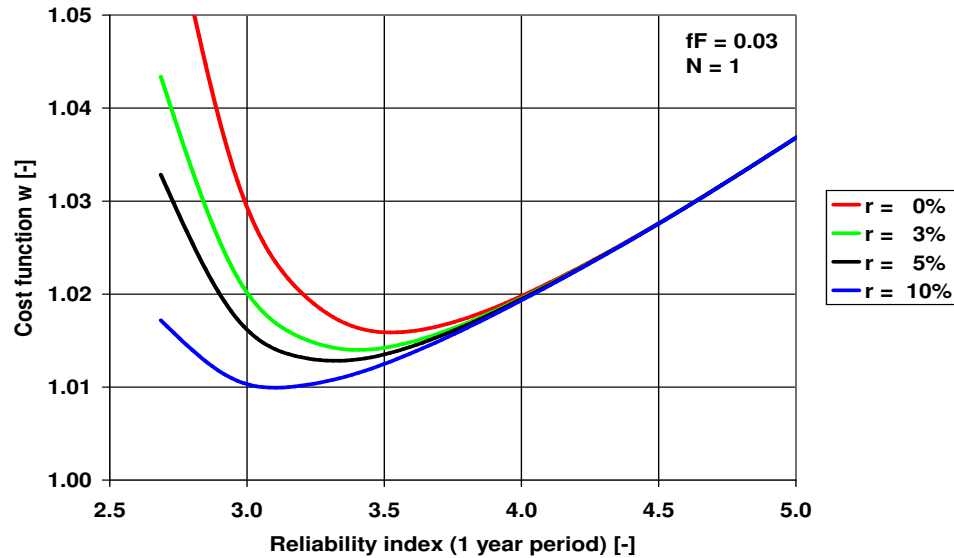
Figure 8.2: Economic weight function w for the tower for various values of the interest rate r. The failure cost fraction $f_F = 0.03$ and the number of critical location is $N = 1$. For $r = 5\%$ optimum system reliability index (period 1 year) is $\beta_1 = 3.32$.

day money is 'expensive'), and to have more failures (since these will occur in the future they are 'cheaper' in present day money than if there were no inflation). It is seen in figure 8.2 that the optimum shifts from $\beta_1 = 3.52$ to $\beta_1 = 3.10$ if the interest rate goes from $r = 0\%$ to $r = 10\%$: dependence is not very strong.

The dependence on the failure cost fraction f_F is even smaller: the minimum hardly shifts (see figure 8.3). This is not strange since replacement of 90% of the entire turbine is more expensive by far than the failure cost.

Figure 8.4 shows the cost function w for any number of critical locations. Obviously the optimal safety factor is smaller in the case of one critical location, than if there are five or ten locations, in particular because failures must be considered to be less than perfectly correlated (if not fully independent). Because the tower is designed to be as light as possible, ideally all locations should have exactly the same stress reserve factor $SRF = 1$. In practice this is not achieved, and stress reserve factors vary typically between 1 and 1.1, with mean value $SRF \simeq 1.05$. This has the effect that (in this particular case) the 32 critical locations in the tower with different stress reserve factors can be treated as 16 equivalent critical locations with $SRF = 1$. The subjects of multiple critical locations with possibly correlated loads and the influence of the size of a critical area are treated in more detail in appendix F.3.
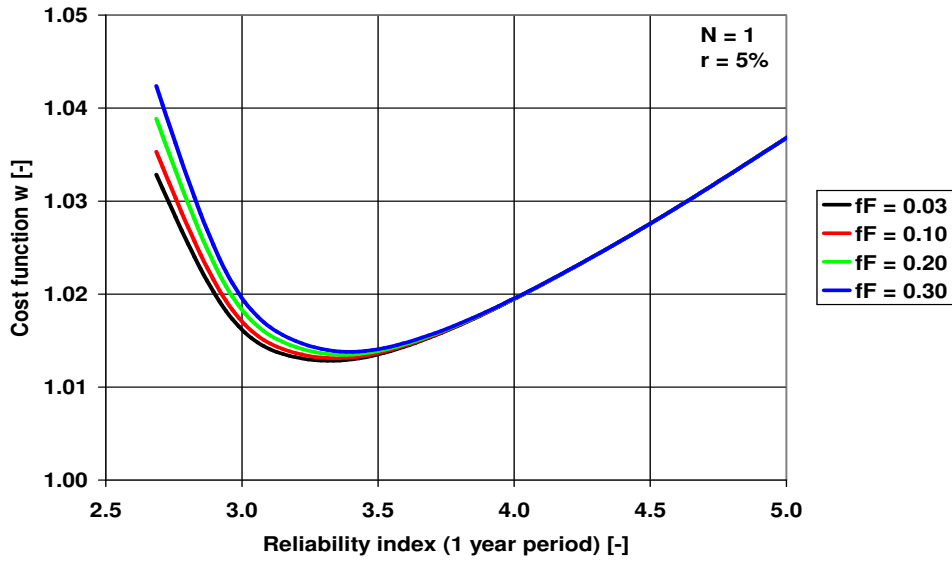
Figure 8.3: Economic weight function w for the tower for various values of the failure cost fraction f_F. The number of critical locations $N = 1$ and the interest rate is $r = 5\%$. For $f_F = 0.03$ optimum system reliability index (period 1 year) is $\beta_1 = 3.32$.
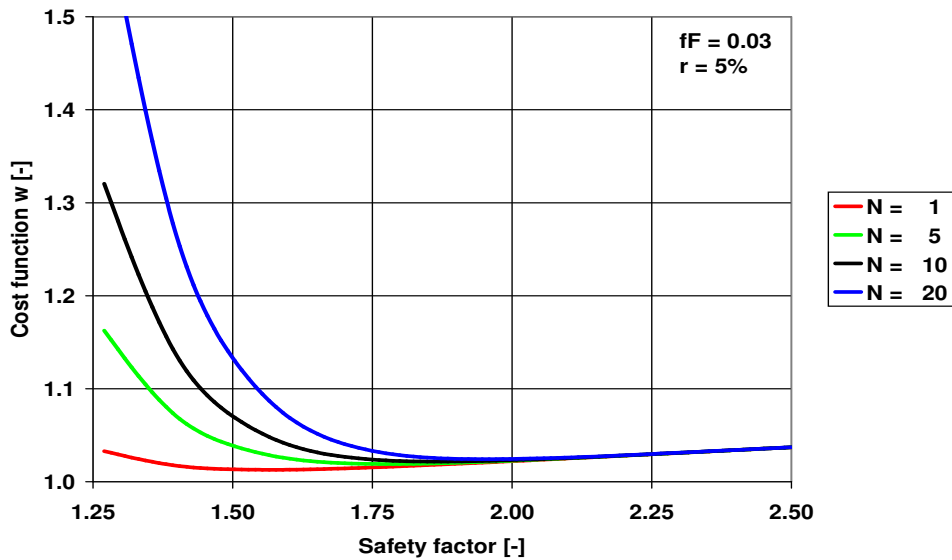
Figure 8.4: Economic weight function w for the tower for various numbers of critical locations N. The failure cost fraction $f_F = 0.03$ and the interest rate is $r = 5\%$. For $N = 1$ the optimal partial factor product is $\gamma = 1.57$.

Blade. For blades the situation is somewhat different, because collapse of a blade does not destroy the whole structure; in most cases only the blade needs to be replaced. Because the cost of replacement is smaller, the optimal reliability index β is shifted to lower values. In the calculation it is assumed that one blade represents 4% of the total investment ($f_R = 0.04$). The normalised mass derivative is:

$$\frac{1}{m_0}\frac{\partial m}{\partial \gamma} = 0.5 \tag{8.34}$$

This number is based on experience with actual blades. Of course for an ideal thin walled structure one would expect unity value. Optimisation results are given in table 8.9 (p152).

Hub. There are two possible failure scenarios for the hub. On one hand it may be argued that there will be no additional damage, and that only the hub is replaced; however this would require that cracks are detected. On the other hand it may be assumed that the whole rotor (hub and blades) must be replaced. This seems to be the more likely case.

The difference with the tower is that the hub is a cast product, and this makes it relatively cheap to strengthen critical areas since material need only be added locally (in the tower the welds are critical, and each weld defines the thickness of a 2.4 m high plate section). It is not easy to say what the normalised mass derivative should be in reality without doing detailed calculations on the hub. Fortunately the influence on the optimal safety factor is not all that large, as can be seen in table 8.7. For now we settle for a value of 0.2, but the value may be determined more accurately if so desired. It is noted that basically one is interested in the cost derivative rather than the mass derivative. However the calculation is not sensitive to the price of cast iron: if the price is higher it is more expensive to strengthen the hub, but on the other hand a failure with hub replacement is also more expensive.

Nacelle. The calculation of the nacelle machine frame is analogous to that of the hub; only failure and replacement is more costly. Different failure modes may be imagined. In the worst case the whole nacelle might fall down: if we assume that the only things that are not damaged are the tower, the foundation and the grid connection, together about 30% of total investment, the damaged fraction would be

Table 8.7: Optimal component reliability index for the hub. The assumed failure mode is collapse of the entire rotor, with replacement costing 20% of the wind turbine ($f_R = 0.2$). Standard calculation according to IEC 61400-1 class II for $L = 20$ years life.

normalised mass derivative	0.1	0.2	0.3	0.4	0.5	1.0
optimal reliability index β_1	3.81	3.64	3.53	3.47	3.39	3.18
optimal safety factor γ						
- number of critical locations $N = 1$	1.59	1.53	1.49	1.47	1.45	1.38
- $N = 10$	1.77	1.72	1.68	1.66	1.64	1.59

$f_R = 0.7$ (see table B.3). In the most favourable scenario (crack detection), only the nacelle would have to be replaced, giving $f_R = 0.1$. Finally in an intermediate case, the rotor would fall down (hub and blades), probably taking with it the main bearing and the main shaft; also the machine frame would have to be replaced. This comes out to about $f_R = 0.4$. Like we did for the hub we consider mass/safety factor derivative 0.1 and 0.2; results are given in table 8.8.

Summary. The results of the optimisation calculations are summarised in table 8.9 (next page). Results are only shown for the worst case load component (sensor); other results are almost identical. The optimal value of the failure probability (and the product of safety factors) depends on the expected damage in relation to the expected cost of making the component stronger. Thus it is economically optimal not to invest much in blade strength, but put the money in stronger machine frames and towers. The safety factors in table 8.9 (next page) are different from the customary factors, especially if we take into account the effect of multiple critical locations.

This means that it is advantageous to make the hub, the nacelle and the tower stronger in the critical areas because the extra material is cheap compared to the fatigue failures that are expected; conversely it pays to make blades less safe because the cost of losing a few blades is small. Of course the value of the economically optimal safety factor says nothing about the desirability of the associated failure probability from a public relations perspective.

The difference with current practice makes it important to analyse how results arise. Fortunately, on the whole calculations are robust (see chapter 9). What is new in the sense that it was not explicitly used in wind turbine calculations before is:

- That variation on CA fatigue strength is combined with variation of the stress factor q_0.

- That the median value of the stress factor q_0 is set to a value smaller than unity i.e. damage prediction is biased to the unconservative side.

- That the increase in failure probability caused by multiple critical locations is taken into account.

Table 8.8: Optimal component reliability index and safety factor for the nacelle for different failure modes and replacement cost. Standard calculation according to IEC 61400-1 class II for $L = 20$ years life.

normalised mass derivative	0.1			0.2		
replacement cost fraction f_R	0.1	0.4	0.7	0.1	0.4	0.7
optimal reliability index β_1	3.89	4.17	4.29	3.71	4.01	4.13
optimal safety factor γ						
- number of critical locations $N = 1$	1.73	1.84	1.89	1.66	1.77	1.83
- $N = 10$	1.94	2.07	2.11	1.88	1.99	2.05

8.9   Reduction of variation

To see where most can be gained by limiting variation of the limit state function, we assume for each variable in turn that it is deterministic instead of stochastic, i.e. that we know its value exactly (we ignore the fact that this is not possible for every variable, for example that natural variability in yearly wind speed cannot be influenced). Arbitrarily we require average yearly failure probability $p_F = 10^{-4}$ ($\beta_1 = 3.72$, $\beta_{20} = 2.88$), and calculate for each case the necessary product of partial factors γ to obtain these values.

Results are shown in table 8.10. The conclusion of this calculation is that wind turbine manufacturers should concentrate their efforts on determining the stress factor q_0 (i.e. the fatigue damage sum) as accurately as possible. For example for the hub, the required total safety factor could be reduced from 1.52 to 1.27 (Mx11h) and from 1.55 to 1.31 (My11h) respectively (note that the exact numerical values depend on the required reliability index). There is no other variable of which perfect knowledge can significantly reduce the overall required safety factor. This does not mean that no improvement is possible if we had better knowledge of a number of other variables, it is just that all individual contributions are swamped by uncertainty of fatigue. This conclusion about the importance of knowing material fatigue properties conforms to what was found by Larsen [120].

Table 8.9: Summary of results of optimisation of reliability index and safety factor. Standard calculation according to IEC 61400-1 class II for $L = 20$ years life.

component	blade	hub	nacelle	tower
material	composite	cast iron	cast iron	welded steel
load used	My11r	My11h	MyNf	Myt0
normalised mass derivative	0.50	0.20	0.20	0.70
replacement cost fraction f_R	0.04	0.20	0.40	0.90
failure cost fraction f_F	0.01	0.01	0.03	0.03
component reliability index β				
- 1 year period	2.70	3.64	4.01	3.32
- 20 year period	1.48	2.78	3.24	2.37
component failure prob. p_F				
- 1 year period	3.5×10^{-3}	1.3×10^{-4}	3.1×10^{-5}	4.5×10^{-4}
- 20 year period	7.0×10^{-2}	2.6×10^{-3}	6.2×10^{-4}	9.0×10^{-3}
target partial factor γ				
- 1 critical location	1.09	1.53	1.77	1.57
- 5 critical locations	1.24	1.66	1.93	1.78
- 10 critical locations	1.29	1.72	1.99	1.86
- 20 critical locations	1.34	1.77	2.07	1.95
standard safety factor	1.50	1.38	1.38	1.27
DNV values (table 2.3)	$\beta_1 = 4.26$; $p_{F,1} = 10^{-5}$			

8.10 Influence on turbine investment

It is not easy to say something definite about the influence of using different safety factors on total cost over the life of the turbine. The turbine total cost (of investment and of replacement of failed components) is the end result of a lengthy calculation based on many assumptions (some of these assumptions are examined more closely in chapter 9). What the optimal safety factor is, depends on the number of critical locations and the (assumed) replacement cost associated with component failure. Also it must be stressed that fatigue may not be the governing load; for example hub dimensions may be determined by stiffness considerations.

In table 8.11 (next page) some indications are given for $N = 10$ critical locations and interest rate $r = 5\%$. For each component the expected total cost (excluding maintenance) over the turbine's life is estimated with the safety factor currently used, and with the optimal safety factor. Calculations are independent in the sense that if one component is considered, all other components are assumed not to fail.

If we take the tower as example, we see that the current safety factor required by IEC 61400-1, $\gamma = 1.27$, results in expected total cost over the turbine's life that is 1.32 times the original investment; if a safety factor $\gamma = 1.86$ is used instead, total cost falls to 1.02 times the initial investment. Apparently the number of failures that

Table 8.10: Required total safety factor if one stochastic variable were exactly known. Factors are only listed if the difference with the case of 'no factors known' is larger than 0.01. Target yearly reliability index $\beta_1 = 3.72$; target yearly failure probability $p_{F,1} = 10^{-4}$. Standard load calculation according to IEC 61400-1 class II for $L = 20$ years life.

Known factor	Mx11r	My11r	Mx11h	My11h	MxNr	MyNf	MzNf	Myf0
None	1.33	1.36	1.52	1.55	1.55	1.66	1.59	1.76
Fatigue strength	1.26	1.29	1.45	1.49	1.48	1.60	1.53	1.63
Stress factor	1.18	1.22	1.27	1.31	1.30	1.43	1.36	1.42
Wind seed								
Geometry	1.31	1.34	1.50	1.54	1.53	1.65	1.58	1.75
FEM	1.27	1.31	1.46	1.50	1.49	1.61	1.54	1.75
Avg. wind speed					1.53	1.62	1.57	1.70
Weibull shape								
Wind dir. dist.								
Turb. intensity		1.34				1.63	1.57	1.75
Spectrum shape								1.75
Wind shear								
Windfarm wake						1.64	1.58	
Aerodyn. model		1.34		1.54	1.53	1.65	1.58	
Yaw error								
Terrain slope								
Low cycle fatigue								
Stop wind speed								

is prevented more than offsets the additional cost associated with a heavier tower.

For the blades, the hub and the nacelle we see that it hardly makes a difference what safety factor we use. The cost function w is very flat, meaning that cost of extra material balances cost of prevented failures. One could say that the bad news is that we cannot save much money, but that the good news is that we can have great reliability at almost no expense. Still 1–2% reduction on total turbine cost is not negligible, because of leverage it may mean 10–20% difference in profitability of a project.

Table 8.11: Indication of influence of optimisation on wind turbine cost. Reliability index β, failure probability p_F and cost function w refer to the component as a whole; there are 10 critical locations, and the interest rate $r = 0.05$. Standard calculation according to IEC 61400-1 class II for $L = 20$ years life.

component	blade	hub	nacelle	tower
material	composite	cast iron	cast iron	welded steel
load used	My11r	My11h	MyNf	Myt0
normalised mass derivative	0.50	0.20	0.20	0.70
replacement cost fraction f_R	0.04	0.20	0.40	0.90
failure cost fraction f_F	0.01	0.01	0.03	0.03
standard situation				
- yearly reliability index β_1	4.26	3.18	2.98	2.69
- yearly failure probability $p_{F,1}$	1.0×10^{-5}	7.5×10^{-4}	1.4×10^{-3}	3.6×10^{-3}
- safety factor γ	1.50	1.38	1.38	1.27
- value of cost function w	1.00	1.01	1.06	1.32
optimal safety factor				
- yearly reliability index β_1	2.70	3.64	4.01	3.32
- yearly failure probability $p_{F,1}$	3.5×10^{-3}	1.3×10^{-4}	3.1×10^{-5}	4.5×10^{-4}
- safety factor γ	1.29	1.72	1.99	1.86
- value of cost function w	1.00	1.00	1.01	1.02

Chapter 9

Sensitivity analysis

9.1 Introduction

In chapter 8 failure probabilities were derived for a turbine which is designed according to IEC 61400-1 wind class II, and placed in a class II environment; the optimal partial factors were calculated, and an estimate made of the effect on total cost if optimal values are used instead of the standard ones.

The results found are somewhat surprising. To take an example: according to table 8.9 (p152), blades might be constructed lighter (γ = 1.29 instead of γ = 1.50) and hub, nacelle machine frame and tower should be made considerably heavier (γ = 1.7–2.0 instead of the usual γ = 1.27–1.38). In fact, if the standard calculation is used, the tower 20 years failure probability is estimated to p_F = 0.07: out of every 100 towers, 7 are supposed to fail due to fatigue (table 8.6, p146).

Two obvious questions that arise are: 'Why are results as they are?' and 'Why are so few wind turbines collapsing if the calculated numbers are to be believed?'. While this is undoubtedly the most intriguing matter, there are other questions too that came up during the calculations. Hence questions treated in this chapter are:

1. Fundamental questions:

    - Why exactly are the optimal safety factors as high as they are?

    - Are failure probabilities found the *real* values?

    - How would results change if certain input parameters were chosen differently?

2. Interesting questions:

    - How do results change if required life is shorter than 20 years?

    - How do results change in complex terrain or for offshore sites?

    - What advantage is gained if calculated loads are verified with measurements?

9.2   Explanation of results

From the information in chapter 8 and especially table 8.10 (p153) the origin of the high failure probabilities may basically be inferred, but because the results seem to defy everyday experience it is worthwhile to discuss the causes in some more detail.

Most of the distributions of stochastic parameters listed in table 8.5 (p145) can be established with good accuracy. Moreover, the end result of the calculation is robust against changes in most distributions. The optimal one year period reliability index $\beta_1 = 3.32$ for the tower is also normal, and agrees with Dalsgaard Sørensen's result [198]. So far there is nothing out of the ordinary.

Two things are different compared to the usual calculations however. Firstly the uncertainty in fatigue life prediction is explicitly taken into account with the stress factor q_0 that is biased towards the unconservative side ($\mu_{q0} < 1$) and has significant variation ($V_{q_0} > 0$); this base calculation is designated '0' in table 9.1. Three additional calculations are now done, where we assume that the stress factor q_0:

1. Has unity mean $\mu_{q0} = 1$ (is unbiased) and coefficient of variation $V_{q_0} > 0$. On average predicted fatigue life corresponds to actual life.

2. Has biased mean $\mu_{q0} \neq 1$ but zero coefficient of variation $V_{q_0} = 0$. Fatigue life is always mispredicted by the same factor.

3. Has unity mean $\mu_{q0} = 1$ and zero coefficient of variation $V_{q_0} = 0$. The factor q_0 plays not role at all. This is the implicit assumption in conventional calculations.

Table 9.1: Influence of different distributions of stress factor q_0 on cumulative 20 years failure probability. Calculation according to IEC class II.

case	μ_{q_0}	V_{q_0}	Mx11r	My11r	Mx11h	My11h	MxNr	MyNf	MzNf	Myf0
Blades (composite)										
0, 1	1.00	0.10	9.1e-5	2.1e-4						
2, 3	1.00	0.00	1.4e-7	2.1e-6						
Hub and nacelle (cast iron)										
0	0.93	0.13			1.0e-2	1.4e-2	1.3e-2	2.9e-2	1.9e-2	
1	1.00	0.13			3.0e-3	4.6e-3	4.2e-3	1.1e-2	6.5e-3	
2	0.93	0.00			1.0e-4	4.0e-4	3.4e-4	4.5e-3	1.4e-3	
3	1.00	0.00			5.8e-6	3.2e-5	2.6e-5	8.5e-4	2.0e-4	
Tower (weld seams)										
0	0.80	0.17								7.2e-2
1	1.00	0.17								7.7e-3
2	0.80	0.00								1.6e-2
3	1.00	0.00								1.8e-4
Optimal p_F				7.0e-2		2.6e-3		6.2e-4		9.8e-3

Results are given in table 9.1. We see that bias and variation of the stress factor together are causing the large estimated failure probability, and by extension the high optimal safety factors (for the blades, predictions were assumed to be unbiased, because there is no information justifying other assumptions). If one could for example show with experiments that the bias assumption is too pessimistic, the tower failure probability would drop by a factor 10.

Secondly there is the issue of multiple critical locations. The usual approach is to look at critical locations individually, without bothering to calculate the system failure probability. Prime motivation is probably ease of calculation, but other arguments for this practice are:

- There are not many really critical locations (with $SRF = 1$), so in reality only one location is relevant. This assumption does not hold any more for today's highly optimised structures, like wind turbine towers.

- The standard is conservative enough to deal with this effect. Calculations done here indicate that this is not the case if the standard is followed to the letter (without hidden safety).

- Loads and material properties are correlated. There is some merit to this argument, but in appendix F.3 it is shown that high correlations are required (say $r \geq 0.7$) to see an effect. It is not known to which extent fatigue properties in various tests cited were correlated. It is therefore possible that correlation plays a significant role in tower welds.

Both the issue of the stress factor and correlation of failures in multiple critical locations should be settled by fatigue tests on material as used in wind turbines, if variation in results is to be limited and partial factors reduced.

9.3 Real failure probability

A question that often comes up when probabilistic calculations are done is: 'Is this the *real* failure probability?'. In this case especially the (calculated) large failure probability of hub, nacelle and tower arouses curiosity: for example, is it true that seven out of one hundred towers fail after 20 years? What we can do is to compare the values found with the probabilities that are used in risk assessments for wind turbines. This is done in table 9.2 (next page); it must be remembered that there are reasons to be somewhat skeptical of the 'Handbook' numbers (see section 2.5), so one does not have to be concerned about a factor 3 difference. On the other hand a factor 10 or more difference merits an explanation, so we should definitely have a closer look at failure probabilities found for the nacelle frame and the tower. The numbers given are (to the author's knowledge) the best estimate if one sticks to the letter of the standard, i.e. designs according to the precise degree of (un)conservatism the standard allows. In practice there is a tendency to do better than the standard, for

example foundries take pride in casting with very few errors; furthermore machine welding can be done with quality superior to what is required by the standard.

Still (to take an example) if there are about 2000 wind turbines in the Netherlands, one should expect 7 fatigue failures per year, which seems too high by one order of magnitude. On top of that the effect of multiple critical locations has not even been incorporated in the calculations. Suppose there are 10 critical weld seams in the tower, then we would expect to see 70 failures per year (even if material fatigue properties are correlated there should still be an increase in total system failure probability). However so many failures are not seen to occur. Possible explanations may be the following:

- Most wind turbines are younger than 10 years, and hence fatigue cracks have not had time to develop.

- Wind turbines are designed according to a class, for example IEC class II, with mean wind speed 8.5 m/s. In the Netherlands all locations but Den Helder have average wind speeds lower than this value. It is probably safe to say that the majority of wind turbines is placed where wind speeds are 0.5–1 m/s lower than the class they were designed for.

- Material quality is better than assumed in the standard. Accurate data are confidential, but it is not unreasonable to assume cast iron fatigue strength to be be 10–20% higher (based on static strength tests), and weld seam fatigue strength 20–30% (based on fatigue tests).

- Fatigue may not be governing. For example the plate buckling failure mode may determine tower plate thickness; also stiffness considerations determine hub and machine frame wall thickness in some cases.

To investigate the plausibility of the explanations offered, some additional calculations were done for cast iron and welded components. Results are given in table 9.3 for material properties and in table 9.4 for wind class and turbine age. It appears that failure probabilities may indeed be brought to levels that do not conflict with reality

Table 9.2: Comparison of component failure probabilities found with values given by Rademakers [173] in the 'Handbook for wind turbine risk assessment' (table 2.5, p21; values converted to 20 years life). Values from this work are for one critical location and for 20 years life (table 8.6, p146).

failure	p_1 (this work)	p_2 (Rademakers)	ratio p_1/p_2
blade fails[1]	1.1×10^{-3}	4.2×10^{-3}	0.3
nacelle and rotor fall down[2]	2.2×10^{-2}	1.2×10^{-3}	19
tower fails	7.2×10^{-2}	4.0×10^{-3}	18

[1]The Handbook value is the probability per turbine that a blade fails. The probability for an individual blade (given here) is ca 3 times lower.

[2]Compared to nacelle machine frame failure probability.

without stretching credulity too much. In fact, if we consider calculation no 4 for example, failure probabilities are close to the Handbook values (table 9.2). For a nacelle failure we have 6.9×10^{-4}–1.8×10^{-3} against the Handbook's 1.2×10^{-3}, while for a tower failure we have 2.0×10^{-3}, where the Handbook gives 4×10^{-3}. These preliminary calculations indicate once more that it is of paramount importance to get the right material and site data to obtain correct results.

9.4   Equivalent load definition

In the reference calculation the equivalent load with mean stress correction was used except for weld seams (see appendix C), where it is better to operate on the assumption that in large constructions there will be significant residual stresses (Olivier [164]). Using this concept means that we assume that the linear Palmgren-Miner rule is valid if mean stress corrected stresses are used, and that there is no fatigue limit (following Eulitz [61]). These assumptions may be wrong, which means that the calculation of the failure probability and the reliability index are off. Nevertheless, using the approximate equivalent load to estimate the sensitivity of the exact equivalent load to stochastic parameters is probably quite accurate, because all calculations

Table 9.3: Influence of hidden material safety on life fatigue failure probability. The equivalent load definition with mean stress influence is used. Calculation according to IEC class II for 20 years life. Calculation 0 is the base calculation, while calculations 1–3 assume different hidden safety factors.

case	hidden safety R_0		hub		nacelle			tower
	cast iron	welds	Mx11h	My11h	MxNr	MyNf	MzNf	Myf0
0	1.00	1.00	1.0e-2	1.4e-2	1.3e-2	2.9e-2	1.9e-2	7.2e-2
1	1.05	1.10	4.6e-3	6.9e-3	6.3e-3	1.5e-2	9.4e-3	3.1e-2
2	1.10	1.20	1.9e-3	3.1e-3	2.8e-3	8.1e-3	4.5e-3	1.2e-2
3	1.15	1.30	8.0e-4	1.3e-3	1.2e-3	4.1e-3	2.2e-3	4.7e-3

Table 9.4: Influence of hidden safety in wind speed and wind turbine age on life fatigue failure probability. The equivalent load definition with mean stress influence is used. The hidden safety on cast iron $R_0 = 1.15$, on weld seams $R_0 = 1.30$. Calculation according to IEC class II for 20 years life. Calculation 3 is the same as in table 9.3, while calculations 4–6 assume different wind speeds and lives.

case	hidden safety		hub		nacelle			tower
	wind speed	life	Mx11h	My11h	MxNr	MyNf	MzNf	Myf0
3	8.5	20	8.0e-4	1.3e-3	1.2e-3	4.1e-3	2.2e-3	4.7e-3
4	8.0	20	6.3e-4	9.3e-4	6.9e-4	1.8e-3	1.0e-3	2.0e-3
5	8.5	10	1.7e-5	4.7e-5	6.7e-5	1.3e-4	1.2e-4	6.3e-4
6	8.0	10	1.4e-5	2.4e-5	5.0e-5	8.6e-5	6.2e-5	2.4e-4

involve comparison of equivalent loads based on similar load spectra, which is bound to give similar deviations from the exact equivalent loads (see appendix C.2). One way to check this contention is to redo the reference calculation of chapter 8 with different definitions of the equivalent load. The mean stress corrections used before in the reference calculation were as follows:

- For weld seams we assume no mean stress influence because of residual stresses.

- For cast iron we have (the hub and the nacelle):

$$\Delta\sigma_{eff} = \Delta\sigma + 2M\,\sigma_{mean} \tag{9.1}$$

  Here M is the mean stress sensitivity (see appendix C.2).

- For composites (the blades) the correction is (see appendix C.2):

$$\Delta\sigma_{eff} = \frac{\Delta\sigma}{1 - \sigma_{mean}/UTS} \tag{9.2}$$

  Here the ultimate tensile strength UTS is set to 1.5 times the largest load in the fatigue spectrum.

Table 9.5: Life failure probability, reliability index and influence factors for standard calculation according to IEC class II for 20 years life. Simplest equivalent load definition: no mean stress correction and no cut off.

	Mx11r	My11r	Mx11h	My11h	MxNr	MyNf	MzNf	Myf0
$p_{F,MC,L}$	9.9e-5	5.3e-4	1.0e-2	2.4e-2	1.8e-2	2.6e-2	2.2e-2	7.3e-2
$p_{F,FORM,L}$	9.6e-5	4.8e-4	1.0e-2	2.3e-2	1.7e-2	2.4e-2	2.1e-2	7.2e-2
$\beta_{L,FORM}$	3.73	3.30	2.31	2.00	2.11	1.97	2.03	1.46
$\beta_{1,FORM}$	4.43	4.07	3.28	3.05	3.13	3.03	3.08	2.69
α^2 [%]								
Fatigue strength	24	19	18	15	16	15	15	23
Stress factor	48	39	62	53	56	51	51	53
Wind seed		1			1			2
Geometry	5	4	3	3	3	3	3	2
FEM	22	17	15	12	13	12	12	2
Avg. wind speed		6		6		6	6	10
Weibull shape								
Wind dir. dist.								
Turb. intensity		6		5	5	6	7	3
Spectrum shape						1		3
Wind shear		1						
Windfarm wake		4		2	2	3	3	1
Aerodyn. model		3		3	3	3	3	2
Yaw error								
Terrain slope								
Low cycle fatigue								
Stop wind speed								

The reference calculation is compared to a calculation where the equivalent load is not corrected for mean stress (table 9.5), and a calculation where small load cycles below the cut off limit produce no fatigue damage (table 9.7). For convenience, results are also summarised in table 9.6. In most cases results are not sensitive to a change in equivalent load definition; the tower is an exception. Note that there is virtually no change in the influence factors, regardless of equivalent load definition.

Table 9.6: Life failure probability for different definitions of equivalent load for standard calculation according to IEC class II for 20 years life. Blades have no cut off.

	Mx11r	My11r	Mx11h	My11h	MxNr	MyNf	MzNf	Myf0
simple	9.6e-5	4.8e-4	1.0e-2	2.3e-2	1.7e-2	2.4e-2	2.1e-2	7.2e-2
mean stress corr.	9.1e-5	2.1e-4	1.0e-2	1.4e-2	1.3e-2	2.9e-2	1.9e-2	2.1e-2
m.s.c. + cut off	9.1e-5	2.1e-4	2.5e-2	1.7e-2	2.2e-2	3.0e-2	2.1e-2	2.1e-1
best estimate	9.1e-5	2.1e-4	1.0e-2	1.4e-2	1.3e-2	2.9e-2	1.9e-2	7.2e-2

Table 9.7: Life failure probability, reliability index and influence factors for standard calculation according to IEC class II for 20 years life. Equivalent loads are corrected for mean stress and fatigue limit (cut off). Blades have no cut off.

	Mx11r	My11r	Mx11h	My11h	MxNr	MyNf	MzNf	Myf0
$p_{F,MC,L}$	9.3e-5	2.3e-4	2.6e-2	1.8e-2	2.2e-2	3.2e-2	2.3e-2	2.1e-1
$p_{F,FORM,L}$	9.1e-5	2.1e-4	2.5e-2	1.7e-2	2.2e-2	3.0e-2	2.1e-2	2.1e-1
$\beta_{FORM,L}$	3.74	3.53	1.96	2.12	2.02	1.88	2.03	0.81
$\beta_{1,FORM}$	4.44	4.26	3.02	3.14	3.07	2.97	3.07	2.31
α^2 [%]								
Fatigue strength	24	21	16	16	16	14	15	20
Stress factor	48	42	56	56	56	46	50	48
Wind seed		1			1			1
Geometry	5	4	3	3	3	3	3	2
FEM	22	18	13	13	13	11	12	2
Avg. wind speed		3	5	3	1	10	7	7
Weibull shape								
Wind dir. dist.								
Turb. intensity		4	3	3	4	8	7	6
Spectrum shape			1			1		10
Wind shear						1		
Windfarm wake		3	2	2	2	4	4	2
Aerodyn. model		4		3	3	2	3	2
Yaw error								
Terrain slope								
Low cycle fatigue								
Stop wind speed								

9.5   Exponent of S-N curve

In the probabilistic calculations the exponent of the S-N curve m was considered to be a fixed number. Although this is not too far from the truth for constant amplitude loading (many tests have been done for glassfibre composites, for cast iron and for welds, that show similar exponents), the situation is less clear for life curves, or for a Liu-Zenner modified curve, the curve that preferably should be used for life predictions since it gives superior results (figure 7.2, p112). Also data for materials as presently used in wind turbines are missing in the literature. In appendix C.5 it is shown that under some reasonable assumptions the estimated slope m from experiments has a distribution with coefficient of variation $V \simeq 5$–10%: for composites ($m = 9$–12) the standard deviation on slope is $\sigma_m \simeq 0.5$, while for cast iron ($m = 5$–8) and weld seams ($m = 3$–4) $\sigma_m \simeq 0.3$. To get an impression of the influence of slope we will look at the original value minus or plus one standard deviation: $m \pm \sigma_m$ (which covers a 68% interval). The slope is correlated to the fatigue strength with $r^2 = 0.77$; for convenience full correlation is used, which means that the fatigue strength changes with the slope (see appendix C.5 for a discussion of this, and all data).

Results are shown in table 9.8. Changes in failure probability are on the threshold of significance, maximally a factor 2. This is almost entirely due to the fatigue strength change, as can be inferred from table 9.9, where only the slope of the S-N curve is changed (suppose we were to use some other material having the same fatigue strength but a different slope S-N curve). Here almost no change in failure probability is seen, regardless of slope. The conclusion is that results are insensitive to errors in the S-N curve exponent m.

Table 9.8: Life failure probability for different slopes m and associated change in fatigue strength distribution. Standard calculation according to IEC class II for 20 years life. For each material the table has 3 lines, with mean minus one standard deviation, mean and mean plus one standard deviation. Slope m and fatigue strength $\Delta\sigma_A$ are assumed to be fully correlated.

slope m	$\Delta\sigma_A$	Mx11r	My11r	Mx11h	My11h	MxNr	MyNf	MzNf	Myf0
11.4	0.98	1.6e-4	3.5e-4						
12.0	1.00	9.1e-5	2.1e-4						
12.6	1.02	4.9e-5	1.2e-4						
6.0	0.98			1.4e-2	2.1e-2	1.9e-2	3.8e-2	2.5e-2	
6.3	1.00			1.0e-2	1.4e-2	1.3e-2	2.9e-2	1.9e-2	
6.6	1.02			7.4e-3	1.0e-2	9.7e-3	2.1e-2	1.3e-2	
3.2	0.96								1.0e-1
3.5	1.00								7.2e-2
3.8	1.04								5.1e-2

Table 9.9: life failure probability for different exponents of the S-N curve m. The distribution of the fatigue strength $\Delta\sigma_A$ is not changed. Standard calculation according to IEC class II for 20 years life.

	Mx11r	My11r	Mx11h	My11h	MxNr	MyNf	MzNf	Myf0
reference	9.1e-5	2.1e-4	1.0e-2	1.4e-2	1.3e-2	2.9e-2	1.9e-2	7.2e-2
composite								
- $m = 9$	8.3e-5	2.1e-4						
- $m = 10$	8.6e-5	2.1e-4						
- $m = 11$	8.8e-5	2.1e-4						
- $m = 12$	9.1e-5	2.1e-4						
cast iron								
- $m = 5$			1.0e-2	1.5e-2	1.4e-2	3.4e-2	1.8e-2	
- $m = 6$			1.0e-2	1.4e-2	1.3e-2	3.0e-2	1.9e-2	
- $m = 7$			1.0e-2	1.5e-2	1.3e-2	2.7e-2	1.9e-2	
- $m = 8$			1.0e-2	1.5e-2	1.3e-2	2.5e-2	1.9e-2	
weld seam								
- $m = 3$								7.2e-2
- $m = 4$								7.3e-2

Table 9.10: Summary of results of optimisation. Comparison of 10 years life and 20 years life (see also table 8.9, p152).

component	blade	hub	nacelle	tower
material	composite	cast iron	cast iron	welded steel
load used	My11r	My11h	MyNf	Myt0
normalised mass derivative	0.50	0.20	0.20	0.70
replacement cost fraction f_R	0.04	0.20	0.40	0.90
failure cost fraction f_F	0.01	0.01	0.03	0.03
component reliability index β				
- 1 year period	2.58	3.58	3.96	3.34
- 10 year period	1.65	2.92	3.37	2.63
component failure prob. p_F				
- 1 year period	5.0×10^{-3}	1.7×10^{-4}	3.8×10^{-5}	4.2×10^{-4}
- 10 year period	5.0×10^{-2}	1.7×10^{-3}	3.8×10^{-4}	4.2×10^{-3}
target safety factor γ (10 years)				
- 1 location	1.06	1.41	1.63	1.37
- 5 locations	1.19	1.53	1.77	1.50
- 10 locations	1.24	1.57	1.82	1.60
- 20 locations	1.28	1.62	1.88	1.66
standard safety factor	1.50	1.38	1.38	1.27
target safety factor γ (20 years)				
- 1 location	1.09	1.53	1.77	1.57
- 5 locations	1.24	1.66	1.93	1.78
- 10 locations	1.29	1.72	1.99	1.86
- 20 locations	1.34	1.77	2.07	1.95

9.6   Wind turbine life

So far all calculations were done with 20 years life. In reality economic life is shorter than that, the main reason for this being the rapid development of wind turbine technology. Therefore it is interesting to investigate if and how the safety factors would change if optimisation were done for 10 years instead of 20. Results are given in table 9.10 (previous page), where it can be seen that results are somewhat different from those for 20 years life (for convenience the numbers from table 8.9 (p152) are repeated). For the blades there is almost no change: optimal partial factors are 4% lower. For the cast iron components factors are 8% lower and for the tower 14%. The difference is significant, but not overwhelming.

9.7   Complex terrain

For complex terrain the modified distributions of stochastic parameters as given in table 4.17 are used, copied here in table 9.11. To get more insight into what is happening, the distributions of the parameters listed in table 9.11 are first changed to the new values one at a time, and then all together. We perceive (table 9.12, cases 0–5) that influence is generally small, except for Mann's shear parameter (case 4): smaller shear in the turbulence field gives considerably larger loads. The design value for

Table 9.11: Adjusted distributions (mean and standard deviation) for complex terrain.

parameter	FSU terrain		Complex terrain	
	mean	std.dev	mean	std.dev.
wind speed [m/s]	U_{avg}	0.07 U_{avg}	U_{avg}	0.20 U_{avg}
turbulence intensity [-]	0.16	0.01	0.16	0.02
wind shear exponent [-]	0.2	0.02	0.1	0.08
Mann's shear parameter [-]	3	0.3	1	0.6

Table 9.12: Influence of modified parameter distributions for complex terrain on life failure probability. Standard calculation according to IEC class II for 20 years life.

case	dist. chgd	Mx11r	My11r	Mx11h	My11h	MxNr	MyNf	MzNf	Myf0
0	reference[1]	9.3e-5	2.3e-4	1.0e-2	1.5e-2	1.3e-2	3.0e-2	2.0e-2	7.2e-2
1	wind speed[1]	1.0e-4	4.5e-4	1.1e-2	1.9e-2	2.0e-2	6.0e-2	3.5e-2	1.3e-1
2	turb. int.[1]	9.8e-5	4.6e-4	1.0e-2	1.7e-2	1.3e-2	4.3e-2	2.8e-2	8.1e-2
3	wind shear[1]	8.3e-5	1.0e-4	9.6e-3	1.0e-2	1.3e-2	1.2e-2	1.3e-2	7.5e-2
4	Mann's Γ[1]	3.1e-4	8.0e-4	1.7e-2	2.8e-2	2.1e-2	1.5e-1	5.7e-2	4.0e-1
5	All[1]	3.3e-4	1.4e-3	1.8e-2	2.7e-2	3.1e-2	1.4e-1	8.4e-2	4.3e-1
6	Mann's Γ[2]	7.8e-5	3.4e-4	9.6e-3	1.2e-2	1.8e-2	2.9e-2	3.1e-2	7.2e-2
7	All[2]	7.8e-5	3.4e-4	9.6e-3	1.2e-2	1.8e-2	2.9e-2	3.1e-2	1.2e-1

[1]Design value of Mann's Γ = 3.9. [2]Design value of Mann's Γ = 1.0.

Mann's shear parameter according to IEC 61400-1 is $\Gamma = 3.9$, while in flat terrain at current hub heights (70–100 m) $\Gamma \sim 3.0$ should be expected (table 4.14, p72) ; this gives only a slight increase in loads. However if the same design is used in complex terrain where the shear parameter is probably closer to $\Gamma = 1.0$, there is a larger increase. If we were to use $\Gamma = 1.0$ in the design phase (as we should, knowing the expected real value) there is no big change in failure probabilities (cases 6 and 7).

Clearly change of the spectral shape must be taken into account if calculations are done for complex terrain. However uncertainty in the calculation is still largely determined by fatigue properties.

9.8 Offshore

For offshore applications the dependence on wind speed is different. One might say that the influence of the wind is amplified through the waves; also the influence of variation of inertia coefficient C_M (determining wave loads) must be taken into account. To investigate all this, again we follow the practice of changing one parameter at a time. Load cases considered are:

case 0   land reference case, IEC class II ($U = 8.5$ m/s), wind from the North
case 1   as case 0, but IEC class I ($U = 10$ m/s)
case 2   offshore, IEC class I, uniform wind direction distribution, $C_M = 2$
case 3   as case 2, but $C_M = N(\mu = 2, \sigma = 0.1)$
case 4   as case 3, but wave forces are multiplied by $S_0 = 1.05$
case 5   as case 4, but $C_M = N(\mu = 2, \sigma = 0.2)$

Only the support construction (tower and monopile) is considered because loads above the yaw system (tower top) are known not to change compared to the land situation. Results are listed in table 9.13. From the numbers it appears that failure probabilities do not change much whatever we do. The only significant influence is the average value of the inertia coefficient C_M, which may be larger than expected (resulting in a wave load increase, simulated by the factor $S_0 = 1.05$), for example because of appurtenances or marine growth.

Table 9.13: Influence of modified parameter distributions for offshore sites on life failure probability. Calculations for 20 years life.

case	site	U	dir	σ_{C_M}	S_0	Myt68	Myt38	Myf0	Myf-10	Myf-20
0	land	8.5	N	–	1	1.7e-2	5.6e-2	7.2e-2	7.2e-2	6.9e-2
1	"	10	"	–	1	1.7e-2	5.4e-2	7.0e-2	6.8e-2	6.7e-2
2	offs.	10	unif.	0.0	1	1.7e-2	5.5e-2	7.2e-2	7.2e-2	6.8e-2
3	"	"	"	0.1	1	1.7e-2	5.6e-2	7.3e-2	7.1e-2	7.1e-2
4	"	"	"	0.1	1.05	1.7e-2	7.1e-2	1.1e-1	1.0e-1	1.0e-1
5	"	"	"	0.2	1.05	1.7e-2	7.9e-2	1.1e-1	1.1e-1	1.1e-1

One may wonder why results are so similar: after all the influence of the wind is increased through wind driven waves. However what is important for the limit state function Z (equation 8.23, p140) are the relative changes in load due to changes in wind speed, given by the derivative:

$$\frac{\partial Z}{\partial U} = \left(\frac{1}{\Delta F_{eq}} \frac{\partial \Delta F_{eq}}{\partial U} \right)_{U=U_{avg}} \tag{9.3}$$

The values of the relevant derivatives are listed in table 9.14. The general picture is that there is almost no change from land to offshore.

Table 9.14: Comparison of equivalent bending moment derivatives for onshore and offshore wind turbine towers. Wöhler exponent $m = 4$.

load	Myt68	Myt38	Myf0	Myf-11	Myf-21
land	0.058	0.087	0.091	0.092	0.093
offshore	0.065	0.087	0.095	0.103	0.105

9.9 Load verification

According to standards one must verify calculated loads by measurements on turbines. This makes sense, and obviously increases the confidence we may have in our calculations. One would therefore expect some reward or penalty depending on the extent of the verification. For example if no tests have been done yet, all calculated loads are to be multiplied by a load factor $\gamma_f = 1.2$; alternatively one could stipulate some reduction in safety factor, if a full load verification had been conducted. Therefore it is interesting to find out what the advantage is of a measurement program compared to calculating *de novo*. Unfortunately (for us) there is now so much experience with wind turbine load calculations, that it is hard to start completely unprejudiced; to get reliable data a special procedure with a tight protocol would have to be organised. This may be quite time consuming, especially since it is not easy to

Table 9.15: Influence of load verification on 20 years failure probability. Standard calculation according to IEC class II. The aerodynamic model has no influence on blade root lead-lag moments, which are dominated by gravity.

case	V_{aero}	Mx11r	My11r	Mx11h	My11h	MxNr	MyNf	MzNf	Myf0
-1	0.00	–	1.6e-4	–	1.3e-2	1.2e-2	2.7e-2	1.7e-2	7.1e-2
0	0.03	9.1e-5	2.1e-4	1e-2	1.4e-2	1.3e-2	2.9e-2	1.9e-2	7.2e-2
1	0.05	–	3.1e-4	–	1.7e-2	1.6e-2	3.1e-2	2.1e-2	7.5e-2
2	0.10	–	1.0e-3	–	2.8e-2	2.6e-2	4.4e-2	3.2e-2	8.8e-2
3	0.15	–	3.5e-3	–	4.5e-2	4.2e-2	6.2e-2	4.9e-2	1.0e-1

define which errors are 'normal' and which errors are 'gross' and would probably be detected in the design procedure.

Nevertheless we have the NASA Ames experiments (see section 6.3), which led us to a coefficient of variation on loads $V = 10$–15% (except for blade root lead-lag moments which are gravity dominated). To see what this does to failure probabilities, some calculations with increased uncertainty on aerodynamics are done. Not surprisingly failure probabilities get smaller if aerodynamic uncertainty decreases (table 9.15). For the blades the effect is considerable (a factor 20) but for cast iron and weld seams influence is smaller (a factor 4 and 1.3 respectively).

Chapter 10

Conclusions and recommendations

In this chapter we look back at the objectives stated in section 1.4 and check to see whether and to what extent they have been satisfied (sections 10.1–10.3). Section 10.4 gives the usual recommendations for further research.

10.1   Uncertainties

A study has been conducted to determine how large total uncertainty is in the fatigue design process, and what the main uncertainties are. These have all been quantified: the distributions of the relevant stochastic parameters have been determined (see table 8.5, p145), and their influence on fatigue damage equivalent loads established. To find the relative importance of each parameter, program tools have been developed: a combination of the wind turbine aeroelastic code Flex5 for load calculations and implementations of FORM and Monte Carlo algorithms that use Flex5 output for failure probability estimates.

The prediction of fatigue strength and the fatigue damage sum (component life) are the most important uncertainties by far, covering 50% or more of total variation of the limit state function. As long as these uncertainties are not reduced, improving other aspects of the design calculations will not yield any great advantage.

10.2   Review of models

In the process some models in common use were reviewed, in particular:
- Low cycle fatigue model. A program was developed to generate artificial wind speed histories to estimate realistic load sequences and calculate the effect on fatigue damage caused by large low frequency load cycles. For the drive train and the tower the effect of low cycle fatigue is significant and should be taken into account.

- Turbulent wind field model. Strictly speaking, within this work no formal comparison was done. We repeat the conclusions of Veldkamp [223]: comparing the Sandia/Veers and the Mann model, no evidence was found that one particular model predicts loads consistently better; however the Mann model is more physical in the sense that the wind fields always have consistent properties.

- Equivalent load definition. Three different definitions of equivalent loads were compared: influence on probabilistic results is limited (a factor ~ 2 on failure probability). For probabilistic calculations any of the three definitions investigated may be used.

- Equivalent turbulence intensity model. Establishing the equivalent turbulence intensity by direct integration of the turbulence intensity (to the power given by the slope m of the S-N curve), yields results that are almost the same compared to the exact calculation using equivalent loads. The 90% fractile turbulence intensity given by IEC 61400-1 is conservative by 0.01-0.02. Since the difference is small and the model simple, it is probably best to stick to the IEC recommendation.

- Mode shape approach. No evidence was found that more than three blade mode shapes improve load calculations. A limited number of modes is sufficient to obtain accurate results.

- Wave load model. Using nonlinear wave modeling has some effect on wave loads (increase by 5–10%). Inertia (acceleration) forces totally dominate drag forces in fatigue loading. Hence most attention should go to accurate estimation of the inertia coefficient.

10.3   Partial safety factors

Given the best available data on the distribution of parameters influencing fatigue loads on wind turbines and fatigue properties of materials, economically optimal safety factors have been derived with a simple cost model (see table 8.9 (p152) for details). These factors differ from the ones prescribed by current design standards:

- Larger safety factors should be used for cast iron (hub and nacelle machine frame) and for welded constructions (tower).

- A smaller safety factor could be used for composites (blades).

The discrepancy with conventional design practice is due to two major causes. Firstly, uncertainty on fatigue life prediction is not taken into account: for the stress factor one assumes no variation and no bias, which is unconservative. Secondly, in modern highly optimised constructions critical locations are treated in isolation, when they should be considered together (as a chain with a weakest link). The fact that current safety factors nevertheless appear to give sufficiently low failure probability in

practice is explained as follows:

- Material quality is better and hence fatigue strength is higher than assumed.

- Fatigue may not govern, and in effect the advocated larger safety may have been obtained already.

- Wind turbines are often placed in environments more benign than they were designed for.

- Due to rapid expansion of the wind turbine market, most turbines are still young (5–10 years old), and fatigue problems may come later.

The best means to reducing uncertainty and improving design practice (i.e. removing hidden safety), is by fatigue testing on materials identical to those used in practice, with specimens of relevant size, both with constant amplitude and variable amplitude loading. Furthermore fatigue damage prediction tools must be examined and calibrated, and the issue of critical locations with correlated properties should be investigated.

The influence of adjusting assumptions and values of input parameters on failure probabilities was investigated (see chapter 9); in general calculations appear to be stable and results robust.

10.4 Recommendations for further research

10.4.1 Design methods

in order to improve accuracy of the results of probabilistic calculations, and gain greater insight into the safety margins actually achieved, fatigue life predictions should be verified against variable amplitude tests on specimens representative of actual components, preferably with load spectra characteristic of wind turbines. In this way reliable data on bias and variation can be obtained; the relative Miner approach may be adopted, using the stress factor q_0. An interesting alternative is the use of fracture mechanics for short cracks (Vormwald [227]) to predict fatigue life.

Due to the large number of critical locations in a wind turbine, their size and the tendency to design for the same stress reserve factor all through a component ('simultaneous failure everywhere'), it is necessary that the combined effect of all the (possibly correlated) critical locations is considered, which could for example result in the partial factor depending on the number of locations. This holds especially true for the tower, having hundreds of metres of weld seam where cracks may start.

10.4.2 Materials

Composites (blades)
Indications are that the current constant life diagram with three stress ratio values is not accurate enough. Current fatigue damage predictions with a limited diagram

should be checked against life estimates based on a more detailed diagram (and of course against tests).

Cast iron (Hub and nacelle). The material in use is probably better than assumed in calculations. Fatigue testing should be done to establish the S-N curve accurately rather than using literature values.

Welded steel (tower). The weld seam quality is probably better than prescribed by standards. Fatigue tests should be done to find the correct S-N curve, to establish whether the variation for machine welding under controlled conditions is smaller than assumed in standards, and whether individual welds are correlated to a significant degree.

Bibliography

[1] M. Anderson. A review of MCP techniques. Technical Report 01327R00022 issue 02, Renewable Energy Systems Ltd, July 2004.

[2] M. Anderson. MCP errors. Technical Report 01327 R 00025, Renewable Energy Systems Ltd, January 2005.

[3] R. Anthes. Ein neuartiges Kurzrissfortschrittsmodell zu Anrisslebensdauer-vorhersage bei wiederholter Beanspruchung. Technical Report (Heft) 57, Institut für Stahlbau und Werkstoffmechanik, 1997.

[4] I. Antoniou, H. Jørgensen, T. Mikkelsen, S. Frandsen, R. Barthelmie, C. Perstrup, and M. Hurtig. Offshore wind profile measurements from remote sensing instruments. In *European Wind Energy Conference*. EWEA, February 2006.

[5] I. Antoniou, S.M. Petersen, J. Højstrup, F. Mouzakis, C. Tiel, U. Follrichs, A. Albers, T. Curvers, H. Verhoef, P. Enevoldsen, and L.C. Christensen. Identification of variables for site calibration and power curve assessment in complex terrain. Technical Report JOR3-CT98-0257, Risø, CRES, WindTest, DEWI, ECN, Bonus and NEG Micon, July 2001.

[6] C. Bak and J. Johansen. Metode til 3D korrektion af profildata. In C. Bak, editor, *Forskning i Aeroelasticitet - EFP-2004 R-1509(DA)*, chapter 2, pages 11–25. Risø, Roskilde, May 2005.

[7] R. Barthelmie, O. Frost Hansen, K. Enevoldsen, and R. Møller. The importance of accurate and reliable wind measurements at turbine hub-height for offshore wind farms. In *Copenhagen Offshore Wind*, October 2005.

[8] R.J. Barthelmie, B. Lange, and M. Nielsen. Wind resources at Rødsand and Omø Stålgrunde. Technical Report I-1456(EN), Risø National Laboratory, Roskilde, October 1999.

[9] R.J. Barthelmie and S.C. Pryor. Can satellite sampling of offshore wind speeds realistically represent wind speed distributions? *Journal of Applied Meteorology*, 42(1):83–94, 2003.

[10] J.H. Bass, M. Rebbeck, L. Landberg, M. Cabré, and A. Hunter. An improved Measure-Correlate-Predict algorithm for the prediction of long term wind climate in regions of complex environment. Technical Report JOR3-CT98-0295, Renewable Energy Systems Ltd (UK), Risø National Laboratory (Denmark), Ecotécnia (Spain), University of Sunderland (UK), July 2000.

[11] I. Bech Lauridzen. Hot spot result deviation in FEM - analyses of the Mk IV V100 hub. Internal report 961602 R0, Vestas, April 2006.

[12] E. Berge, F. Nyhammer, L. Tallhaug, and Ø. Jacobsen. An evaluation of the WAsP model at a coastal mountainous site in Norway. *Wind Energy*, 9:131–140, 2006.

[13] H. Bergström and A.-S. Smedman. Stably stratified flow in a marine atmospheric surface layer. *Boundary-Layer Meteorology*, 72:239–265, 1995.

[14] W. Bierbooms and H.F. Veldkamp. Time domain comparison of simulated and measured wind turbine loads using constrained wind fields. In *Euromech Colloquium 464b Wind Energy Oldenburg - International Colloquium on Fluid Mechanics and Mechanics of Wind Energy Conversion*. ForWind, Springer, October 2005.

[15] G.T. Bitsuamlak, T. Stathopoulos, and C. Bédard. Numerical evaluation of wind flow over complex terrain. *J. Aerosp. Engng.*, 17(4):135–145, October 2004.

[16] A. Björck. Aerodynamic engineering calculations of blade tower interaction. In B. Maribo Pedersen, editor, *IEA Annex XI Aerodynamics of Wind Turbines 13th Symposium*, number ISSN 0590-8809, pages 173–186. FFA, Technical University of Denmark, November 1999.

[17] G.K. Boerstra. The multislope model: a new description for the fatigue strength of glassfibre reinforced plastic. In *Proceedings of the European Wind Energy Conference and Exhibition, Athens (available online)*. EWEA, February 2006.

[18] J. Böhm and K. Heckel. Die Vorhersage der Dauerschwingfestigkeit unter Berücksichtigung des statistischen Größeneinflusses. *Z. Werkstofftech.*, 13:120–128, 1982.

[19] I.P. Bond. Fatigue life prediction of GRP subjected to variable amplitude loading. *Composites: Part A*, 30:961–970, 1999.

[20] E.A. Bossanyi. Individual blade pitch control for load reduction. *Wind Energy*, 6(2):119–128, 2003.

[21] E.A. Bossanyi. Wind turbine control for load reduction. *Wind Energy*, 6(3):229–244, 2003.

[22] E.A. Bossanyi. Further load reductions with individual pitch control. *Wind Energy*, 8(4):481–485, 2005.

[23] H. Bouillon, P. Fösel, J. Neubarth, and W. Winter. Wind report 2003. Technical report, E.ON Netz GmbH, Bayreuth, Germany, 2004.

[24] H. Braam, J.J.D. van Dam, C.J. Christensen, M.L. Thøgersen, G.C. Larsen, and K.O. Ronold. Methods for probabilistic design of wind turbines. Technical Report R-1082(EN), Risø National Laboratory, Roskilde, December 1998.

[25] P. Brandt Christensen. Stateline Windfarm FPL - Investigation results and proposed solutions. Internal report, Vestas, January 2003.

[26] P. Brøndsted, H. Lilholt, and A. Lystrup. Composite materials for wind power turbine blades. *Annu. Rev. Mater. Res.*, 35:505–538, 2005.

[27] A. Buch, T. Seeger, and M. Vormwald. Improvement of fatigue life prediction accuracy for various realistic loading spectra by use of correction factors. *Int. J. Fatigue*, 8:175–185, October 1986.

[28] A. Buch, M. Vormwald, and T. Seeger. Anwendung von Korrekturfaktoren für die Verbesserung der rechnerischen Lebensdauervorhersage. Technical Report FF-16/1985, Technische Hochschule Darmstadt / Technion - Israel Institute of Technology, Darmstadt, 1985.

[29] R. Burrows, R.G. Tickell, D. Hames, and G. Najafian. Morison wave force coefficients for application to random seas. *Applied Ocean Research*, 19:183–199, 1997.

[30] T. Burton, D. Sharpe, N. Jenkins, and E. Bossanyi. *Wind Energy Handbook*. Wiley, 2001.

[31] M.P. Byfield and D.A. Nethercot. Material and geometric properties of structural steel for use in design. *The Structural Engineer*, 75:363–367, November 1997.

[32] I. Carlén and G.C. Larsen. Fatigue analysis of structures subjected to wind loading - a model for low frequency load cycles. Technical report, Teknikgruppen AB, Sollentuna, Sweden, November 2002.

[33] D.J. Cerda Salzmann and J. van der Tempel. The impact of different wind and wave data sources on the fatigue of offshore wind turbines. In *European Wind Energy Conference London*. EWEA, November 2004.

[34] H. Chandler. Wind energy the facts - an analysis of wind energy in the EU-25. CD, European Wind Energy Association, 2004.

[35] H. Charnock. Wind stress over a water surface. *Q. J. R. Meteor. Soc.*, 81:639–640, 1955.

[36] P.W. Cheng. *A Reliability Based Design Methodology for Extreme Responses of Offshore Wind Turbines*. PhD thesis, Delft University Wind Energy Research Institute, October 2002.

[37] S. Chib and E. Greenberg. Understanding the Metropolis-Hastings algorithm. *The American Statistician*, 49(4):327–335, Nov 1995.

[38] G. Claus and U. Steinhagen. Generation by numerical simulation of predetermined nonlinear wave sequences in random seaways. In *Proceedings OMAE'01 Rio De Janeiro*, June 2001.

[39] K. S. Correa Bomholt Pedersen. Relative damge on offshore wind turbines induced by linear and nonlinear wave loadings. Master's thesis, Denmark's Technical University, Lyngby, August 2005.

[40] G.P. Corten. *Flow separation on Wind Turbine Blades*. PhD thesis, University of Utrecht, Utrecht, January 2001.

[41] G.P. Corten and H.F. Veldkamp. Aerodynamics: Insects can halve wind-turbine power. *Nature*, 412:41–42, July 2001.

[42] M.S. Courtney and P. Hummelshøj. Murdochville turbulence measurements. Internal report, Vestas, February 2003.

[43] M. Dankert. Ermüdungsrisswachstum in Kerben - Ein einheitliches Konzept zur Berechnung von Anriss- und Rissfortschrittslebensdauern. Technical Report (Heft) 60, Institut für Stahlbau und Werkstoffmechanik, 1999.

[44] Dansk Ingeniørforening. *Last og sikkerhed for vindmøllekonstruktioner (Dansk Ingeniørforening's Code of Practice for Loads and Safety of Wind Turbine Constructions)*. Teknisk Forlag - Normstyrelsens Publikationer, 1st edition, 1992.

[45] Det Norske Veritas. *Guidelines for Certification of Wind Turbine Power Plants*. DNV, 1992.

[46] Det Norske Veritas. *Design of Offshore Wind Turbine Structures - Offshore Standard DNV-OS-J101*. DNV, 2004.

[47] Det Norske Veritas and Risø National Laboratory. *Guidelines for Design of Wind Turbines*. DNV/Risø, second edition, 2002.

[48] R.P. Downey. Uncertainty in wind turbine life equivalent load due to variation of site conditions. Master's thesis, Technical University of Denmark, Fluid Mechanics Section, Lyngby, April 2006.

[49] P.E. Duncan and K.R. Drake. A note on the simulation and analysis of irregular nonlinear waves. *Applied Ocean Research*, 17:1–8, 1995.

[50] V. Dünkel. *Schwingfestigkeit von Schraubenverbindunge - Optimierte Ver-*

suchsführung und deren Anwendung bei der Untersuchung von Randschicht und Oberflächenzuständen. PhD thesis, TU Darmstadt, 1999.

[51] A.T. Echtermeyer, C. Kensche, P. Bach, M. Poppen, H. Lilholt, S.I. Andersen, and P. Brøndsted. Method to predict fatigue lifetimes of GRP wind turbine blades and comparison with experiments. In *European Union Wind Energy Conference Göteborg*, May 1996.

[52] B. Efron. *The Jackknife, the Bootstrap and Other Resampling Plans*. CBMS 38. Society for Industrial and Applied Mathematics, 1982.

[53] B. Efron and R.J. Tibshirani. *An Introduction to the Bootstrap*. Monographs on Statistics and Applied Probability 57. Chapman and Hall, 1993.

[54] K.J. Eidsvik. A system for wind power estimation in mountainous terrain. prediction of Askervein Hill data. *Wind Energy*, 8:237–249, 2005.

[55] S. Elgar, R.T. Guza, and R.J. Seymour. Wave group statistics from numerical simulation of a random sea. *Applied Ocean Research*, 7:93–96, 1985.

[56] ESDU. Characteristics of atmospheric turbulence near the ground part I: Definitions and general information. Technical Report 74030, ESDU, October 1976.

[57] ESDU. Integral length scales of turbulence over flat terrain with roughness changes. Technical Report 86035, ESDU, April 1993.

[58] ESDU. Characteristics of atmospheric turbulence near the ground part II: Single point data for strong winds (neutral atmosphere). Technical Report 85020, ESDU, August 2001.

[59] ESDU. Characteristics of atmospheric turbulence near the ground part III: Variations in space and time for strong winds (neutral atmosphere). Technical Report 86010, ESDU, August 2001.

[60] K.G. Eulitz. Lebensdauervorhersage I - Verbesserung der Lebensdauerabschätzung durch systematische Aufarbeitung und Auswertung vorliegender Versuchsreihen. Technical report, TU Dresden, June 1994.

[61] K.G. Eulitz. *Beurteilung der Zuverlässigkeit von Lebensdauervorhersagen nach dem Nennspannungkonzept und dem Örtlichen Konzept anhand einer Sammlung von Betriebsfestigkeitsversuchen.* PhD thesis, TU Dresden - Fakultät für Maschinenwesen, Dresden, May 1999.

[62] L. Flacelière and F. Morel. Probabilistic approach in high-cycle multiaxial fatigue: volume and surface effects. *Fatigue Fract. Engng Mater. Struct.*, 27:1123–1135, 2004.

[63] European Commission Directorate General for Research. External costs - research results on socio-economical damages due to electricity and transport.

Technical Report EUR 20198, European Commission, 2003.

[64] S.T. Frandsen. Turbulence and turbulence-generated structural loading in wind turbine clusters. Technical Report R-1188(EN), Risø National Laboratory, Roskilde, October 2005.

[65] H.P. Frank, S.E. Larsen, and J. Højstrup. Simulated wind power offshore using different parametrizations for the sea surface roughness. *Wind Energy*, 3:67–79, 2000.

[66] H.P. Frank, E.L. Pedersen, R. Hyvönen, and B. Tammelin. Calculations on the wind climate in Northern Finland: the importance of inversions and roughness variations during the seasons. *Wind Energy*, 2:113–123, 1999.

[67] P. Fuglsang and K. Thomsen. Cost optimization of wind turbines for large scale offshore windfarms. Technical Report R-1000(EN), Risø National Laboratory, Roskilde, 1998.

[68] E. Gassner. U0+ Verfahren zur treffsicheren Vorhersage von Betriebsfestigkeits-Kennwerten nach Wöhler-Versuchen. *Materialprüfung*, 22(4):155–159, April 1980.

[69] E. Gassner. Ermittlung von Betriebsfestigkeits-Kennwerten auf der Basis einer reduzierten Bauteil-Dauerfestigkeit. *Materialprüfung*, 26(11):394–398, November 1984.

[70] Germanischer Lloyd. *Rules and Regulations IV - Non-Marine Technology Part 1 - Wind Energy*. Germanischer Lloyd, 1993.

[71] Germanischer Lloyd. *Rules and Regulations - Non-Marine Technology Part 2 - Offshore Wind Energy*. Germanischer Lloyd, 1995.

[72] Germanischer Lloyd. *Rules and Guidelines IV Industrial Services Guideline for the Certification of Offshore Wind Turbines (final draft)*. Germanischer Lloyd, 2004.

[73] J.M.R. Graham and C.J. Brown. ROTOW - Investigation of the aerodynamic interaction between wind turbine rotor blades and its impact on wind turbine design. Technical report, Imperial College of Science and Medicine, London, UK, September 2000.

[74] H. Gudehus and H. Zenner. *Leitfaden für eine Betriebsfestigkeitsrechnung - Empfehlung zur Lebensdauerabschätzung von Maschinenbauteilen*. VBFEh/VDEh, 4th edition, 1999.

[75] O.T. Gudmestad. Measured and predicted deep water wave kinematics in regular and irregular seas. *Marine Structures*, 6:1–73, 1993.

[76] O.T. Gudmestad and G. Moe. Hydrodynamic coefficients for calculation of hydrodynamic loads on offshore truss structures. *Marine Structures*, 9:745–

758, 1996.

[77] E. Haibach. *Betriebsfestigkeit - Verfahren und Daten Zur Bauteilberechnung*. Springer/VDI, 2nd edition, 2002.

[78] W. Hanenkamp. Untersuchungen zur Zeit- und Dauerfestigkeit von hochfesten Schraubenbolzen (10.9) im Durchmesserbereich M36 bis M72. *Konstruktion*, 44:255–260, 1992.

[79] K.S. Hansen and G.C. Larsen. Parameterisation of turbulence intensity. In *European Wind Energy Conference Madrid*. EWEA, EWEA, June 2003.

[80] L.P. Hansen. Wind analysis Syros Island Greece, V47-600 kW, Turbines 15888-4 and 15889-2. Internal report, Vestas, February 2006.

[81] L.P. Hansen. Wind analysis Tursillagh windfarm, Ireland, Park no. 21 Turbine 1775. Internal report, Vestas, February 2006.

[82] C.B. Hasager, M. Bruun Christensen, M. Nielsen, and R. Barthelmie. Using satellite data for mapping offshore wind resources and wakes. In *Copenhagen Offshore Wind*, October 2005.

[83] C.B. Hasager, M. Nielsen, P. Astrup, R. Barthelmie, E. Dellwik, N.O. Jensen, B.H. Jørgensen, S.. Pryor, O. Rathmann, and B.R. Furevik. Offshore wind resource estimation from satellite SAR wind field maps. *Wind Energy*, 8:403–419, 2005.

[84] W.K. Hastings. Monte Carlo sampling methods using Markov chains and their applications. *Biometrika*, 57(1):97–109, 1970.

[85] E. Hau. *Wind Turbines, Fundamentals, Technologies, Application, Economics*. Springer, 2nd edition, 2005.

[86] S.A. Herman. DOWEC Cost Model - Implementation. Technical Report DOWEC-068 / DOWEC F1W2-SH02-068/01C / ECN-CX-02-048, ECN, Petten, 2003.

[87] S.A. Herman, H.J.T. Kooijman, H.B. Hendriks, M. Zaayer, E. van de Brug, W. op den Velde, A. Winnemuller, and R. van den Berg. Variations on a 500 MW offshore windfarm design. In *Offshore Wind Energy in the Mediterranean and other European Seas (Naples)*, April 2003.

[88] P. Heuler, M. Vormwald, and T. Seeger. Relative Miner-regel und U0-Verfahren - eine bewertende Gegenüberstellung. Technical Report FF-18, Technische Hochschule Darmstadt - Fachgebiet Werkstoffmechanik, 1984.

[89] P. Heuler, M. Vormwald, and T. Seeger. Relative Miner-regel und U0-Verfahren - eine bewertende Gegenüberstellung. *Materialprüfung*, 28:65–72, 1986.

[90] A. Hobbacher. Fatigue design of welded joints and components. Technical Report XIII-1539-96/XV-845-96, IIW Joint Working Group XIII-XV, 1996.

[91] M. Høgedal. *Experimental Study of Wave Forces on Vertical Circular Cylinders in Long and Short Crested Sea.* PhD thesis, Aalborg University, Dept of Civil Engineering, Hydraulic and Coastal Engineering Laboratory, Aalborg, August 1993.

[92] D. Hollis and J. Ashcroft. Techniques for estimating the local wind climatology. Technical Report W/11/00400/REP, ETSU, 1995.

[93] International Electrotechnical Committee. *IEC 61400-1: Wind turbines part 1: Design Requirements.* IEC, 3rd edition, 2005.

[94] International Electrotechnical Committee. *IEC 61400-3 Wind turbines part 3: Design Requirements for Offshore Wind Turbines (committee draft).* IEC, 1st edition, 2005.

[95] ISO TC67 and SC 7N288. *Petroleum and Natural Gas Industries - Fixed Steel Offshore Structures (ISO/CD 19902).* ISO, 2001.

[96] Joint Committee on Structural Safety. JCSS probabilistic model code part 3: Resistance models. Technical Report 3rd draft, JCSS, April 2006.

[97] H.E. Jørgensen, S.Frandsen, and P. Volund. Wake effects on Middelgrund windfarm. Technical Report R-1415(EN), Risø National Laboratory, Roskilde, July 2003.

[98] J.C. Kaimal. Turbulence spectra, length scales and structure parameters in the stable surface layer. *Boundary-Layer Meteorology*, 4:289–309, 1973.

[99] J.C. Kaimal, J.C. Wyngaard, Y. Izumi, and O.R. Coté. Spectral characteristics of surface-layer turbulence. *Quart. J.R. Met. Soc.*, 98:563–589, 1972.

[100] F.C. Kaminsky, R.H. Kirchhoff, C.Y. Syu, and J.F. Manwell. A comparison of alternative approaches for the synthetic generation of a wind speed time series. *Transactions of the ASME*, 113:280–289, November 1991.

[101] T. von Kármán. Progress in the statistical theory of turbulence. *Journal of Marine Research*, 7:252–264, 1948.

[102] T. Kashef and S.R. Winterstein. Relating turbulence to wind turbine blade loads: Parametric study with multiple regression analysis. *Transactions of the ASME*, 121:156–161, August 1999.

[103] H. Kaufmann. Zur schwingfesten Bemessung dickwandiger Bauteile aus GGG-40 unter Berücksichtigung gießtechnisch bedingter Gefügeungänzen. Technical Report FB-214, Fraunhofer Institut Betriebsfestigkeit LBF, 1998.

[104] H. Kaufmann and C.M. Sonsino. Schwingfestigkeit von reinigungs- und ver-

festigungsgestrahlten duktilen Eisen-Graphit-Gußwerkstoffen unter konstanter und zufallsartiger Belastung. *Giessereiforschung*, 41(3):99–106, 1989.

[105] H. Kaufmann and D.B. Wolters. Zyklische Beanspruchbarkeit dickwandiger Bauteile aus ferritischem Gußeisen mit Kugelgraphit. *Konstruieren + Gießen*, 27(1):4–27, 2002.

[106] N.D. Kelley and H.J. Sutherland. Damage estimates from long term structural analysis of a wind turbine in a US wind farm environment. In *ASME/AIAA Wind Energy 1997*. AIAA, 1997.

[107] C. King and B. Hurley. The SpeedSort, DynaSort and Scatter wind correlation methods. *Wind Engineering*, 29:217–241, 2005.

[108] K.H. Kloos and W. Thomala. Zur Dauerhaltbarkeit von Schraubenverbindungen Teil 1-4. *Verbindungstechnik*, 11, 1979.

[109] K.L. Kotte and K.-G. Eulitz. Datensammlung Betriebsfestigkeit - Zuverlassigkeit von Lebensdauerabschätzungen (Data pool structural integrity - reliability of lifetime prediction methods). *Mat.wiss. u. Werkstofftech.*, 34(9):836–842, 2003.

[110] K.L. Kotte and H. Zenner. Lifetime prediction - comparison between calculation and experiment on a large data base. In K.-T. Rie and P.D. Portella, editors, *Low Cycle Fatigue and Elasto-Plastic Behaviour of Materials*, pages 721–728. Elsevier Science Ltd, 1998.

[111] V.B. Köttgen, R. Olivier, and T. Seeger. Fatigue analysis of welded connections based on local stresses. Technical Report XIII-1408-91, International Institute of Welding, 1992.

[112] V.B. Köttgen, R. Olivier, and T. Seeger. Der Schaden an der Großen Windkraftanlage GROWIAN - Schwingfestigkeitsanalyse der versagenskritischen Schweißverbindungen. *Konstruktion*, 45:1–9, 1993.

[113] H. Kouwenhoven. Windfarm investment strategy. Personal communication (telephone conversation and email), 18 April 2006.

[114] L. Kristensen, P. Kirkegaard, and J. Mann. Sampling statistics of atmospheric observations. *Wind Energy*, 5:301–313, 2002.

[115] M. Kühn. *Dynamics and Design Optimisation of Offshore Wind Energy Conversion Systems*. PhD thesis, Delft University Wind Energy Research Institute, Delft, 2001.

[116] D.J. Laino, A.C. Hansen, and J.E. Minnema. Validation of the Aerodyn subroutines using NREL unsteady aerodynamics experiment. *Wind Energy*, 5, 227-244 2002.

[117] L. Landberg and N.G. Mortensen. A comparison of physical and statistical

methods for estimating the wind resource at a site. In K.F. Pitcher, editor, *Wind Energy Conversion 1993 - Proc. 15th BWEA Conference*, London, October 1993. Mech. Eng. Publ. Ltd.

[118] B. Lange. *Modelling the Marine Boundary Layer for Offshore Wind Power Utilisation*. PhD thesis, University of Oldenburg, December 2002.

[119] C.H. Lange. Probabilistic fatigue methodology and wind turbine reliability. Technical Report SAND96-1246 UC-1211, Sandia National Laboratories, Albuquerque, 1996.

[120] G. Larsen and A.M. Hansen. Usikkerhed ved opstilling af lastgrundlag. In H. Aagaard Madsen, editor, *Forskning i Aeroelasticitet - EFP-2000 R-1272(DA)*, chapter 11, pages 89–102. Risø, Roskilde, July 2001.

[121] G.C. Larsen. Offshore fatigue design turbulence. *Wind Energy*, 4:107–120, 2001.

[122] G.C. Larsen and K.S. Hansen. Spatial coherence of the longitudinal turbulence component. In *Proceedings of the European Wind Energy Conference (EWEC), Madrid*. EWEA, June 2003.

[123] G.C. Larsen and K. Thomsen. Low cycle fatigue loads. Technical report, Risø National Laboratory, Roskilde, September 1996.

[124] N.A. Last and M. Duijvendijk. Enhanced reliability of simulation models of welded wind turbine components. In *Proceedings of DEWEK International Technical Wind Energy Conference Wilhelmshaven*. DEWI, published on CD, October 2004.

[125] H.A. Lausen. Woolnorth turbine no 15330 (complex terrain). Internal report, Vestas, February 2005.

[126] H. van Leeuwen, D. van Delft, J. Heijdra, H. Braam, E.R. Jørgensen, D. Lekou, and P. Vionis. Comparing fatigue strength from full scale blade tests with coupon-based predictions. *Journal of Solar Energy Engineering*, 124:404–411, November 2002.

[127] J.G. Leishman. Challenges in modelling the unsteady aerodynamics of wind turbines. *Wind Energy*, 5:85–132, 2002.

[128] M. Lenzen and J. Munksgaard. Energy and CO2 life-cycle analyses of wind turbines - review and applications. *Renewable Energy*, 26:339–362, 2002.

[129] B.T. Madsen and P. Krogsgaard. International wind energy development world market update (issued yearly). Technical report, BTM Consult, 1997-2006.

[130] P.A. Madsen, H.B. Bingham, and Hua Liu. A new Boussinesq method for fully nonlinear waves from shallow to deep water. *J. Fluid. Mech.*, 462:1–30, 2002.

[131] T. Maeda, S. Homma, and Y. Ito. Effect of complex terrain on vertical wind profile measured by SODAR technique. *Wind Engineering*, 28(6):667–678, 2004.

[132] J.F. Mandell, D.D. Samborsky, and N.K. Wahl. New fatigue data for wind turbine blade materials. *Journal of Solar Energy Engineering*, 125:506–514, November 2003.

[133] J. Mann. The spatial structure of neutral atmospheric surface-layer turbulence. *J. Fluid. Mech.*, 273:141–168, 1994.

[134] J. Mann. Wind field simulation. *Prob. Engng. Mech.*, 13:269–282, 1998.

[135] J. Mann. Simulation of turbulence, gusts and wakes for load calculations. In *Euromech Colloquium 464b Wind Energy Oldenburg - International Colloquium on Fluid Mechanics and Mechanics of Wind Energy Conversion*. ForWind, Springer, October 2005.

[136] J. Mann, F. Bingöl, H.E. Jørgensen, T. Mikkelsen, G.C. Larsen, A. Coffey, and M. Harris. Fast laser Doppler wake measurements. In *Proceedings of the European Wind Energy Conference and Exhibition, Athens (available online)*. EWEA, February 2006.

[137] J. Mann, M.S. Courtney, and P. Hummelshøj. Lacedonia and Roseto turbulence measurements. Technical report, Risø National Laboratory, Roskilde, December 2000.

[138] J. Mann, L. Kristensen, and M.S. Courtney. The Great Belt coherence experiment - a study of atmospheric turbulence over water. Technical Report R-596, Risø National Laboratory, Roskilde, Aug 1991.

[139] J. Mann, G.C. Larsen, and T.J. Larsen. Towards more realistic extreme load predictions. In *Proceedings of the European Wind Energy Conference and Exhibition, Athens (available online)*, February 2006.

[140] E.P.D. Mansard, S.E. Sand, and P. Klinting. Sub and superharmonics in natural waves. *Transactions of the ASME*, 110:210–217, August 1988.

[141] L. Manuel, P.S. Veers, and S.R. Winterstein. Parametric models for estimating wind turbine fatigue loads for design. In *A Collection of the 2001 ASME Wind Energy Symposium*, number AIAA-2001-0047, pages 276–287. AIAA/ASME, January 2001.

[142] J.F. Manwell, J.G. McGowan, and A.L. Rogers. *Wind Energy Explained: Theory, Design and Application*. John Wiley, 2002.

[143] D. McQueen and S. Watson. Validation of wind speed prediction methods at offshore sites. *Wind Energy*, (in press), 2006.

[144] R.E. Melchers. *Structural reliability analysis and prediction*. Wiley, second

edition, 1999.

[145] D. Milborrow. Uncovering truths behind capacity factors. *WindStats Newsletter*, 16(3):1–3, Summer 2003.

[146] K. Mittendorf and W. Zielke. Nonlinear irregular wave forces on the support structure of wind energy turbines. In *Euromech Colloquium 464b*. ForWind, Springer, October 2005.

[147] E.E. Morifadakis, G.L. Glinou, and M.J. Koulouvari. The suitability of the von Kármán spectrum for the structure of turbulence in a complex terrain wind farm. *J. Wind Eng. Ind. Aerodyn.*, 62:237–257, 1996.

[148] M. Motta, R.J. Barthelmie, and P. Vølund. The influence of non-logarithmic wind speed profiles on potential power output at Danish offshore sites. *Wind Energy*, 8:219–236, 2005.

[149] T. Mousten, S. Sørensen, and L. Strandgaard. Udmattelses- og sikkerhedsanalyse af samlingsdetalje i vindmølletårn. Master's thesis, Aalborg Universitetet, Det Teknisk-Naturvidenskabelige Fakultet, Aalborg, 2003.

[150] G. Najafian, R.G. Tickell, R. Burrows, and J.R. Bishop. The UK Christchurch bay compliant cylinder project: analysis and interpretation of Morison wave force and response data. *Applied Ocean Research*, 22:129–153, 2000.

[151] J. Nathwani, N.C. Lind, and M.D. Pandey. *Affordable Safety by Choice: The Life Quality Method*. Institute for Risk Research, University of Waterloo, Canada, 1995.

[152] O. Nerdahl and O. Ørjasæter. SN data for nodular cast iron according to Windcast quality. Technical Report STF24 F01305, SINTEF, December 2001.

[153] L. B. Nielsen. Madeira mesurement report Vestas V47 WTG nos 12124 and 12127. Internal report, Vestas, February 2003.

[154] M. Nielsen, K.S. Hansen, and B.J. Pedersen. Validity of the assumption of Gaussian turbulence. Technical Report R-1195(EN), Risø National Laboratory, Roskilde, 2000.

[155] M. Nielsen, G.C. Larsen, J. Mann, S. Ott, K.S. Hansen, and B.J. Pedersen. Wind simulation for extreme and fatigue loads. Technical Report R-1437(EN), Risø National Laboratory, Roskilde, December 2003.

[156] P. Nielsen, L. Bo Albinus, T. Sørensen, M.V. Sørensen, M.L. Thøgersen, S. Chun, and N.G. Mortensen. Twenty case studies for predicting and verifying wind farm energy production. In *European Wind Energy Conference Madrid*. EWEA, EWEA, June 2003.

[157] R. Nijssen, O. Krause, C. Kensche, T. Philippides, and A. van Wingerde. Basic static and fatigue data from the OPTIMAT BLADES project. In *European*

Wind Energy Conference Athens. EWEA, March 2006.

[158] R.P.L. Nijssen. *Spectrum fatigue life prediction and strength degradation of wind turbine rotor blade composites*. PhD thesis, Technical University Delft, 2006.

[159] R.P.L. Nijssen, V. Paasipoularidis, A. Smits, g. Dutton, and T. Philippides. Fatigue and residual strength of rotor blade materials. In *European Wind Energy Conference Athens*. EWEA, March 2006.

[160] R.P.L. Nijssen, D.D. Samborsky, J.F. Mandell, and D.R.V. van Delft. Strength degradation and simple load spectrum tests in rotor blade composites. In *A Collection of the 2005 ASME Wind Energy Symposium: Technical Papers Presented at the 43rd AIAA Aerospace Sciences Meeting and Exhibit, Reno, Nevada 10-13 january 2005*, pages 28–38, Reston, January 2005. AIAA/ASME, AIAA.

[161] R.P.L. Nijssen, D.R.V. van Delft, and A.M. van Wingerde. Alternative fatigue lifetime prediction formulations for variable amplitude loading. *Journal of Solar Energy Engineering*, 124:396–403, November 2002.

[162] Det Nordiske Komité for Bygningsbestemmelser. Retningslinier for last- og sikkerhedsbestemmelser for bærende konstruktioner. Technical Report 35, NKB, November 1978.

[163] R. Olivier. Experimentelle und numerische Untersuchungen zur Bemessung schwingbeanspruchter Schweißverbindungen auf der Grundlage örtlicher Beanspruchungen. Technical Report (Heft) 62, Institut für Stahlbau und Werkstoffmechanik, 2000.

[164] R. Olivier and W. Ritter. Catalogue of S-N-curves of wleded joints in structural steels parts 1-5: Uniform statistical analysis of fatigue test results. Technical Report 56/I-II-II-IV-V, Deutscher Verband fur Schweisstechnik e.V. (DVS), 1980-85.

[165] S. Øye. Dynamic stall model. In K.F. McAnulty, editor, *Proceedings of the Fourth IEA Symposium on the Aerodynamics of Wind Turbines*, number N-118. IEA, January 1991.

[166] D.J. Peters, C.J. Shaw, C.K. Grant, J.C. Heideman, and D. Szabo. Modelling the North Sea through the North European storm study. In *25th Annual Offshore Technology Conference Houston*, pages 479–489, May 1993.

[167] W.H. Press, B.P. Flannery, S.A. Teukolsky, and W.T. Vetterling. *Numerical Recipes in Pascal - The Art of Scientific Computing*. Cambridge University Press, 1989.

[168] W.H. Press, B.P. Flannery, S.A. Teukolsky, and W.T. Vetterling. *Numerical Recipes in C - The Art of Scientific Computing*. Cambridge University Press,

2nd edition, 1992.

[169] S.C. Pryor, R.J. Barthelmie, and J.T. Schoof. Inter-annual variability of wind indices across Europe. *Wind Energy*, (in press), 2006.

[170] S.C. Pryor, M. Nielsen, R.J. Barthelmie, and J. Mann. Can satellite sampling of offshore wind speeds realistically represent wind speed distributions? Part II Quantifying uncertainties associated with distribution fitting methods. *Journal of Applied Meteorology*, 43(5):739–750, 2004.

[171] R. Rackwitz. The philosophy behind the life quality index and empricial verification. Updated memorandum to JCSS, Technical University Munich, Munich, November 2005.

[172] R. Rackwitz and H. Streicher. Optimization and target reliabilities. In *AS-RANET Conference Glasgow*, July 2002.

[173] L. Rademakers, H. Braam, H. Brinkman, K. Ham, F. Verheij, H. Cleijne, and L. Folkerts. *Handboek Risicozonering Windturbines*. NOVEM, 1.1 edition, July 2002.

[174] F. Rasmussen, M. Hartvig Hansen, K. Thomsen, T. Juul Larsen, F. Bertagnolio, J. Johansen, H. Aagaard Madsen, C. Bak, and A. Melchior Hansen. Present status of aeroelasticity of wind turbines. *Wind Energy*, 6:213–228, 2003.

[175] W. Ritter. Kenngrößen der Wöhlerlinien für Schweißverbindungen aus Stählen. Technical Report (Heft) 53, Institut für Stahlbau und Werkstoffmechanik, 1994.

[176] K.O. Ronold and C.J. Christensen. Optimization of a design code for wind-turbine rotor blades in fatigue. *Engineering Structures*, 23:993–1004, 2001.

[177] K.O. Ronold and G.C. Larsen. Reliability based design of wind turbine rotor blades against failure in ultimate loading. *Engineering Structures*, 22(6):565–574, 1999.

[178] K.O. Ronold, J. Wedel-Heinen, and C.J. Christensen. Calibration of partial safety factors for design of wind-turbine rotor blades against fatigue failure in flapwise bending. In *European Union Wind Energy Conference Göteborg*, May 1996.

[179] K.O. Ronold, J. Wedel-Heinen, and C.J. Christensen. Reliability-based fatigue design of wind turbine rotor blades. *Engineering Structures*, 21:1101–1114, 1999.

[180] S.E. Sand and E.P.D. Mansard. Reproduction of higher harmonics in irregular waves. *Ocean Engng*, 13(1):57–83, 1986.

[181] P. Schaumann and M. Seidel. Ermüdung von Ringflanschverbindungen - Ermüdungsbeanspruchung geschraubter Ringflanschverbindungen bei Wind-

energieanlagen. Technical Report (Forschungsheft) 268, Forschungskuratorium Maschinenbau e.V., January 2002.

[182] J. Schijve. Fatigue prediction and scatter. *Fatigue Fract. Engng Mater. Struct.*, 17:381–396, 1994.

[183] J. Schijve. *Fatigue of Structures and Materials*. Kluwer Academic, 2001.

[184] S. Schreck (editor). Analysis and modeling of the NREL full-scale wind tunnel experiment. *Wind Energy*, 5:77–257, 2002.

[185] W. Schütz. Fatigue life prediction by calculation: facts and fantasies. In Shinozuka and Yao, editors, *Structural Safety and Reliability*, pages 1125–1131. Balkema, 1994.

[186] G. Schweiger and K. Heckel. Statistischer Größeneinfluß bei zufallsartiger Schwingbeanspruchung. *Z. Werkstofftech.*, 15:257–264, 1984.

[187] G. Sedlacek, A. Hobbacher, J.B. Schleich, and A. Nussbaumer. First draft of the background document prEN 1993-1-9. Technical report, RWTH Institute of Steel Construction, December 2002.

[188] M. Shafiee-Far. *Hydrodynamic Interaction Between Fluid Flow and Oscillating Slender Cylinders*. PhD thesis, Technical University Delft, Delft, March 1997.

[189] W.Z. Shen, M.O.L. Hansen, and J.N. Sørensen. Determination of angle of attack (AoA) for rotating blades. In *Euromech Colloquium 464b*. Springer, October 2005.

[190] M. Shinozuka and C.-M. Jan. Digital simulation of random processes and its applications. *Journal of Sound and Vibrations*, 25:111–128, 1972.

[191] D. Simms, S. Schreck, M. Hand, and L.J. Fingersh. NREL unsteady aerodynamics experiment in the NASA-Ames wind tunnel: A comparison of predictions to measurements. Technical Report TP-500-29494, NREL, Golden, Colorado, June 2001.

[192] A.-S. Smedman, H. Bergström, and U. Högström. Spectra, variances and length scales in a marine stable boundary layer dominated by a low level jet. *Boundary-Layer Meteorology*, 76:211–232, 1995.

[193] H. Snel. Review of the present status of rotor aerodynamics. *Wind Energy*, 1:46–69, 1998.

[194] H. Snel and J.G. Schepers. Joint investigation of dynamic inflow effects and implementation of an engineering method. Technical Report C-94-107, ECN, Petten, 1994.

[195] G. Solari and F. Tubino. A turbulence model based on principal components.

Prob. Engng. Mech., 17:327–335, 2002.

[196] C.M. Sonsino, H. Kaufmann, and A. Engels.   Schwingfestigkeit von festgewalzten, induktionsgehärteten sowie kombiniert behandelten Eisen-Graphit-Gußwerkstoffen unter konstanten und zufallsartigen Belastungen. *Giessereiforschung*, 42(3):110–121, 1990.

[197] C.M. Sonsino and M. Küppers. Fatigue life of welded joints under multiaxial variable amplitude loading - damage accumulation and the effective equivalent stress hypothesis. *Mat-wiss. u. Werkstofftech.*, 31:81–95, 2000.

[198] J.D. Sørensen and N.J. Tarp-Johansen. Cost-optimal structural reliability of offshore wind turbines. In *The Science of Making Torque from Wind (CD)*. EWEA, April 2004.

[199] J.D. Sørensen and N.J. Tarp-Johansen. Optimal structural reliability of offshore wind turbines. In *ICOSSAR Rome*. ICOSSAR, June 2005.

[200] N.N. Sørensen and J.A. Michelsen. Detaljeret 3D CFD beregning med programmet EllipSys3D på National Renewable Energy Laboratory's (NREL) 10 m rotor. In H. Aagaard Madsen, editor, *Forskning i Aeroelasticitet - EFP-2000 R-1272(DA)*, chapter 3, pages 15–26. Risø, Roskilde, July 2001.

[201] U. Steinhagen. *Synthesizing Nonlinear Transient Gravity Waves in Random Waves*. PhD thesis, TU Berlin, May 2001.

[202] H.J. Sutherland and J.F. Mandell. Optimised Goodman diagram for the analysis of fiberglass composites used in wind turbine blades. In *A Collection of the 2005 ASME Wind Energy Symposium: Technical Papers Presented at the 43rd AIAA Aerospace Sciences Meeting and Exhibit, Reno, Nevada 10-13 january 2005*, pages 18–27, Reston, January 2005. AIAA/ASME, AIAA.

[203] N.J. Tarp-Johansen. Examples of fatigue lifetime and reliability evaluation of larger wind turbine components. Technical Report R-1418(EN), Risø National Laboratory, Roskilde, March 2003.

[204] N.J. Tarp-Johansen, P. Hauge Madsen, and S. Frandsen. Partial safety factors in the 3rd edition of IEC 61400-1: Wind turbine generator systems - part 1: Safety requirements. Technical Report R-1319(EN), Risø National Laboratory, Roskilde, March 2002.

[205] T.O. Tengs, M.E. Adams, J.S. Pliskin, D.G. Sfaran, J.E. Siegel, M.C. Weinstein, and J.D. Graham. Five-hundred life-saving interventions and their cost-effectiveness. *Risk Analysis*, 15:369–390, 1995.

[206] K. Thomsen. Få parametre kan beskrive komplekse vindforhold. Technical Report AED-RB-3b, Risø National Laboratory, Roskilde, September 1998.

[207] K. Thomsen. The statistical variation of wind turbine fatigue loads. Technical

Report R-1063(EN), Risø National Laboratory, Roskilde, September 1998.

[208] K. Thomsen. Turbulensmodelleringens betydning for tårnlaster. Technical report, Risø National Laboratory, Roskilde, 2002.

[209] K. Thomsen, E.R. Jørgensen, and E.C. Miranda. Afklaring af usikkerhed på beregning af tårnlaster. In C. Bak, editor, *Forskning i Aeroelasticitet - EFP-2004 R-1509(DA)*, chapter 4, pages 43–54. Risø, Roskilde, May 2005.

[210] K. Thomsen and H. Aagaard Madsen. A new simulation method for turbines in wake - applied to extreme response during operation. *Wind Energy*, 8:35–47, 2005.

[211] K. Thomsen and H.A. Madsen. A new simulation method for turbines in wake - applied to extreme response during operation. In G.A.M. van Kuik, editor, *The Science of Making Torque from Wind*, pages 425–432. Duwind/ECN, Duwind, Delft University of Technology, April 2004.

[212] K. Thomsen, H.A. Madsen, and G.C. Larsen. En ny metode kan forudsige detaljerede laster for møller i parker. Technical Report AED-RB-16, Risø National Laboratory, Roskilde, 2003.

[213] H.W. Tieleman. Universality of velocity spectra. *J. Wind Eng. Ind. Aerodyn.*, 56:55–69, 1995.

[214] I. Troen and E. Lundtang Pedersen. *European Wind Atlas*. Risø National Laboratory, Roskilde, 1989.

[215] J.M.V. Trumars, N.J. Tarp-Johansen, and T. Krogh. The effect of wave modelling on offshore wind turbine fatigue loads. In *Copenhagen Offshore Wind*, October 2005.

[216] M.J. Tucker, P.G. Challenor, and D.J.T. Carter. Numerical simulation of a random sea: a common error and its effect upon wave group statistics. *Applied Ocean Research*, 6(2):118–222, 1984.

[217] S.E. Tuller and A.C. Brett. The characteristics of wind velocity that favor the fitting of a Weibull distribution in wind speed analysis. *Journal of Climate and Applied Meteorology*, 23:124–134, 1984.

[218] P.S. Veers. Three-dimensional wind simulation. Technical Report SAND88-0152 UC-261, Sandia National Laboratories, Albuquerque, 1988.

[219] P.S. Veers. All wind farm uncertainty is not the same: the economics of common versus independent causes. In *AWEA Windpower '95, Washington DC*, pages 195–204. AWEA, March 1995.

[220] P.S. Veers and S.R. Winterstein. Application of measured loads to wind turbine fatigue and reliability analysis. *Journal of Solar Energy Engineering*, 120:233–239, November 1998.

[221] P.S. Veers, S.R. Winterstein, C.L. Lange, and T.A. Wilson. User's manual for FAROW: Fatigue and reliability of wind turbine components. Technical Report SAND94-2460, Sandia National Laboratories, Albuquerque, 1994.

[222] H.F. Veldkamp. Flex5 modifications (blade modes). Technical Report RDT 156 A, NEG Micon, September 2003.

[223] H.F. Veldkamp. Influence of wind field modelling on wind turbine fatigue loads. In *European Wind Energy Conference Madrid*. EWEA, 2003.

[224] H.F. Veldkamp and J. van der Tempel. Influence of wave modelling on the prediction of fatigue for offshore wind turbines. *Wind Energy*, 8:49–65, 2005.

[225] Verein Deutsche Ingenieure. VDI 2230 Systematische Berechnung hochbeanspruchter Schraubenverbindungen Zylindrische Einschraubenverbindungen, February 2003.

[226] L.J. Vermeer, J.N. Sørensen, and A. Crespo. Wind turbine wake aerodynamics. *Progress in Aerospace Sciences*, 39:467–510, 2003.

[227] M. Vormwald. Anrißlebensdauervorhersage auf der Basis der Schwingbruchmechanik für kurze Risse. Technical Report (Heft) 47, Institut für Stahlbau und Werkstoffmechanik, 1989.

[228] M. Vormwald. Crack initiation in weld seam test specimens. Personal communication (email), 13 April 2006.

[229] M. Vormwald and T. Seeger. The consequences of short crack closure on fatigue crack growth under variable amplitude loading. *Fatigue Fract. Engng Mater. Struct.*, 14:205–225, 1991.

[230] J.K. Vrijling, W. van Hengel, and R.J. Houben. A framework for risk evaluation. *Journal of Hazardous Materials*, 43:245–261, March 1995.

[231] J.K. Vrijling and A.C.W.M. Vrouwenvelder. *Probabilistic Design*. TU Delft, 2005.

[232] A.C.W.M. Vrouwenvelder. Failure probability for N correlated failure modes. Personal communication (email), 10 April 2006.

[233] A.C.W.M. Vrouwenvelder and J.K. Vrijling. *Probabilistisch Ontwerpen*. TU Delft, 2000.

[234] J.D. Wheeler. Method for calculating forces produced by irregular waves. *Journal of Petroleum Technology*, 22:359–367, 1970.

[235] J. Wieringa and P.J. Rijkoort. *Windklimaat van Nederland (Wind Climate of the Netherlands)*. KNMI/Staatsuitgeverij, Den Haag, 1983.

[236] S.R. Winterstein and P.S. Veers. Theory manual for FAROW version 1.1: A numerical analysis of the fatigue and reliability of wind turbine components.

Technical Report SAND94-2459, Sandia National Laboratories, January 2000.

[237] J.C. Woods and S.J. Watson. A new matrix method for producing long-term wind roses with MCP. *Wind Engineering and Industrial Aerodynamics*, 66:85–94, 1997.

[238] F. Yamazaki and M. Shinozuka. Digital generation of non-Gaussian stochastic fields. *J. Engng. Mech. ASSC*, 114:1183–1197, 1988.

[239] H. Zenner and J. Liu. Vorschlag zur Verbesserung der Lebensdauerabschätzung nach dem Nennspannungskonzept. *Konstruktion*, 44:9–17, 1992.

Index

Appendix A

Coordinate system and nomenclature

A.1 Coordinate sytem

In this report the coordinate system of Germanischer Lloyd is used (figure A.1):

- X is the wind direction
- Z is upwards
- Y is to the left when looking at the wind turbine from an upwind position.
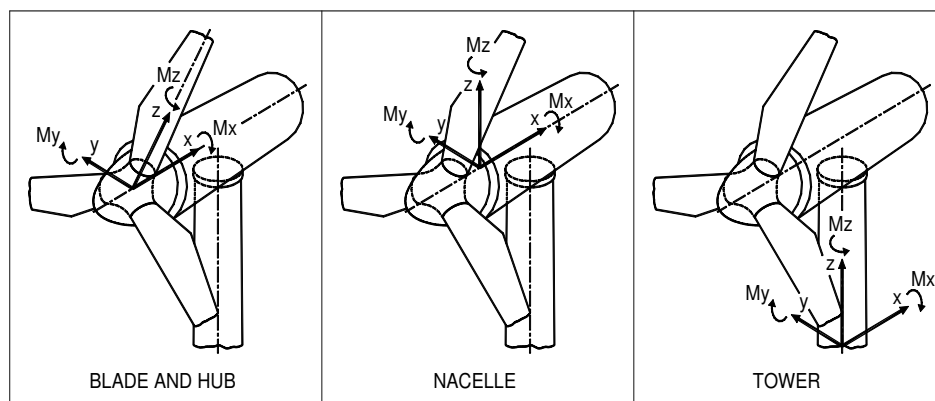

Figure A.1: Definition of co-ordinate systems according to Germanischer Lloyd [70]

The same definition holds for any location in the wind turbine (with a blade pointing upwards).

A.2   Load components

Wind turbine loading is characterised by fatigue damage equivalent bending moment ranges at important location in the structure, such as the blade root and the tower base. The convention for load component names is in line with the GL coordinate system (see figure A.1). Because equivalent loads are used, it is necessary to assign an S-N curve exponent m to each load, which corresponds to the material that is normally used (see table A.1).

Table A.1: Names of relevant load components and description; default material and corresponding slope of the S-N curve m.

load	load (sensor) description	material	slope
Mx1r	blade root edgewise moment (rotating with blade)	composite	12
My1r	blade root flapwise moment (rotating with blade)		
Mx1h	hub edgewise moment (fixed, not rotating with blade)	cast iron	6
My1h	hub flapwise moment (fixed, not rotating with blade)		
MxNr	main bearing driving moment	cast iron	6
MyNf	main bearing tilt moment		
MzNf	main bearing yaw moment		
Mxt0	tower base side-side moment	weld	4
Myt0	tower base fore-aft moment		
Mxf-10	foundation side-side moment 10 m below SWL	weld	4
Myf-10	foundation fore-aft moment 10 m below SWL		

A.3   Acronyms

BEM	blade element-momentum method
CA	constant amplitude
CFD	computation fluid dynamics
DNV	Det Norske Veritas
ECMWF	European Centre for Medium-Range Weather Forecsts
FEM	finite element method
FORM	first order reliability method
GL	Germanischer Lloyd
HIRLAM	HIgh Resolution Limited Area Model
IEC	International Electrotchnical Commission
JONSWAP	JOint North Sea WAve Project
LIDAR	LIght Detection And Ranging

MC	Monte Carlo
MCP	Measure-Correlate-Predict
MD	Multibody Dynamics
NBCC	National Building Code of Canada
NCAR	National Center for Atmospheric Research
NCEP	National Centers for Environmental Prediction
PM	Palmgren-Miner
PM	Pierson-Moskowitz
PRVS	pitch regulated variable speed
rpm	revolutions per minute
SAR	Synthetic Aperture Radar
SODAR	Sound Detection and Ranging
SRF	stress reserve factor
SWL	still water level
VA	variable amplitude
WAsP	Wind Atlas Analysis and Application Program
WT	wind turbine

A.4   Symbols

Note: some parameters are general, and may have different units dependent on where they are used; for example loads may be forces or moments. In such cases the unit is given as [*].

Latin symbols

A	rotor swept area [m^2]
A	(highly stressed) area [m^2]
A	constant in Charnock's formula [-]
A	geometry matrix [*]
A	Weibull scale factor [m/s]
A_0	reference surface [m^2]
a	constant [*]
B	benefits over a turbine's life [€]
b	yearly benefits [€/year]
b	constant [*]
C	Weibull scale factor [*]
C_D	hydrodynamic drag coefficient [-]
C_F	failure cost [€]
C_I	investment cost [€]
C_M	hydrodynamic inertia coefficient [-]
C_P	power coefficient [-]

C_R replacement (repair) cost [€]

c constant in IEC turbulence formula [m/s]

c constant for fatigue strength mean stress correction [-]

c investment cost [€/kW]

c_m specific investment cost [€/kg]

c_{tf} factor for laod conservatism in tower and foundation [-]

Coh root coherence function [-]

D diameter [m]

d water depth [m]

d' water depth corrected for tidal influence [m]

d_i partial fatigue damage [-]

E energy yield [kWh]

E von Kármán energy spectrum [-]

e capacity factor (mean power divided by rated power) [-]

F force [N]

F load [*]

F cumulative probability distribution [-]

ΔF_{eq} fatigue damage equivalent load range [*]

f force [N/m]

f fraction of investment [-]

f frequency [Hz, 1/day]

f probability density [-]

f_0 resonance frequency [Hz]

f_F failure cost fraction [-]

f_p spectrum peak frequency [Hz]

f_R replacement cost fraction [-]

g acceleration of gravity = 9.81 m/s^2

H wind turbine hub height [m]

H_{m0} significant wave height [m]

H_s significant wave height [m]

h height [m]

I turbulence intensity [-]

I_{eff} effective turbulence intensity [-]

I_{ref} IEC reference turbulence intensity (mean value at 15 m/s) [-]

J_1 Bessel function [-]

Kc Keulegan-Carpenter number [-]

k wave number [1/m, -]

k Weibull shape factor [-]

L Monin-Obukhov length [m]

L turbine life [year]

L_c turbulence length scale for coherence function [m]

L_k turbulence length scale [m]

M	fatigue strength mean stress sensitivity [-]
M	moment [Nm]
M	location parameter in lognormal distribution
M_N	location parameter in fatigue life distribution [-]
m	component mass [kg]
m	median of Weibull distribution [m/s]
m	slope of S-N curve (Wöhler curve) [-]
m_{ij}	element of Markov matrix (transition probability) [-]
N	cumulative normal distribution function [-]
N	number of cycles [-]
N	number of critical spots [-]
N	number of neighbouring wind turbines [-]
N	number of (numerical) experiments [-]
N	number of time steps [-]
N_D	number of cycles at knee point in S-N curve [-]
N_{eq}	number of cycles for which the equivalent load is calculated [-]
N_F	number of failures [-]
N_{di}	number of deaths in activity i [-]
N_p	number of persons (population) [-]
N_{pi}	number of persons involved in activity i [-]
N_S	number of meteorological stations [-]
n	stochastic variable with normal distribution [-]
n_i	number of load cycles of range i [-]
P	power [W]
P_{fi}	probability of an accident in activity i [-]
p	pressure [Pa]
p	probability [-]
p_d	probability of fatal injury (death) [-]
p_E	endurance probability [-]
p_F	failure probability [-]
p_w	fixed probability for wake effect calculation [-]
q_0	stress factor (reduction for load sequence effects) [-]
R	covariance (matrix) [-]
R	ratio predicted wind speed / actual wind speed [-]
R	resistance [*]
R	stress ratio (minimum stress divided by maximum stress) [-]
Re	Reynolds number [-]
R_i	factor in resistance product function [-]
r	correlation coefficient [-]
r	discount (interest) rate [-]
r	distance [m]
S	covariance matrix [*]

S	inflow angle ('terrain slope') [rad, deg]	
S	power spectral density [*]	
S	load [*]	
S	scale parameter in lognormal distribution [*]	
S_i	factor in load product function [-]	
S_N	scale parameter in fatigue life distribution [-]	
s	turbulent speed fraction [-]	
s_i	distance between turbines divided by rotor diameter [-]	
SRF	stress reserve factor [-]	
T	absolute temperature [K]	
T	main shaft tilt angle [rad, deg]	
T	time constant [day]	
T	time period [s]	
T	wave period [s]	
T_D	scatter parameter for fatigue damage sustained $(= D_{10\%}/D_{90\%})$	
T_N	scatter number for fatigue life [-]	
T_p	spectrum peak period [s]	
T_z	spectrum zero crossing period [s]	
T_σ	scatter number for fatigue strength $(= \Delta\sigma_{10\%}/\Delta\sigma_{90\%})$	
ΔT	time step [s]	
t	time [s]	
U	wind speed [m/s]	
u	turbulent wind speed (in wind direction) [m/s]	
u	standard normally distributed variable [-]	
$u*$	friction velocity [m/s]	
UTL	ultimate tensile load [N, Nm]	
UTS	ultimate tensile strength [Pa]	
V	coefficient of variation [-]	
V	(highly stressed) volume [m^2]	
v	turbulent wind speed (in horizontal direction) [m/s]	
v	standard normally distributed variable [-]	
W	cost function [€]	
W	section modulus [m^3]	
W	wind direction [rad, deg]	
w	normalised cost function [-]	
w	turbulent wind speed (in vertical direction) [m/s]	
x	stochastic variable [*]	
$\underline{x}^*$	design point (vector) in FORM [*]	
$\underline{x}_{char}$	characteristic parameter vector [*]	
$x_{\Delta\sigma_A}$	fatigue strength stochastic variable [-]	
Y	yaw angle [rad, deg]	
Y_1	Bessel function [-]	

Z	limit state function [*]
z	height [m]
z_0	terrain roughness [m]
z_r	reference height [m]

Greek symbols

α	angle [rad, deg]
α	constant in formula for Jonswap spectrum [-]
α	exponent for wind shear power law [-]
α	influence factor [-]
α	phase lag [rad]
β	reliability index [-]
β	policy factor [-]
Γ	Mann's shear parameter [-]
Γ	gamma function [-]
γ	Jonswap spectrum peak parameter [-]
γ	product of all partial (safety) factors [-]
γ_0	standard product of partial (safety) factors [-]
γ_f	load factor [-]
γ_m	material factor [-]
γ_n	consequence-of-failure factor [-]
ϵ	error [*]
η	water surface elevation [m]
κ	von Kármán's constant ($\simeq 0.4$) [-]
Λ	IEC length scale [m]
μ	distribution mean [*]
ν	kinematic viscosity [m^2/s]
ρ	correlation coefficient [-]
ρ	density [kg/m^3]
σ	stress [Pa]
σ	distribution standard deviation [*])
σ_U	turbulence (standard deviation on wind speed) [m/s]
$\Delta\sigma$	stress range [Pa]
$\Delta\sigma_A$	fatigue strength (at knee point in S-N curve) [Pa]
Φ	spectral tensor [-]
ϕ	random phase angle [rad, deg]
Ψ	stability function [-]
ψ	rotation angle [rad, deg]

Subscripts

10	at 10 m height
10%	10% fractile
$1year$	one year average, one year period
$3h$	three hour average
50%	50% fractile (median)
70	at 70 m height
90%	90% fractile
a	ambient
avg	average
c	(IEC) class
$char$	characteristic
D	fatigue damage
D	knee point in S-N curve
d	design
d	death (fatal injury)
dim	dimension
eff	effective
eq	equivalent
F	failure
$FORM$	First Order Reliability Method
f	foundation
I	investment
in	cut in (start)
inv	inverse
J	JONSWAP
k	speed component number, k=1 (u), 2 (v), 3 (w)
L	life
lcf	low cycle fatigue
M	Mann
MC	Monte Carlo
max	maximum
min	minimum
msr	measured
m	mass
m	mean
N	cycles, life
out	cut out (stop)
PM	Pierson-Moskowitz
P	prediction
p	peak

$pred$	predicted
R	repair, replacement of component
r	reference
rat	rated
ref	reference
rel	relative
rms	root mean square
S	station
s	significant
s	site
$seed$	seed for wind field generation
std	standard
t	tower
U	wind speed
u	in wind direction (turbulence)
v	horizontal, perpendicular to wind direction (turbulence)
w	wake
w	vertical (turbulence)
wf	wind farm
wdd	wind direction distribution
x	exact
z	zero crossing
σ	stress
σ	turbulence

Appendix B

Wind turbine data

B.1 Wind turbine

In many calculations the NM92/2750-70 wind turbine is used (for a picture see the back cover of the book), which serves as a standard representative machine with the following properties:

Table B.1: Properties of standard turbine NM92/2750-70

Turbine name	NM92-2750-70
Rated power	2750 kW
Rotor diameter	92 m
Rotor position	upwind
Rotor tilt	5 deg
Number of blades	3
Hub height	70 m
Control	Pitch regulated variable speed
Generator speed	800–1200 rpm
Start wind speed	3 m/s
Rated wind speed	15 m/s
Stop wind speed	25 m/s

B.2 Wind turbine component cost

Below some data on relative cost of components are given. Table B.3 has a summary of the data that may be used for comparison. Numbers for blades and hub show reasonable agreement, but this is not so for the nacelle and the tower. For the nacelle this must be due to differing definitions of what to include (for the present work we are only concerned with the front part machine frame); for the tower there are

probably differences in height. For completeness full data as found in the references are given in additional tables:

Table B.2: Properties of main components NM92/2750-70. Total estimated turbine price: $1100 \times 2750 = $ k€ 3025.

Component	Blade (1)	Hub	Nacelle	Tower
Material	composite	cast iron	cast iron	welded steel
Mass [kg]	10,000	25,000	10,000	100,000
Price [€/kg] (Hau [85])	12	2	2	1.3
Price [€]	120,000	50,000	20,000	130,000
Relative price [%]	4	2	1	4
Standard safety factor γ_0 [-]	1.50	1.38	1.38	1.27
Derivative $1/m \; \partial m/\partial \gamma$ [-]	0.5	0.1–0.2	0.1–0.2	0.7

Table B.3: Wind turbine component relative cost summary (onshore) [%].

Source	table	Blades (3)	Hub	Nacelle[1]	Tower
Fuglsang [67]	B.4	18	3	11	18
Hau [85]	B.5	28	2	5[2]	21
Herman[3] [86, 87]	B.6	12	6	36	24
This work	B.3	12	2	1	4

[1]Definition of what is included in 'nacelle' is not clear.

[2]Machine frame only.

[3]Estimated from table B.6

Table B.4: Wind turbine component relative cost [%] for 1.5 MW passive stall turbine. Source: Fuglsang [67]

Component	Cost onshore	Cost offshore
Blades	18.3	12.9
Tower	17.5	12.4
Gearbox	12.5	8.8
Nacelle	10.8	7.6
Grid connection	8.3	17.6
Generator	7.5	5.3
Main shaft	4.2	2.9
Yaw system	4.2	2.9
Controller	4.2	2.9
Foundation	4.2	17.6
Hub	2.5	1.8
Assembly	2.1	2.9
Transport	2.0	2.9
Brake system	1.7	1.2
TOTAL	100.0	100.0

- Table B.4 is based on a recent book by Hau [85, 2005]; figures for the 1.5 MW machine are most relevant to our calculations.

- Table B.5 is based on the work of Fuglsang [67], and figures are for a 1.5 MW passive stall turbine. This means that the cost of the controller (pitch system) and the electrical system (generator/converter) probably represent larger fractions of the total in current wind turbines. This makes the other components accounting for a smaller share. From the cost of the blades it can be inferred that the offshore version of the turbine considered is 18.3/12.9 ≈ 1.4 times more expensive than the land turbine.

- Table B.6 has some data from the DOWEC project (Herman [86, 87]). Figures given are for a modern offshore wind farm.

Table B.5: Wind turbine component relative cost [%] for 750 kW stall turbine and 1.5 MW variable speed turbine (onshore). Source: Hau [85].

Component	750 kW stall	1500 kW var. speed
Blades	34.0	21.0
Blade bearings	-.-	3.1
Pitch system	0.8	4.0
Tower	16.4	20.7
Gearbox	12.5	13.6
Nacelle	10.7	6.3
Generator and converter	7.5	10.9
Main shaft (incl. bearings)	3.7	4.3
Yaw system	2.4	3.4
Controller	5.0	7.4
Hub	2.0	2.1
Brake system etc	5.0	3.2
TOTAL	100.0	100.0
Assembly	5.0	5.0

Table B.6: Relative cost [%] for a 500 MW offshore wind farm. Source: DOWEC (Herman)
[86, 87]

Component	Cost share of subassembly	Cost share of total
Hardware incl. transport onshore	53	53
Operation and maintenance	27	27
Assembly, transport and installation	11	11
Retrofit and overhaul	7	7
Decommissioning	1	1
Windfarm design	1	1
Hardware subdivision		
Support structure	43	23
Nacelle	32	17
Rotor	25	13
Rotor subdivision		
Blades	44	6
Hub	23	4
Pitch system	33	3

Appendix C

Fatigue and equivalent load

C.1 Equivalent load

The advantage of the fatigue damage equivalent load concept is that it reduces a long history of random fatigue loads to one number, which makes it very easy to compare different load situations and design modifications. It is derived as follows. If we test some component with a sinusoidal load (say) we will typically find that the number of cycles until rupture (life) varies inversely with the load range: the larger the load range, the shorter the life (see figure C.1, next page). In many cases there is some limit below which the component life is infinite, or at least very long. This is called the fatigue strength ΔF_D (ΔF_D may for example be a force range, or a stress range); if we do an experiment with a load range slightly larger we will get a life of N_D cycles. In double logarithmic representation the Wöhler curve (or S-N curve) will approximately consist of two straight lines that meet in the knee point $(N_D, \Delta F_D)$ where the left part has slope $1/m$ and the right part is horizontal. For every load $\Delta F_i \geq \Delta F_D$ the number of cycles until failure is smaller than N_D and it is found with the relation describing the curve:

$$N_i \Delta F_i^m = N_D \Delta F_D^m \tag{C.1}$$

or:

$$N_i = N_D \left(\frac{\Delta F_D}{\Delta F_i} \right)^m \tag{C.2}$$

Miner's hypothesis is that if some load occurs n_i times rather than the allowed number N_i, a fraction $d_i = n_i/N_i$ of the component's life has been used. The fraction d_i is called partial damage; if the sum of all partial damage $\sum d_i = 1$ the component fails. With this hypothesis we may find the total damage D of all loads combined:

$$D = \sum_{i=1}^{n} d_i = \sum_{i=1}^{n} \frac{n_i}{N_i} = \sum_{i=1}^{n} \frac{n_i}{N_D} \left(\frac{\Delta F_i}{\Delta F_D} \right)^m \tag{C.3}$$
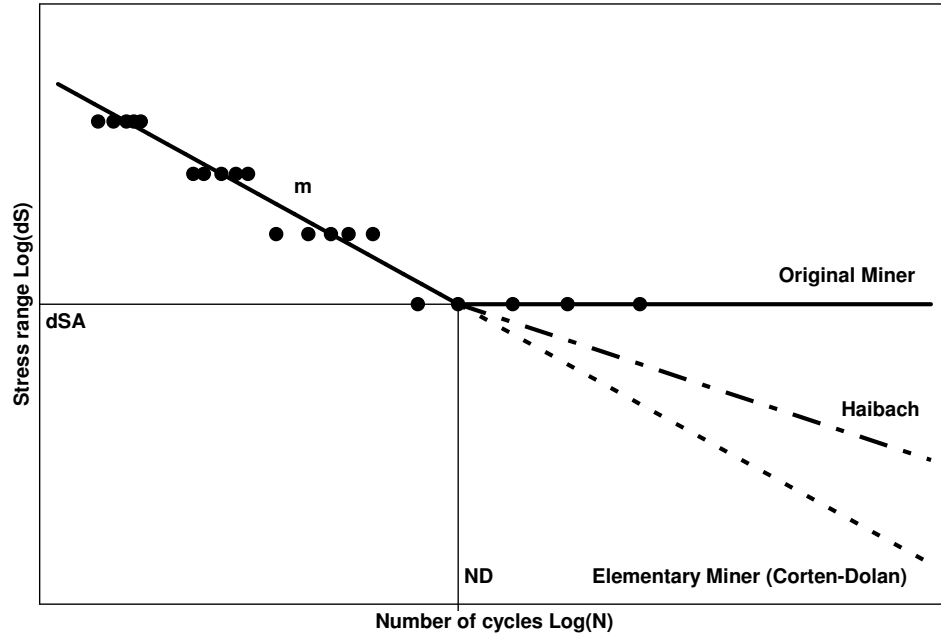
Figure C.1: Wöhler curves (S-N curve)

The fatigue damage equivalent load, is the load that for some arbitrarily chosen number of cycles N_{eq} would produce the same damage as all actual loads combined, so:

$$\frac{N_{eq}}{N_D}\left(\frac{\Delta F_{eq}}{\Delta F_D}\right)^m = \sum_{i=1}^{n}\frac{n_i}{N_D}\left(\frac{\Delta F_i}{\Delta F_D}\right)^m \tag{C.4}$$

Which works out to:

$$\Delta F_{eq} = N_{eq}^{1/m}\left(\sum_{i=1}^{n}n_i\Delta F_i^m\right)^{1/m} \tag{C.5}$$

Common values for N_{eq} are $N_{eq} = 5\times10^6$, $N_{eq} = 10^7$ or $N_{eq} = L$, where L is the component's life in [s], which assumes that the equivalent load has 1 Hz frequency (this makes it possible to compare load situations of different duration). If we extend the line with slope m to the right of the knee we may incorporate all load cycles in the equivalent load. Basically this is not correct, however no great additional error is introduced. Firstly both design loads and site loads are treated in this way, which makes it likely that any error in the whole procedure will be cancelled in a comparison; secondly Eulitz [61] shows that the correctness of damage prediction

depends only very weakly on how small cycles are treated; all proposals to do this are just as good (or bad).

The equivalent load assumption also makes it possible to estimate the relative damage distribution. Using 1 Hz equivalent load ranges, the relative of damage created by some load case i occurring is:

$$d_{rel,i} = \frac{d_i}{D} = \frac{L_i \, \Delta F_{eq,i}^m}{L \, \Delta F_{eq}^m} \tag{C.6}$$

Where L_i is determined by the wind speed distribution. With these considerations it is easily shown that fatigue damage created by loads with wind speed $U < 10$ m/s and $U > 25$ m/s may normally be neglected (see table 4.13, p68).

C.2   Mean stress correction

Composites.   Especially for composites (blade materials), the mean load level has large influence on the fatigue strength, and a modified definition of the equivalent load is necessary. For convenience we assume the following (see figure C.2, next page):

- The relation life-fatigue strength is the usual one: $N\sigma^m = C$.

- Stress and strain are always proportionally related.

- The fatigue strength decreases linearly from the maximum value for zero mean stress to zero if the mean stress equals the ultimate tensile strength (UTS).

- The Goodman diagram is symmetric around mean stress zero, in particular the ultimate compressive strength (UCS) equals the ultimate tensile strength (UTS).

While being appealing for their simplicity, these assumption are in fact not true; nevertheless they may be allowed because the purpose of the equivalent load is to compare different situations rather than to make lifetime predictions. In a comparison errors will tend to cancel each other. To give this statement some mathematical background, consider the derivative of the exact equivalent load: $\partial \Delta F / \partial x$ is :

$$\frac{\partial \Delta F}{\partial x} \approx \frac{\Delta F(x_2) - \Delta F(x_1)}{x_2 - x_1} = \frac{\Delta F_2 - \Delta F_1}{x_2 - x_1} \tag{C.7}$$

while the approximation $\partial \Delta F' / \partial x$ is:

$$\frac{\partial \Delta F'}{\partial x} \approx \frac{\Delta F_2' - \Delta F_1'}{x_2 - x_1} = \frac{(\Delta F_2 + \varepsilon_2) - (\Delta F_1 + \varepsilon_1)}{x_2 - x_1} \tag{C.8}$$

Because of the similarity of load spectra we have for the errors ε:

$$\varepsilon_1 \approx \varepsilon_2 \tag{C.9}$$

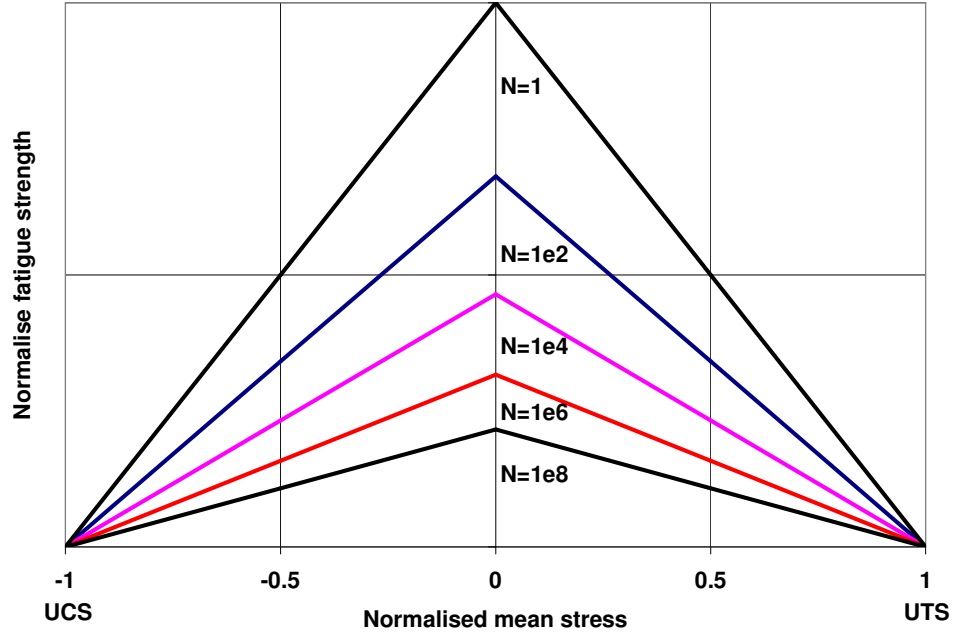**Figure C.2:** Goodman diagram (idealised)

and:

$$\frac{\partial \Delta F'}{\partial x} \approx \frac{\partial \Delta F}{\partial x} \tag{C.10}$$

If we set the mean stress $\sigma_m = 0$, then we get (note that we are using amplitudes $\sigma = \Delta\sigma/2$ rather than ranges $\Delta\sigma$):

$$N_i \sigma_i^m = N_D \sigma_D^m \tag{C.11}$$

or:

$$N_i = N_D \left(\frac{\sigma_D}{\sigma_i}\right)^m \tag{C.12}$$

However to find correct life N_i for stress amplitude σ_i the fatigue strength $\sigma_D(\sigma_m = 0)$ must be modified for the influence of non zero mean stress σ_m. The simplest modification is:

$$\sigma_D(\sigma_m) = \sigma_D(0) \left(1 - \frac{|\sigma_m|}{UTS}\right) \tag{C.13}$$

which gives:

$$N_i = N_D \left(\frac{\sigma_D(0)}{\sigma_i} \left(1 - \frac{|\sigma_m|}{UTS} \right) \right)^m \tag{C.14}$$

Then the damage D is:

$$D = \sum_{i=1}^n d_i = \sum_{i=1}^n \frac{n_i}{N_i} = \sum_{i=1}^n \frac{n_i}{N_D} \left(\frac{\sigma_i}{\sigma_D(0) \left(1 - \frac{|\sigma_m|}{UTS} \right)} \right)^m \tag{C.15}$$

We require the same damage D if the equivalent stress $\sigma_{eq}(0)$ is applied N_{eq} times:

$$D = \frac{N_{eq}}{N_D} \left(\frac{\sigma_{eq}(0)}{\sigma_D(0)} \right)^m = \sum_{i=1}^n \frac{n_i}{N_D} \left(\frac{\sigma_i}{\sigma_D(0) \left(1 - \frac{|\sigma_m|}{UTS} \right)} \right)^m \tag{C.16}$$

which finally yields:

$$N_{eq}\sigma_{eq}^m(0) = \sum_{i=1}^n n_i \left(\frac{\sigma_i}{\left(1 - \frac{|\sigma_m|}{UTS} \right)} \right)^m \tag{C.17}$$

Note that equation (C.17) is equivalent to equation (C.5) if $\sigma_m = 0$ (or $UTS = \infty$). It is easiest to use it if the actual stress combinations (σ_i, σ_{mi}) and UTS are known. However in many cases these will not be known, and apart from that we would like to apply the concept to loads rather than stresses. Therefore we must set a reasonable value for the ultimate tensile load (UTL). Clearly to avoid 'immediate collapse' in case the extreme load occurs we must have:

$$UTL \geq SRF \, \gamma_f \, \gamma_m \max(F_i + F_{mi}) \tag{C.18}$$

For ultimate load calculations, it is common practice to have $SRF \; \gamma_f \gamma_m \; \geq \; 1.5$. Usually ultimate design load situations are defined as to produce higher loads than found from the fatigue calculations. Therefore it seems reasonable to calculate the equivalent load ranges for blades with safety margins $SRF \; \gamma_f \gamma_m = 1.5 \ldots 2$. The sensitivity of the calculations to the choice of $SRF \; \gamma_f \, \gamma_m$ will be investigated.

Metals. For metallic materials the situation is similar. However a different mean stress correction is used[1]. The dependence of the fatigue strength (amplitude) σ_A on mean stress σ_m is approximated by:

$$\sigma_A(\sigma_m) = \sigma_A(0) - M\sigma_m \tag{C.19}$$

---

[1]If weld details are not stress relieved, usually no mean stress correction is applied.

The number M is called the mean stress sensitivity. The expression is easily converted to stress ranges:

$$\Delta\sigma_A(\sigma_m) = \Delta\sigma_A(0) - 2M\sigma_m \tag{C.20}$$

If fatigue tests are available for stress ratios $R = -1$ and $R = 0$, then the value of the mean stress sensitivity is found with:

$$M = \frac{\Delta\sigma_A(\sigma_m = 0)}{\Delta\sigma_A(\sigma_m = \Delta\sigma_A/2)} - 1 = \frac{\Delta\sigma_A(R = -1)}{\Delta\sigma_A(R = 0)} - 1 \tag{C.21}$$

The fatigue damage d_i caused by n_i load cycles of range $\Delta\sigma_i$ and mean stress σ_{mi} is:

$$d_i = \frac{n_i}{N_D}\left(\frac{\Delta\sigma}{\Delta\sigma_A(0) - 2M\sigma_{mi}}\right)^m \tag{C.22}$$

We may determine the effective (fatigue damage equivalent) stress range that would have given the same fatigue damage:

$$\Delta\sigma_{i,eff} = \frac{\Delta\sigma_i}{1 - \frac{2M\sigma_{mi}}{\Delta\sigma_A(0)}} \tag{C.23}$$

If $2M\sigma_{mi}/\Delta\sigma_A(0) \ll 1$ then:

$$\Delta\sigma_{i,eff} \approx \Delta\sigma_i + 2M\sigma_{mi}\frac{\Delta\sigma_i}{\Delta\sigma_A(0)} \tag{C.24}$$

If furthermore $\Delta\sigma_i \simeq \Delta\sigma_A(0)$ then:

$$\Delta\sigma_{i,eff} \approx \Delta\sigma_i + 2M\sigma_{mi} \tag{C.25}$$

This is the equation used by Eulitz [60, 61]. Clearly it is not equivalent to equation (C.23), but the advantage is that we do not need to know the fatigue strength $\Delta\sigma_A$. Finally:

$$N_{eq}\Delta\sigma_{eff}^m = \sum_{i=1}^{n} n_i\left(\Delta\sigma_i + 2M\sigma_{mi}\right)^m \tag{C.26}$$

This means for example that for steel S355 the mean stress correction factor is (R_m = 500 MPa): $M = 0.075$, and for cast iron GGG40.3 (R_m = 400 MPa): $M = 0.19$. In fact the mean stress corrections are somewhat more complex, with modification of M for other stress ratios, but this sophistication is unwarranted for present use.

Note that the Goodman diagram is not symmetrical around zero mean stress: for metallic materials compressive stresses are favourable, and completely negative load cycles produce zero fatigue damage.

C.3   Fatigue limit

An objection against the equivalent loads presented so far may be that the existence of a fatigue limit is not taken into account, which may give a significant difference for metals. To do this, the calculation of the equivalent load is simply modified to reject any load cycle below the fatigue strength. The only problem is how to determine the fatigue strength in terms of loads. A practical solution is the following. Assume that in the reference situation a component is just designed to the limit, which means it can withstand a load ΔF if it is applied N_D times (the number of cycles corresponding to the knee in the Wöhler curve):

$$\Delta F = SRF \, \gamma_f \, \gamma_m \, \Delta F_D \tag{C.27}$$

If we set the equivalent number of load cycles $N_{eq} = N_D$, then the $\Delta F_D = \Delta F_{eq}$ and the fatigue limit is just $\Delta F = SRF \, \gamma_f \, \gamma_m \, \Delta F_{eq}$. We cannot neglect all load cycles smaller than this because cycles below the fatigue limit can still enlarge an existing crack, but a reasonable cut off limit is (for example used in Eurocode 3):

$$\Delta F_{CO} = 0.5 \, SRF \, \gamma_f \, \gamma_m \, \Delta F_{eq} \tag{C.28}$$

Finally it must be remarked that the argument presented here is somewhat circular because basically in establishing the cut off value the fact that some cycles cause no fatigue damage should be taken into account, while to do this the cut off value must be known. Of course the problem could be solved iteratively, but in the light of the inaccuracy of the whole concept of equivalent load this is not necessary.

C.4   Equivalent turbulence

In this section it is shown that the equivalent turbulence approach yields good, slightly conservative estimates of the equivalent fatigue load, and that the IEC 61400-1 recommendation to use the 90% fractile turbulence is (perhaps) a little overconservative. We start by looking at the moments of a lognormal distribution around zero.

Table C.1: Fatigue strength mean stress sensitivity M (R_m is the tensile strength in [MPa]).

material	treatment	sensitivity	source
steel	smooth	$M = 0.00035 \, R_m - 0.1$	Gudehus [74]
cast iron	smooth	$M = 0.00035 \, R_m + 0.05$	Gudehus [74]
cast iron	as cast	$M = 0.28$	Kaufmann [104], table 7.6
weld seams	as welded	$M = 0$ (no sensitivity)	Hobbacher [90]
weld seams	stress relieved	$M = 0.33$	Hobbacher [90]
weld seams	stress relieved	$M = 0.40$	Köttgen [112], table 7.8

Let the parameter x be lognormally distributed according to:

$$f(x) = \frac{1}{S\sqrt{2\pi}\,x} \exp\left(-\frac{(\ln x - M)^2}{2S^2}\right) \tag{C.29}$$

Then the mean and standard deviation of the distribution are:

$$\mu_x = \exp(M + \frac{1}{2}S^2) \tag{C.30}$$

$$\sigma_x = \mu_x\sqrt{\exp(S^2) - 1} \tag{C.31}$$

In general the mth moment around zero is given by:

$$\int_0^\infty x^m f(x)dx = \exp\left(mM + \frac{1}{2}m^2 S^2\right) \tag{C.32}$$

This can be proved with the substitution $\ln x = y$ (and $x = e^y$):

$$\int_0^\infty \frac{x^m}{S\sqrt{2\pi}\,x} \exp\left(-\frac{(\ln x - M)^2}{2S^2}\right) dx =$$

$$\int_{-\infty}^\infty \frac{e^{my}}{S\sqrt{2\pi}\,e^y} \exp\left(-\frac{(y - M)^2}{2S^2}\right) de^y =$$

$$\int_{-\infty}^\infty \frac{e^{my}}{S\sqrt{2\pi}} \exp\left(-\frac{(y - M)^2}{2S^2}\right) dy =$$

$$\int_{-\infty}^\infty \frac{1}{S\sqrt{2\pi}} \exp\left(-\frac{y^2 - (2M + 2mS^2)y + M^2}{2S^2}\right) dy =$$

$$\int_{-\infty}^\infty \frac{1}{S\sqrt{2\pi}} \exp\left(-\frac{(y - (M + mS^2))^2}{2S^2} + \frac{2mMS^2 + m^2 S^4}{2S^2}\right) dy =$$

$$\exp(mM + \frac{1}{2}m^2 S^2) \int_{-\infty}^\infty \frac{1}{S\sqrt{2\pi}} \exp\left(-\frac{(y - (M + mS^2))^2}{2S^2}\right) dy =$$

$$\exp(mM + \frac{1}{2}m^2 S^2) \tag{C.33}$$

It is seen that the equation for the mean μ_x (C.30) is a special case ($m = 1$) of the general formula (C.33). If the turbulence σ is likewise lognormally distributed, then the equivalent turbulence σ_{eq} is:

$$\sigma_{eq} = \left[\int_0^\infty \sigma^m d\sigma \right]^{1/m} = \exp\left(M + \frac{1}{2} m S^2 \right) \tag{C.34}$$

Most equivalent load ranges may be expressed in good approximation as:

$$\Delta F = a\sigma + b \tag{C.35}$$

Then the equivalent load range is:

$$\Delta F_{eq} = \left[\int_0^\infty f(\sigma) \Delta F^m(\sigma) d\sigma \right]^{1/m} = \left[\int_0^\infty f(\sigma)(a\sigma + b)^m d\sigma \right]^{1/m} \tag{C.36}$$

The standard IEC 61400-1 advocates the use of 90% fractile turbulence based on the assumption that the equivalent turbulence approach is valid. We may ask how accurate this is compared to the exact calculation of equation (C.36). The integral for the equivalent load can be solved analytically using equation (C.33):

$$\left[\int_0^\infty f(\sigma)(a\sigma + b)^m d\sigma \right]^{1/m} = \left[\sum_{k=0}^m \binom{m}{k} a^k b^{m-k} \exp(kM + \frac{1}{2} k^2 S^2) \right]^{1/m} \tag{C.37}$$

We may rewrite this as:

$$\Delta F_{eq} = \left[\sum_{k=0}^m \binom{m}{k} \left(a \exp(M + \frac{1}{2} k S^2) \right)^k b^{m-k} \right]^{1/m} \tag{C.38}$$

Because $k \leq m$:

$$\Delta F_{eq} \leq \left[\sum_{k=0}^m \binom{m}{k} \left(a \exp(M + \frac{1}{2} m S^2) \right)^k b^{m-k} \right]^{1/m} \tag{C.39}$$

$$\Delta F_{eq} \leq \left[\left(a \exp(M + \frac{1}{2} m S^2) + b \right)^m \right]^{1/m} \tag{C.40}$$

$$\Delta F_{eq} \leq a \exp(M + \frac{1}{2} m S^2) + b \tag{C.41}$$

$$\Delta F_{eq} \leq a\sigma_{eq} + b \tag{C.42}$$

By this we have proved that the equivalent turbulence approach is conservative. We may further investigate how conservative it is. Clearly the expression is exact for cases where either $a = 0$ or $b = 0$, and a good approximation when S is small.

To check the equations given above, the average turbulence intensity was calculated for the important wind speed interval 10-20 m/s. It turns out that equivalent turbulence intensity according to equation (C.34) is a good approximation of the exact load equivalent turbulence intensity (equation C.38), as can be seen in tables C.2–C.4. The 90% fractile tends to be 0.01–0.02 too conservative; in other words, instead

Table C.2: Comparison of different fatigue load equivalent turbulence intensities for IEC 61400-1 (Class A, $I_{ref} = 0.16$) [93]. Average for $10 < U < 20$ m/s.

Effective turbulence intensity	$m = 4$		$m = 8$		$m = 12$	
90% fractile (IEC)		0.176		0.176		0.176
Equation (C.34)		0.163		0.165		0.166
Exact	Mxt0	0.162	Mx11h	0.163	Mx11r	0.163
	Myt0	0.162	My11h	0.160	My11r	0.165
			MxNf	0.166		
			MyNf	0.165		
			MzNf	0.165		

Table C.3: Comparison of different fatigue load equivalent turbulence intensities for Lammefjord (measured turbulence distribution from DNV [47]). Average for $10 < U < 20$ m/s.

Effective turbulence intensity	$m = 4$		$m = 8$		$m = 12$	
90% fractile (IEC)		0.160		0.160		0.160
Equation (C.34)		0.143		0.147		0.151
Exact	Mxt0	0.137	Mx11h	0.140	Mx11r	0.141
	Myt0	0.142	My11h	0.144	My11r	0.147
			MxNf	0.148		
			MyNf	0.146		
			MzNf	0.145		

Table C.4: Comparison of different fatigue load equivalent turbulence intensities for Vindeby (measured turbulence distribution from Hansen [79]). Average for $10 < U < 20$ m/s.

Effective turbulence intensity	$m = 4$		$m = 8$		$m = 12$	
90% fractile (IEC)		0.099		0.099		0.099
Equation (C.34)		0.088		0.091		0.094
Exact	Mxt0	0.082	Mx11h	0.079	Mx11r	0.080
	Myt0	0.083	My11h	0.086	My11r	0.089
			MxNf	0.087		
			MyNf	0.084		
			MzNf	0.084		

of adding 1.3 times the turbulence intensity standard deviation to the mean turbulence intensity, 0.5 times the standard deviation would be enough (however equation (C.34) is to be preferred).

C.5 Estimation of S-N curve from tests

Because of the method of equivalent loads that is used for all calculations, it is convenient to treat the exponent (or slope) of the S-N curve m as a fixed variable. While it may be true that the slope is fixed, we do not know exactly what the value is. In practice, the S-N curve used for the fatigue damage estimates would be found as follows:

1. The constant amplitude S-N curve is established with tests.

2. The life curve is found with tests using representative variable amplitude load spectra;

3. The Liu-Zenner correction (or something similar) is applied to the original curve;

4. The stress factor q_0 is adjusted to make life predictions based on the Liu-Zenner curve fit experiments;

5. Steps 2–4 may be repeated with different VA load spectra to get the best curve for life predictions.

One might skip step 1, and only use the life curve without any correction for life predictions; but hope is that the approach sketched here has more general validity. However, whichever curve is used, it is necessarily established on the basis of a limited number of experiments.

To get more insight in how accurately we can establish an S-N curve with this procedure (and whether our assumption of treating m as fixed is justified), we do some idealised numerical Monte Carlo experiments. Because we are only interested in the how much the slope m varies if it is derived from experiments, we may bypass all things that make it difficult to find representative S-N curves: we simply assume that there is some underlying S-N curve of the usual shape, and that test results scatter around it. Random test data are generated and the S-N curve derived, as would be done if real experimental data were available. If one scans the literature, it appears that some reasonable assumptions about typical fatigue experiments for finding the curve are:

- The real material fatigue behaviour can be described with a one slope power law curve $N\sigma^m = c$.

- The experimental lives of individual speciments scatter around the median according to a lognormal distribution, and the scatter number T_N is constant along the curve.

- The fatigue strength amplitude is one third of the yield strength (for convenience we set the real median fatigue strength $\sigma_A = 1$) at some fixed number of cycles N_D (since we are interested in uncertainty in the estimate of m it is immaterial here what value N_D has).

- Three times 10 'experiments' are done at stress levels $\sigma = 2$, 1.5 and 1.0 times the fatigue strength. Other set ups are possible, and one may discuss how many test at which levels should be done –for example tests at intermediate levels do not yield much information: to fix a slope it is better to test 'at the ends' of the line– but some experimentation shows that in essence Monte Carlo results do not change much under different strategies; most important is the total number of experiments.

With the Monte Carlo method 1000 pseudo-experimental sets of results are generated. At each stress level the maximum likelihood median is determined, and through the 3 points a least squares line is drawn (this works better than a least squares fit through all points, which tends to yield curves that are too flat). This gives us estimates of the exponent $\widehat{m}$ and the constant $\widehat{c}$. Hence the estimate of the curve is given by:

$$N\sigma^{\widehat{m}} = \widehat{c} \tag{C.43}$$

And the estimated fatigue strength $\widehat{\sigma}_A$:

$$\widehat{\sigma}_A = \left(\frac{\widehat{c}}{N_D} \right)^{1/\widehat{m}} \tag{C.44}$$

Note that it is not necessary to estimate the number of cycles N_D; because we assumed a one slope curve, it is fully determined by the slope m and the fatigue strength σ_A at N_D cycles.

Results are given in table C.5. It turns out that all estimates are normally distributed. The slope $\widehat{m}$ and the fatigue strength $\widehat{\sigma}_A$ at N_D are correlated with $r^2 = 0.6$ i.e. larger slope corresponds to larger fatigue strength. This is just a matter of geometry: if the fatigue strength had been defined at stress level 1.5 (the midpoint of the line), correlation would have been close to zero.

Table C.5: Estimates of parameters defining the S-N curve (1000 simulations): slope m and fatigue strength σ_A.

material	table	inputs			estimates (mean and std deviation)			
		slope	scatter		slope		fatigue strength	
		m	T_N	T_σ	$\widehat{\mu}_m$	$\widehat{\sigma}_m$	$\widehat{\mu}_{\sigma_A}$	$\widehat{\sigma}_{\sigma_A}$
composite	7.12	9.00	8.40	1.27	9.02	0.52	1.00	0.027
composite	-	12.00	10.00	1.21	12.01	0.56	1.00	0.022
cast iron	7.6	6.33	3.45	1.21	6.34	0.30	1.00	0.023
weld seam	7.8	3.50	3.63	1.41	3.52	0.32	1.00	0.043

It is seen that the coefficient of variation on slope $V_m = \sigma_m/\mu_m \sim 5$–$10\%$. Fortunately the standard deviation on fatigue strength σ_{σ_A} is only a few percent, which is much smaller than standard deviation on individual test results.

Appendix D

Wind data

Table D.1: Variation in yearly average wind speed and Weibull shape factor for some stations in the Netherlands. Coefficients of variation are calculated for 1 year average values; $r(U,k)$ is the correlation coefficient for wind speed U_{10} and shape factor k_{10}. Source: KNMI.

Station	period [year]	U_{10} [m/s]	U_{80} [m/s]	$V_{U_{10}}$ [-]	k_{10} [-]	$V_{k_{10}}$ [-]	$r(U,k)$ [-]
s225 IJmuiden	46	6.5	8.8	0.071	2.1	0.059	0.33
s229 Texelhors	19	7.2	9.8	0.058	2.2	0.087	0.50
s235 Den Helder	29	6.1	8.3	0.045	2.0	0.062	0.24
s240 Schiphol	52	5.4	7.3	0.059	1.9	0.058	-0.04
s242 Vlieland	7	7.2	9.8	0.047	2.1	0.055	0.64
s250 Terschelling	26	6.9	9.4	0.049	2.1	0.076	0.35
s252 K13	14	7.8	9.7	0.082	2.3	0.058	0.29
s254 Noordwijk	12	7.5	9.4	0.037	2.1	0.051	0.46
s270 Leeuwarden	41	5.3	7.1	0.054	1.9	0.079	0.49
s310 Vlissingen	42	5.5	7.5	0.050	2.0	0.047	-0.06
s321 Europlatform	15	7.8	9.8	0.062	2.2	0.054	0.47
s330 Hoek van Holland	41	6.5	8.8	0.106	2.1	0.098	0.77
s343 Geul	18	6.0	8.1	0.082	2.2	0.042	0.09
s348 Cabauw	16	4.7	6.4	0.048	1.8	0.066	0.38
s350 Gilze-Rijen	42	4.5	6.0	0.073	1.9	0.079	0.39
Average	28	6.3	8.4	0.062	2.1	0.065	0.35

Table D.2: Variation in yearly average wind speed at 10 m height for some stations in Denmark. Source: Energi og Miljødata.

region	period	average speed [m/s]	std deviation [m/s]	COV [-]
North Jutland	1989–2001	5.1	0.25	0.050
West Jutland	1989–2001	5.6	0.28	0.049
Bornholm	1989–2001	5.1	0.24	0.047
Fyn	1989–2001	4.4	0.19	0.044
Average (1 year)		5.0	0.24	0.047

Table D.3: Variation in yearly average wind speed and Weibull shape factor at 10 m height for some stations in Germany. Source: Deutsche Wetterdienst.

station	period	U_{10} [m/s]	σ_U [m/s]	V_U [-]	k [-]	σ_k [-]	V_k [-]
Sylt	1960–99	7.2	0.32	0.044	2.6	0.25	0.097
Schleswig	1960–99	4.3	0.25	0.057	1.9	0.08	0.042
Hamburg	1960–99	4.3	0.33	0.064	1.9	0.12	0.064
Helgoland	1960–99	7.4	0.61	0.082	2.1	0.19	0.088
Average (1 year)				0.065			0.073

Table D.4: Variation in yearly wind energy index for some countries. Source: Pryor *et al.* [169].

Country	NCEP/NCAR 1960-89			ECMWF 1990–2001		
%	Mean	StDev	COV	Mean	StDev	COV
Denmark	88	9	0.10	88	8	0.09
Norway	89	8	0.09	87	11	0.13
Sweden	90	10	0.11	94	9	0.10
Finland	92	8	0.09	96	10	0.10
Baltic States	91	11	0.12	101	12	0.12
Iceland	91	8	0.09	83	10	0.12

Table D.5: Wind speed estimates for Nysted (Rødsand). Source: Barthelmie [8].

Method	Description	Wind speed
WAsP	Rødsand 96–98/Tystofte 83–97	8.7
Weibull	Rødsand 96–98/Tystofte 83–97	8.8
MCP	Rødsand 96–98/Tystofte 83–97	8.6
WAsP	Rødsand 96–99/Tystofte 83–97	9.0
Weibull	Rødsand 96–99/Tystofte 83–97	9.0
MCP	Rødsand 96–99/Tystofte 83–97	8.6
Observed	Rødsand 96–99	9.5
	Average error [m/s]	-0.7
	Coefficient of variation [-]	0.021

Table D.6: Wind speed estimates for Omø Stålgrunde (Source: Barthelmie [8].

Method	Description	Wind speed
WAsP	Omø Stålgrunde 96–98/Tystofte 83–97	8.3
Weibull	Omø Stålgrunde 96–98/Tystofte 83–97	8.3
MCP	Omø Stålgrunde 96–98/Tystofte 83–97	8.1
WAsP	Omø Stålgrunde 96–99/Tystofte 83–97	8.3
Weibull	Omø Stålgrunde 96–99/Tystofte 83–97	8.3
MCP	Omø Stålgrunde 96–99/Tystofte 83–97	8.1
Observed	Omø Stålgrunde 96–99	7.8
	Average error [m/s]	+0.4
	Coefficient of variation [-]	0.012

Table D.7: Prediction of wind speeds and turbulence intensity at hub height H from measurements at low height in [m/s]. Source: Downey [48]. The terrain roughness z_0 is estimated from the turbulence intensity at the lowest height; the wind shear exponent α is estimated for the largest height. In the calculations all available data between 10 and 20 m/s were used.

station	type	height	wind speed [m/s]			turbulence intensity [-]		
	(z_0 in [m])	[m]	U_{msr}	U_{pred}	ΔU	I_{msr}	I_{pred}	ΔI
Egmond	offshore	116	13.6	14.1	0.4	0.054	0.071	0.018
	$z_0 = 9.1e\text{-}5$	70	13.0	13.5	0.5	0.061	0.074	0.013
	$\alpha = 0.09$	21	12.3	12.3	0.0	0.081	0.081	0.000
Horns Rev	offshore	62	14.7	14.5	−0.3	0.070	0.086	0.016
	$z_0 = 5.8e\text{-}4$	45	14.1	14.1	−0.1	0.078	0.089	0.011
	$\alpha = 0.13$	30	13.6	13.5	0.0	0.085	0.092	0.007
		15	12.7	12.7	0.0	0.099	0.099	0.000
Læsø	offshore	62	14.5	13.8	−0.7	0.066	0.080	0.014
	$z_0 = 2.3e\text{-}4$	45	13.9	13.4	−0.5	0.070	0.082	0.012
	$\alpha = 0.13$	30	13.2	13.0	−0.2	0.078	0.085	0.007
		15	12.2	12.2	0.0	0.090	0.090	0.000
Skipheia	coastal	101	16.6	17.0	0.5	0.065	0.096	0.031
	$z_0 = 3.0e\text{-}3$	72	15.9	16.5	0.6	0.072	0.099	0.027
	$\alpha = 0.12$	41	15.3	15.6	0.3	0.086	0.105	0.019
		20.5	14.4	14.4	0.0	0.104	0.113	0.010
		11	13.4	13.4	0.0	0.122	0.122	0.000
Tjæreborg	coastal	90	16.1	14.9	−1.1	0.084	0.105	0.022
	$z_0 = 6.9e\text{-}3$	60	14.7	14.3	−0.5	0.096	0.110	0.014
	$\alpha = 0.21$	30	13.2	13.2	0.0	0.119	0.119	0.000
Toboel	pastoral	62	16.2	15.5	−0.7	0.126	0.140	0.014
	$z_0 = 4.8e\text{-}2$	45	15.2	14.8	−0.4	0.139	0.146	0.007
	$\alpha = 0.20$	30	13.9	13.9	0.0	0.158	0.155	−0.003
		15	12.4	12.4	0.0	0.174	0.174	0.000
Cabauw	pastoral	200	17.1	17.0	−0.1	0.074	0.100	0.026
	$z_0 = 9.3e\text{-}3$	140	17.2	16.4	−0.7	0.086	0.104	0.018
	$\alpha = 0.16$	80	15.7	15.5	−0.3	0.107	0.110	0.004
		40	14.2	14.3	0.1	0.128	0.120	−0.009
		20	13.1	13.1	0.0	0.130	0.130	0.000
Oak Creek	complex	79	16.6	17.9	1.3	0.088	0.097	0.010
	$z_0 = 2.8e\text{-}3$	65	16.7	17.6	0.9	0.094	0.099	0.005
	$\alpha = \text{-}0.02$	50	16.3	17.1	0.8	0.099	0.102	0.003
		10	14.3	14.3	0.0	0.122	0.122	0.000

Appendix E

Low cycle fatigue

E.1 Transition matrix

It has often been argued that the conventional approach to load calculations in which only 10 minute (or 1 hour) intervals are considered, characterised by a mean wind speed and (Gaussian) turbulence, misses large load cycles that are created by very low frequency wind speed variations (periods of days). To estimate the size of this effect we consider an artificial sequence of these load calculations that is representative for real wind speed histories.

It is not entirely straightforward how to generate wind speed history of 10 minute or 1 hour intervals with the right properties. For example, if a one step Markov chain is used we may run into trouble because the correlation function for such a chain is rapidly decaying, and low frequency phenomena are not well represented. If on the other hand we use the method of Shinozuka [190] (combined with Yamazaki's [238] algorithm to obtain the desired Weibull wind speed distribution), we will tend to find persistence that is larger than in reality, because the methods disregards phase information (phase angles are assumed to be random). Kaminsky [100] advocates the use of an embedded Markov procedure, in which a low and high frequency chain are superposed. In investigating this method it was found however that a single chain based on 1 hour average wind speeds yields spectra that are quite similar to measured ones. Moreover, the transition matrices and spectra for various sites are so similar that is seems justified to represent them by one synthetic matrix.

The Markov transition matrix is found as follows. First all wind speeds are transformed to the height where the mean wind speed would have been 8.5 m/s. Then each 1 h period is binned into 2 m/s intervals (0–3, 3–5, ..., 23–25, 25 and over). Each transition is characterised by the *from* wind speed and the *to* wind speed. A transition $U_j \rightarrow U_i$ is counted by increasing matrix element m_{ij} by 1. There is no reason why we should not look at the signal in reverse, so we also increase element m_{ji} by 1. This will ensure detailed balance (see below), and that the eigenvector of the matrix

equals the wind speed distribution. When we are done, every column is normalised to make the sum of probabilities equal to unity.

It turns out that the transition probabilities from one wind speed bin to another are well described by Weibull distributions. For average wind speed 8.5 m/s and 2 m/s bins, Weibull curve fitting yields the result that the Weibull size factor A and the median m are given by linear functions (in good approximation):

$$A = a_A U_{from} + b_A \tag{E.1}$$

$$m = a_m U_{from} + b_m \tag{E.2}$$

Where:

A	Weibull scale factor [m/s]
a_A	constant = 0.969
a_m	constant = 0.960
b_A	constant = 0.723 m/s
b_m	constant = 0.458 m/s
m	median [m/s]
U_{from}	'from' bin wind speed mean value [m/s]

Because the median of a Weibull distribution and the scale factor are related:

$$m = A \left(\ln 2\right)^{1/k} \tag{E.3}$$

The shape factor k can be found with:

$$k = \frac{\ln \ln 2}{\ln(m/A)} \tag{E.4}$$

This prescription yields a transition matrix that is very close to the average of 10 measured ones (for each site the wind speed history was blown up to achieve average wind speed 8.5 m/s, i.e. wind speeds were transformed to the height where this speed would occur), and the matrix will yield a wind speed distribution close to the desired one ($U = 8.5$ m/s, $k = 2$), but not exactly. A problem with the synthetic matrix is that it generates a signal which is not time reversible, i.e. if we take the signal generated, reverse it and regenerate the matrix, the new matrix will not be identical to the original one. To get time reversibility and the correct wind speed distribution, we must have the following. Let the transition matrix be M and the desired wind speed frequency is p_i for wind speed interval i, then for any m_{ij}:

$$p_j m_{ij} = p_i m_{ji} \tag{E.5}$$

This property, which is also called 'detailed balance' means that the process moves from wind speed interval i to j just as often as it moves from wind speed interval j to i. [1]

---

[1]Note that our definition of the transition matrix has columns summing to unity, not rows.

The matrix built from measurements has the first property automatically if we build the matrix by counting transitions and input every transition in elements m_{ij} and m_{ji} and in p_i and p_j. The wind speed distribution will of course be the measured one, and not necessarily the desired one.

The synthetic matrix will only approximately have the desired properties. We may rectify this by applying the Metropolis-Hastings algorithm (see Hastings [84] and Chib [37]). The original algorithm modifies the matrix by shifting probability mass from off-diagonal element to main diagonal elements; unfortunately this tends to destroy the fit of the individual Weibull distributions. For our purpose it is better to use a modified, iterative version of the algorithm that relies on redistributing probability mass between sets of mirror off-diagonal elements m_{ij} and m_{ji}:

1. Redistribute probability mass over m_{ij} or m_{ji} to comply with equation (E.5). Set the new elements m'_{ij} and m'_{ji} to:

$$
\begin{aligned}
m'_{ij} &= \frac{p_i}{p_i + p_j} \left(m_{ij} + m_{ji} \right) \\
m'_{ji} &= \frac{p_j}{p_i + p_j} \left(m_{ij} + m_{ji} \right)
\end{aligned}
\tag{E.6}
$$

2. Apply this procedure to all pairs (m_{ij}, m_{ji}) where $i \neq j$.

3. Renormalise all columns to restore unity column sums.

4. Go to step 1 and repeat the procedure until detailed balance is achieved.

This simple tweaking procedure by and large preserves the original matrix: only small changes are made in some elements. The matrix found with the Weibull distribution given above and subsequent correction is given as table E.2 (next page).

Table E.1: Meteo stations used

station	period	time [h]	measuring height [m]	average wind speed at measuring height [m/s]
Netherlands				
Cabauw (s348)	1988–2003	121,900	10.0	4.7
Den Helder (s235)	1974–2002	262,600	10.0	6.1
Europlatform (s321)	1985–2003	158,200	29.1	8.8
K13 (s252)	1981–2001	154,100	73.8	9.6
MP Noordwijk (s254)	1991–2002	112,700	27.6	8.4
Texelhors (s229)	1973–2002	246,000	10.0	7.2
Vlieland (s242)	1996–2002	61,400	10.0	7.2
Denmark				
Risø	1996–2002	14,700	125.0	7.6
Tystofte	1982–1999	149,300	39.3	6.5
Sweden				
Nasudden	1992–1995	29,100	96.0	7.5

Apart from wind speed changes something must be assumed for wind direction changes. It turns out that the change in wind direction for 1 hour means is well (enough) described by a normal distribution with 0 mean and standard deviation 15°. Figure E.1 shows the power spectral density of a wind speed history generated with the matrix given above. It is seen that the Markov chain signal fits the measured signal well, and is also close to the (unity normalised, one-sided) spectrum for Tystofte derived by Kristensen [114]:

$$S(f) = \frac{4T}{1 + (2\pi fT)^2} \tag{E.7}$$

where:

f frequency [1/day]
S power spectral density [m^2/s^2/day]
T time constant = 0.84 days

While this method is fine for generating wind speed histories, the wind direction history is not completely satisfactory: the resulting wind direction distribution is uniform, while in reality the wind is known to have a dominant direction. This could be solved by generating separate histories for E-W and N-S wind speeds, which have normal distributions with non-zero means (for North-Western Europe) and are uncorrelated.

Table E.2: Markov transition matrix for IEC class II wind regime (U=8.5 m/s, k=2)

A	1.41	2.82	4.60	6.49	8.43	10.37	12.33	14.27	16.24	18.18	20.13	21.94	23.98	26.20
m	1.10	2.48	4.25	6.14	8.06	10.00	11.95	13.88	15.83	17.75	19.68	21.46	23.47	25.66
k	1.50	2.97	4.65	6.62	8.45	10.09	11.88	13.09	14.40	15.57	16.37	16.82	17.31	19.35
U	0.5	2	4	6	8	10	12	14	16	18	20	22	24	26
0.5	0.53	0.06												
2	0.43	0.70	0.13											
4	0.04	0.24	0.65	0.17	0.01									
6		0.01	0.21	0.63	0.19	0.01								
8			0.01	0.19	0.61	0.21	0.02							
10				0.01	0.18	0.60	0.23	0.02						
12					0.01	0.17	0.59	0.24	0.03	0.01				
14						0.01	0.16	0.57	0.25	0.04	0.01			
16							0.01	0.15	0.56	0.27	0.05	0.01		
18								0.01	0.14	0.54	0.28	0.05	0.01	
20									0.01	0.14	0.53	0.29	0.06	0.02
22										0.01	0.13	0.51	0.29	0.07
24											0.01	0.12	0.48	0.28
26												0.02	0.15	0.63
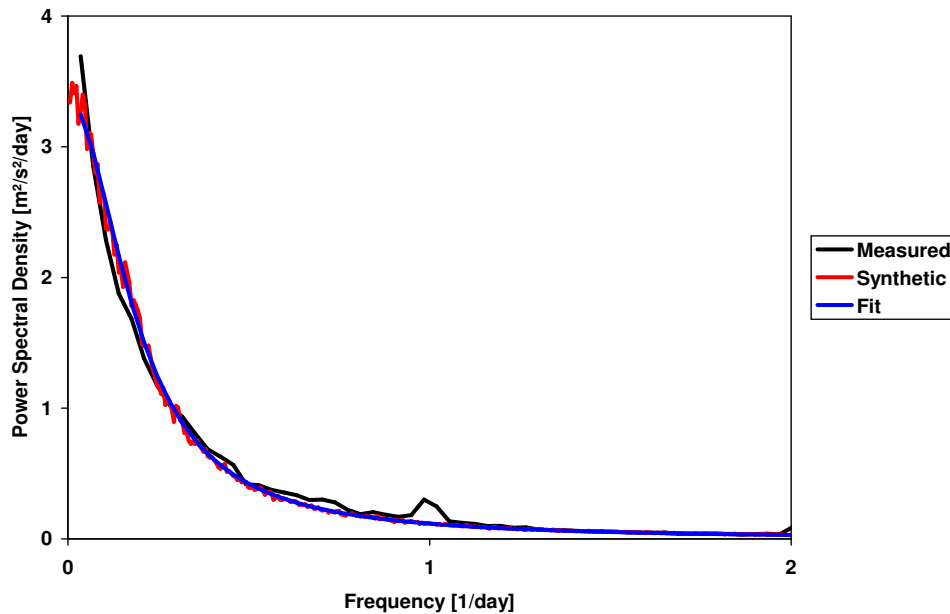
Figure E.1: Power spectral density of 1 hour mean wind speed for Tystofte (unity normalised area). The fit is according to equation (E.7).

E.2 Calculations

A total of $13 \times 12 = 156$ load calculations were done for wind speeds 3, 4, 6, . . ., 24, 30 m/s; for every wind speed 12 calculations of 10 minutes were done, at angles 0, 30, . . ., $330°$. Once we have a wind history, either from measurements or an artificial one, it is possible to construct long term load time series, simply by stringing together 10 minute time series according to this history. The load histories are rainflow counted, and the equivalent load is calculated and compared to the conventionally calculated one for the same load history.

For the artificial time series, which wind direction to select is determined by finding the new wind direction from the old one by adding a random angle from the appropriate normal distribution $N(0°, 15°)$, which results in a series of 1 hour mean wind directions having any value between $0°$ and $360°$ with a uniform distribution. To determine which load case to use, the new angle is rounded to the nearest multiple of $30°$.

Table E.3 (p232) presents the ratios of equivalent loads incorporating large cycles with conventional calculations, for the standard IEC class II calculation with uniform wind speed distribution and for 5 meteo stations for which measured wind histories are available (turbine hub height is assumed to be at the level where the average wind
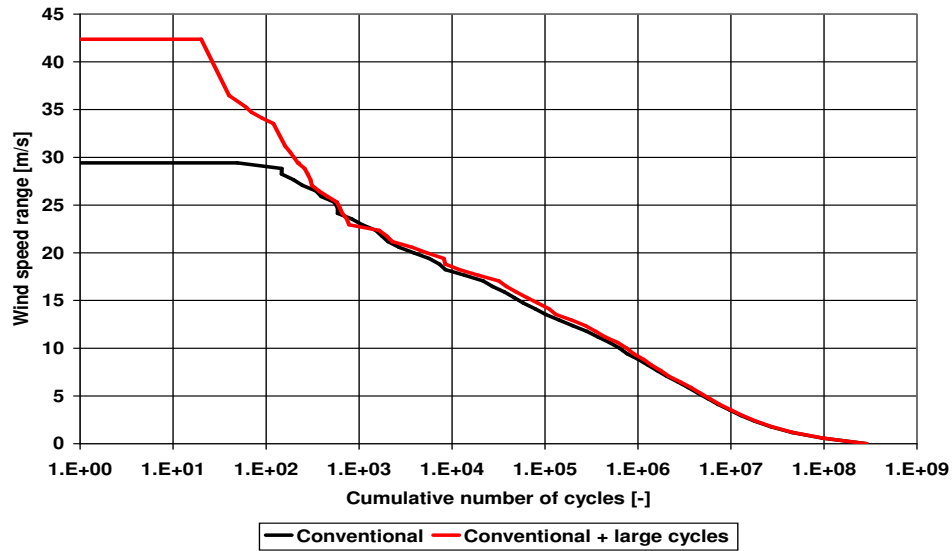
Figure E.2: Large cycles due to low frequency wind speed variations: wind speed.

speed is 8.5 m/s). Results for various stations agree very well with each other, and also with the IEC class II calculations. Some graphical results of the calculations are given in figures E.2–E.5.

Table E.3: Influence of large low frequency load cycles on equivalent fatigue loads. Table numbers are the ratio of calculations with and without large load cycles, for the same measured wind speed and direction histories, which are normalised to average wind speed 8.5 m/s. Note that the wind speed distributions thus obtained are not necessarily Weibull; nor are wind direction distributions uniform. Hourly wind directions for the IEC II wind regime are generated with a random walk process, where change in wind speed is governed by the normal distribution $\Phi(\mu = 0°, \sigma = 15°)$.

Load	Mx11r	My11r	Mx11h	My11h	MxNr	MyNf	MzNf	Mxt0	Myt0
Exponent m	12	12	6	6	6	6	6	4	4
IEC II	1.00	1.02	1.00	1.03	1.06	1.01	1.01	1.03	1.03
IEC II[1]	1.00	1.04	1.00	1.04	1.06	1.02	1.03	1.05	1.06
Cabauw	1.00	1.02	1.00	1.03	1.07	1.01	1.01	1.02	1.03
Den Helder	1.00	1.02	1.00	1.03	1.06	1.01	1.01	1.02	1.03
K13	1.00	1.02	1.00	1.03	1.05	1.01	1.01	1.02	1.03
Vlissingen	1.00	1.02	1.00	1.03	1.06	1.01	1.01	1.02	1.03
Tystofte	1.00	1.03	1.00	1.04	1.09	1.01	1.01	1.03	1.05

[1]Results as in first line, but normalised against exact Weibull distribution.
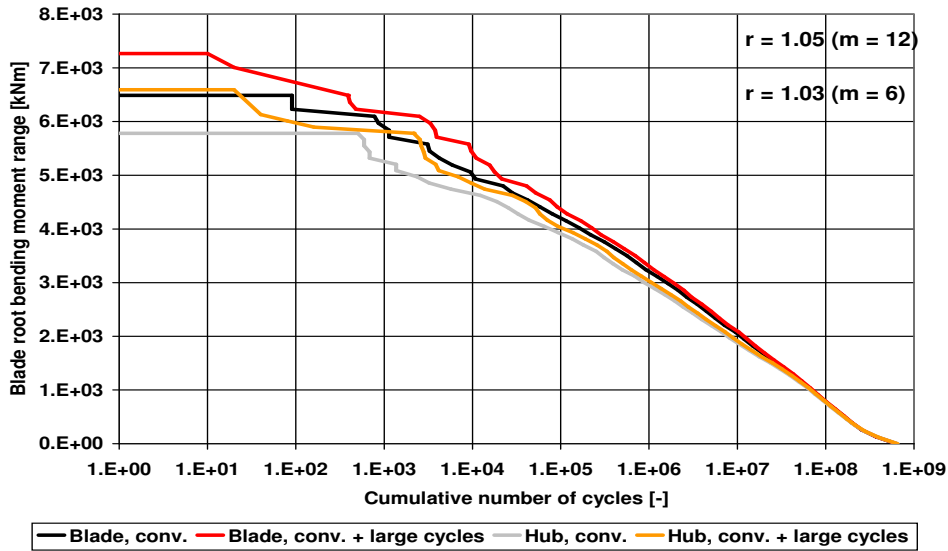
Figure E.3: Large cycles due to low frequency wind speed variations: blade root flap moment. Load ratio $r = 1.05$ for exponent $m = 12$ (blade) and $r = 1.03$ for $m = 6$ (hub).
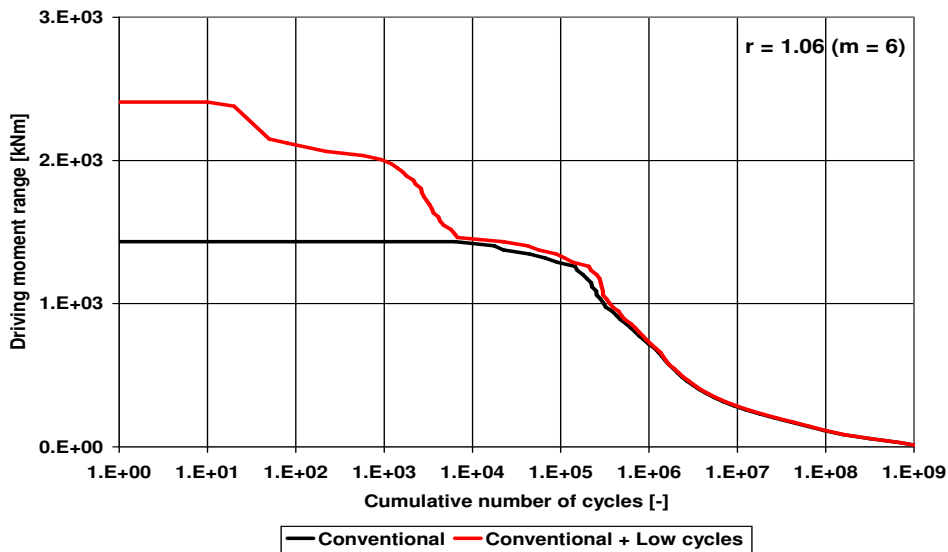
Figure E.4: Large load cycles due to low frequency wind speed variations: main shaft driving moment. Load ratio $r = 1.06$ for exponent $m = 6$.
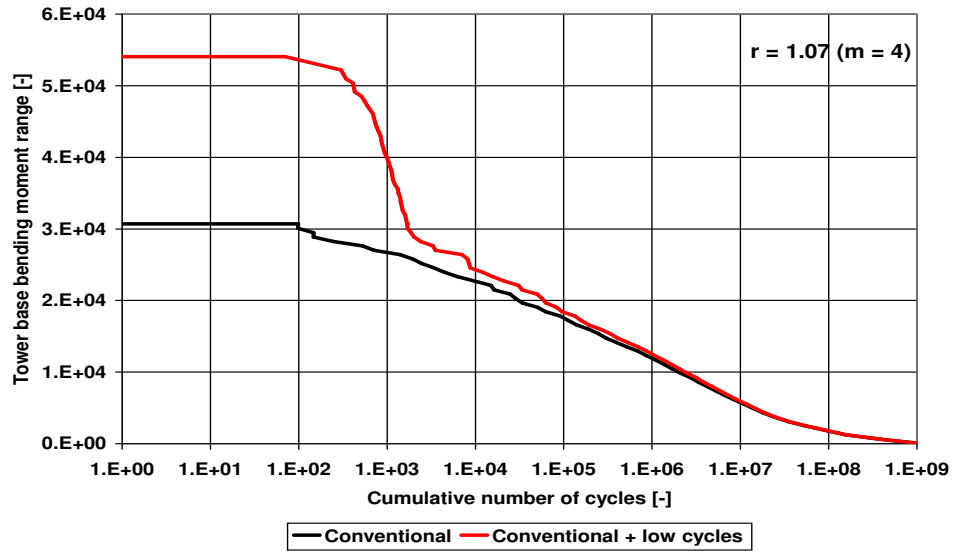
Figure E.5: Large load cycles due to low frequency wind speed variations: tower base bending moment. Load ratio $r = 1.07$ for exponent $m = 4$.

Of course from the time series the number of start stop cycles may be derived as well, see table E.4, which would for example enable us to judge the effect of setting stop wind to different values.

Table E.4: Start stop cycles. Average of 5 wind histories. Note: start-stop hysteresis at high wind speeds was not taken into account.

start wind speed	stop wind speed	IEC I; $U = 10$ m/s		IEC II; $U = 8.5$ m/s	
		cycles	cycle time	cycles	cycle time
[m/s]	[m/s]	[-]	[h]	[-]	[h]
4	4	2,564	45	3,328	43
4	25	158	116	46	136
25	4	153	126	43	122
25	25	221	24	29	13
all	all	3,095	52	3,446	45

Appendix F

Some notes on probabilistic methods

F.1 First Order Reliability Method

The idea of the First Order Reliability Method is to linearise the limit state function Z around the design point $\underline{x}^*$, which is the point fulfilling $Z(\underline{x}) = 0$ with the highest probability density ('the point with the highest failure probability'). This means that the surface $Z = 0$ is approximated by a hyperplane. If all distributions of the vector $\underline{x}$ are (approximated by) normal distributions, the amount of probability mass in the region where $Z < 0$ is found from the distance β (the reliability index) of point $\underline{x}^*$ to the point of the mean value of Z:

$$\beta = \frac{\mu_Z}{\sigma_Z} \tag{F.1}$$

The reliability index β is found with an iterative method. Schemes of various degrees of sophistication are found in books on probabilistic design; this particular one is taken from Vrouwenvelder and Vrijling [231, 233], and is valid for non-correlated variables.

What we need to do is find the design point $\underline{x}^*$, which is the point of the hyperplane where Z has the highest probability density, and the point that will give us the most accurate linearisation of Z:

$$Z(x_i^*) = 0 \tag{F.2}$$

The first estimate of the design point x^* is:

$$x_i^* = \mu_i = \mu_{x_i} \tag{F.3}$$

The expected value of the limit state function μ_Z is:

$$\mu_Z = Z(\mu_i) \tag{F.4}$$

The variance of Z in the design point is found with:

$$\sigma_Z^2 = \sum_{i=1}^{n} \left(\sigma_i \left(\frac{\partial Z}{\partial x_i} \right)_{x_i = x_i^*} \right)^2 \tag{F.5}$$

For later use, we calculate the influence factors α_i:

$$\alpha_i = \frac{\sigma_i}{\sigma_Z} \left(\frac{\partial Z}{\partial x_i} \right)_{x_i = x_i^*} \tag{F.6}$$

As long as β has not been calculated (see equation F.9), we use the estimate:

$$\beta = \frac{\mu_Z}{\sigma_Z} \tag{F.7}$$

This gives us a new estimate of the design point:

$$x_i^* = \mu_i - \alpha_i \beta \sigma_i \tag{F.8}$$

We repeat the calculations of equations (F.5–F.8) until a stable design point $\underline{x}^*$ is found. If this is the case we get an improved value of β with:

$$\beta = \frac{Z(\underline{x}^*) + \sum_{i=1}^{n} \frac{\partial Z}{\partial x_i} (\mu_i - x_i^*)}{\sigma_Z} \tag{F.9}$$

and start the cycle to find $\underline{x}^*$ again, until β is also stabilised. Finally the failure probability p_F is:

$$p_F = N(-\beta) \tag{F.10}$$

So far we have assumed normality for all distributions. However if the distribution of some component x_i is not normal, it is replaced by a normal distribution that has the same cumulative probability and probability density in point x_i^* before evaluating equation (F.5). This is done as follows: for the equivalent normal distribution $N(\mu_N, \sigma_N)$ to have the same cumulative probability as the actual distribution, we must choose mean μ_N and standard deviation σ_N in such a way that:

$$x_i^* = \mu_N + k\sigma_N \tag{F.11}$$

We may find k from the cumulative probability F:

$$k = N_{std,inv} (F(x_i^*)) \tag{F.12}$$

For the derivatives (or probability density functions f) we have (ϕ is the marginal normal distribution approximation of f):

$$f(x_i^*) = \phi(x_i^*, \mu_N, \sigma_N) = \frac{\phi_{std}(k)}{\sigma_N} \tag{F.13}$$

Hence:

$$\sigma_N = \frac{\phi_{std}(k)}{f(x_i^*)} \tag{F.14}$$

Finally the mean μ_i' and the standard deviation σ_i' of the replacement normal distribution are:

$$\sigma_i' = \sigma_N = \frac{\phi(0, k)}{f(x_i^*)} \tag{F.15}$$

$$\mu_i' = \mu_N = x_i^* - k\sigma_i' \tag{F.16}$$

This method is used in its standard form, except for the fact that the limit state function Z and its derivatives are approximated instead of calculated exactly (see next section), because it is too expensive to evaluate Z in every point $\underline{x}$.

F.2 Approximation of limit state function

In section 8.5 the following equation for the limit state function $Z(\underline{x})$ was derived:

$$Z'(\underline{x}) = q_0 x_{dim} x_{\Delta\sigma_A} SRF \gamma_f \gamma_m - \prod_j \frac{S(\underline{x} = \underline{x}_{char}, x_j \neq x_{char,j})}{S_{avg}(\underline{x}_{char})} \tag{F.17}$$

The site load $S(\underline{x})$ is approximated by a product function, rather than a first order Taylor expansion, because this improves accuracy. Figures F.1 to F.4 (p238–239) show how the product approximation performs for the two important site parameters wind speed and turbulence intensity; it is seen that accuracy is satisfactory over the ranges $7.5 \leq U \leq 10$ m/s and $0.05 \leq I \leq 0.30$. For the tower base bending moment the Taylor approximation is also plotted (figure F.4). The Taylor expansion from the central point ($U = 8.5$ m/s, $I_{15} = 0.15$) cannot capture the divergent behaviour of the lines representing actual loads, while the product approximation can.
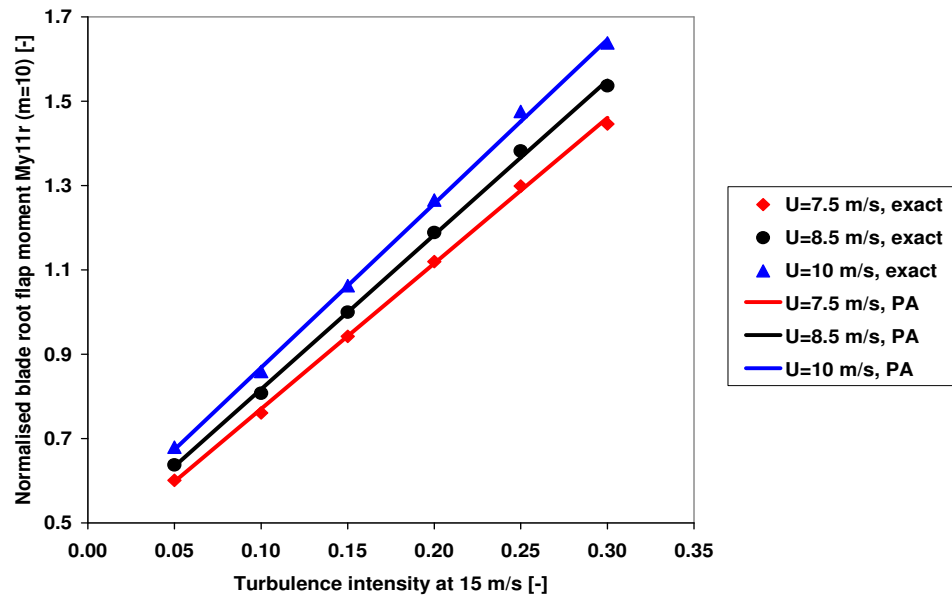
Figure F.1: Estimation of equivalent blade root moment with product approximation (PA).
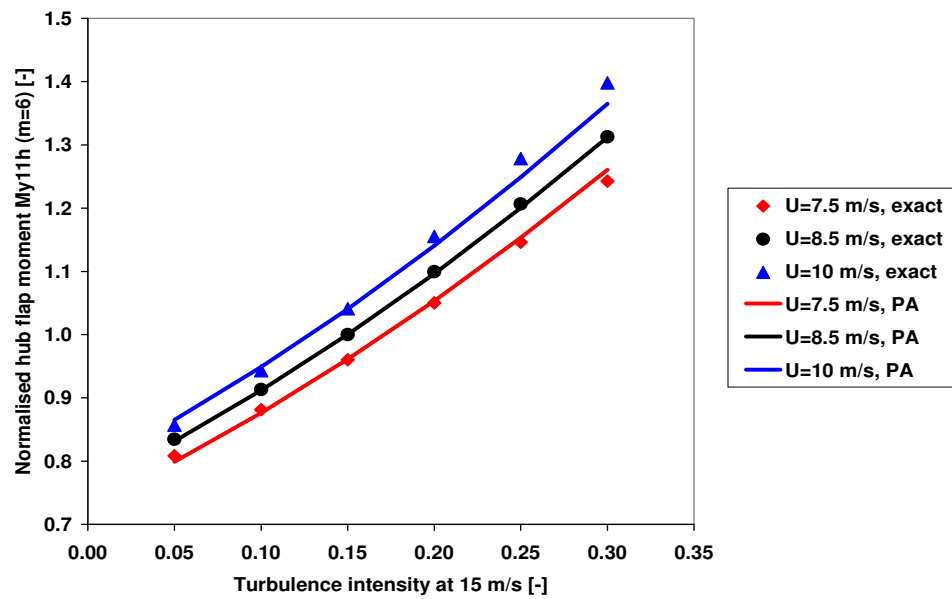
Figure F.2: Estimation of equivalent hub root moment with product approximation (PA).
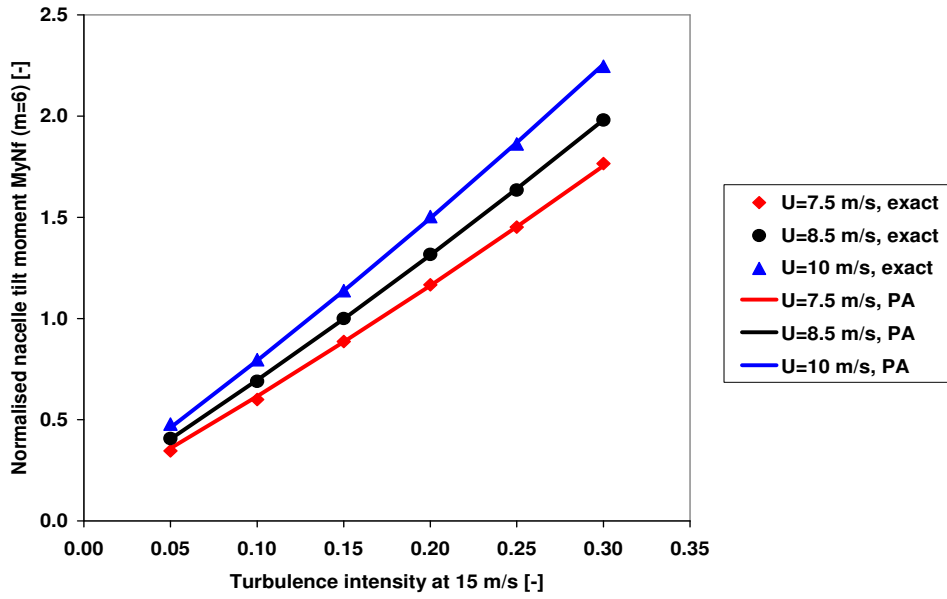
Figure F.3: Estimation of nacelle tilt moment with product approximation (PA).
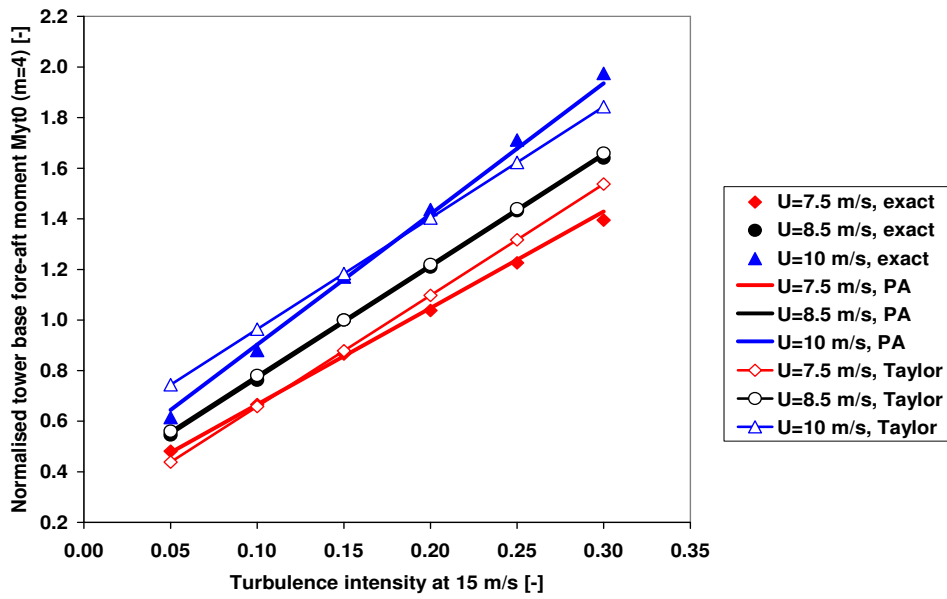
Figure F.4: Estimation of tower base fore-aft moment with product approximation (PA) and Taylor approximation.

F.3   Multiple critical locations

In the main section of the book it is tacitly assumed that all possible failures in critical locations are completely independent of each other. This is a reasonable assumption since most variation is in fatigue properties, and the variation that is used is in fact variation that was found in fatigue tests with identical loading, i.e. possible common cause failure because of correlated loads has been taken into account already; still in the case of a structure like a tower it may be argued that the entire component was probably welded in the same way with the same quality, and fatigue properties of individual critical locations may well be correlated.

Let us look a little further into the matter. In the tower under consideration there are 32 weld seams, and hence $N = 32$ possibly critical locations. If we go for complete independence ($\rho = 0$), this means that the failure probability of the tower is approximately 32 times larger than the failure probability of a single critical location. In fact if all locations have the same failure probability, then:

$$p_{F,N}(\rho = 0) = 1 - (1 - p_{F,1})^N \approx N p_{F,1} \tag{F.18}$$

Now let us assume that failures are correlated with some correlation coefficient ρ.
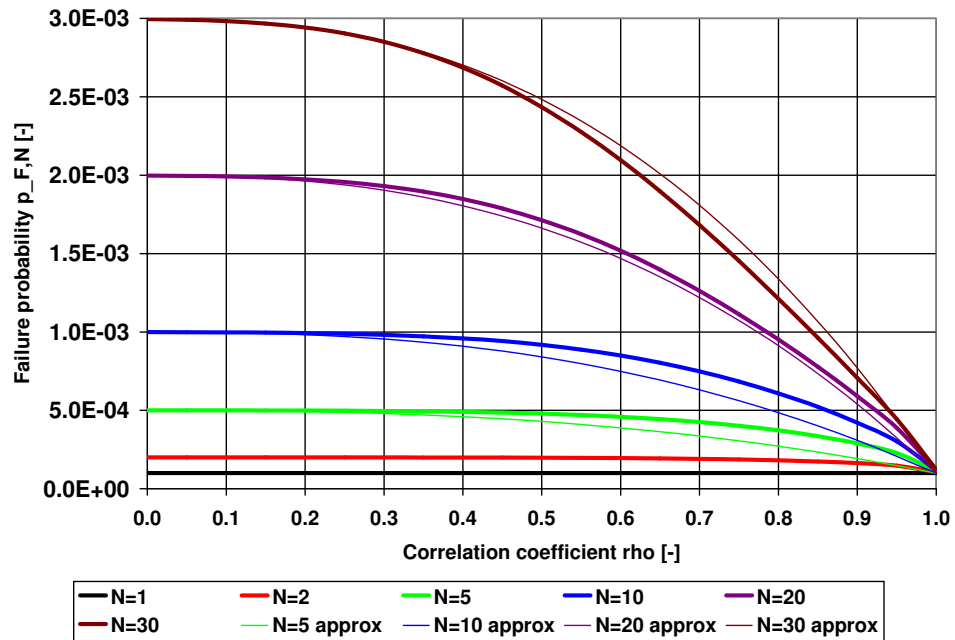
Figure F.5: System yearly failure probability as function of number of critical locations N and correlation coefficient ρ. The failure probability for one location is 10^{-4} ($\beta = 3.72$).

Obviously if there is perfect correlation $\rho = 1$, and:

$$p_{F,N}(\rho = 1) = p_{F,1} \tag{F.19}$$

We are looking for an expression for $p_{F,N}$ for all values $0 \leq \rho \leq 1$. We assume that all critical locations have the same limit state function Z_i, which is:

$$Z_i = \beta - u_i\sqrt{1-\rho} - v\sqrt{\rho} \tag{F.20}$$

Here u_i and v are standard normally distributed variables. Because all Z_i have the component $v\sqrt{\rho}$ in common, they will be correlated with correlation coefficient ρ. Since u and v are independent, the variance of Z_i is:

$$var(Z_i) = \sigma_{Z_i}^2 = 1 - \rho + \rho = 1 \tag{F.21}$$

and hence the correlation $\rho(Z_i, Z_j)$ is:

$$\rho(Z_i, Z_j) = \frac{covar(Z_i, Z_j)}{\sqrt{var(Z_i)\,var(Z_j)}} = \rho \tag{F.22}$$

The failure probability for all failure modes combined is (limit state function $Z < 0$):

$$p_{F,N} = p(Z < 0) = \int_{-\infty}^{\infty} p\left(Z_1 < 0 \vee ... \vee Z_N < 0\right)\,f(v)dv \tag{F.23}$$

This integration can be done with the Monte Carlo method, but it is also possible to use normal integration (Vrouwenvelder [232]):

$$p_F = \int_{-\infty}^{\infty} \left(1 - \left[1 - N(-\beta')\right]^N\right)\,f(v)dv \tag{F.24}$$

with:

$$\beta' = \frac{\beta - v\sqrt{\rho}}{\sqrt{1-\rho}} \tag{F.25}$$

Results of the integration are given in figure F.5. The value chosen for the yearly failure probability of one location is $p_{F,1} \sim 10^{-4}$, corresponding to reliability index $\beta = 3.72$. It turns out that a reasonable approximation of the curves is:

$$p_{F,N}(\rho) = \left(1 - \rho^2\right)p_{F,N}(0) + \rho^2 p_{F,1} \tag{F.26}$$

With the approximation for small failure probabilities:

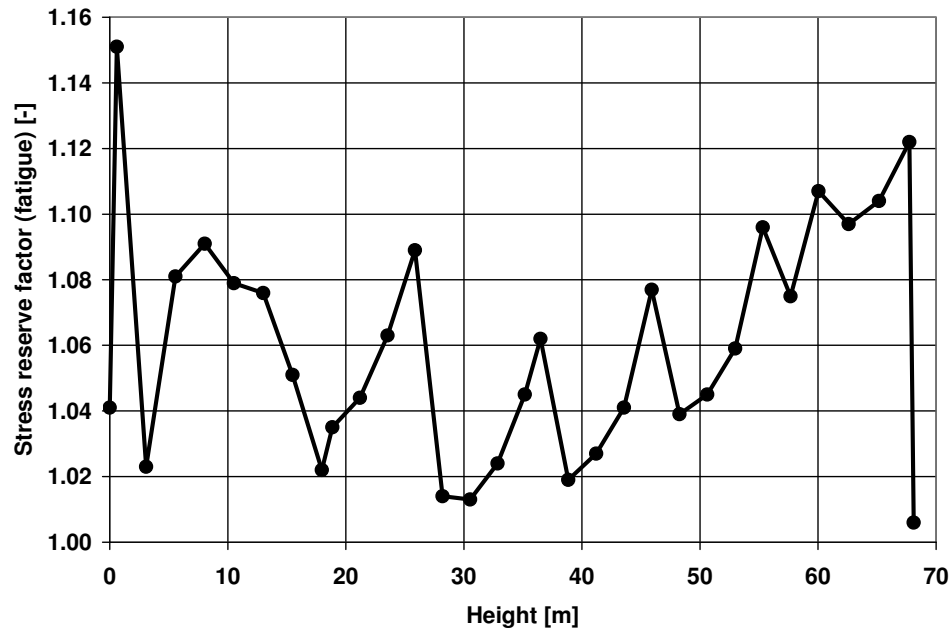$$p_{F,N}(\rho) = \left(N - N\rho^2 + \rho^2\right)p_{F,1} \tag{F.27}$$

Figure F.6: Distribution of fatigue stress reserve factors for tower critical locations.

So far we assumed that all critical locations had the same failure probability: actually this is not the case. A typical example of a tower optimised with respect of fatigue is given in figure F.6. It is seen that all factors are larger than unity; the average value is $SRF = 1.06$. This means that we are conservative if we demand that the failure probability for individual locations is the system failure probability divided by N. The question is: given usual design practice, which failure probability should we demand for individual locations? For this particular case the answer is that we require the failure probability to be 14 times smaller than the system failure probability index (see table F.1). If all critical locations had $SRF = 1$ the requirement woud be a factor 32; however since the average stress reserve factor is $SRF = 1.06$ the total effect of the 32 locations is the same as 14 locations with $SRF = 1$.

Dalsgaard Sørensen [198, 199] considered a 3-piece tower design with only 6 critical locations (because each piece has constant wall thickness), of which only 2 locations contribute significantly to total failure probability. Given current design practice resulting in highly optimised towers, this may be to be too optimistic. While material fatigue properties may be correlated, it is seen that a high correlation coefficient is required (say $r \geq 0.7$) to have significant effect. Hence the failure probability requirement for individual locations should be more stringent than in the case of one location (figure F.5).

F.4   Size of critical location

Besides the matter of the number of critical locations, we have to consider the statistical size effect. This is the effect that if two components of the same shape are compared, the larger one will have smaller fatigue strength, simply because the highly stressed surface area where a crack might start is larger. This can be made precise with the Weibull weakest link model. If the fatigue strength of a specimen with reference area A_0 is Weibull(C, k) distributed, then the failure probability p_{F,A_0} given load $\Delta\sigma$ is:

$$p_{F,A_0} = p(\Delta\sigma_A < \Delta\sigma) = 1 - \exp\left[-\left(\frac{\Delta\sigma}{C}\right)^k\right] \tag{F.28}$$

where $\Delta\sigma_A$ is the fatigue strength. The probability of endurance (survival) p_{E,A_0} is:

$$p_{E,A_0} = 1 - p_{F,A_0} = \exp\left[-\left(\frac{\Delta\sigma}{C}\right)^k\right] \tag{F.29}$$

If there are n small areas, with stress ranges $\Delta\sigma_i$ the total endurance probability is found by multiplying individual probabilities, which comes down to adding exponents:

$$p_E = \exp\left[-\sum_{i=1}^{n}\left(\frac{\Delta\sigma_i}{C}\right)^k\right] \tag{F.30}$$

For an arbitrary stress distribution over an area A this generalises to:

$$p_E = \exp\left[-\int_A \left(\frac{\Delta\sigma_i}{C}\right)^k \frac{dA}{A_0}\right] \tag{F.31}$$

The scale parameter is related to the median fatigue strength with:

$$C = \frac{\Delta\sigma_{A0,50\%}}{(\ln 2)^{1/k}} \tag{F.32}$$

Table F.1: Calculation details for tower (reference period 1 year). The safety factor γ is chosen to obtain yearly failure probability $p_F = 10^{-3}$ for one location; there are 32 critical locations with average $SRF = 1.06$.

Location	Stress reserve factor	Failure probability	Reliability index
Worst location	1.00	1.0×10^{-4}	3.72
System (32 locations)	1.00	3.2×10^{-3}	2.73
System (32 locations)	1.06	1.4×10^{-3}	2.99
Equivalent number of critical locations: $1.4\times10^{-3}/1.0\times10^{-4}$ = 14			

Hence the endurance probability is:

$$p_E = \exp\left[-\ln 2 \int\limits_A \left(\frac{\Delta\sigma_i}{\Delta\sigma_{A0,50\%}}\right)^k \frac{dA}{A_0}\right] \tag{F.33}$$

Now we may derive an equivalent stress range, by comparing the real stress situation with an arbitrary stress pattern with the standard situation where we have constant stress range $\Delta\sigma_{eq}$ over an area A_0, and demanding that the endurance probabilities are the same:

$$\exp\left[-\ln 2 \int\limits_A \left(\frac{\Delta\sigma}{\Delta\sigma_{A,50\%}}\right)^k \frac{dA}{A_0}\right] = \exp\left[-\ln 2 \left(\frac{\Delta\sigma_{eq}}{\Delta\sigma_{A,50\%}}\right)^k \frac{A_0}{A_0}\right] \tag{F.34}$$

This may be simplified to:

$$\int\limits_A \Delta\sigma^k \frac{dA}{A_0} = \Delta\sigma_{eq}^k \tag{F.35}$$

and finally we get:

$$\left[\int\limits_A \Delta\sigma^k \frac{dA}{A_0}\right]^{1/k} = \Delta\sigma_{eq} \tag{F.36}$$

Suppose that we have two components with the same shape but with different sizes A_1 and A_2; the stress patterns are the same, for example the same constant stress in both cases. Then the equivalent stresses are related as:

$$\frac{\Delta\sigma_{eq,2}}{\Delta\sigma_{eq,1}} = \left(\frac{A_2}{A_1}\right)^{1/k} \tag{F.37}$$

This means that the larger part acts *as if* it sees a stress that is larger than the actual stress by a factor $(A_2/A_1)^{1/k}$.

The Weibull shape factor k is found by equating the coefficient of variation of a Weibull distribution with the standard deviation (on stress) of the S-N curve:

$$\sqrt{\frac{\Gamma(1+2/k)}{\Gamma^2(1+1/k)} - 1} = V_\sigma \tag{F.38}$$

The astute reader will have noticed that the assumption that the fatigue strength is Weibull distributed is contrary to the assumption of lognormality used so far. However the Weibull distribution is just used as an analytical convenience, basically the integration can be done for any distribution. From equation (F.36) it is clear that only

Table F.2: Weibull shape factor k as function of coefficient of variation V_σ.

Coefficient of variation V_σ	0.05	0.10	0.15	0.20
Weibull shape factor k	24.95	12.15	7.91	5.80

stresses close to the maximum in some critical location contribute, because the stress ratio is raised to some power k; in the literature one sees usually values $k > 10$. This justifies the usual critical location approach, where it is assumed that only the (infinitesimally small) critical location may be considered without doing the stress integral.

It is a matter of some debate whether the integration should be over length, surface area or volume. This depends of course on where cracks are likely to start, and geometry. For example Kaufmann [104] gives a simple volume recipe for cast iron: the reduction factor on fatigue strength is:

$$\frac{\Delta\sigma_{V_2}}{\Delta\sigma_{V_1}} = \left(\frac{V_{90\%,1}}{V_{90\%,2}}\right)^v \tag{F.39}$$

where:

$V_{90\%}$	volume with stress larger than 90% of maximum stress [mm^3]
v	exponent
	$v = 0.09$ for $300 \le V_{90\%} \le 8000$ mm^3
	$v = 0.01$ for $V_{90\%} > 8000$ mm^3
$\Delta\sigma$	fatigue strength [Pa]

We may check the value $k = 1/0.09 \simeq 11$ against the known coefficient of variation on the S-N curve for cast iron, which is $V_\sigma = 0.07$, giving $k = 17.6$. Although the values are not quite the same, at least the magnitude is all right; the difference may (for example) have to do with the fact that Kaufmann used a volume integral, while a surface integral might be more appropriate.

For the case of weld seams a fatigue strength reduction factor dependent on thickness is prescribed in Eurocode 3, but there is no reduction based on seam length.

Indications are that the Weibull model conforms to reality: for example Haibach [77] (citing Böhm [18]) and Flacelière [62] report reasonable agreement to theory. Still a model like this needs calibration: reference fatigue strength and the reference volume must be determined (the exponent k can be found from the distribution of fatigue strength).

For a cast structure like the hub it is straightforward to apply the model; it is not clear whether the model could be used for circular weld seams in the tower. Still it seems obvious that the longer a weld seam, the larger the failure probability must be.

Appendix G

Wind field generation methods

G.1 One dimensional case

For ease of understanding, first the 1-dimensional case of wind generation for one point in space is considered in some detail. Suppose we consider the wind speed variation in time $u(t)$ in the rotor plane. For N samples, the wind speed signal $u(t)$ can be written as a sum of cosines and sines:

$$u(t) = \sum_{j=0}^{j=N/2} A_j \cos j2\pi\Delta ft + B_j \sin j2\pi\Delta ft \tag{G.1}$$

The total time considered is T, and there are N samples ΔT apart. Hence:

$$N\Delta T = T \tag{G.2}$$

And the lowest non zero frequency is:

$$\Delta f = \frac{1}{N\Delta T} = \frac{1}{T} \tag{G.3}$$

With $N/2$ frequencies the highest (Nyquist) frequency is:

$$f_{N/2} = \frac{N}{2}\Delta f = \frac{1}{2\Delta T} \tag{G.4}$$

If the mean wind speed is U, a box of length $L = UT$ is transported through the wind turbine rotor. Define the wave number k_j:

$$k_j = j\Delta k = j\frac{2\pi}{L} = j\frac{2\pi}{UT} \tag{G.5}$$

Then the wind speed can be written as a function of the spatial co-ordinate in the box $x = Ut$ (Taylor's frozen turbulence hypothesis):

$$u(x) = \sum_{j=0}^{j=N/2} A_j \cos j\Delta kx + B_j \sin j\Delta kx \tag{G.6}$$

From which it immediately follows that:

$$\Delta k = \frac{2\pi}{U}\Delta f \tag{G.7}$$

Let us consider the two-sided power spectrum S_2. The covariance R of the signal at 2 points in space as a function of the distance r is defined as the expectation value of the product of the 2 signals:

$$R(r) = \langle u(x)u(x+r)\rangle \tag{G.8}$$

And the spectral density $S_2(k)$ is the Fourier transform of R:

$$S_2(k) = \frac{1}{2\pi}\int R(r)e^{-ikr}dr \tag{G.9}$$

In practice the power spectral density $S_2(k)$ is known, and our task is to generate an artificial wind signal $u(t)$ from it that has the right power as a function of frequency and has the same probability distribution as measured wind (in many cases a normal distribution is assumed, for the validity of this assumption see Nielsen [155]).

The fast Fourier transform (FFT) of the wind speed signal $u(t)$ (equation G.1) is a vector Z, with N complex components. The question is now: how must the components of Z be chosen to arrive at a wind speed signal with the right properties after the inverse FFT? The requirement is that for each component of Z (that represents a sinusoid) the power (expectation of the square of the signal) must fit the integral of the power spectral density S_2 over a wave number interval:

$$\langle Z_{-j}^2\rangle = \langle Z_j^2\rangle = \int_{(j-\frac{1}{2})\Delta k}^{(j+\frac{1}{2})\Delta k} S_2(k)dk \tag{G.10}$$

The vector Z does not contain the amplitudes A and B from equation (G.6), but rather a linear combination of them (this is a consequence of the FFT). For each combination of negative and positive wave numbers $k = (-j\Delta k \quad j\Delta k)$ we have a partial vector $\Delta\underline{Z}(-k,k)$ defined as:

$$\Delta\underline{Z}(-k,k) = (Z_{-j}\ Z_j) \tag{G.11}$$

If all partial vectors are inverse FFT'ed, one finds:

$$u(t) = \sum_{j=1}^{j=N/2} (Z_{-j} + Z_j)\cos j\Delta kx + (Z_{-j} - Z_j)\sin j\Delta kx \tag{G.12}$$

Comparing this to the earlier definition (G.6):

$$u(x) = \sum_{j=0}^{j=N/2} A_j \cos j\Delta kx + B_j \sin j\Delta kx \tag{G.13}$$

It is clear that:

$$A(k) = Z_j + Z_{-j} \quad B(k) = Z_{-j} - Z_j \tag{G.14}$$

Conversely, the numbers Z_{-j} and Z_j can be expressed as combinations of A and B:

$$\Delta \underline{Z}(-k, k) = \begin{pmatrix} Z_{-j} \\ Z_j \end{pmatrix} = \begin{pmatrix} \frac{A(k) - iB(k)}{2} \\ \frac{A(k) + iB(k)}{2} \end{pmatrix} \tag{G.15}$$

The partial variance $\Delta \sigma^2(f)$ is:

$$\begin{aligned}
\Delta \sigma^2 &= \frac{A^2 + B^2}{2} = \frac{(\Delta Z_j + \Delta Z_{-j})^2 + (\Delta Z_j - \Delta Z_{-j})^2}{2} \\
&= 2\Delta Z_{-j}^2 = 2\Delta Z_j^2
\end{aligned} \tag{G.16}$$

Combining with equation (G.10) it is found that:

$$\Delta \sigma^2 = 2\Delta Z_{-j}^2 = 2 \int\limits_{(j-\frac{1}{2})\Delta k}^{(j+\frac{1}{2})\Delta k} S_2(k) dk = \int\limits_{(j-\frac{1}{2})\Delta k}^{(j+\frac{1}{2})\Delta k} S_1(k) dk \tag{G.17}$$

So if the components of Z fit the variance requirement, the resulting sinusoids with amplitudes A,B fit it too, as required. It only remains to generate the right Z_j.

Define $C(k)$ as follows:

$$C(k) = \sqrt{\int\limits_{(j-\frac{1}{2})\Delta k}^{(j+\frac{1}{2})\Delta k} 2S_2(k') dk'} = \sqrt{\int\limits_{(j-\frac{1}{2})\Delta k}^{(j+\frac{1}{2})\Delta k} S_1(k') dk'} \tag{G.18}$$

Then the right expectation value for the partial variance $\Delta \sigma^2 = (A^2 + B^2)/2$ may be obtained by setting:

$$A = \sqrt{2}C \cos\phi \quad B = \sqrt{2}C \sin\phi \tag{G.19}$$

With φ a random phase angle uniformly distributed over $[0, 2\pi]$. The corresponding Z-values are easily found from A and B (equation G.15). Another possibility is:

$$Z_{-j} = Cn_1 \quad Z_j = Cn_2 \tag{G.20}$$

Where n_1 and n_2 are random numbers drawn from a standard normal distribution $N(0, 1)$. This last possibility is usually preferred because the process now is truly gaussian.

G.2 Veers method

For a complete description of this method (also known as the Sandia method) see Veers [218]. Consider a number of points in space $p = 1 \ldots P$. For point p amplitudes A_{pj} and B_{pj} are found for every frequency (for example with the uniform phase angle method) (eqn G.19):

$$u_p(t) = \sum_{j=0}^{j=N/2} A_{pj} \cos j2\pi \Delta f t + B_{pj} \sin j2\pi \Delta f t \tag{G.21}$$

To elaborate:

$$\varphi_{pj} = \arg(A_{pj} + iB_{pj}) \tag{G.22}$$

$$A_{pj} = \sqrt{A_{pj}^2 + B_{pj}^2} \cos \varphi_{pj} \tag{G.23}$$

$$B_{pj} = \sqrt{A_{pj}^2 + B_{pj}^2} \sin \varphi_{pj} \tag{G.24}$$

All speeds are uncorrelated. To obtain the desired coherence between two points r (= row) and c (= column) one needs the coherence matrix element:

$$Coh_{rc}(f, \Delta r, \overline{U}) = \frac{S_{rc}(f, \overline{U})}{\sqrt{S_{rr}(f, \overline{U})S_{cc}(f, \overline{U})}} \tag{G.25}$$

Element Coh_{rc} contains the coherence for frequency $f = j\Delta f$ and speed $\overline{U}$ for two points r and c, distance Δr apart; it is easily derived that the 'co-coherence' for two sinusoids with phase difference $\Delta \varphi$ is:

$$Coh_C = \cos \Delta \varphi \tag{G.26}$$

While the 'quad coherence' is:

$$Coh_Q = i \sin \Delta \varphi \tag{G.27}$$

Since the coherence matrix is positive definite, it may be Cholesky decomposed:

$$HH^T = Coh \tag{G.28}$$

The diagonal of the matrix Coh has unity elements, while all off diagonal elements will contain numbers between -1 and $+1$, typically smaller when the distance between points gets larger. Now the desired correlated speed signal for each point p is:

$$u_{p,cor}(t) = \sum_{j=1}^{N/2} \sum_{i=p}^{P} A_{pj} \cos j2\pi \Delta f t + B_{pj} \sin j2\pi \Delta f t \tag{G.29}$$

This means that the correlated signal for point p is made up of contributions from point p itself and from all other points with higher numbers. For reasons of efficiency, the summation will not be done in the time domain, but in the frequency domain, and the time signal generated with the inverse FFT. The procedure is repeated three times for all three wind speed components.

An advantage of the Veers method is that the points may have any position, and that an efficient circular grid may be used for wind turbine applications. Somewhat inelegant is the fact that mass conservation is not obeyed, that the correlation between speed components u and w is zero, and that autospectra and co-spectra (or coherence functions) must be input by hand.

G.3   Modified Veers method

It is not difficult to introduce the right (u, w) coherence, following a proposal by Tubino and Solari [195] (there is no need to do something about the other coherences (u, v) and (v, w) because they are very close to zero anyway). The idea is to generate uncorrelated amplitudes in some co-ordinate system rotated over an angle. The correlated amplitudes for u and w are then found by projection. Since both speed components are linear combinations of the same set of amplitudes, they will be correlated. The equations are given below. Start with the 1-point (u, v, w) covariance matrix S, which is (assume $S_{uv} = S_{vw} = 0$):

$$S(f, U_m, r) = \begin{pmatrix} S_{uu} & 0 & S_{uw} \\ 0 & S_{vv} & 0 \\ S_{uw} & 0 & S_{ww} \end{pmatrix} \tag{G.30}$$

The variances S are thought of as vectors along the x, y and z-axis. The eigenvalues γ of this matrix represent power spectral densities (vectors) in a new co-ordinate system. They are:

$$\gamma_1 = \frac{1}{2} \left(S_{uu} + S_{ww} + \sqrt{(S_{uu} - S_{ww})^2 + 4S_{uw}^2} \right)$$
$$\gamma_2 = S_{vv} \tag{G.31}$$
$$\gamma_3 = \frac{1}{2} \left(S_{uu} + S_{ww} - \sqrt{(S_{\mathrm{u}} - S_{ww})^2 + 4S_{uw}^2} \right)$$

The corresponding eigenvectors represent (the directions of) two independent stochastic processes. They are found by rotating the u and w unit vectors over an angle ψ given by:

$$\psi = \arctan \left(\frac{S_{uu} - S_{ww} - \sqrt{(S_{uu} - S_{ww})^2 + 4S_{uw}^2}}{2S_{uw}} \right) \tag{G.32}$$

The wind speeds (u, v, w) may be found from projections of γ on the original axes, as follows:

$$u(f, t) = \sqrt{2\gamma_1 \Delta f} \cos \psi \cos(2\pi f t + \phi_1) + \sqrt{2\gamma_3 \Delta f} \sin \psi \cos(2\pi f t + \phi_3)$$

$$v(f, t) = \sqrt{2\gamma_2 \Delta f} \; \cos(2\pi f t + \phi_2) \tag{G.33}$$

$$w(f, t) = -\sqrt{2\gamma_1 \Delta f} \sin \psi \cos(2\pi f t + \phi_1) + \sqrt{2\gamma_3 \Delta f} \cos \psi \cos(2\pi f t + \phi_3)$$

The speeds u and w are formed as linear combinations of independent stochastic processes, and have the desired 1-point coherence. The (u, w) correlated speeds for every point go into the Veers procedure described above. The co-spectrum S_{uw} used may for example be the one found by Kaimal with total correlation $\rho = 0.5$ [98, 99]. A value for the correlation ρ of this magnitude was also found by Bergstrøm [13] and with the Mann method if $\Gamma = 3.9$ to obtain the Kaimal spectra [133].

If $S_{uu} \geqq S_{ww}$ then for the zero coherence case $S_{uw} = 0$, one finds: $\gamma_1 = S_{uu}$, $\gamma_2 = S_{vv}$, $\gamma_3 = S_{ww}$, $\psi = 0$, and the original Veers method is recovered. If $S_{uu} < S_{ww}$ then γ_1 and γ_3 must be exchanged to maintain consistency with the $S_{uw} = 0$ case, and

$$\psi = \arctan \left(\frac{S_{ww} - S_{uu} - \sqrt{(S_{uu} - S_{ww})^2 + 4S_{uw}^2}}{2S_{uw}} \right) \tag{G.34}$$

For details and background refer to the paper by Solari and Tubino [195].

G.4   Incorporating measured wind

A nice thing about the Veers method is that measured wind can easily be incorporated into the artificial wind field, which makes it possible to reproduce measured wind fields, at least in some circular area around the position of an anemometer. This is a consequence of the way the Veers method works:

1. Sinusoids with independent random phase angles are generated for point 1.

2. The same is done for point no 2, but the originally independent random phase angles are modified to satisfy coherence with point 1.

3. The same is done for all subsequent points P ($3 \leq P \leq N$). For every point P, the random phase angles are modified to satisfy coherence with preceding points $1 \ldots P - 1$.

Because one is completely free to chose the phase angles for the first point, one may just as well feed in the angles found from a Fourier transform of the measured wind. This procedure may be extended to the first N_m measurement points; there is no need to worry about coherence because the measurement points automatically have the right coherence. The rest of the procedure goes through exactly as before. Of course one still has to input the spectrum and coherence by hand. The best estimate

for the spectrum is probably the average of the measured spectra, while the coherence function can be made to resemble the measured coherence.

Mann's method (see below) is capable of incorporating any predefined wind event in 3 dimensions (gust, shear, direction changes), but the mathematics is more complex (see Nielsen [155] for a description of methods, and Mann [135, 139] for examples).

G.5   Three dimensional case (Mann's method)

All the above is generalised into 3 dimensions in the Mann method, which is described in detail in publications by Mann himself [133, 134, 138]. However when the method was programmed for this work, it appeared that there are some tricky technicalities that make it difficult to get the desired results with the method; therefore it seemed worthwhile to record some of the author's experience.

The method starts out with the 3×3 covariance matrix R, which gives the covariance of speed components u_i and u_j a function of a separation vector $\underline{r}$ between 2 points in space:

$$R_{ij}(\underline{r}) = \langle \underline{u}_i(\underline{x})\underline{u}_j(\underline{x} + \underline{r}) \rangle \tag{G.35}$$

The spectral tensor $\Phi_{ij}(\underline{k})$ is the 3-dimensional Fourier transform of the covariance matrix R (in the 3D Fourier transform (for example) the wind speed is seen as the product of 3 sine functions in the 3 directions x, y and z). The spectral tensor (matrix) Φ_{ij} is a function of the wave number vector $\underline{k} =^T (k_1 \ k_2 \ k_3)$:

$$\Phi_{ij}(\underline{k}) = \frac{1}{8\pi^3} \int R_{ij} \exp(-i\underline{k}.\underline{r}) dr_1 dr_2 dr_3 \tag{G.36}$$

The spectral tensor is the 3D generalisation of the 1D power spectral density S, also giving the component cross-spectral densities. Now as before, suppose that the wind speed vector $\underline{u}$ is given by the inverse Fourier transform of a process $\underline{Z}(\underline{k})$ (which is a $N \times 3$ matrix of random numbers). Part of $\underline{Z}(\underline{k})$ is $\Delta\underline{Z}(\underline{k})$:

$$\Delta\underline{Z}(\underline{k}) = \begin{pmatrix} A_x & A_y & A_z \end{pmatrix} \tag{G.37}$$

With $\Delta\underline{Z}$ constrained by:

$$\langle \Delta\underline{Z}_j^T(\underline{k})\Delta\underline{Z}_j(\underline{k}) \rangle = \iiint\limits_{\Delta k_1 \Delta k_2 \Delta k_3} \Phi_{ij}(\underline{k}) dk_1 dk_2 dk_3 \tag{G.38}$$

The expected value of the transpose of $\Delta\underline{Z}_i$ multiplied by $\Delta\underline{Z}_j$ (the covariance matrix of ΔZ) equals the spectral tensor integrated over a volume $\Delta\underline{k} = \Delta k_1 \Delta k_2 \Delta k_3$ (centred on $\underline{k}$) representing an amount of variance in a block $\Delta\underline{k}$. The constraint is met if $\Delta\underline{Z}$ is defined as:

$$\Delta\underline{Z} = C\underline{n} \tag{G.39}$$

The 3-row column vector $\underline{n}(0,1)$ has three components which are random numbers that are standard normally distributed ($\mu = 0$, $\sigma = 1$). The matrix C is the (non unique) 'square root' of the spectral tensor $\Phi(\underline{k})$ integrated over $\Delta \underline{k} = \Delta k_1 \Delta k_2 \Delta k_3$:

$$C^T(\underline{k})C(\underline{k}) = \iiint\limits_{\Delta k_1 \Delta k_2 \Delta k_3} \Phi_{ij}(\underline{k})dk_1 dk_2 dk_3 \tag{G.40}$$

The matrix C may be found with the Cholesky decomposition, but in a large part of wave number space (where $k = |\underline{k}| \geq 3$) the spectral tensor function Φ is smooth, and it is a good enough approximation to write:

$$C^T(\underline{k})C(\underline{k}) \approx \Phi(\underline{k})\Delta k_1 \Delta k_2 \Delta k_3 \tag{G.41}$$

In that case a matrix C may be found directly with:

$$C(\underline{k}) \approx \sqrt{\frac{E(k_0)}{4\pi k_0^2}\Delta k_1 \Delta k_2 \Delta k_3} \begin{pmatrix} \frac{k_2 \zeta_1}{k_0} & \frac{k_3 - k_1 \zeta_1 + \beta k}{k_0} & -\frac{k_2}{k_0} \\ \frac{k_2 \zeta_2 - k_3 - \beta k_1}{k_0} & -\frac{k_1 \zeta_2}{k_0} & \frac{k_1}{k_0} \\ \frac{k_0 k_2}{k^2} & -\frac{k_0 k_1}{k^2} & 0 \end{pmatrix} \tag{G.42}$$

A complete overview of the underlying equations is given in Mann [133, 134] and in IEC 61400-1 [93]. Here it is only important to note that the expression under the square root sign represents the total energy (half the variance), which is the energy density multiplied by the volume of a box $\Delta \underline{k}$. The matrix expression produces a linear combination of the components of vector $\underline{n}$ multiplied by the right variance. The special (or maybe magical is a better word) thing about the matrix is that a vector with three independent random numbers is transformed into a vector that represents 3 wind speed components that obey mass conservation and the Navier Stokes equation. Of course the magic is really in the equation of the tensor Φ, in which mass conservation and Navier-Stokes equations have been incorporated.

Finally the wind field is found with the inverse Fourier transform:

$$\underline{u} = \sum_{k_1 k_2 k_3} e^{i\underline{x}.\underline{k}} \Delta \underline{Z}(\underline{k}) \tag{G.43}$$

Or:

$$\underline{u} = \sum_{k_1 k_2 k_3} e^{i\underline{x}.\underline{k}} C(\underline{k})\underline{n}(\underline{k}) \tag{G.44}$$

Note that for each wind speed component (u, v, w) a separate 3D Fourier transform must be done.

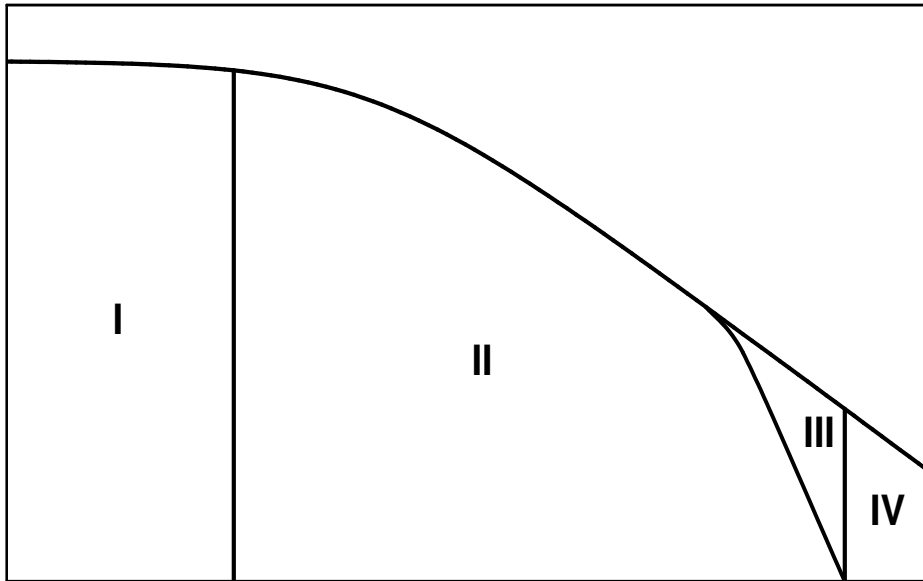**Figure G.1:** Loss of variance in generation of wind fields (schematic). Note logarithmic scales.

G.6   Technicalities

Loss of variance. The ideal spectra stretch from zero frequency to infinity, which is not the case for simulated spectra. A typical practical simulation period is 614 s (a little over 10 min), thus the lowest non-zero frequency found in the FFT 4096 points) is 1/614 = 0.0016 Hz, and the highest (2048/614 = 3.3333 Hz. Hence the simulated spectrum covers the frequency interval 0.0008–3.3341 Hz. All variance outside the interval is lost (figure G.1, areas I and IV). However in measurements the variance is found with:

$$\sigma_U^2 = \frac{\displaystyle\sum_{i=1}^{N} (U_i - \overline{U})^2}{N - 1} \tag{G.45}$$

 This amounts to removing the zero frequency component of the signal, which is exactly area I; furthermore it is easily verified that area IV amounts to only a few percent, so in the Sandia-Veers method areas II+III can be 'blown up' to compensate, In the Mann method that leaves us to deal with the loss in area III, which is a consequence of the fact that not the entire wave space is sampled, but only part of

it, especially in crosswind directions. One argument is that this loss does not matter, since it constitutes high frequencies that would be filtered out by the turbine anyway. However some informal investigations with more points in the rotor plane indicated that the variance loss in area III does have some influence on loads, and that it is probably better to normalise the variance of the turbulence field (area II) back to the desired value (for instance measured with sonic equipment). For the IEC 61400-1 Kaimal spectrum, the variance loss in areas I and IV is found as:

$$\Delta\sigma^2 = \int_0^{\Delta f/2} S_1(f) df + \int_{(N+1)\Delta f/2}^{\infty} S_1(f) df =$$

$$= \int_0^{\Delta f/2} \frac{4L/U}{(1 + 6fL/U)^{5/3}} + \int_{(N+1)\Delta f/2}^{\infty} \frac{4L/U}{(1 + 6fL/U)^{5/3}} =$$

$$= 1 - (1 + 3\Delta fL/U)^{-2/3} + (1 + 3(N+1)\Delta fL/U)^{-2/3} \qquad \text{(G.46)}$$

where:

L	length scale [m]
N	number of samples [-]
S_1	One sided spectral density [m2/s]
U	wind speed [m/s]
Δf	frequency interval [Hz]
$\Delta\sigma^2$	variance loss [m2/s]

Trends. Another problem is whether measured turbulence should be detrended or not. Trends will increase measured variance. Since the simulated wind signal has no trend, the 'trend variance' appears elsewhere in the spectrum. The correct procedure would perhaps be to measure the trend distribution, and add a similar random trend to the generated wind field.

Variation between 10 minute turbulence values. Turbulence measurements show variation between measurements (see for example Hansen [79]). One does not find the same variation in artificial wind fields, although the gaussian amplitude method give some. However as long as one is interested in mean loads (and not extremes) it is perfectly justified to use unity normalised turbulence fields without variation.

Periodicity. Wind fields generated with the Veers method are periodic in u-direction, while wind fields generated with the Mann method are periodic in all 3 directions. Periodicity in u-direction is no problem, since the time scale in u-direction is large. Problems with periodicity in v and w direction are avoided by generating a wind field with dimensions $2D \times 2D = 4D^2$, of which only the centre $D \times D$ is used (D = rotor diameter).

Of this square finally only $\pi D^2/4 \approx 80\%$ is used, which is 20% of the original points.

Zero wave numbers. The sheared tensor cannot be calculated for $k_1 = 0$ because zeros appear in the denominator in some matrix elements, and they become undefined. However since wave number $k_1 = 0$ represents the constant wind speed, it is no problem to leave this wave number out, except for variance loss. The variance that *is* taken into account is the variance in two blocks in wave number space defined by:

$$
\begin{aligned}
\frac{k_1}{\Delta k_1} &\in \left[-\frac{N_1 + 1}{2}; -\frac{1}{2}\right] \cup \left[\frac{1}{2}; \frac{N_1 + 1}{2}\right] \\
\frac{k_2}{\Delta k_2} &\in \left[-\frac{N_2 + 1}{2}; \frac{N_2 + 1}{2}\right] \\
\frac{k_3}{\Delta k_3} &\in \left[-\frac{N_3 + 1}{2}; \frac{N_3 + 1}{2}\right]
\end{aligned}
\tag{G.47}
$$

Box dimensions. The dimensions of the box that is transported through the rotor are chosen as follows. The length of the box in wind direction is $L_1 = N_1 U \Delta T$, with $N_1 = 2048$ or 4096 and $\Delta T = 0.15$ s. This yields time series of 307 or 614 seconds (5 or 10 minutes). For the Mann algorithm $L_2 = L_3 = 2D$ (of which only $D \times D$ output). The number of points is 32×32, of which 16×16 are output. This strategy yields cells that are not cubic. For example for an 80 m rotor at 16 m/s wind speed:

$$
\begin{aligned}
\Delta x &= U \, \Delta t = 16 \times 0.15 = 2.4 \, m \\
\Delta y &= 80 \, / \, 16 = 5 \, m \\
\Delta z &= 80 \, / \, 16 = 5 \, m
\end{aligned}
$$

IEC 61400 [1] recommends that points represent cubes, but this is impractical with a view to loss of variance and frequency content. At present the author does not see any objection to bricks rather than cubes: all the statistics of the wind field appear to be all right.

Fast Fourier transform. The fast Fourier transform used in the program is FourN (Press [167, 168]). Basically this would be inefficient, because only real numbers need to be transformed (not complex). However this is remedied by producing two wind fields at the same time, using the real and the imaginary part of the transform.

For $N_1 = 4096$, $N_2 = N_3 = 32$, a total of $4096 \times 32 \times 32 = 4,194,304$ numbers need to be stored for each Fourier transform. With 4 byte reals, this means ca 17 MB. Because the FourN algorithm uses complex numbers, this must be multiplied by 2, to get 33 MB. Finally there are 3 wind speed components, giving a memory requirement of ca 100 MB. This is no problem for modern PCs.

Recently even faster FFTs have appeared; there is a web site devoted to the 'Fastest Fourier Transform in the West' (www.fftw.org).

Efficient calculation of C matrix and spectral tensor. For every wave vector $\underline{k}$ the spectral tensor must be calculated i.e. the average value of the tensor elements over a volume $\Delta k_1 \Delta k_2 \Delta k_3$.

$$C^T(\underline{k})C(\underline{k}) = \iiint\limits_{\Delta k_1 \Delta k_2 \Delta k_3} \Phi_{ij}(\underline{k}) dk_1 dk_2 dk_3 \tag{G.48}$$

For large k ($|k| \geq 3$) it is not necessary to calculate the spectral tensor integral, since Φ is smooth, and it is accurate enough to approximate it with:

$$C^T(\underline{k})C(\underline{k}) \approx \Phi(\underline{k}) \Delta k_1 \Delta k_2 \Delta k_3 \tag{G.49}$$

In this case the decomposition 'by hand' (the C matrix, equation G.42) can be used, and the tensor need not be calculated. Some further increase in efficiency is gained by pre-computing some common coefficients, such as squares of the wave numbers and the value of the von Kármán energy spectrum.

If $|k| < 3$ however, the integration must be performed because the approximation is not accurate enough. Because the k_1 increment Δk_1 is small, the 3-dimensional integral can however be approximated by a 2-dimensional one:

$$C^T(\underline{k})C(\underline{k}) \approx \Delta k_1 \iint\limits_{\Delta k_2 \Delta k_3} \Phi_{ij}(\underline{k}) dk_2 dk_3 \tag{G.50}$$

The 2-dimensional integration may for example be done with a nested application of the routine **qromb**, which uses trapezoid integration with Richardson extrapolation (Press [167, 168]). It is a good idea to do integration in double precision, and check on relative and absolute error.

Mann advocates transforming the integral with the use of the $sinc(x) = sin(x)/x$ function, but the author found no advantage in doing this. It is possible that the integrand becomes somewhat smoother, and easier to integrate. However the integration described above works fine.

Arctan function. To evaluate C (or Φ), a help parameter C_2 must be calculated, which is given by Mann [133]:

$$C_2 = \frac{k_2 k_0^2}{(k_1^2 + k_2^2)^{3/2}} \arctan\left(\frac{\beta k_1 \sqrt{k_1^2 + k_2^2}}{k_0^2 - \beta k_{30} k_1}\right) \tag{G.51}$$

It is important to realise that the arctan function to be used is the arctan that yields a value between $-\pi$ and π, i.e. expression G.51 is equivalent to:

$$C_2 = \frac{k_2 k_0^2}{(k_1^2 + k_2^2)^{3/2}} \arg(x + yi) \tag{G.52}$$

With:

$$x = k_0^2 - \beta k_{30} k_1 \tag{G.53}$$

$$y = \beta k_1 \sqrt{k_1^2 + k_2^2}$$

And the argument normalised to a value between $-\pi$ and π. This arctan function is called *arctan2* in some programming languages.

Energy integral. For every vector $\underline{k}$ (with length k) a help parameter β must be calculated, that uses the integral of the von Kármán energy spectrum. Mann's article calls for the use of the hypergeometric function $_1F_2$. He points out that the value is proportional to the integral of the three dimensional energy function (half the power spectral density) $E(\underline{k}) = E(k)$:

$$\beta(\underline{k}) = \frac{\gamma}{k^{2/3} \sqrt{_1F_2\left(\frac{1}{3}, \frac{17}{6}, \frac{4}{3}, -\frac{1}{k^2}\right)}} = \frac{c\gamma}{k \sqrt{\displaystyle\int_{|\underline{k}|}^{\infty} E(p)dp}} \tag{G.54}$$

In fact the proportionality constant c is:

$$c = \sqrt{\frac{55}{6} \frac{\Gamma(5/6)}{\sqrt{\pi}\Gamma(1/3)}} \approx 1.476 \tag{G.55}$$

The energy spectrum $E(k)$ is the non-dimensionalised von Kármán spectrum, given by:

$$E(k) = \frac{55}{9} \frac{\Gamma(5/6)}{\sqrt{\pi}\Gamma(1/3)} \frac{k^4}{(1+k^2)^{17/6}} \approx \frac{1.453k^4}{(1+k^2)^{17/6}} \tag{G.56}$$

For each vector $\underline{k}$ the energy spectrum integral must be calculated, so it pays to pre-compute it. This is done as follows:

1. Set $k = 0$.
2. Calculate $\int E(k)$ from k to ∞ (= 1.5 if $k = 0$).
3. Calculate $\int E(k+1) = \int E(k)$ minus the integral $\int E(k)$ over $[k, k+1]$.
4. Go to step 2.

Through the table values cubic splines are constructed. For large k (for example $k > 400$) the integral can also be approximated by:

$$\int_k^{\infty} E(p)dp \approx \int_k^{\infty} \frac{1.453p^4}{(1+p^2)^{17/6}} dp \approx \int_k^{\infty} \frac{1.453}{p^{5/3}} dp = \frac{2.180}{k^{2/3}} \tag{G.57}$$

It is easier to use the energy integral because this makes it unnecessary to get a routine for the (somewhat obscure) hypergeometric function. However the two functions are equivalent, so it is really a matter of taste.

G.7   Some results

All auto- and cross spectra can be found by integration of the spectral tensor:

$$S_{ij}(k_1, \Delta y, \Delta z) = \int_{-\infty}^{\infty} \int_{-\infty}^{\infty} \Phi_{ij}(\underline{k}) \exp(ik_2 \Delta y + ik_3 \Delta z) dk_2 dk_3 \qquad (G.58)$$

For autospectra the distances in y and z direction are zero ($\Delta y = \Delta z = 0$), and the expression simplifies to ($i = j$:

$$S_{ij}(k_1) = \int_{-\infty}^{\infty} \int_{-\infty}^{\infty} \Phi_{ij}(\underline{k}) dk_2 dk_3 \qquad (G.59)$$

For shear parameters from $\Gamma = 0$ to $\Gamma = 5$ the total variance was calculated (the integration was done from $k_1 = 0.001$ to $k_1 = 100$, for $k_1 \leq 0.001$ the spectrum was assumed to be constant, and for $k_1 \geq 100$ decreasing according to the $-5/3$ power law). The figures given in table G.1 agree well with the values taken from figures published by Mann [133, 134].

As an interesting sidelight it is noted that if the variances for wind speed components u, v, and w can be measured with sufficient accuracy (for example with a sonic anemometer), the shear parameter Γ can immediately be estimated from the turbulence ratios; and this parameter in turn fixed the shape of all autospectra and cross spectra (coherence functions), except for the length scale.

In figure G.2 a comparison is given between the spectra found with direct integration and (average) spectra recovered from a wind field generated with Mann's method. Clearly it can be seen that there is large variation at low frequencies, and variance loss at high frequencies.

Comparison of known spectra with integration For the von Kármán spectrum the coherence functions are known analytically. For example the lateral coherence for speed component U is (see Mann [138, p19]):

$$Coh(k_1, D) = \frac{2}{\Gamma(5/6)} \left(\frac{\zeta}{2} \right)^{5/6} \left(K_{5/6}(\zeta) - \frac{\zeta}{2} K_{1/6}(\zeta) \right) \qquad (G.60)$$

Table G.1: Variance values.

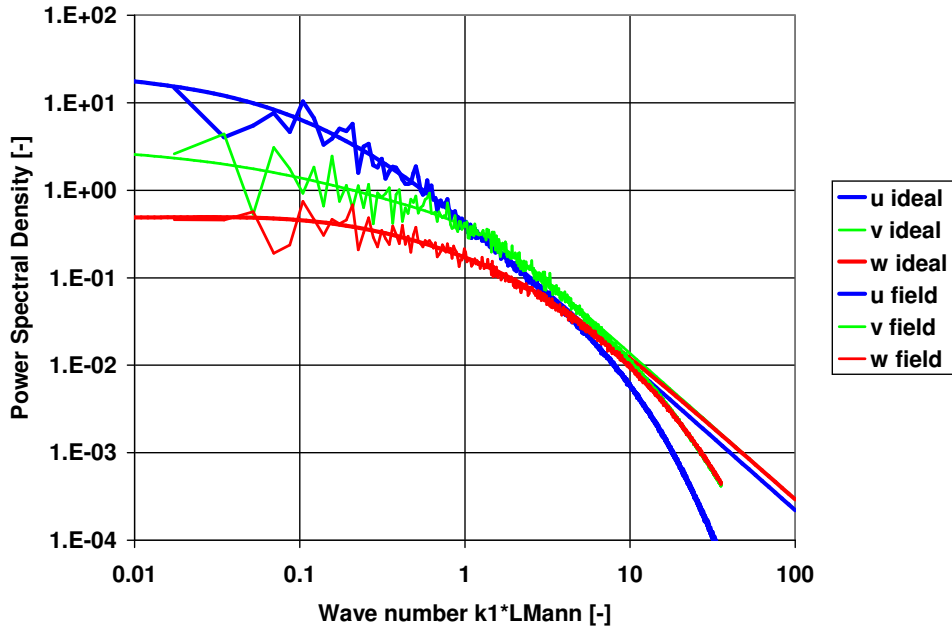| shear	variance			variance ratios		
Γ	σ_u^2	σ_v^2	σ_w^2	σ_u^2/σ_u^2	σ_v^2/σ_u^2	σ_w^2/σ_u^2
0	1.00	1.00	1.00	1.00	1.00	1.00
1	1.16	1.06	1.04	1.00	0.91	0.90
2	1.65	1.24	1.02	1.00	0.75	0.62
3	2.41	1.46	0.95	1.00	0.61	0.39
4	3.34	1.66	0.87	1.00	0.50	0.26
5	4.40	1.85	0.80	1.00	0.42	0.18

Figure G.2: Comparison of Mann spectra found by direct integration and recovered from a generated wind field. The shear parameter $\Gamma = 3.9$, which produces the Kaimal spectra.

with:

$$\zeta = \sqrt{k_1^2 D^2 + D^2/L^2} \tag{G.61}$$

where:

D	separation distance [m]
K	modified Bessel function of second kind of fractional order
k_1	wave number [1/m]
L	length scale [m]
ζ	help parameter [-]

The coherence can also be found by integrating:

$$Coh(k_1, \delta) = \frac{\displaystyle\int\limits_{-\infty}^{\infty}\int\limits_{-\infty}^{\infty} \Phi_{ij}(\underline{k})e^{ik_2\delta}dk_2 dk_3}{\displaystyle\int\limits_{-\infty}^{\infty}\int\limits_{-\infty}^{\infty} \Phi_{ij}(\underline{k})dk_2 dk_3} \tag{G.62}$$

This is a difficult integral to find numerically, but Mann [138, appendix A] gives a procedure with cubic splines which is very effective.

Appendix H

Curriculum vitae

Herman Frederik Veldkamp was born on 27 March 1961 in Kokonao, Netherlands New-Guinea (now Irian Jaya, Indonesia).

He attended grammar school at the Eerste Christelijk Lyceum in Haarlem, where he obtained his diploma (Gymnasium-β) in 1978. After this he studied at the Technical University of Delft, finishing with an MSc degree in Mechanical Engineering and a teacher's degree in mathematics in 1986.

He then worked with water pumping windmills at CWD (Consultancy Services Wind Energy Developing Countries, a government project aimed at introducing wind pump technology overseas) from 1986 to 1990. When the project ended he started the wind energy consultancy firm 'Goezinne & Veldkamp' (together with colleague Frank Goezinne), in which he worked until going to Denmark in 1995 for a job at wind turbine manufacturer Micon. Since then he has been working at the same firm (from 2000 in the Netherlands), which during that time first changed name to NEG Micon and then to Vestas.

He is married and has three daughters. His hobbies are science (applied mathematics and evolution biology), languages and music (bagpipe, guitar, piano).